

# NASA Contractor Report 3694

NASA  
CR  
3694  
c.1

## The NCOREL Computer Program for 3D Nonlinear Supersonic Potential Flow Computations

TECH LIBRARY KAFB, NM  
0062309

Michael J. Siclari

LOAN COPY: RETURN TO  
AFWL TECHNICAL LIBRARY  
KIRTLAND AFB, NM 87117

CONTRACT NAS1-16758  
AUGUST 1983



25th Anniversary  
1958-1983

NASA



## **NASA Contractor Report 3694**

# **The NCOREL Computer Program for 3D Nonlinear Supersonic Potential Flow Computations**

**Michael J. Siclari**  
*Grumman Aerospace Corporation*  
*Bethpage, New York*

**Prepared for**  
**Langley Research Center**  
**under Contract NAS1-16758**



National Aeronautics  
and Space Administration

**Scientific and Technical  
Information Branch**



## CONTENTS

<u>Section</u>		<u>Page</u>
1	SUMMARY.....	1
2	INTRODUCTION.....	3
3	ANALYTICAL APPROACH.....	5
4	GENERAL METHODOLOGY.....	7
	4.1 Transformations.....	7
	4.2 Relaxation Schemes.....	8
	4.3 Boundary Conditions.....	13
	4.4 Mesh Refinement.....	14
	4.5 Bow Shock Methods.....	14
	4.5.1 Bow Shock Capture (BSC).....	14
	4.5.2 Bow Shock Fit (BSF).....	18
5	GEOMETRY AND MAPPING REQUIREMENTS.....	27
	5.1 Mapping Requirements.....	27
	5.2 Geometry Options.....	30
6	AERODYNAMIC FORCES AND MOMENTS.....	39
7	GEOMETRIC RESTRICTIONS.....	47
8	TYPICAL APPLICATIONS.....	51
	8.1 Conical Flows.....	51
	8.2 Nonconical Flows.....	55
	8.2.1 Analytic Forebodies.....	55
	8.2.2 Missile Bodies.....	59
	8.2.3 Analytic Arrow Wing.....	65
	8.2.4 Supersonic Cruise Aircraft.....	68
	8.2.5 Zero Lift Wave Drag of a Delta Wing.....	73
	8.2.6 NASA/Grumman Demonstration Wing.....	75
9	COMPUTER PROGRAM DESCRIPTION.....	83
	9.1 Organizational Structure & Segmentation.....	83
	9.2 Subroutine Description.....	87
	9.3 Common Blocks.....	93
	9.4 I/O Unit Devices.....	97

<u>Section</u>		<u>Page</u>
10	NCOREL USER MANUAL.....	101
	10.1 Input Parameters.....	101
	10.2 Printed Output.....	108
	10.3 Sample Cases.....	115
11	REFERENCES.....	159

## ILLUSTRATIONS

<u>Figure</u>		<u>Page</u>
1	Ring and Column Relaxation Methods.....	10
2	Convergence Rates for conical Flow Solutions, Ring vs Column SLOR.....	12
3	Effect of Mesh Refinement.....	15
4	Bow Shock Capture Methods (BSC).....	17
5	Mach Cone Relationship to Type of Surface for Bow Shock Fit Method (BSF).....	21
6	Bow Shock Guess Generation.....	24
7	Examples of Conical Bow Shock Fit Solutions, (16 x 16 Mesh)..	25
8	Singularity Placement and CONUSE Logic Used in NCOREL.....	29
9	Geometrical Parameters Used in Defining Analytical Wings (IOPTG = 2).....	31
10	Analytical Geometry Package Definitions (IOPTG = 2).....	33
11	Sample Analytic Wing Geometries.....	34
12	Conical Wing-Body Geometry Generation.....	35
13	General Interpolation Scheme for Arbitrary Planforms Used for Aerodynamic Computation.....	40
14	NCOREL Aerodynamic Output: Areas, Lift and Drag Coefficients	42
15	NCOREL Aerodynamic Output, Moment Coefficients.....	45
16	Conical Surface Pressure Distributions for Two Dissimilar Cross Sections ( $M_\infty = 2.0$ , $\theta_c = 20^\circ$ ).....	52
17	Conical Bow Shock Fit Crossflow Streamline Patterns.....	54
18	Conical Bow Shock Fit Crossflow Streamline Patterns for a Thin Elliptic Cone, $\theta_c = 20^\circ$ , $\delta_c = 2^\circ$ , and $\alpha = 10^\circ$ .....	56
19	Conical Bow Shock Fit Crossflow Streamline Patterns for a Wing-Body Cross Section, $M_\infty = 2.0$ , $\alpha = 10^\circ$ , $\theta_c = 20^\circ$ .....	56
20	Conically Cambered Wing.....	57

<u>Figure</u>		<u>Page</u>
21	Spanwise Pressure Distributions on a Conical Cambered and Flat Wing Section, $M_\infty = 1.62$ .....	58
22	Axial Pressure Distribution on a Parabolic Arc Body with Lobed Cross Sections at $M_\infty = 1.70$ .....	60
23	Azimuthal Pressure Distribution on a Parabolic Arc Body with Lobed Cross Section, $M_\infty = 1.70$ , $\alpha = 10.35^\circ$ .....	61
24	Axial Pressure Distribution on a Fuselage Forebody Shape, $M_\infty = 1.70$ .....	62
25	Azimuthal Pressure Distribution on a Fuselage Forebody $M_\infty = 1.70$ , $\alpha = 1^\circ$ .....	63
26	Missile Body Moment and Normal Force Characteristics at $M_\infty = 2.0$ .....	64
27	Arrow-wing Wind-tunnel Model Showing Pressure Orifice Locations (Ref. 14).....	66
28	Spanwise Pressure Distribution on an Analytically Defined Arrow Wing, $M_\infty = 2.36$ , $\alpha = 6^\circ$ .....	67
29	Input Panel Model of Supersonic Cruise Aircraft Showing Pressure Data Stations used for Comparison.....	70
30	Isometric View of Spanwise Cross Sections and Pressure Distributions ( $\Delta X = 2$ ).....	70
31	Comparison of Computed Wing Alone and Wing-Body Configurations with Pressure Data for $M_\infty = 2.30$ , $\alpha = 4.82^\circ$ .....	72
32	Comparison with Surface Pressure Data for a Supersonic Cruise Aircraft at $M_\infty = 2.30$ , $\alpha = 2.81^\circ$ and $4.82^\circ$ .....	72
33	Computed and Measured Zero Lift Wave Drag on the Squire Delta Wing.....	74
34	NCOREL Comparisons with DEMO Wing Surface Pressure Data, $M_\infty = 1.62$ , $\alpha = 9.92^\circ$ .....	76
35	NCOREL Comparisons with DEMO Wing Surface Pressure Data, $M_\infty = 1.62$ , $\alpha = 11.93^\circ$ .....	77
36	NCOREL Comparisons with DEMO Wing Surface Pressure Data, $M_\infty = 1.62$ , $\alpha = 13.92^\circ$ .....	79
37	NCOREL Comparisons with DEMO Wing Surface Pressure Data, $M_\infty = 2.00$ , $\alpha = 11.80^\circ$ .....	80
38	Computed Isobar Patterns for the DEMO Wing, $M_\infty = 1.62$ .....	81

<u>Figure</u>		<u>Page</u>
39	Computed Isobar Patterns at $C_L = 0.40$ , $M_\infty = 1.62$ .....	82
40	NCOREL Subroutine and Branch Organizational Chart.....	84
41	Subroutine Dependence in INITN Branch.....	85
42	Segmentation Directives for NCOREL.....	86
43	Segmentation Tree Diagram for NCOREL.....	88
44	Sample of CONUSE Subroutines.....	117
45	Sample Input Data Sets.....	119
46	Sample Printed Output for BSF Method.....	120
47	Sample Printed Output for BSC Method.....	134
48	Summary of Convergence History.....	148
49	Spanwise and Chordwise Interpolation Output.....	149
50	Aerodynamic Output.....	155



## 1 SUMMARY

An innovative computational technique, Nonconical Relaxation (NCOREL), has been established for the treatment of three dimensional supersonic flows. The method is nonlinear in that it solves the nonconservative finite difference analog of the full potential equation and can predict the formation of supercritical cross flow regions, embedded and bow shocks.

The method implicitly computes a conical flow at the apex ( $R = 0$ ) of a spherical coordinate system and uses a fully implicit marching technique to obtain three dimensional cross flow solutions. This implies that the radial Mach number must remain supersonic. The cross flow solutions are obtained by using type dependent transonic relaxation techniques with the type dependency linked to the character of the cross flow velocity (i.e., subsonic/supersonic).

The spherical coordinate system and marching on spherical surfaces is ideally suited to the computation of wing flows at low supersonic Mach numbers due to the elimination of the subsonic axial Mach number problems that exist in other marching codes that utilize Cartesian transverse marching planes.

NCOREL has been applied successfully to a wide variety of body and wing configurations in the Mach number range from 1.5 to 3. The method represents a significant advancement in accuracy over linear methods. This report describes the practical application and use of the computer program NCOREL.



## 2 INTRODUCTION

A new computational technique, Nonconical Relaxation (NCOREL), utilizing the full potential flow equation has been established for the prediction of inviscid nonlinear supersonic aerodynamics. This method has proven to be remarkably accurate for predicting flows in the low to moderate supersonic Mach number regime (i.e., 1.5 to 2.5). Unlike linear potential methods (e.g., panel methods), NCOREL can predict the formation of supercritical cross flow regions, bow and embedded shocks.

Nonlinear effects are important to the aerodynamicist in the supersonic regime because he cannot intelligently or reliably tailor a wing to optimize lift and drag without knowledge of the formation of "embedded crossflow shocks" which can significantly alter the wing characteristics. Embedded crossflow shocks not only induce drag but can also lead to boundary layer separation. The high lift characteristics of supercritical crossflow regions can be beneficial to the aerodynamicist if he can exercise control over the formation and strength of crossflow shocks which are typically synonymous with these supercritical crossflow regions. Strong embedded cross flow shocks are most prevalent on wings that have subsonic leading edges. The strength of the crossflow shock is proportional to the angle of attack or lift coefficient, cross sectional thickness, and leading edge radius of curvature for an uncambered wing. Nonlinear effects are also important on wings that have supersonic leading edges or bodies whose slope is greater than the Mach angle. For this class of configurations, significant errors become prominent in linear theory and a nonlinear theory becomes necessary. Linear panel methods must use approximate techniques to compute bodies that have panels inclined greater than the Mach angle. Hence, significant departures from linear methods can be expected locally in regions of supercritical crossflow and more globally in regions where the bow shock position differs significantly from the Mach cone as is the case for wings or bodies with supersonic boundaries (i.e., normal Mach number greater than one).

The primary intent of this report is to document and illustrate the use of the computer program NCOREL. The name NCOREL is an acronym for Non-CONical RELaxation which is the basic technique used in NCOREL to obtain numerical solutions to the three dimensional nonconservative full potential

equation. NCOREL has in its ancestry the COREL code which was developed for supersonic conical flows (Ref. 1,2). A computer program called SUNPOT for SUPersonic Nonlinear POTential flow was developed prior to NCOREL for the Air Force Wright Aeronautical Laboratory (see Ref. 3,4). This early version of NCOREL captured all shocks and was lacking in numerical efficiency compared to the present code.

The success of COREL in its application to the design of a SC3 Conceptual Conical wing (i.e., SuperCritical Conical Camber) detailed in Ref. 5, paved the way for its extension to NCOREL. A landmark application of NCOREL to a three dimensional high lift maneuver wing (Ref. 6,7) demonstrated that for the first time aerodynamicists could reliably predict the detailed spanwise behavior of realistic supersonic wings in a high lift maneuver regime.

### 3 ANALYTICAL APPROACH

The approach used in NCOREL consists of casting the nonconservative full potential equation in a spherical coordinate system. Conformal mappings are then used, if necessary, to generate a grid in the spherical cross flow plane capable of resolving typically large gradients in the vicinity of the wing leading edge. The three dimensional full potential equation written in a spherical coordinate system reduces identically to the conical two dimensional equation at  $r = 0$ . The primary advantage to this formulation is that a three dimensional computation can be automatically initiated with a conical flow at the apex using the same set of equations. Other supersonic marching codes either require a separate conical computation or another code to generate starting plane data. Unlike other supersonic methods utilizing nonlinear equations, NCOREL is a fully implicit marching technique which is not hindered by CFL constraints. The only constraint in the marching direction is that due to geometric accuracy. Hence, a three dimensional wing computation can be achieved in 10 to 50 steps depending upon accuracy requirements and geometric variation in the marching direction.

The radial spherical coordinate is used as the marching direction. This is an absolute necessity for a method oriented toward wing flow fields at low supersonic Mach numbers. Other marching methods that utilize the axial cartesian coordinate as the marching direction very quickly encounter subsonic axial Mach numbers below Mach 2 for wings that are not highly swept. Explicit marching codes that use conformal mappings also typically encounter difficulty for wing geometries at low supersonic Mach numbers because the mesh size in the vicinity of the leading edge tends to diminish greatly. The vanishing mesh size and CFL condition in combination greatly restrict the step size in the marching direction, making the computation impractical.

In NCOREL, finite difference solutions to the nonconservative full potential equation are obtained at each spherical crossflow station commencing at the apex,  $R = 0$ , with a conical solution for the geometry obtained at  $R = \Delta R$ . Transonic type dependent relaxation techniques form the basis for the numerical finite difference crossflow plane solutions. The current finite difference equations are second order accurate in elliptic crossflow regions and first order accurate in the hyperbolic crossflow region and spherical

marching direction. A rotated difference scheme (Ref. 8) is used in the supersonic crossflow region. The type dependency is coupled to the character of the crossflow Mach number on the spherical surface. The character of the crossflow terms switch from elliptic to hyperbolic as the crossflow Mach number exceeds sonic conditions. The numerical technique allows for the capture of both embedded crossflow and bow type shocks. Recently, in Ref. 9, the bow shock was fitted isentropically as a boundary. It was found that fitting the bow shock further increased the accuracy of the technique. As will be demonstrated in a later section, NCOREL has exhibited a high level of success for flows over isolated bodies and wings.

## 4 GENERAL METHODOLOGY

### 4.1 TRANSFORMATIONS

The method uses a series of three transformations from the physical cartesian (x,y,z) or spherical ( $\omega, \phi, r$ ) coordinates to the computational evenly spaced rectangular crossflow mesh. The coordinate transformations are:

#### I Spherical Coordinates ( $\omega, \phi, r$ )

$$\begin{aligned}x &= r \cos \omega \sin \phi \\y &= r \sin \omega \sin \phi \\z &= r \cos \phi\end{aligned}\tag{1}$$

Note that the Cartesian coordinate sytem used in NCOREL is atypical of the standard aircraft coordinate system in that the Z direction is axial and (X,Y) are the transverse plane coordinates.

#### II Stereographic Projection (p,q,t)

$$\begin{aligned}p &= \cos \omega \tan \phi/2 \\q &= \sin \omega \tan \phi/2 \\t &= r\end{aligned}\tag{2}$$

#### III Conformal Joukowski Mapping ( $\rho, \theta, R$ )

$$\frac{S-S_0}{S+\bar{S}_0} = \left( \frac{R-S_0/2}{R+\bar{S}_0/2} \right)^2\tag{3}$$

where  $S = p + iq$ ,  $R = \rho e^{i\theta}$  and  $S_0(r)$  is the singularity location.

#### IV Shearing Transformation (X,Y,Z)

$$\begin{aligned}X &= \theta \\Y &= \frac{\rho-B}{C-B} \\Z &= R = r\end{aligned}\tag{4}$$

where  $\rho = B(\theta, R) \equiv$  Body Surface

$\rho = C(\theta, R) \equiv$  Outer Boundary or Bow Shock Surface

#### 4.2 RELAXATION SCHEMES (SLOR)

The three dimensional full potential equation in a spherical coordinate system can be represented by,

$$L_c(\phi) + RL_{nc}(\phi) = 0 \quad (5)$$

where  $L_c$  is a conical operator and  $L_{nc}$  is a nonconical operator. At  $R = 0$ , the above equation reduces to the conical quasi two dimensional full potential equation. A perturbation potential is introduced as

$$\vec{Q} = \vec{q} + \vec{q}_\infty = \nabla\phi + \vec{q}_\infty \quad (6)$$

where

$$\vec{Q} = U\vec{i}_\theta + V\vec{i}_\rho + W\vec{i}_r$$

This potential is further reduced to

$$\phi = RF(\rho, \theta, R) \quad (7)$$

The mapped space velocities are then defined as,

$$U = \frac{F_\theta}{\rho H} + U_\infty$$

$$V = \frac{F_\rho}{H} + V_\infty$$

$$W = F + RF_r + W_\infty$$

where  $U_\infty$ ,  $V_\infty$ , and  $W_\infty$  are the freestream velocity components in the mapped  $\theta$ ,  $\rho$ , and  $r$  directions, respectively.  $H$  is the metric of the two conformal mapping transformations.

If the Joukowski mapping singularity  $S_0$  is a function of  $r$ , the following mesh derivatives are generally nonzero and defined by,

$$h_1 = \partial\rho/\partial r$$



$$h_2 = \frac{1}{\rho} \partial \theta / \partial r$$

These mesh derivatives are used in the following transformation,

$$\frac{\partial}{\partial r} = \frac{\partial}{\partial R} + h_1 \frac{\partial}{\partial \theta} + h_2 \frac{\partial}{\partial p}$$

The finite difference analog of the nonconservative full potential equation in the computational domain can be written as,

$$(A_1 - B_1) F_{xx} + (A_2 - B_2) F_{xy} + (A_3 - B_3) F_{yy} + \quad (8)$$

$$+ B_8 F_{zz} + B_9 F_{xz} + B_{10} F_{yz} + B_{11} F_z = 0$$

where the coefficients  $B_i = R \bar{B}_i$  vanish for conical flows. The X and Y terms are crossflow plane derivatives evaluated according to the type of crossflow. (i.e., subsonic/elliptic or supersonic/hyperbolic). The Z terms in the marching direction are always assumed to be hyperbolic. This implies the condition that the radial velocity must remain supersonic. The Z derivatives are evaluated using first order accurate upwind differences. The first order accurate second derivative  $F_{zz}$  requires that the potential at two previous spherical planes be stored. Hence, the potential at a total of three cross flow stations must be stored.

Figure 1 shows the coordinate meshes in the mapped crossflow plane and in the sheared computational domain. The conformal mapping transforms the cross sectional projected geometry into a near circle which clusters grid points in the vicinity of the leading edge in the physical space. Two basic types of shocks can occur, the bow shock or Y-shock and the crossflow shock or X-shock. Since the freestream must always be supersonic, a bow shock will always be present. If the bow shock is captured within the mesh (BSC method), the bow shock is defined by a crossflow sonic line. The crossflow velocity beyond the bow shock position will be supersonic and inside the bow shock only subsonic crossflow will exist if a crossflow shock or X-shock is not present. If the flow around the leading edge accelerates to supersonic velocities an embedded crossflow shock will also exist. For most flows, the Y or bow shock is due to the V component of velocity being negative (towards the body) and supersonic and for the X-shock, or crossflow shock, the U component of velocity becomes positive and supersonic if  $\alpha > 0$ .

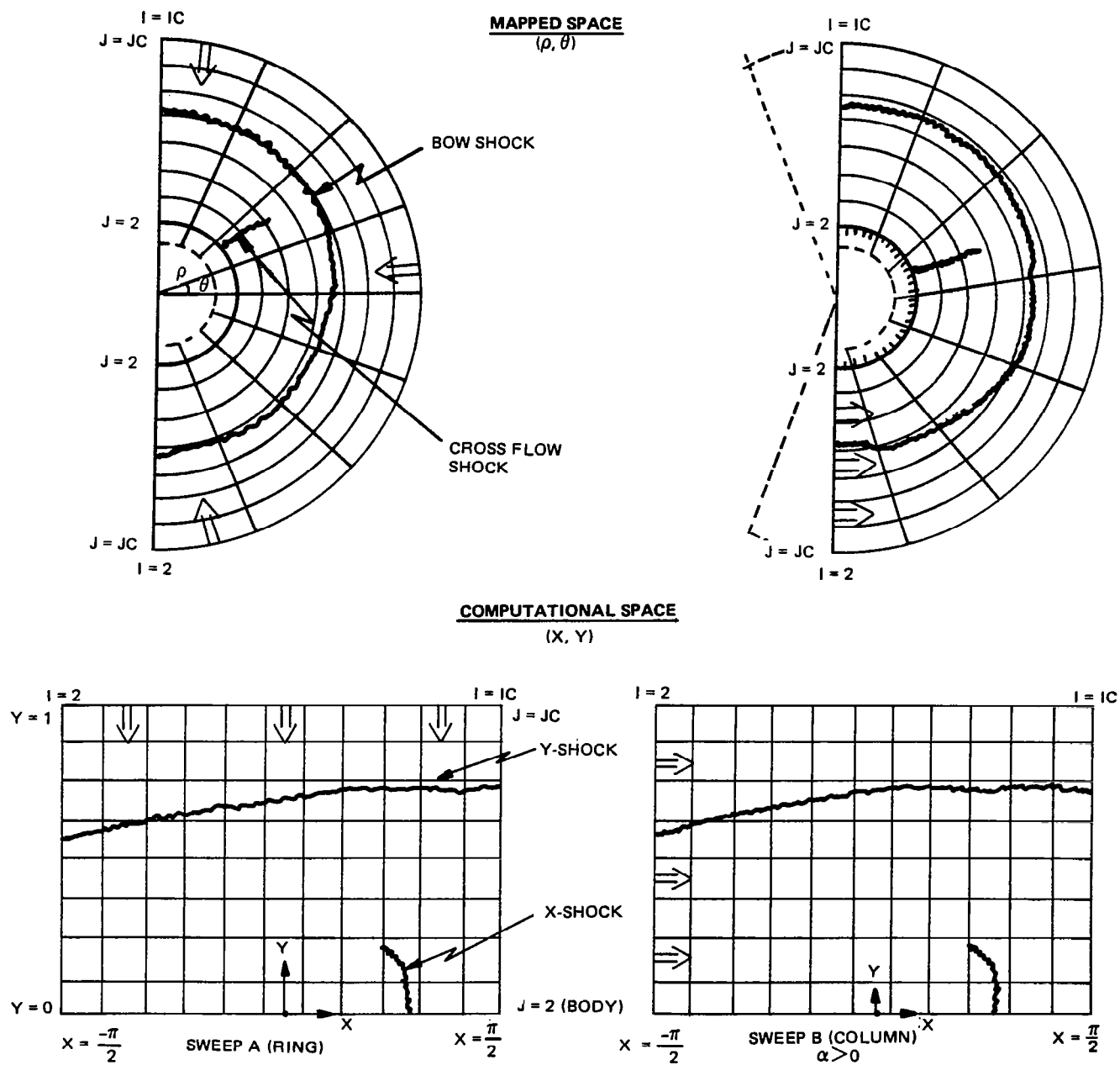
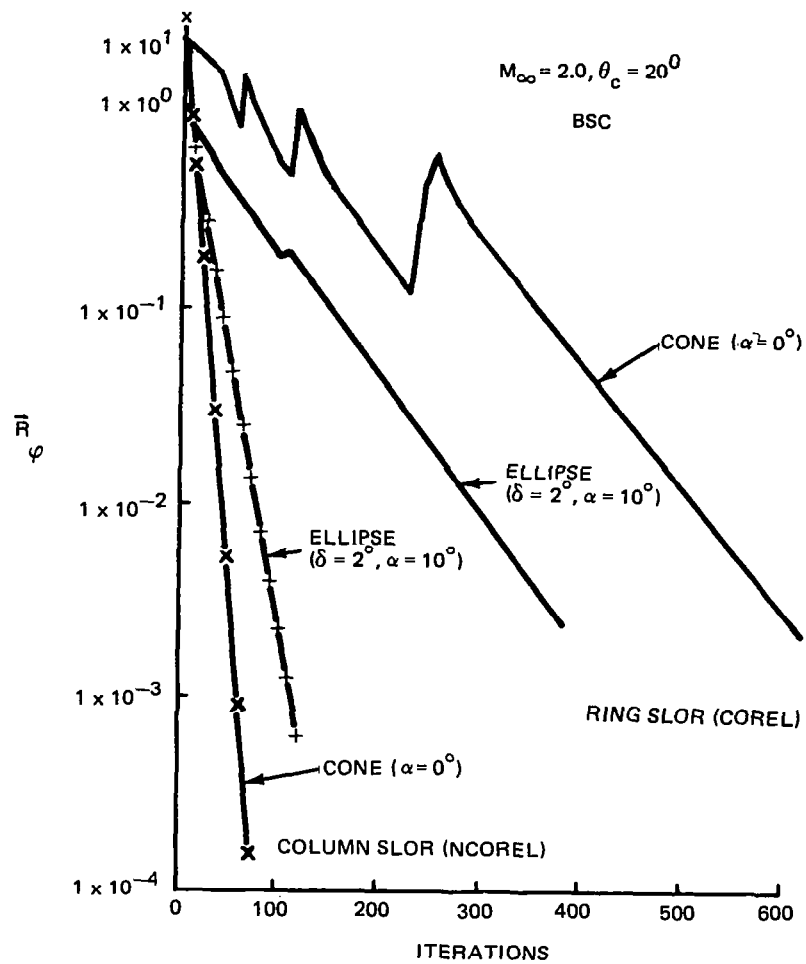


Figure 1 Ring and Column Relaxation Methods

Successive Line Over Relaxation (SLOR) is used as the basic numerical procedure in the computer program NCOREL. In SLOR, the values of the potential on any given computational coordinate line  $X = \text{constant}$  or  $Y = \text{constant}$  are over-relaxed if the flow is subsonic and the equation is elliptic in nature. To determine the value of the correction to the potentials on a given line, a tridiagonal matrix must be solved using the appropriate boundary conditions as end conditions in a Gaussian elimination procedure. The efficient convergence of a SLOR scheme is best achieved when the sweep direction is not opposite to any supersonic zones. Hence, two sweep directions are then possible for the present problem as illustrated in Fig. 1. In sweep A, values for the correction are determined on a  $Y = \text{constant}$  line (Ring) and the sweep direction is towards the surface or decreasing  $J$ . For sweep B, values for the correction are determined on an  $X = \text{constant}$  line (column) and the sweep direction is around the body towards increasing  $I$  or increasing  $\theta$ . Both sweeps are in the direction of the supersonic zones if  $\alpha > 0$ . Each of these methods have been applied to the current problem. Sweep A is the original COREL method of Ref. 1 and 2. Sweep B was later implemented in Ref. 9. The test of which method is the best is how well they perform on problems of practical interest. Figure 2 shows a comparison of the two methods on some sample conical flow problems. The column method turns out to be two to five times faster than the ring relaxation method. The supersonic flow problem is largely determined by the formation of the bow shock. The column relaxation method inverts the tridiagonal matrix from the body to the outer boundary. Hence, the body boundary condition immediately affects or is felt by the bow shock. In the ring relaxation method, it takes approximately  $N$  iterations, where  $N$  is the number of grid points in the  $Y$  direction, for the outer boundary to feel the effect of the surface boundary condition. This is the major reason why the column sweep method is more efficient. There may be a region for a particular class of shapes or for a very high angle of attack where the ring relaxation method may be more efficient. For most practical cases, the Column Relaxation Method has been found to be more efficient for both conical and three dimensional flows and is used in the present NCOREL computer program.



2246-014W

**Figure 2 Convergence Rates for Conical Flow Solutions,  
Ring vs Column SLOR**

### 4.3 BOUNDARY CONDITIONS

For the symmetric half plane problem, periodic end conditions are used at the boundaries  $I = 2$  and  $I = IC$ . This symmetry condition is enforced by storing the reflected potential at  $I = 1$  and  $I = IC + 1$ . The values of the potential are set as:

$$\begin{aligned} F(1,J) &= F(3,J) \\ F(IC+1,J) &= F(IC-1,J) \end{aligned} \tag{9}$$

If quarter plane symmetry exists at zero angle of attack, a reflected boundary condition is enforced at  $I = 1 + IC/2$  and the sweep is conducted from  $I = 1 + IC/2$  to  $I = IC$ .

The body or surface boundary condition of flow tangency or the vanishing of normal velocity is implemented by defining a dummy mesh ring inside the body at  $J = 1$  (see Fig. 1). The boundary condition of zero normal velocity is then used to determine values of  $F(I,1)$  as a function of  $F(I,2)$  and  $F(I,3)$  and the body geometry by solving for the  $Y$  derivative of the potential. In this way, the surface boundary condition is automatically implemented when centered values of the derivative  $F_Y$  are determined at the body surface  $J = 2$ . The surface boundary condition is implemented for each iteration of the relaxation scheme until convergence. For the bow shock capture method (BSC), the value of the potential at the two outermost rings is set equal to zero. This assumes that the two outermost rings are at the freestream conditions, and an outer end condition of zero correction will be imposed in the tridiagonal solution. Hence, care must be taken so that the bow shock is captured within these coordinate rings. Generally, the bow shock should be captured with at least two rings beyond its position where freestream supersonic crossflow velocities exist, not including the two rings held fixed; or  $J$  of the bow shock should be at least  $J_C - 3$  to insure the proper solution. This occurs because the bow shock is captured across three mesh lines. One point will occur on the lower pressure or freestream side and another on the high pressure side of the bow shock with one point in between at approximately sonic conditions. If the outer boundary is chosen incorrectly, no supersonic crossflow velocities will occur within the two fixed rings at  $J_C$  and  $J_C - 1$ , and erroneous results can occur.

In the Bow Shock Fit (BSF) Method, the boundary condition of zero potential is imposed only at the outermost ring. In this method, the outermost ring will be the bow shock, and in the absence of a crossflow shock, only subsonic crossflow velocities will exist for the entire mesh. The restrictions and requirements on the outer boundary that occur in the BSC Method are absent in the BSF method. The first derivative of the potential  $F_Y$  is second order and taken one sided into the mesh or

$$F_Y = \frac{1}{2\Delta Y} (3F_{i,j} - 4F_{i,j-1} + F_{i,j-2})$$

This derivative is necessary to determine the bow shock jump conditions. The different bow shock methods and their implementation will be explained more fully in a subsequent section.

#### 4.4 MESH REFINEMENT

Mesh refinement is currently used in NCOREL to obtain the conical starting solution. A coarse mesh is used to initiate the solution with zero potential (i.e., freestream conditions) used as starting potential values. This mesh is then halved to obtain a finer mesh. The potential solution from the coarser mesh is interpolated onto the finer mesh as a starting solution for the potential. Mesh refinement can speed up the computation by as much as a factor of four or five. Figure 3 shows a sample computation with and without mesh refinement. At little computational cost, a coarse mesh will very quickly establish the salient features of the flow field, such as the bow shock and embedded supersonic crossflow region. This flow field then becomes the starting guess for the next mesh. This is the primary reason for the enhanced computational efficiency. A total of two mesh refinements (i.e., or three grids) can be used in NCOREL for the conical solution. The nonconical solutions are then obtained by marching on the finest grid using the potential solution at the previous station as a starting solution for the new station.

#### 4.5 BOW SHOCK METHODS

##### 4.5.1 Bow Shock Capture (BSC)

The capture of the bow shock and its position within the computational grid is largely determined by the prescription of the crossflow plane outer boundary. If the shape of the outer boundary is much different from that of the captured bow shock, the captured shock position in the crossflow plane may look somewhat like that depicted in Fig. 4a. The outer crossflow sonic line

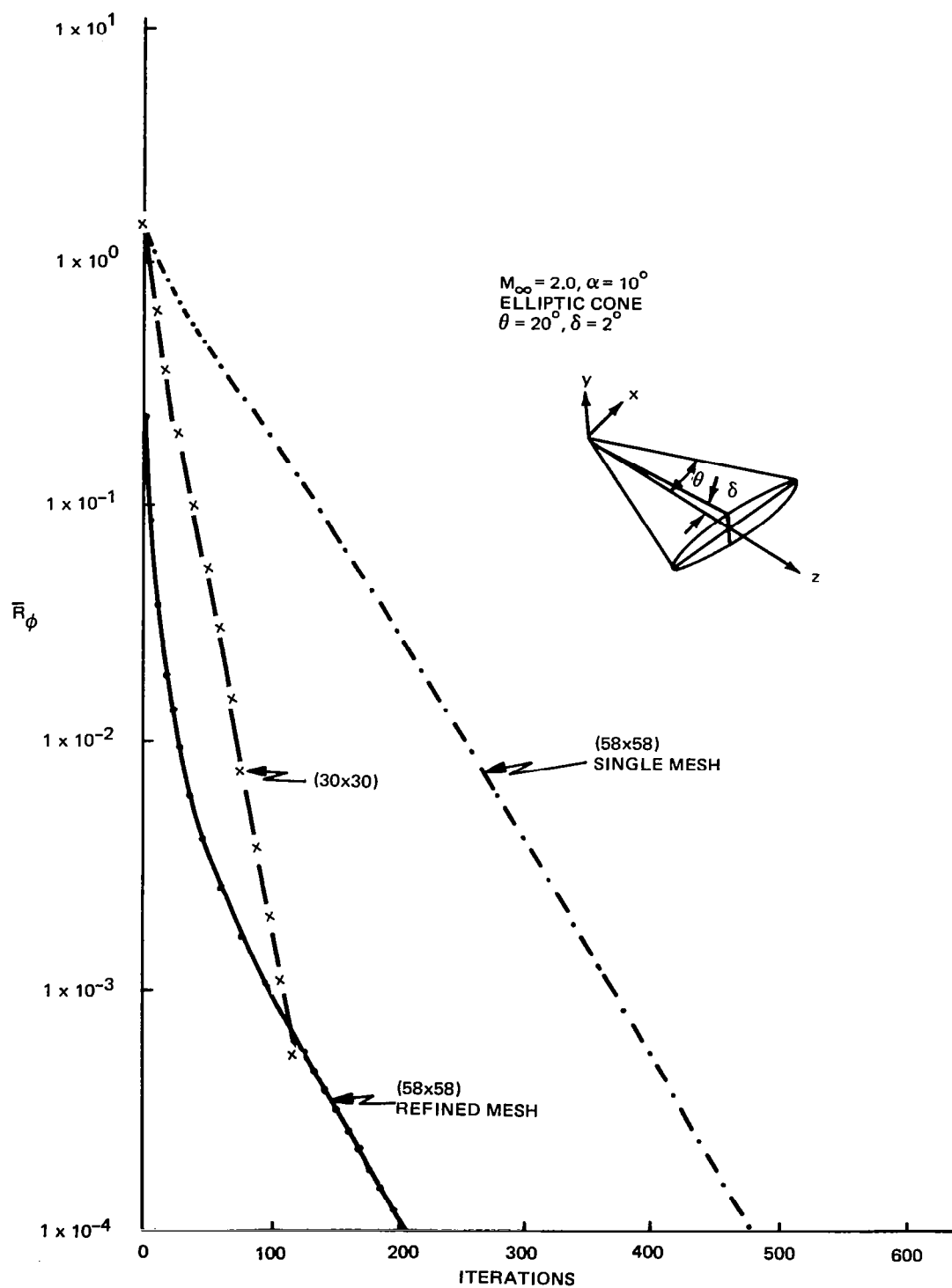


Figure 3 Effect of Mesh Refinement

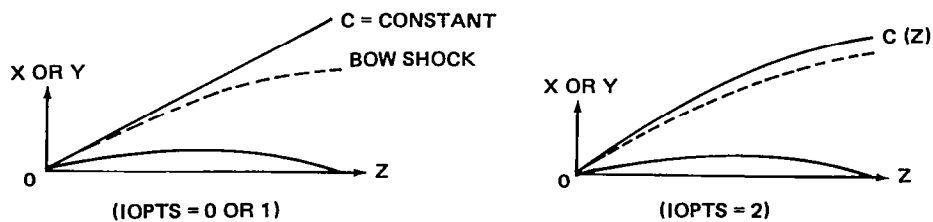
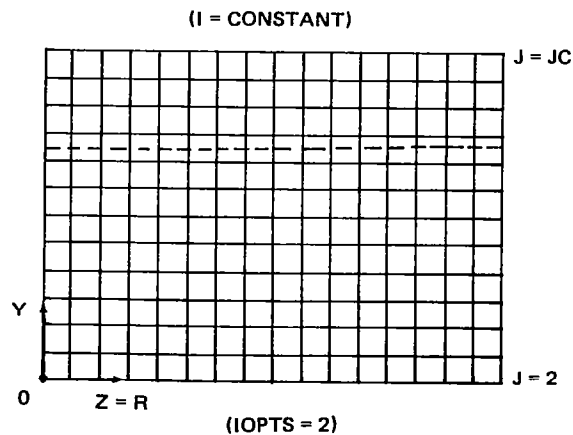
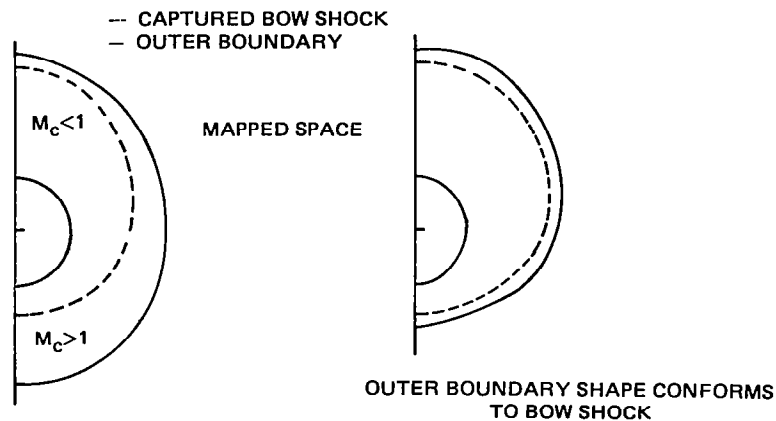
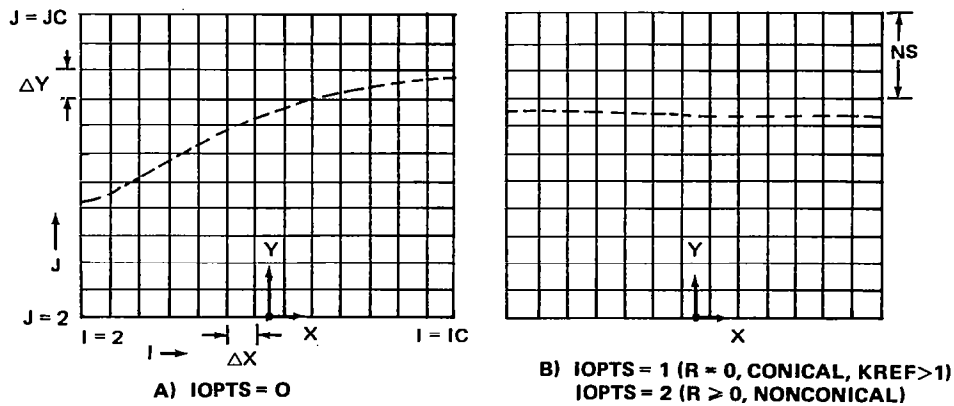
(i.e., captured bow shock) can cut through several J rings or J lines in the computational grid. This is computationally inefficient in that many grid points of freestream conditions outside the bow shock will be carried along in the computation. To compensate for this and to better control the position of the bow shock, a method is used to align the bow shock with the computational grid. This procedure is beneficial not only in that the number of freestream mesh points beyond the bow shock can be controlled, but also in that it aligns the grid with the bow shock, which should yield a better captured shock solution and increased accuracy.

Three bow shock capturing options have been included in NCOREL designated by the parameter IOPTS.

Figure 4 illustrates each of these options. The first option (IOPTS = 0) is the default option. In this option the outer crossflow boundary is held constant and equal to a factor (EP - 1) times the rotated Mach cone for both conical and nonconical stations. Hence, the bow shock will typically cut through the cross flow computational mesh, as illustrated in Fig. 4a. For nonconical stations, the location of the bow shock will generally move within this mesh. Axially expanding bodies will cause the captured bow shock to move toward the surface ( $J = 2$ ) and compression surfaces will cause the shock to move toward the outer boundary ( $J = JC$ ). Hence, holding the outer boundary fixed can cause problems in that the movement of the bow shock has to be anticipated in positioning the outer boundary for the conical solution. If this is not done, the bow shock can hit the outer boundary causing erroneous results. In theory, the outer boundary could be tailored a priori to the particular body shape as a prevention technique. Instead, two other options were built into NCOREL.

The first option (IOPTS = 1) is illustrated in Fig. 4b. This option will be initiated only at the conical station with a mesh refinement ( $KREF > 1$ ). The first mesh will capture the bow shock as illustrated in Fig. 4a. The position and shape of the bow shock will be interpolated from the coarse grid. A new outer boundary will be automatically determined with the same crossflow shape as the interpolated bow shock. This shape will then be imposed NS grid lines or  $NS \times \Delta Y$  beyond the interpolated bow shock sonic line to allow for proper capture. Hence, the parameter NS will approximately control the number of freestream mesh lines beyond the bow shock position.





**C) AXIAL MESHES**

**Figure 4 Bow Shock Capture Methods (BSC)**

The coarse mesh solution will then be interpolated onto this new finer mesh as a starting solution. The resulting solution on the finer mesh will look similar to that shown in Fig. 4b. The captured bow shock will now be aligned approximately with a Y grid line in the computational space. The number of Y grid lines beyond the shock is roughly determined by the parameter NS which shall be set  $> 4$ .

The option IOPTS = 2 is similar to IOPTS = 1 but will occur at nonconical stations. This option, shown in Fig. 4c, not only aligns the captured bow shock with the cross flow grid, but also controls the vertical position of the bow shock by deforming the outer boundary as the marching solutions are obtained. Since mesh refinement is not used at nonconical stations, the previous station's interpolated bow shock shape and position will be imposed at the current station. This will prevent the captured bow shock from moving significantly through the mesh.

For IOPTS = 0 and IOPTS = 1, the outer boundary will be held fixed in the nonconical computation. In IOPTS = 2, the outer boundary will move with the bow shock as the marching solutions are obtained. This causes R derivatives to be nonzero for the outer boundary. IOPTS = 0 is the fastest scheme and IOPTS = 2 requires the most computational time. The extra computational time is caused by the imposition of the interpolated solution onto a new mesh causing a somewhat slower convergence rate.

A detailed study of the effect of each of these options on the solution has not been carried out.

#### 4.5.2 Bow Shock Fit (BSF)

The bow shock fitting eliminates the need for capturing the bow shock within a prescribed outer boundary. Instead the outer boundary at  $J = J_C$  becomes the bow shock. Its shape is governed by an isentropic shock jump condition,

$$\left( \frac{\bar{\rho}}{\rho_{\infty}} Q_{\text{NORM}} = Q_{\infty} \right) \quad (10)$$

where  $\bar{\rho}$  is the density and insures continuity of mass flow across its boundary. In potential flow, the potential is continuous across a shock wave. Its normal derivative or normal velocity is discontinuous causing a pressure discontinuity or jump. The tangential derivative or velocity is also continuous across the shock wave. The reduced potential everywhere outside the bow shock in the cross flow plane is zero due to the freestream outer condition. Hence, its value at the bow shock boundary must also be zero. The value of the potential at the bow shock is then known, and its normal derivative is a function of the internal flow solution and the shape and location of the bow shock boundary. The normal derivative of the potential in Eq (10) is computed at the bow shock by a second order, one sided difference formula into the internal flow field.

In the BSF method, the conical starting solution is by far the most difficult to determine because the bow shock boundary is not known a priori. An initial guess for its shape must be prescribed and iterated upon. At a nonconical station, the bow shock boundary is known and held fixed, and the slope of the bow shock in the marching direction is iterated upon. Iterating and perturbing the bow shock as a boundary for conical flow is also time consuming in a computational sense in that the entire cross flow mesh changes with the iteration process. As a result, the mapping metrics and freestream velocities must be recomputed after each iteration. In addition, the new bow shock shape must be underrelaxed so as not to disturb the convergence of the internal flow field. In a successful calculation, the internal flow residuals or errors associated with the potential flow Eq (8) and those associated with the shock jump condition Eq (10) will both diminish as the iteration procedure progresses.

In conical flow, the isentropic shock jump condition Eq (10), can be written in a recursive tridiagonal form,

$$-\frac{\bar{\rho}U}{2\Delta\theta} C_{i+1}^+ + \bar{\rho} V C_i^+ + \frac{\bar{\rho}UC_{i-1}^+}{2\Delta\theta} = CV_\infty - U_\infty C_\theta \quad (11)$$

where the RHS of Eq (11) is determined using old values of the shock boundary  $C$ , and the LHS is then solved by Gaussian elimination for updated values of the shock boundary  $C^+$ . Equation (11) was found to be the only stable method

to determine the bow shock boundary because it couples all the bow shock points. Periodic end conditions are used in the Gaussian elimination. The updated values of the bow shock position or shape  $C^+$  are then under-relaxed.

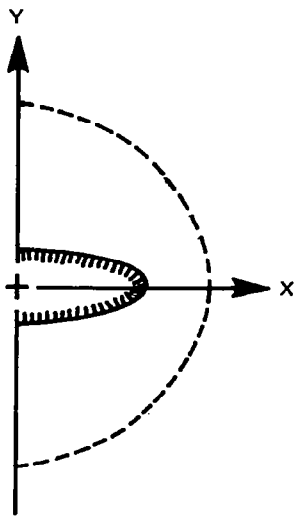
For nonconical flow, Eq (11) becomes

$$-pWRH C_R^+ = \frac{C_\theta}{C} (\rho U - U_\infty) - \rho V + V_\infty + RH(h_1 - \frac{h_2 C_\theta}{C})(W_\infty - pW) - W_\infty RHC_R \quad (12)$$

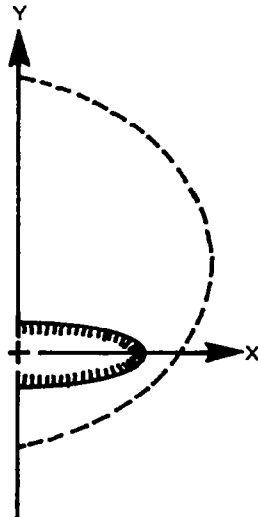
In Eq (12), the slope of the bow shock location  $C_R$  at each point is determined as the internal flow is iterated upon. Because the crossflow mesh is held fixed, the nonconical calculation is not as sensitive, and the updated values of the shock slope in the marching direction  $C_R^+$  can be over-relaxed. When both the internal flow converges and Eq (12) is satisfied, the new shock slopes are then used to determine a new shock boundary and mesh at the next nonconical station using the first order accurate expression:

$$C_i(R + \Delta R) = C_i(R) + C_{R_i} \Delta R \quad (13)$$

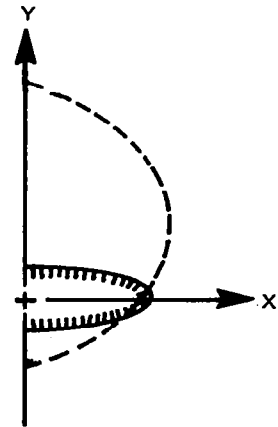
For the conical starting flow, an initial guess for the outer boundary must be prescribed that meets certain requirements. For subsonic leading edge crossflow shapes, the rotated Mach cone is usually a reasonable initial shape. Figure 5 illustrates some of the possible relationships between the rotated Mach cone and body shape in the cross flow plane. For other flows, the prescription of an initial guess is not as simple. The rotated Mach cone can not be used for near sonic or supersonic leading edge shapes since the Mach cone will touch or be within the boundary of the body surface (i.e., usually around the leading edge). For body shapes, this condition can also be encountered at high angles of attack on the leeward surface. For other body shapes and freestream conditions where  $M_\infty \sin \phi_B$  is everywhere greater than one for the body, the Mach cone may lie entirely within the body. A crossflow mesh and a solution can only be generated when the initial guess is everywhere outside the body shape. Hence, the rotated Mach cone must be modified in such a way that an initial guess is prescribed that is everywhere within the boundary of the true bow shock and outside or coincident with the Mach wave. A solution may not be computed if any part of the initial guess lies within the rotated Mach cone or outside the true shock location. If a large part or all of the initial boundary lies outside the true shock location, the method



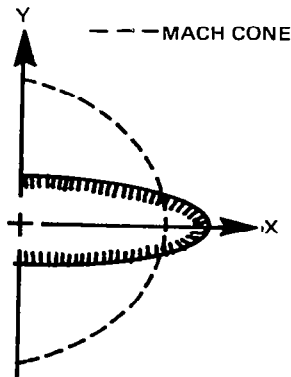
**TYPE IA**  
SUBSONIC BODY ( $\alpha = 0$ )



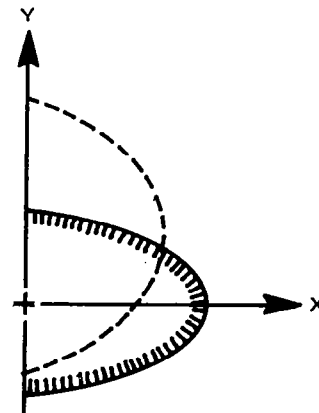
**TYPE IB**  
SUBSONIC BODY ( $\alpha > 0$ )



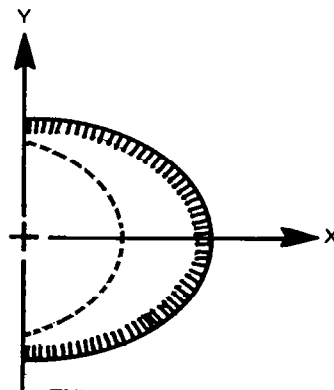
**TYPE IC**  
SUBSONIC BODY (HIGH  $\alpha$ )  
OR  
NEAR SONIC LEADING EDGE ( $\alpha > 0$ )



**TYPE IIA**  
SUPERSONIC LEADING EDGE ( $\alpha = 0$ )



**TYPE IIB**  
SUPERSONIC LEADING EDGE  
(HIGH  $\alpha$ )



**TYPE III**  
SUPERSONIC BODY

2246-009W

**Figure 5 Mach cone Relationship to Type of Surface for Bow Shock Fit Method (BSF)**

will attempt to capture the bow shock and is designed to fail to prevent this from happening. Since freestream conditions or zero potential is used as initial values for the potential, the initial information generated at the prescribed bow shock boundary may be erroneous. This is another reason that under-relaxation must be used so as not to update the bow shock boundary too quickly causing an overshoot of the true bow shock position until the internal flow has somewhat converged. In a conical computation, supersonic crossflow velocities may occur within the boundary at a certain number of initial iterations. These supersonic crossflow points will vanish as the internal flow converges if a good shock guess has been prescribed, meaning that a compression is caused by the body which propagates toward the initial bow shock boundary and merges with it. A better way to initiate the conical BSF calculation might be to hold the boundary fixed ( $\omega_s = 0.0$ ) until the internal flow converges. This would cause the internal flow to converge, the compression to reach the boundary and supersonic crossflow points to disappear, and then allow for a higher bow shock relaxation value to be used because better information is obtained at the boundary. Since this is in general difficult to automate, NCOREL updates the boundary simultaneously with the internal flow iterations, and slightly smaller under-relaxation values must be used. The initial imposed shape for the conical bow shock on the crude grid can be checked by running NCOREL with zero for the bow shock relaxation parameter and then inspecting the crossflow velocities at the bow shock guess after a certain number of iterations (e.g., 25-40). If the crossflow velocities are sonic or subsonic, then a good guess has been achieved for the bow shock.

Low relaxation values ( $\omega_s < .10$ ) are used for difficult conical BSF solutions. Difficult BSF solutions are those that fall into the Type II or Type III categories illustrated in Fig. 5. A crude grid (16 x 16) is used initially to determine the bow shock and solution. If mesh refinement is used, it is not essential for the crude grid bow shock jump conditions to converge totally, especially since a very low bow shock relaxation parameter may have to be used initially.

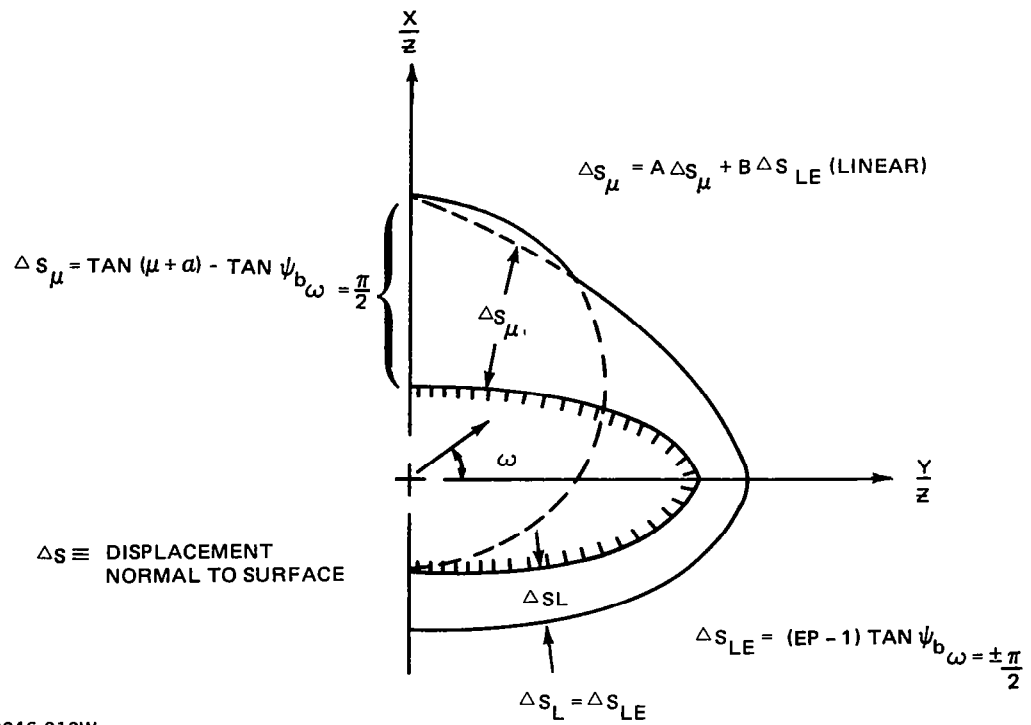
Hence, given a reasonable initial guess, the bow shock fit method will iterate on the internal flow field and the bow shock shape simultaneously. The new shape of the bow shock at each iteration required to fulfill the shock

jump condition at each shock point will be under-relaxed. The solution is considered converged when both internal flow field residuals vanish or become small and the shock jump conditions are met at the shock boundary.

Figure 6 illustrates the basic procedure for generating an initial guess for a bow shock boundary. The bow shock guess is generated by a combination of the rotated Mach cone and a normal displacement of the body surface boundary. The outermost boundary of these two shapes is then used as the initial shape. The displaced body boundary is controlled by an input parameter  $EP > 1$ . A factor  $(EP - 1.0)$  times the centerline half angle of the body is used as the basic displacement  $\Delta S_{LE}$  at the leading edge. So as not to yield a too discontinuous shape, the centerline displacement  $\Delta S_{\mu}$  is taken to be the greater of the leading edge displacement or the displacement due to the Mach cone. The displacement at the leading edge and at the upper and lower centerlines are then faired linearly to determine the displaced body shape. If the Mach cone lies outside the displaced body, then that portion of the displaced body shape is replaced by the Mach cone. Other more clever bow shock guess generators may be found, but this procedure was found to be easiest to manipulate and the safest.

Figure 7 illustrates several examples of actual conical flow BSF computations on a  $(16 \times 16)$  grid for each of the type flow situations depicted in Fig. 5. Figure 7 shows the rotated Mach cone, initial shock guess and converged shock boundary.

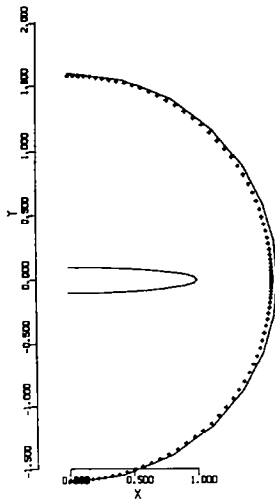
Mesh refinement is almost always used in conjunction with the conical BSF method since the first mesh solution is the most difficult to achieve because of the need for an initial shock guess. Refined meshes use the previous mesh solution for the bow shock boundary shape.



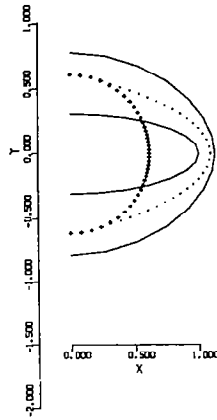
2246-010W

Figure 6 Bow Shock Guess Generation

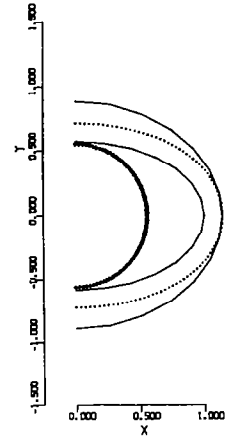




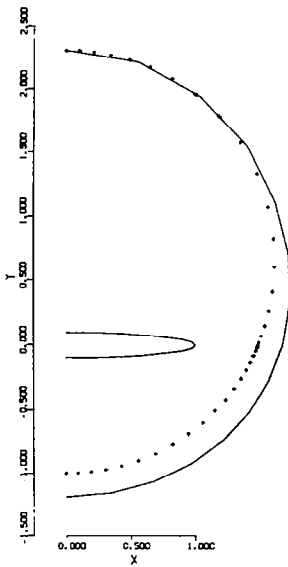
a)  $M_{\infty} = 2.0, \alpha = 0^{\circ}$   
 $\Theta_c = 20^{\circ}, \delta_c = 2^{\circ}$   
 $\omega_s = .50, EP = 1.0$



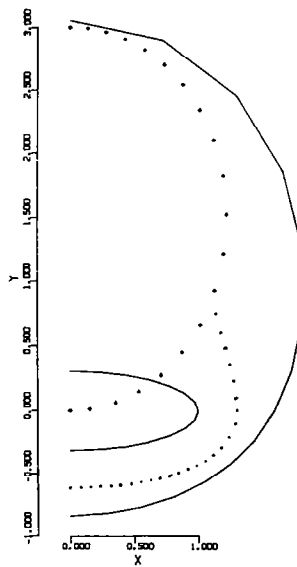
b)  $M_{\infty} = 3.0, \alpha = 0^{\circ}$   
 $\Theta_c = 30^{\circ}, \delta_c = 10^{\circ}$   
 $\omega_s = .20, EP = 1.3$



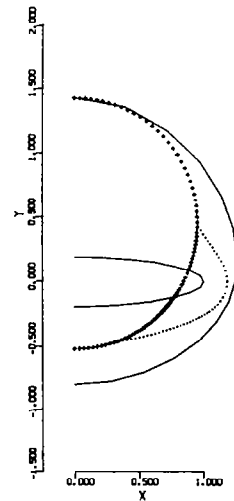
c)  $M_{\infty} = 4.0, \alpha = 0^{\circ}$   
 $\Theta_c = 25^{\circ}, \delta_c = 15^{\circ}$   
 $\omega_s = .05, EP = 1.25$



d)  $M_{\infty} = 2.0, \alpha = 10^{\circ}$   
 $\Theta_c = 20^{\circ}, \delta_c = 2^{\circ}$   
 $\omega_s = .75, EP = 1.0$



e)  $M_{\infty} = 2.0, \alpha = 30^{\circ}$   
 $\Theta_c = 30^{\circ}, \delta_c = 10^{\circ}$   
 $\omega_s = .75, EP = 2.0$



f)  $M_{\infty} = 2.50, \alpha = 10^{\circ}$   
 $\Theta_c = 25^{\circ}, \delta_c = 5^{\circ}$   
 $\omega_s = .05, EP = 2.0$

————— COMPUTED BOW SHOCK  
 ..... INITIAL SHOCK GUESS



## 5 GEOMETRIC AND MAPPING REQUIREMENTS

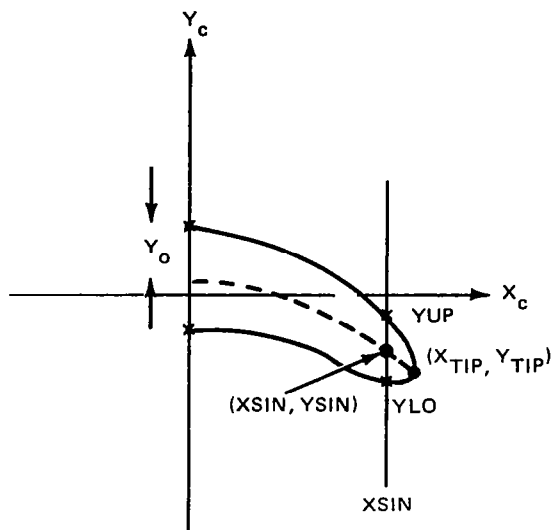
The full potential equation is solved in a spherical coordinate system. Hence, geometric cross sectional coordinates must be generated on successive spheres  $r = \text{constant}$ . A conical apex or nose cap is always assumed by defining the geometry between  $r = 0$  and  $r = \Delta r$  (i.e.,  $\Delta r$  is the marching step) as a constant and equal to the cross sectional geometry at  $r = \Delta r$ . The geometry is defined one step ahead of the calculation. This is necessary to define the conical apex geometry and also to generate numerical second order accurate geometric derivatives (i.e., slopes, etc.). This technique inherently assumes that the geometry is smooth. Any discontinuities in the geometry will be smoothed to the order of the marching step size. At each spherical station, NG cross sectional points will be determined from the geometry routines. At a given  $r$  station, the leading edge coordinates are first determined in order to scale the points. Typically the NG geometry points will be clustered in the vicinity of the leading edge for better accuracy by a cosine or sine variation. This set of geometric points usually exceeds the number of points in the actual cross sectional final computational mesh for accuracy. The geometry points will then be transformed to the mapped space given a singularity location for the particular cross section. Periodic cubic spline coefficients are then generated for the NG mapped space coordinates. The actual IC mesh points, at equally spaced  $\theta$ , are then found by interpolation from the NG input geometry points in the mapped space. A transformation of these interpolated mapped body points at equal  $\theta$  back to the physical space will then generate a mesh where points will be clustered in the vicinity of the wing leading edge. All geometric or surface derivatives are generated numerically in the mapped space.

### 5.1 MAPPING REQUIREMENTS

The mapping transformation will, in general, be a function of  $r$  if the geometric cross sections are nonconical and change in character as a function of  $r$ . The functional dependence on  $r$  comes about from the  $r$  variation of the singularity location. This variation of the mapping transformation with  $r$  results in mesh derivatives defined as  $h_1 = \rho_r$  and  $h_2 = \rho \theta_r$ . If the geometry is conical, or if the singularity location is fixed with  $r$  for nonconical flows, these mesh derivatives will vanish or  $h_1 = h_2 = 0$ .

In general, the best choice for the singularity location is the center of radius of curvature of the wing leading edge. In practice, using a fine mesh, the solution is somewhat sensitive to the precise placement of the singularity location. The exception to this would be the special case of sharp (e.g., small leading edge radius of curvature wings.) For this special case, the singularity must be placed at the center of radius of curvature. Hence, the singularity location is determined by the following approximate procedure. The leading edge coordinates are first determined ( $x_{tip}$ ,  $y_{tip}$ ,  $z_{tip}$ ). The centerline half thickness at  $x = 0$  is determined. The lateral or  $x$  location of the singularity is then determined as the focus of an ellipse or  $x_{sin}^2 = y_{tip}^2 - y_{x=0}^2$ . The  $y$  location ( $y_{sin}$ ) of the singularity is further determined to be on the mean line at the location  $x_{sin}$ . Given the singularity location ( $x_{sin}$ ,  $y_{sin}$ ), the mapping transformation is then defined and the set of NG input geometric points can be transformed to the mapped space. At each  $r$ -station, the cross sectional geometry and singularity location are also determined at  $r + \Delta r$ . This is necessary because the  $r$  derivative of the singularity location is required to determine the mesh derivatives  $h_1$  and  $h_2$ . Numerical second order accurate singularity derivatives are computed at  $r + \Delta r$ , requiring the location of the singularity at the upstream station ( $r + 2\Delta r$ ).

The premise for geometry generation in formulating NCOREL was that users, in general, will not have spherical geometry at their disposal. Hence, the computer code has been tailored to the availability of transverse ( $z = \text{constant}$ ) cross sectional geometry. The code then internally iterates for the spherical geometry given transverse geometry data. The procedure is illustrated in Fig. 8a. An initial iteration takes place to determine the leading edge coordinates at a given  $r$ -station. Since the lateral singularity location is determined approximately as the focus of an equivalent ellipse, an additional approximation is made by determining the centerline thickness at  $z = z_{tip}$  and not on the spherical surface. The singularity location is then determined solely by the transverse data at  $z = z_{tip}$ . The premise for this approximation is that the cross section at  $r = \text{constant}$  will not differ dramatically from the cross sectional characteristic shape at  $z = z_{tip}$ . This may not always be the case and a more exact placement of the singularity may be necessary. This approximation, though, greatly simplifies the generation of the singularity coordinates.



**IFLAG = 0**

GIVEN  $Z_c$ , COMPUTE:

1)  $X_{TIP}, Y_{TIP}$

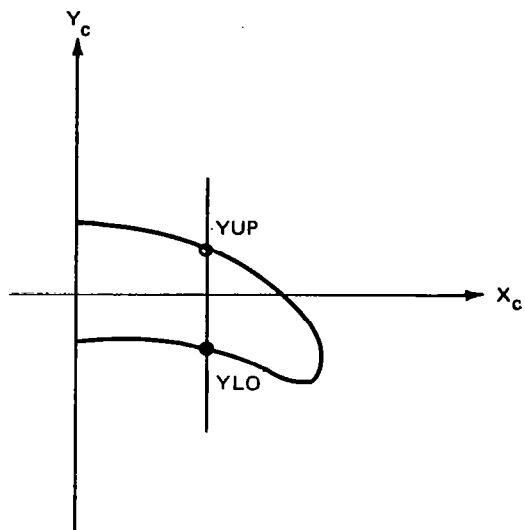
2)  $Y_0 = \frac{1}{2} (Y^+ + Y^-)_{X=0}$

3)  $X_{SIN} = \sqrt{X_{TIP}^2 - Y_0^2}$   
OR

$X_{SIN} \equiv$  CENTER OF L.E. RADIUS  
OF CURVATURE

4)  $Y_{SIN} = \frac{1}{2} (Y^+ + Y^-)_{X=X_{SIN}}$

2246-011W



**IFLAG = 1, 2**

GIVEN  $Z_c, X_c$ , COMPUTE:

1)  $IFLAG = 1, Y = YUP$

2)  $IFLAG = 2, Y = YLO$

**Figure 8 Singularity Placement and CONUSE Logic Used in NCOREL**

## 5.2 GEOMETRY OPTIONS

Several geometry options have been built into NCOREL based on the availability of transverse geometric cross section data being as follows.

### IOPTG = 1: (Axisymmetric bodies of revolution)

A routine is supplied that will generate cross sectional coordinates given the radius of the body as a function of  $z$ .

### IOPTG = 2: (Analytical Geometry Package)

A geometry definition based on simple conical parameters was developed and was found to be very useful in defining both conical and three dimensional wings, bodies, and wing-body configurations. The cross section was simply defined as the superposition of a spanwise thickness and camber distribution. The basic wing cross section is restricted to spanwise elliptical thickness and circular arc camber.

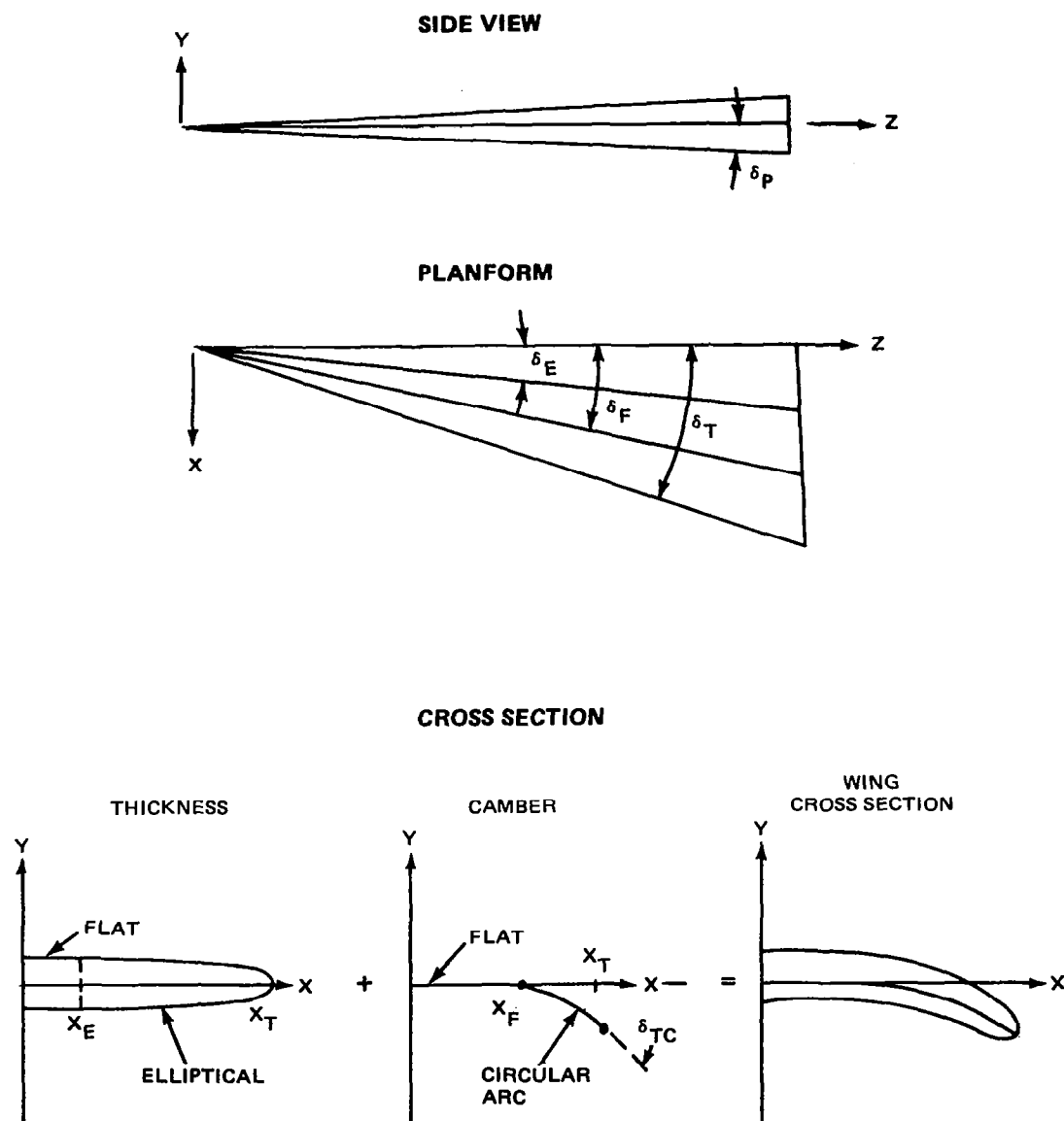
In this analytical representation of the wing geometry, the geometric parameters are specified as parametric angles. Thus, a wing cross section can be entirely specified by five angles:  $\delta_F$ ,  $\delta_E$ ,  $\delta_T$ ,  $\delta_{TC}$ ,  $\delta_P$ . The symbols  $\delta_F$ ,  $\delta_E$  and  $\delta_T$  represent planform angles defining the body lines of the wing and  $\delta_P$  is an angle controlling the centerline thickness variation, and  $\delta_{TC}$  the leading edge camber angle in the cross sectional plane (see Fig. 9). Cubic equations are used to axially curve fit the angles in the general form:

$$\delta(z) = a(z - z_i)^3 + b(z - z_i)^2 + c(z - z_i) + d$$

The spatial location of the body lines can then be simply defined as:

$$x = z \tan (\delta(z))$$

The thickness of the wing was assumed elliptical but was allowed to have an inboard flat section. The camber line, defined separately, was also allowed to have a flat inboard section with a circular arc camber line to the leading edge. To define the maximum camber and twist of the cross section, a leading edge camber angle is specified ( $\delta_{TC}$ ). The thickness and camber flats are defined separately and, thus, do not have to coincide. The wing cross sectional geometry was then simply defined by adding and subtracting the elliptical thickness to the camber line.



2246-016W

Figure 9 Geometrical Parameters Used in Defining Analytical Wings (IOPTG = 2)

The present capability of this geometry package allows for a transition from a cone to a conically cambered wing section. A further deformation from a conical wing section to a conical wing-body cross section can also be generated. Figure 10 illustrates the basic capability of the geometry package. This package can be used to generate conical wing or body or wing-body cross sections for conical solutions. It can also be tailored to generate three dimensional deforming geometries of the above types by a judicious choice of input parameters. Variable sweep wings can also be generated with this definition. Figure 11 shows some sample geometries that can be generated. Figure 11a shows a typical body line deformation to a conical delta wing. Figure 11b shows a cross sectional deformation from a circular cone to an elliptical cross section. Figure 11c shows the deformation from an elliptical cross section to a cambered cross section. The last section of the geometry can deform into a wing-body cross section defined as shown in Fig. 12a. The last conical section of the geometry requires one additional angle for the body definition. If the body angle is made equal to the wing thickness angle the cross section will degenerate into a wing cross section. Figure 12b shows an example of the geometry that can be generated.

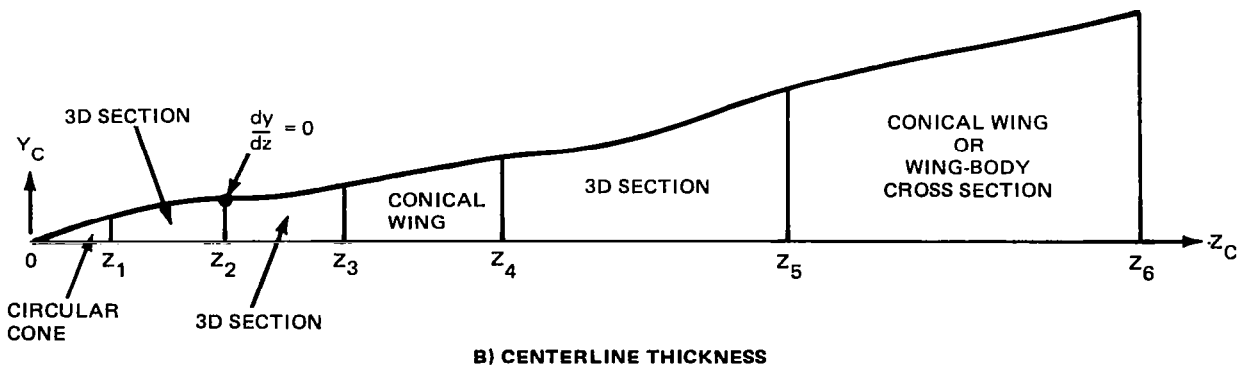
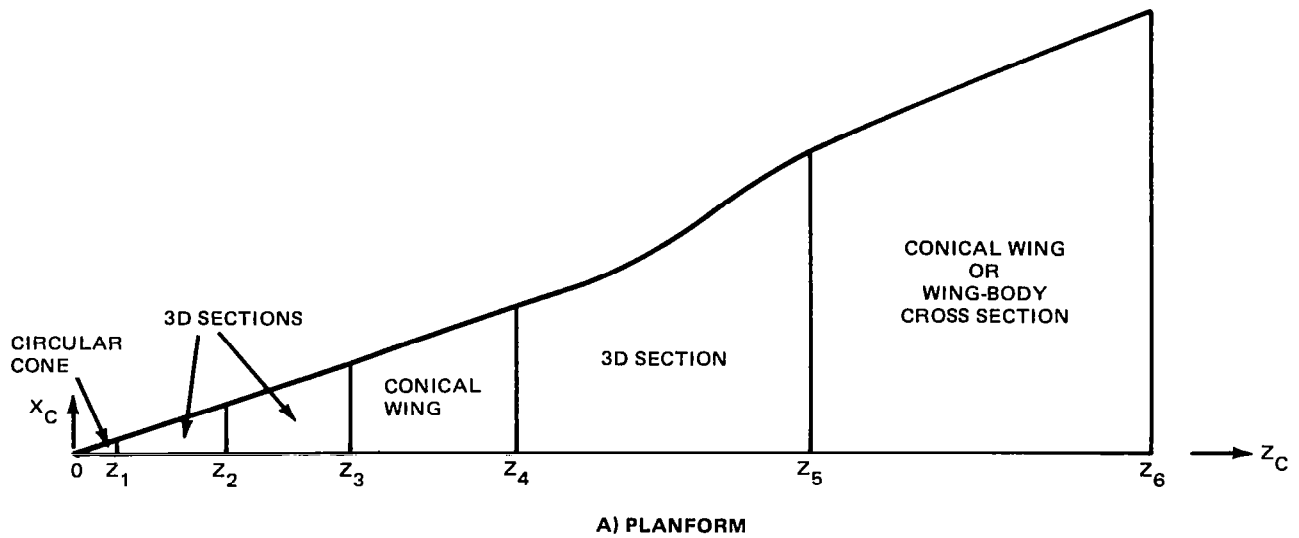
#### IOPTG = 3: (Analytical User Supplied Geometry)

This geometry package is supplied by the user in terms of a subroutine. The basic requirements of the subroutine are illustrated in Fig. 8 and solely requires that the transverse geometry be defined (i.e  $z = \text{constant}$ ). Figure 8a illustrates the use of the subroutine in finding the leading edge coordinates and singularity location for a call to the subroutine with IFLAG = 0. Figure 8b illustrates the general usage of the subroutine for defining the cross sectional points. The code will then use this information to generate the spherical cross sectional geometry. Note that the user is not restricted as to the placement of the singularity as the focus of an ellipse.

#### IOPTG = 4: (Bi-cubic Surface Patch Geometry)

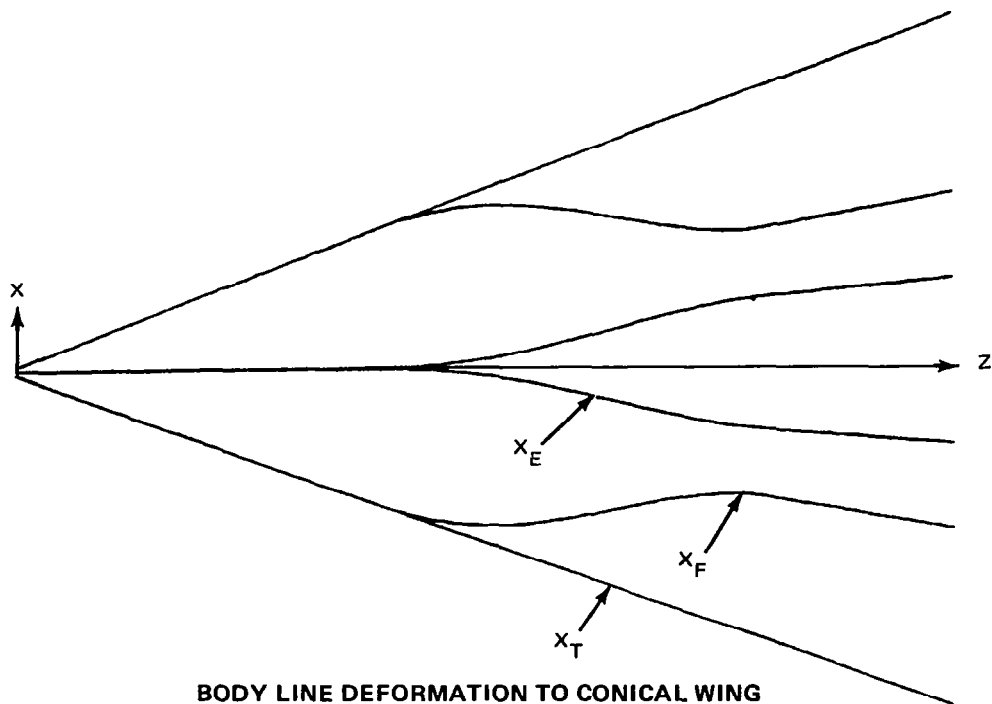
This is a somewhat more flexible geometry package although a much more computationally time consuming package. This geometry package uses the Harris Wave Drag Input where a wing is defined by airfoil sections whose thickness and camber are specified as a set of input points. A body or fuselage is defined as a set of transverse cross sections where the coordinates of each cross section are specified as input. The geometry package is an adaptation

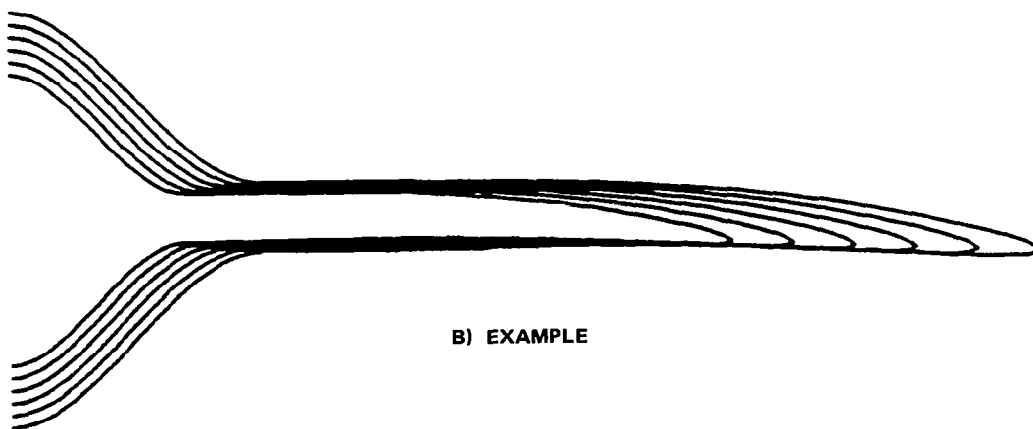
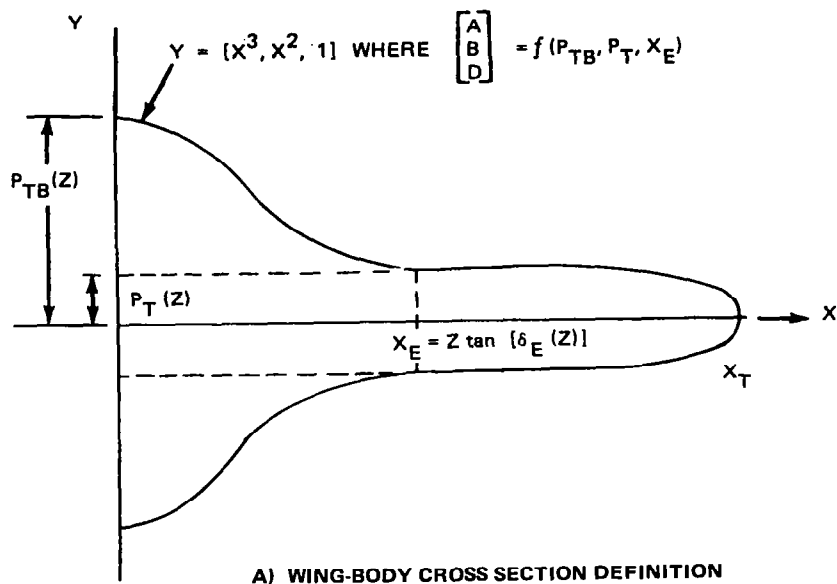




2246-013W

Figure 10 Analytical Geometry Package Definitions (IOPTG = 2)





2246-017W

Figure 12 Conical Wing-Body Geometry Generation

of the Craidon bi-cubic surface patch geometry program of Ref. 10. It was chosen because the Harris Wave Drag Input format is widely used by aerodynamicists and by NASA in defining geometries and also is compatible with many linear panel codes. The bi-cubic surface patch definition was chosen because a continuously defined and smooth geometry must be available to NCOREL. The geometry package as adapted to NCOREL can generate arbitrary wings, bodies, or wing-body geometries based on point wise input. It treats wing and body components individually and superimposes these cross sections to determine a wing-body cross section. This geometry package also works well with the constraint that the individual wing or body geometries are smooth. A detailed description of the basic geometry package and mathematics of the bi-cubic surface patches and spline fitting can be found in Ref. 10. Essentially, a set of input points are converted to quadrilaterals. Each quadrilateral is then defined to be a bi-cubic surface patch defined by a  $4 \times 3$  boundary matrix. Since a large number of patches (e.g., 2000) can be defined for a vehicle, all of the patch matrices can not be stored. The entire set of patch matrices are written on disk and read when needed. In the adaptation of the patch geometry to NCOREL, it was found necessary to store the patches required to define the geometry for a particular spherical cut. The I/O time required to read and sort through the entire set of patch matrices for one cross sectional point was found to be prohibitive. Hence, for each spherical cut the patch matrices are read and sorted only once and the required patches stored. This increases the core requirements of NCOREL but reduces the I/O related CPU time enormously. Since the patches are defined parametrically by two cubics in U and W coordinates, a Newton iteration in two variables has to be used in order to determine an arbitrary surface coordinate. This is also costly in computational time and causes the patch geometry to be the slowest geometry option in NCOREL but the most user oriented.

It should be noted that the Craidon patch geometry routines use the standard aircraft coordinate system denoted by  $(X_A, Y_A, Z_A)$  where  $X_A$  is axial,  $Y_A$  is spanwise and  $Z_A$  is vertical, whereas NCOREL uses a nonstandard coordinate system  $(X_C, Y_C, Z_C)$  where  $Z_C$  is axial,  $X_C$  is spanwise and  $Y_C$  is vertical. These coordinate systems are referenced to and used interchangeably in NCOREL.

In general, any geometry package that can conform to the simple format illustrated in Fig. 8 can be coupled to NCOREL.



## 6 AERODYNAMIC FORCES AND MOMENTS

To tailor NCOREL to the specific needs of aerodynamicists, a detailed knowledge of forces and moments generated by a configuration is essential. Since NCOREL computes spherical solutions, an adaptation is required to generate forces and moments that are useful to the engineer. To do this, an interpolation scheme is used that first recomputes all of the  $\Delta R$  spherical surface data to  $\Delta z$  spanwise ( $z = \text{constant}$ ) data. The interpolated data is then used to compute axial incremental forces and moments on each spanwise segment  $\Delta z$ . These incremental spanwise forces and moments are then integrated to yield a running account of the axial force and moment generation. To accomodate wings with variable or constant sweep trailing edges, a special interpolation scheme was developed to determine the forces and moments aft of the centerline trailing edge station. Figure 13 illustrates the basic technique. The  $z$ -station interpolation proceeds with the same step size as the spherical surface data until the trailing edge station. At the centerline trailing edge,  $z = ZTEC$ , spanwise data is interpolated.

For all of these stations, each radial grid line is used for interpolation to  $z = \text{constant}$  stations. Hence, IC-1 mesh lines are interpolated to yield IC-1 interpolated points for a  $z = \text{constant}$  station. Aft of the centerline trailing edge station,  $z = ZTEC$ , the  $z$  location of the interpolated stations is governed by the intersection of a radial grid line with the trailing edge. The actual interpolated  $z$  values and number of trailing edge stations is governed by the number of grid lines used in the computation. Hence, for each of the interpolated  $z$  stations aft of the trailing edge the number of interpolated values will diminish by two. Finally, at  $z = ZTIP$ , only one value will be interpolated and the interpolation scheme will terminate. If the computation to  $R = ZTIP$  has not been completed the interpolation scheme will terminate when the interpolation from  $x = x_{TE}$  to  $x = x_{LE}$  can not be completed. The interpolated  $z$ -station data for the surface coordinates and pressure coefficients is then written onto TAPE2.

The trailing edge computation is contingent upon a user supplied subroutine XTES which yields a ZTE value given XTE. If a delta wing or body is being computed, the last interpolated station occurs at a  $z = \text{constant}$  station specified in the input.

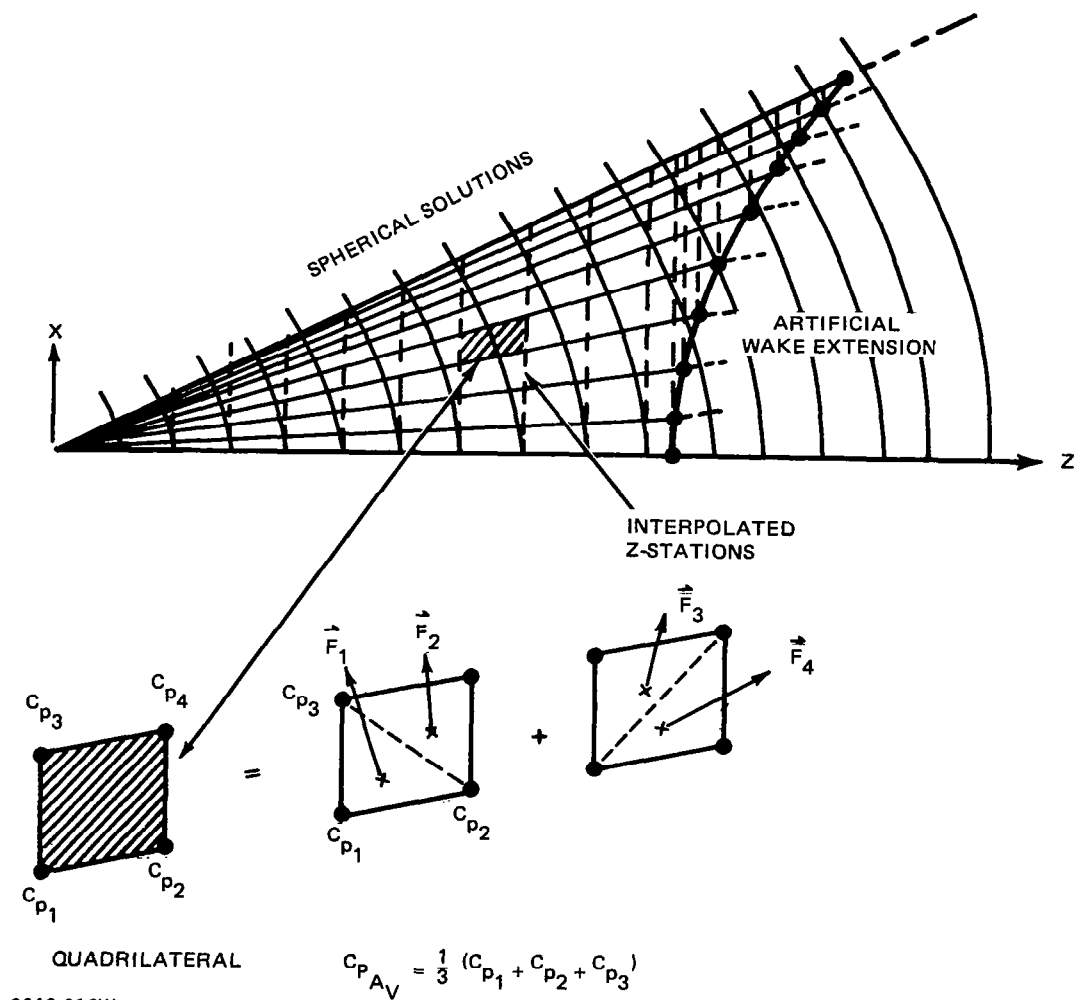


**Figure 13 General Interpolation Scheme for Arbitrary Planforms  
Used for Aerodynamic Computation**

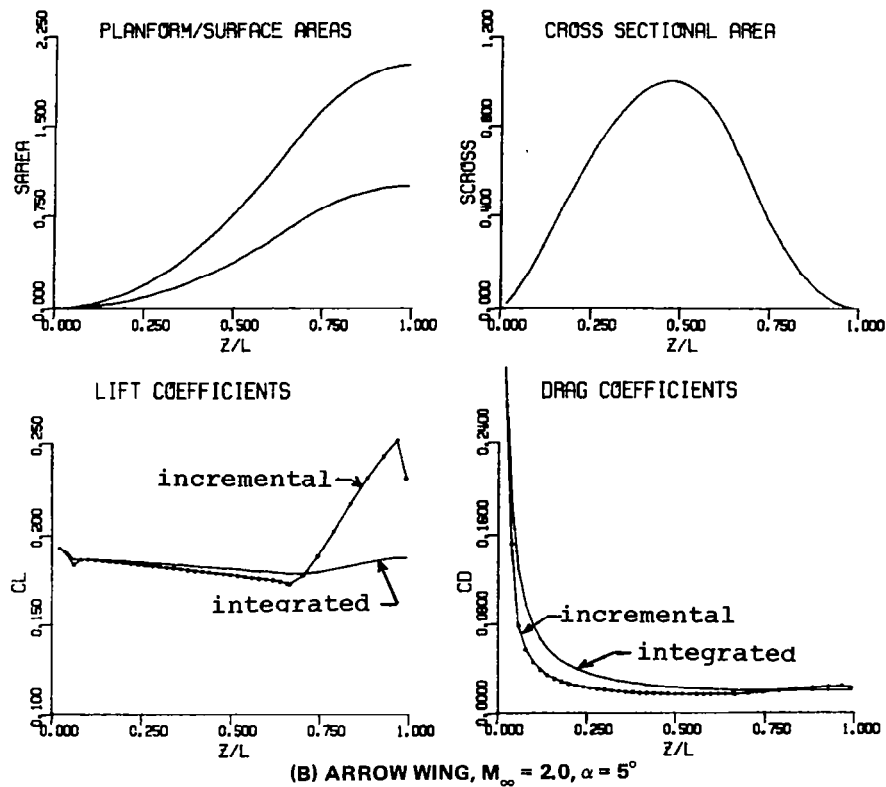
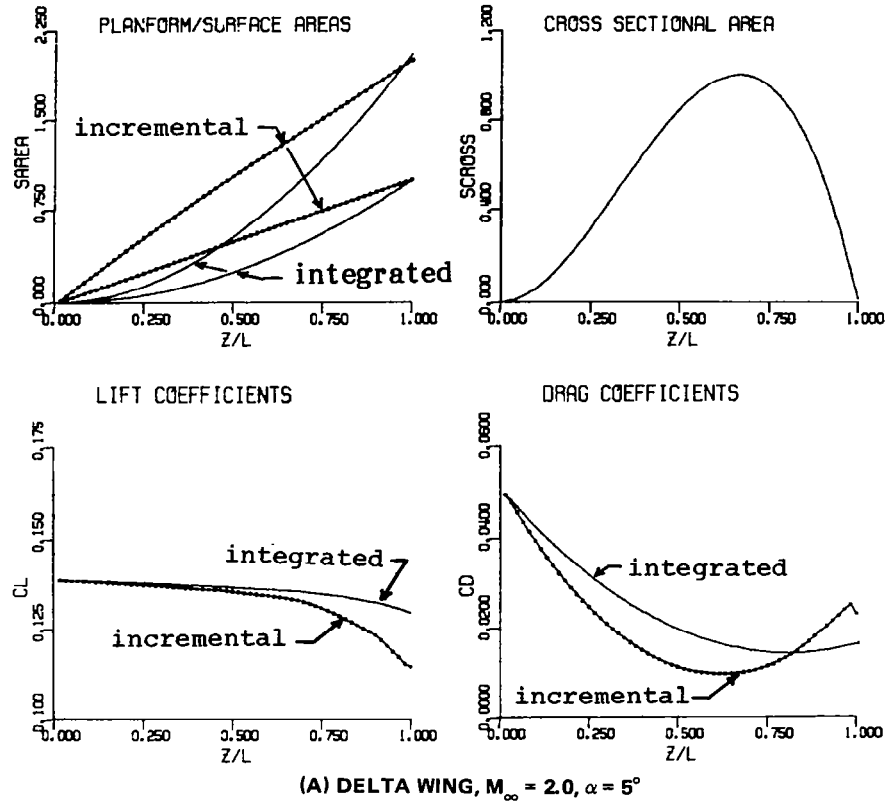


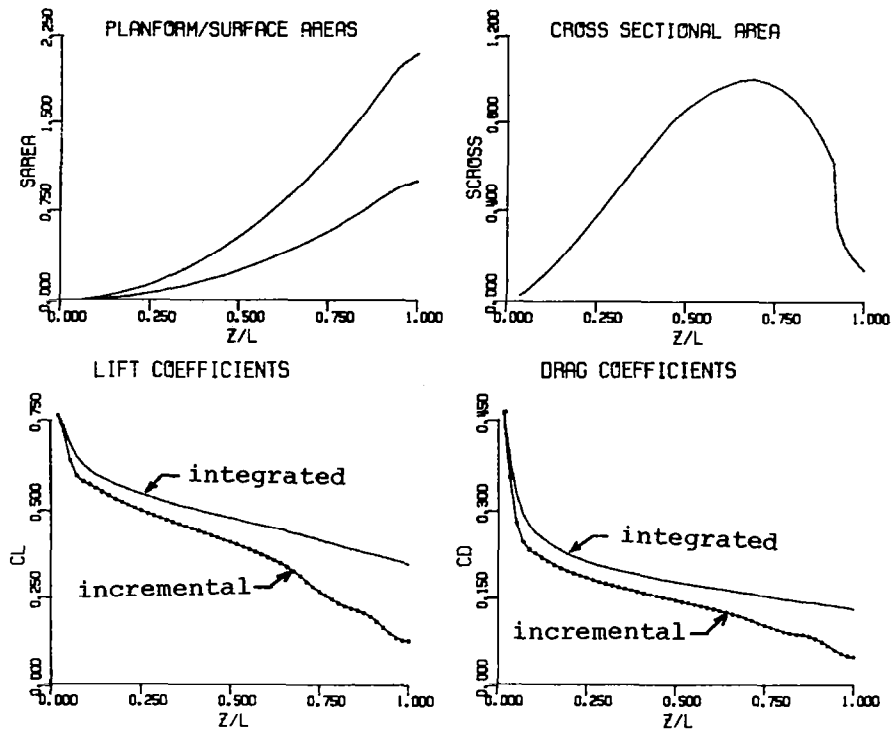
After the interpolation has been completed, a force subroutine is called which reads the interpolated  $z = \text{constant}$  data from TAPE2. The wing or body is now divided into a set of quadrilateral panels where the four pressure coefficients are known at each corner point. For variable sweep trailing edges, the spanwise sections contain quadrilaterals and two triangular panels which include the trailing edge points. To compute the force and moment on each quadrilateral, the quadrilateral is divided into four different triangular planes or two pairs of triangles governed by the two quadrilateral diagonals. The normal, axial force, moment and areas are then computed for each pair of triangular planes and averaged. This is done because if only one set of triangular planes was used, the projection of an upper surface quadrilateral onto a lower surface quadrilateral will result in different triangular planes for the two elements. Hence, for a symmetrical wing, exact cancellation of normal forces might not occur, resulting in a net small but finite normal force on the vehicle. By taking both sets of triangular planes, an exact cancellation of these normal forces will occur, if quarter plane symmetry exists in the geometry and pressure coefficients, yielding a more exact computation. The pressure acting at the centroid of each panel is assumed to be one third of the pressure at the corner points.

The forces, moments and areas are summed spanwise at each  $z$  - station. Projected planform area, surface area and cross sectional areas are all computed. The user can monitor the forces, moments and areas generated by each  $z$  increment. These incremental values are then integrated yielding an axial account of the total forces, moments and areas.

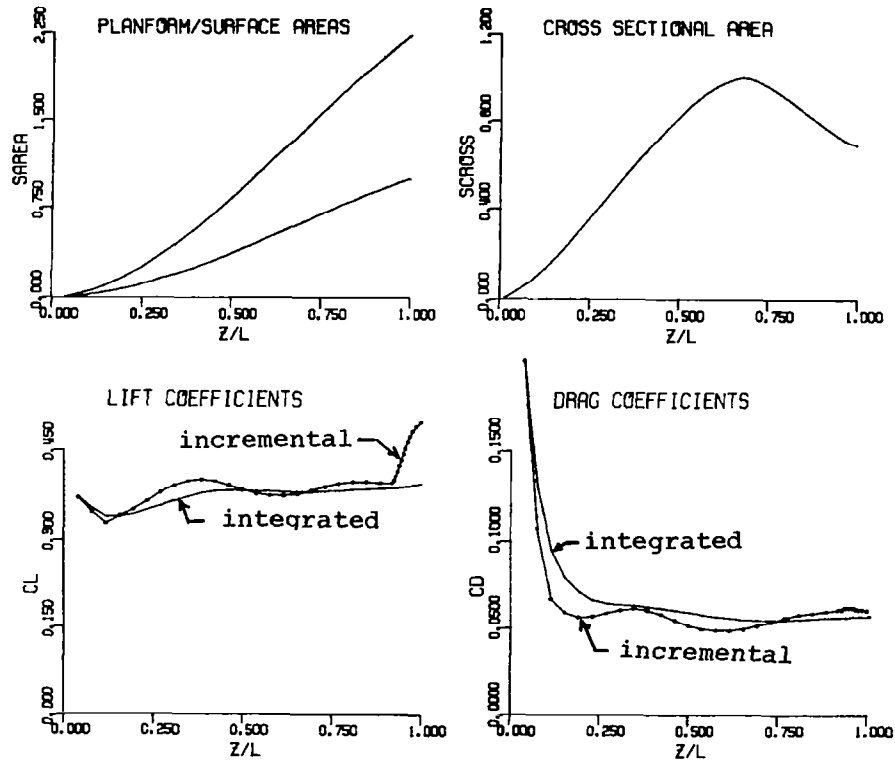
Normal and axial forces are computed as well as normal and axial force coefficients, lift and drag coefficients, and moment coefficient.

Figure 14 illustrates several examples of both incremental and integrated aerodynamic output by NCOREL. The first portion of the figure illustrates the planform and surface area of the configuration nondimensionalized by the maximum planform area; the surface area is always slightly greater than twice the planform area depending upon the cross sectional character. The second portion of the figure shows the cross sectional area nondimensionalized by its maximum value. The remaining two portions of each figure show lift-coefficient and drag-coefficient information. Figure 14a shows results for a simple symmetrical delta wing with a subsonic leading edge, elliptical cross





(C) VARIABLE SWEEP WING,  $M_\infty = 1.62$ ,  $\alpha = 11.93^\circ$

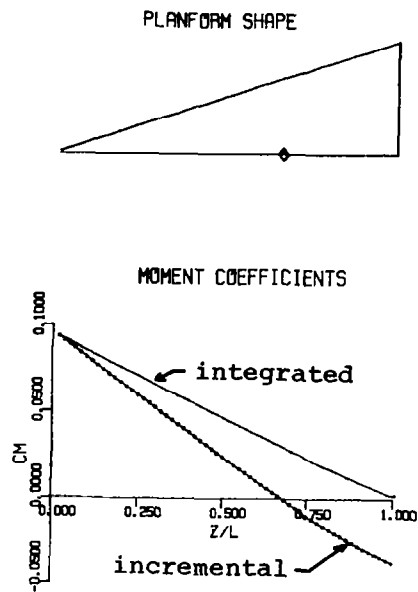


(D) ELLIPTIC MISSILE BODY,  $M_\infty = 2.0$ ,  $\alpha = 20^\circ$

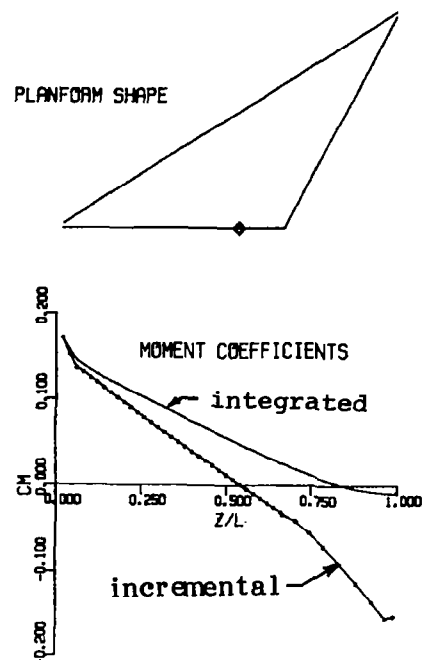
2246-038W

Figure 14. NCOREL Aerodynamic Output: Areas, Lift and Drag Coefficients (Sheet 2 of 2)

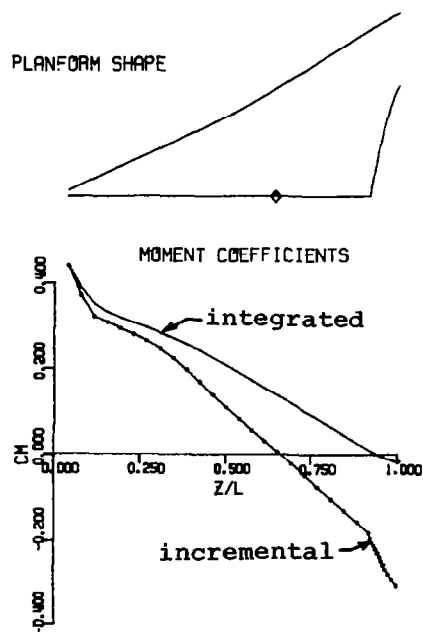
section and a parabolic centerline thickness. Figure 14b shows results for a symmetrical, supersonic-leading-edge, arrow wing with a 4% thick, four digit NACA airfoil section and a highly swept trailing edge. Downstream of the centerline trailing edge of the arrow wing, the sectional lift coefficients increase significantly, causing an overall increase in integrated lift coefficient. The axial variation of drag coefficient is distinctly different for the two wings. Figure 14c shows a typical output for a wing with variable sweep leading and trailing edges. The sectional spanwise lift coefficients also increase significantly aft of the centerline trailing edge. Figure 14d shows the aerodynamic output for a lifting missile body with an elliptical 3 to 1 cross section and a Haack-Adams area distribution at high  $\alpha$ . The forward half of the body has high lift characteristics. The decreasing lifting characteristics are due to the expansion of the body. Figure 15 shows the moment coefficients for the four different configurations. The aerodynamic output represented in Fig. 14 and 15 can be very useful to the designer in tailoring the behavior of a particular configuration.



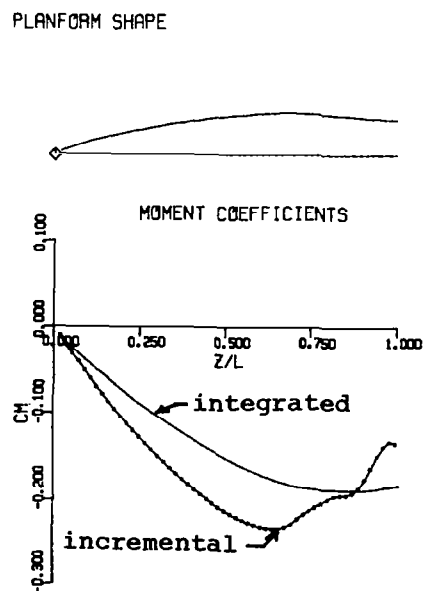
(a) DELTA WING,  $M_{\infty} = 2.0$ ,  $\alpha = 5^{\circ}$



(b) ARROW WING,  $M_{\infty} = 2.0$ ,  $\alpha = 5^{\circ}$



(c) VARIABLE SWEEP WING,  $M_{\infty} = 1.62$ ,  $\alpha = 11.93^{\circ}$



(d) ELLIPTIC MISSILE BODY,  $M_{\infty} = 2.0$ ,  $\alpha = 20^{\circ}$



## 7 GEOMETRIC RESTRICTIONS

Several geometric restrictions currently exist in NCOREL. NCOREL was originally developed for the computation of three dimensional flow over smooth bodies and wings. Any abrupt or discontinuous change in geometry will result in a discontinuous expansion or embedded shock. Currently NCOREL captures all embedded shocks. Theoretically, it can compute embedded supersonic shocks. This shock is different from the embedded cross flow shock because the flow across an embedded cross flow shock changes from supersonic/hyperbolic to subsonic/elliptic. This characteristic change does not occur across a supersonic shock. The interaction of embedded supersonic shocks with the fitted or captured bow shock has not been tested in NCOREL. A supersonic shock can be generated by an abrupt change in leading edge sweep of a wing or body angle. The occurrence of this shock in combination with a supercritical cross flow region and shock also has not been tested in NCOREL. NCOREL will capture these supersonic shocks but will have a tendency to smear them across several mesh points, making their accuracy questionable.

Conical flow computations are limited to attached flow conditions where the bow shock remains attached to the apex of the surface. Detachment can occur for a given Mach number at a high angle of attack or at a given Mach number as the local surface deflection angle is increased. Typically, just prior to detachment, subsonic total Mach numbers will be found in the conical solution. These solutions can not be used as a starting solution for a marching computation.

High angle of attack computations over thin wing cross sections may fail under certain conditions. If the cross section is thin and as the angle of attack is increased, a small region of near limiting suction pressure (i.e.,  $C_{p_{lim}} = \frac{-2}{\gamma M_\infty^2}$ ) may appear on the leeward surface. Further increase in the angle of attack may cause the computation to diverge or fail. Two explanations are possible: either not enough resolution or mesh points are available to resolve the large gradients in the vicinity of the leading edge or an inviscid solution does not exist. Sometimes very thin conical wings must be started on finer grids in order to converge and a large coefficient of artificial viscosity must be used. If these two devices fail, then the above explanations probably hold.

NCOREL computations are also limited to detached leading edge bow shocks. The bow shock will become attached to the leading edge for supersonic leading edges with zero radius of curvature. This condition can not be computed with NCOREL because a computational grid between body and bow shock can not be generated at the leading edge. Although this exact condition can not be computed, wings with small leading edge radii can be computed which approach this condition but still have the bow shock at a small but finite standoff distance.

In its application to wings, only wings with supersonic trailing edges can be treated at the present time. An embedded supersonic shock will be generated at the trailing edge of this wing (i.e., Mach number normal to trailing edge remains supersonic). An approximation for the wake is made by extending the camber line of the wing into the centerline inboard of the wing trailing edge. The wake surface is then treated as a flat plate with the boundary condition of flow tangency. This results in erroneous wake pressures that are not matched but should not affect the wing pressures if the wing has a supersonic trailing edge. This approximation becomes exact for a symmetrical wing at zero angle of attack. Because the actual wing trailing edge point is not demarcated in the cross flow plane, some smearing of this shock and a slight upstream effect on the wing will occur in the solution. This behavior will be corrected and an extension to subsonic trailing edges will be included in a future version of NCOREL which treats the wake properly.

Another area of difficulty in wing applications is the planform of a clipped delta or trapezoidal wing where the abrupt change in leading edge angle has been smoothed. The difficulty occurs when the flow expands around the leading edge. At zero angle of attack, the flow must expand through an angle equal to the planform angle of the wing. This usually does not present a problem to NCOREL. A realistic wing will typically approach zero thickness in this region of the wing. At angle of attack, the flow approaching this region may already have a low pressure supercritical region on its leeward surface. The flow then has to be expanded further through the half planform angle of the wing. NCOREL does not always yield a solution for this type of geometry in the clipped region of the wing. Limiting pressures may be obtained associated with large crossflow Mach numbers. It is suspected that in some cases an inviscid solution to this flow does not exist and the only way



that a solution can be obtained by NCOREL is to modify the leading edge geometry making the expansion less severe. This adverse behavior is a function of the planform angle or sweep, thickness and camber in the vicinity of the expansion and the angle of attack and may not always occur.

Wing-body cross sections can be treated with NCOREL with no apparent difficulties as long as the necessary mesh resolution is available. Difficulty will be encountered in treating a wing body planform where the wing emerges abruptly and at a position significantly downstream of the apex of the vehicle. In this situation, a strong embedded shock will be generated by the wing emergence. NCOREL will capture this shock but will have difficulty resolving the flow field if the initial cross section of the wing is thin and a supercritical region has developed. An insufficient number of mesh points may lie between the captured wing shock and wing surface, causing convergence difficulties. A blended wing-body configuration with strake blending is most suitable to be treated by NCOREL.

Since it is impossible to evaluate every application that NCOREL could possibly be applied to, it is left up to the user to evaluate its capability when going beyond the limit of isolated smooth bodies and wings. In applying NCOREL to a particular configuration, the user should keep in mind the possible areas of difficulty mentioned above.



## 8 APPLICATIONS

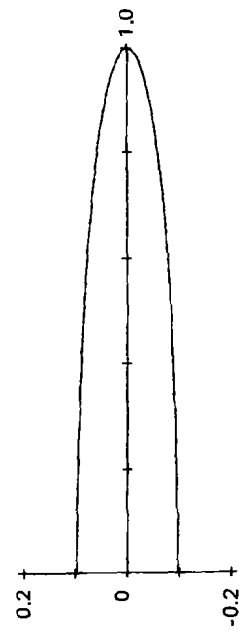
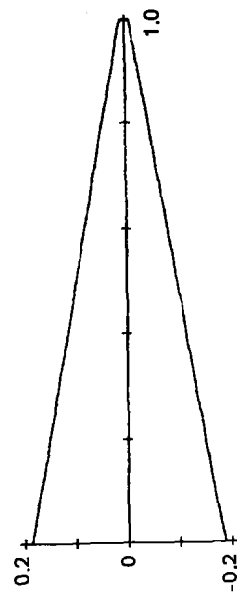
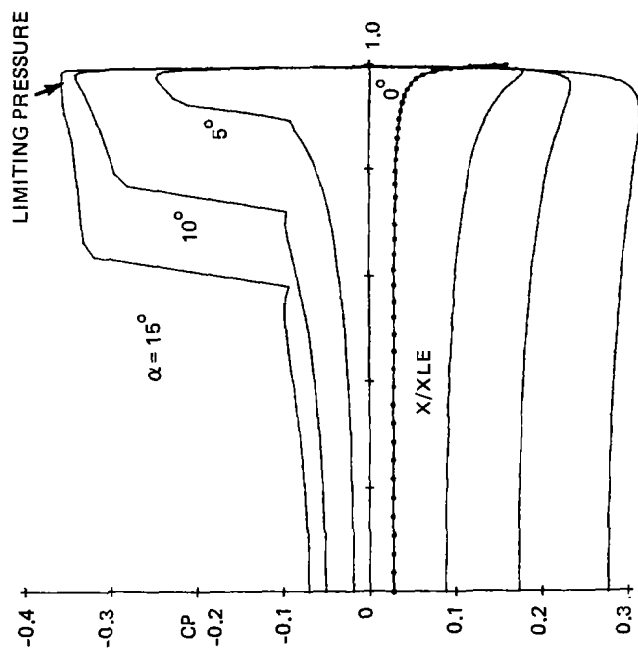
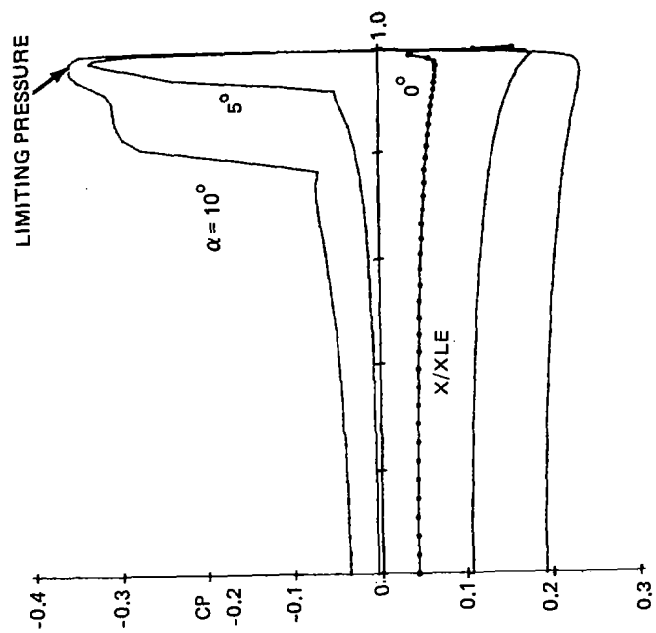
NCOREL has been applied successfully to a variety of conical flows and three dimensional isolated bodies and wings. Several simple wing-body configurations have also been treated successfully. The wing-body problem still needs further investigation, and the user should keep this in mind in attempting this type of computation.

### 8.1 CONICAL FLOWS

NCOREL can treat almost any kind of conical body, wing or wing-body configuration. Conical flows can be treated using any of the geometry packages or a user supplied routine where the cross section is invariant with the axial coordinate. This can be achieved analytically or with a simple nondimensional point wise input. The first station solution at  $R = 0$  is always treated as a conical solution. The only inherent limitation in NCOREL is that the bow shock remain attached at the apex. The typical solution preceding detachment will contain subsonic total Mach numbers. NCOREL will fail at some point when the angle of attack, Mach number, or surface angle exceeds the condition of an attached bow shock.

NCOREL will also fail for a thin wing at some high angle of attack. Preceding the failure or divergence of a solution, a region of limiting suction pressure or near vacuum pressures will typically occur on the leeward surface near the leading edge. The divergence of the solution indicates one of two things: either a lack of resolution (i.e., need for a finer mesh) or that an inviscid solution can not be achieved under those flow conditions.

Figure 16a shows an example of some typical conical surface pressure coefficient distributions obtained by NCOREL on a very fine mesh (86 x 58) at  $M_\infty = 2.0$  and angles of attack up to  $15^\circ$  for a thin elliptic cone. A cross flow shock has formed at  $\alpha = 5^\circ$  and gets stronger and moves inboard with increasing  $\alpha$ . At  $\alpha = 15^\circ$ , a small portion of the suction plateau is close to limiting or vacuum pressure. Higher angles of attack could not be computed because of the presence of these limiting pressures that correspond to very high cross flow Mach numbers. Figure 16b shows a similar set of surface pressure distributions for a wedge wing cross section with a small leading edge radius of curvature. At  $\alpha = 5^\circ$ , a large cross flow shock appears on the



b). WEDGE WITH SMALL LEADING EDGE RADIUS

a). ELLIPTIC

Figure 16 Conical Surface Pressure Distributions for Two Dissimilar Cross Sections ( $M_\infty = 2.0$ ,  $\theta_c = 20^\circ$ )

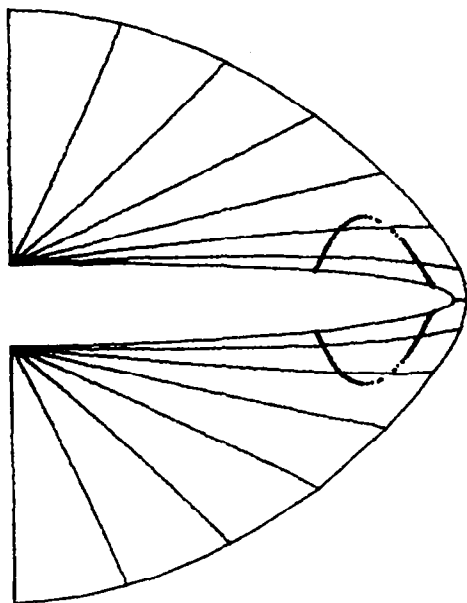
2246-052W

leeward surface. At  $\alpha = 10^\circ$ , a small leeward region of near limiting pressures has already occurred. Higher angles of attack could not be computed even with this fine mesh. Figure 16b shows clearly why leading edge separation occurs early on wings with small leading edge radii.

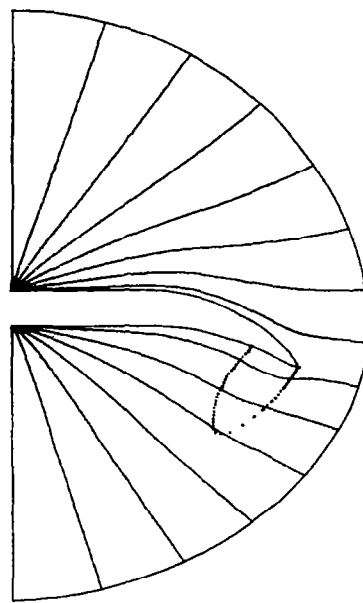
Figures 17 and 18 show a variety of interesting bow shock fit conical flows that can be computed with NCOREL. These figures show the cross section, cross flow sonic line, and cross flow streamline pattern. Supersonic cross flow velocities exist everywhere within the sonic line which is usually terminated by a cross flow shock. The cross flow streamlines emanate from the bow shock (i.e., the outer boundary line) and terminate at the body surface either at a vortical singularity or cross flow saddle point all of which are cross flow stagnation points (i.e.,  $U = V = 0$ ). Winglike cross sections will have three stagnation points, two of which will be vortical singularities located in the leeward and windward symmetry planes. The third cross flow stagnation point will occur near the leading edge of the wing. Body like cross sections will not have the leading edge stagnation point.

Figure 17a shows the solution for a thin supersonic elliptic cone at zero incidence showing the formation of a supersonic cross flow zone on both leeward and windward surfaces. The leading edge bow shock is also approaching an attachment condition. Hence, supersonic cross flow regions can appear on both upper and lower surfaces depending upon the freestream and geometric conditions. An interesting phenomenon can occur on cambered wings at low angle of attack. Figure 17b shows a highly cambered wing at zero incidence. In this flow a supersonic bubble and cross flow shock occurs on the lower surface of the wing.

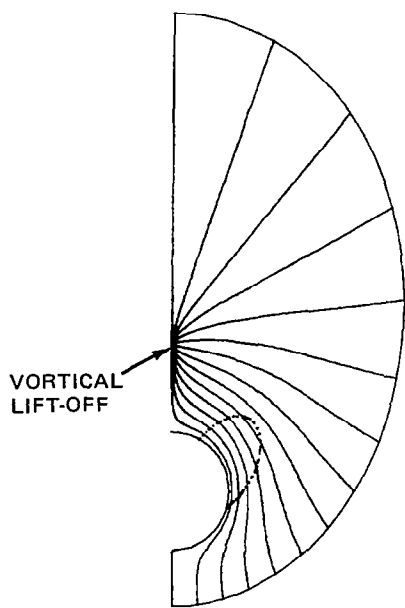
Figure 17c shows a subsonic cone at high incidence. In this flow the leeward vortical singularity lifts off the body surface. Figure 17d shows an interesting flow over a subsonic elliptic cone where a large supersonic cross flow bubble exists on the leeward surface terminating in a very strong cross flow shock. Another sonic line exists on the windward surface. This is a total Mach number sonic line and subsonic total Mach number flow exists within



a)  $M_{\infty} = 3.0, \alpha = 0^{\circ}$   
 $\theta_c = 30^{\circ}, \delta_c = 3^{\circ}$

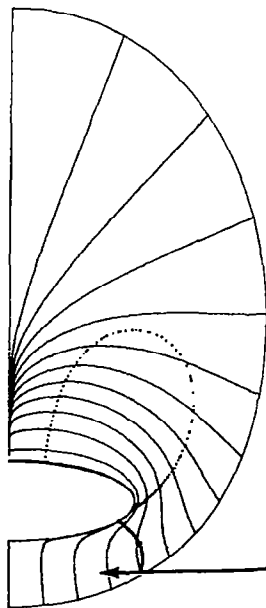


b)  $M_{\infty} = 2.0, \alpha = 0^{\circ}$   
 $\theta_c = 30^{\circ}, \delta_c = 2^{\circ}, \delta_{Tc} = -30^{\circ}$



c)  $M_{\infty} = 2.0, \alpha = 25^{\circ}$   
 $\theta_c = 10^{\circ}$

2246-020W



d)  $M_{\infty} = 2.0, \alpha = 35^{\circ}$   
 $\theta_c = 30^{\circ}, \delta_c = 10^{\circ}$

SUBSONIC  
TOTAL MACH NUMBER

Figure 17 Conical Bow Shock Fit Crossflow Streamline Patterns

Figures 18 a, b and c show the solutions for a thin elliptic cone at incidence and Mach numbers corresponding to subsonic, near sonic and supersonic leading edges. The cross flow region becomes larger and the cross flow shock moves inboard with increasing Mach number until finally the cross flow region extends all the way to the bow shock.

Figure 19 shows two conical wing-body flow solutions. Figure 19a shows a very blended wing-body cross section, and Fig. 19b shows a more abrupt wing-body juncture. It is interesting to note that an additional stagnation point occurs in Fig. 19b at the windward wing-body juncture. The windward vortical singularity moves from the symmetry plane to the wing-body juncture.

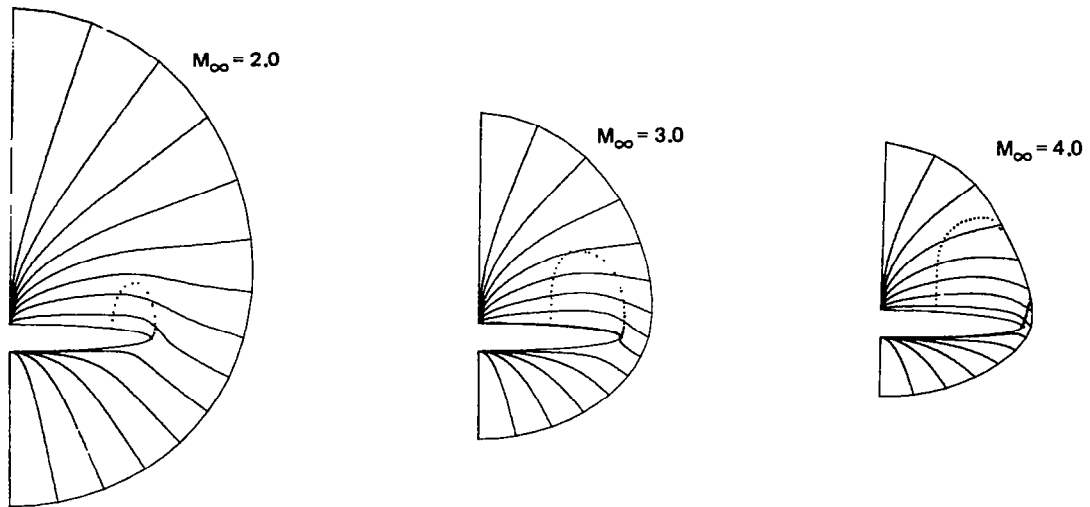
Figure 20a shows spanwise experimental pressure distributions for a conical cambered wing designed with the use of COREL (see Ref. 2). Figure 20a also shows the computed NCOREL solutions for both the BSC and BSF methods. Both methods compare well at the near sonic condition  $M_\infty = 1.66$ . At the higher Mach number, supersonic leading edge condition, the BSF method yields better windward correlation with the pressure data. Figure 20b shows the corresponding differences between the computed bow shock locations for the two methods.

In addition to the cambered wing that was designed for a shockless recompression at  $M_\infty = 1.62$  and  $C_L \sim 0.40$ , the equivalent flat or uncambered wing was tested. Figure 21 shows the cambered and flat wing cross sections at the design lift condition of  $C_L \sim 0.40$ . Excellent correlation and validation of the method was achieved at the design condition for the cambered wing, indicating a virtually shockless recompression. In comparison, the flat wing shows a higher suction pressure plateau and stronger cross flow shock. The comparison with NCOREL is good everywhere except in the vicinity of the cross flow shock. Some boundary layer separation may be occurring that is not accounted for in the inviscid NCOREL solutions.

## 8.2 NONCONICAL FLOWS

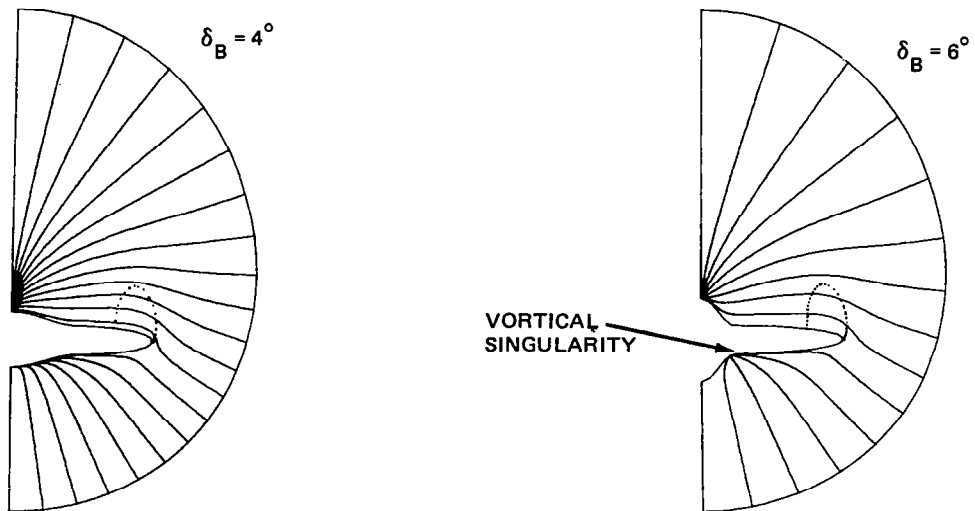
### 8.2.1 Analytic Body Shapes

A series of analytically defined forebodies was tested at supersonic speeds ranging from  $M_\infty = 1.70$  to 4.50, and the pressure data are available in Ref. 11. Two of these body shapes were chosen to determine the accuracy of NCOREL with respect to surface pressure data at  $M_\infty = 1.70$ . All the



2246-021W

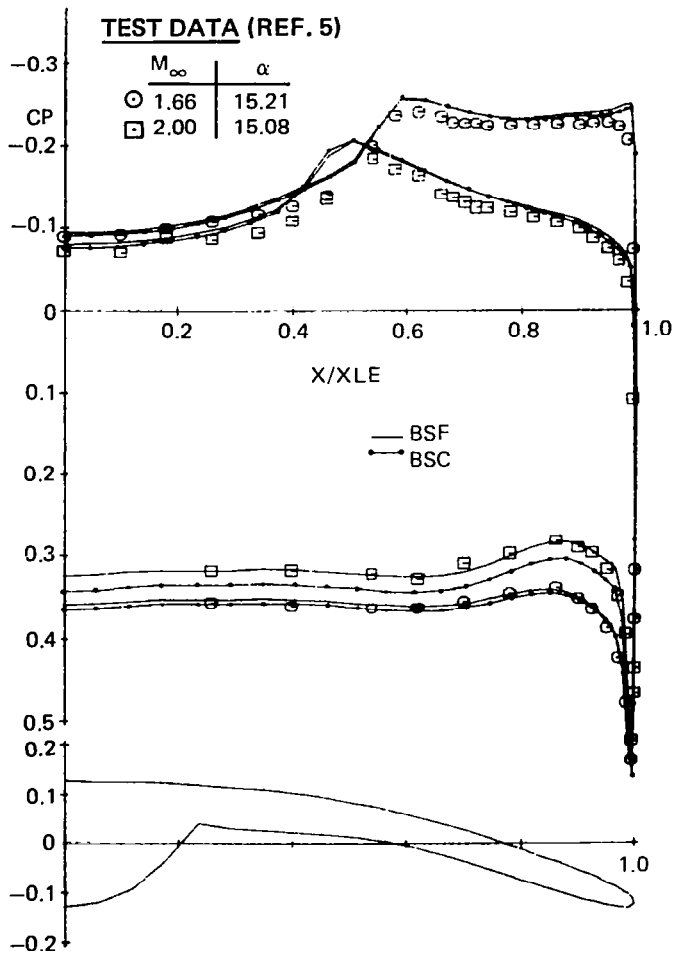
**Figure 18 Conical Bow Shock Fit Crossflow Streamline Patterns for a Thin Elliptic Cone,  $\theta_c = 20^\circ$ ,  $\delta_c = 2^\circ$ , and  $\alpha = 10^\circ$**



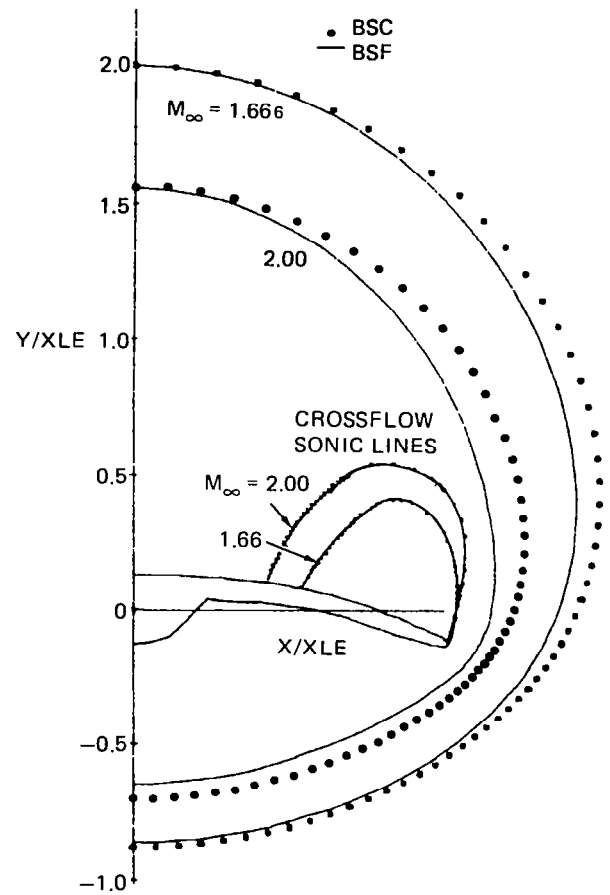
2246-022W

**Figure 19 Conical Bow Shock Fit Crossflow Streamline Patterns for a Wing-Body Cross Section,  $M_\infty = 2.0$ ,  $\alpha = 10^\circ$ ,  $\theta_c = 20^\circ$**





(A) SPANWISE PRESSURE DISTRIBUTIONS



(B) COMPUTED BOW SHOCK LOCATIONS

2246-042W

Figure 20 Conically Cambered Wing

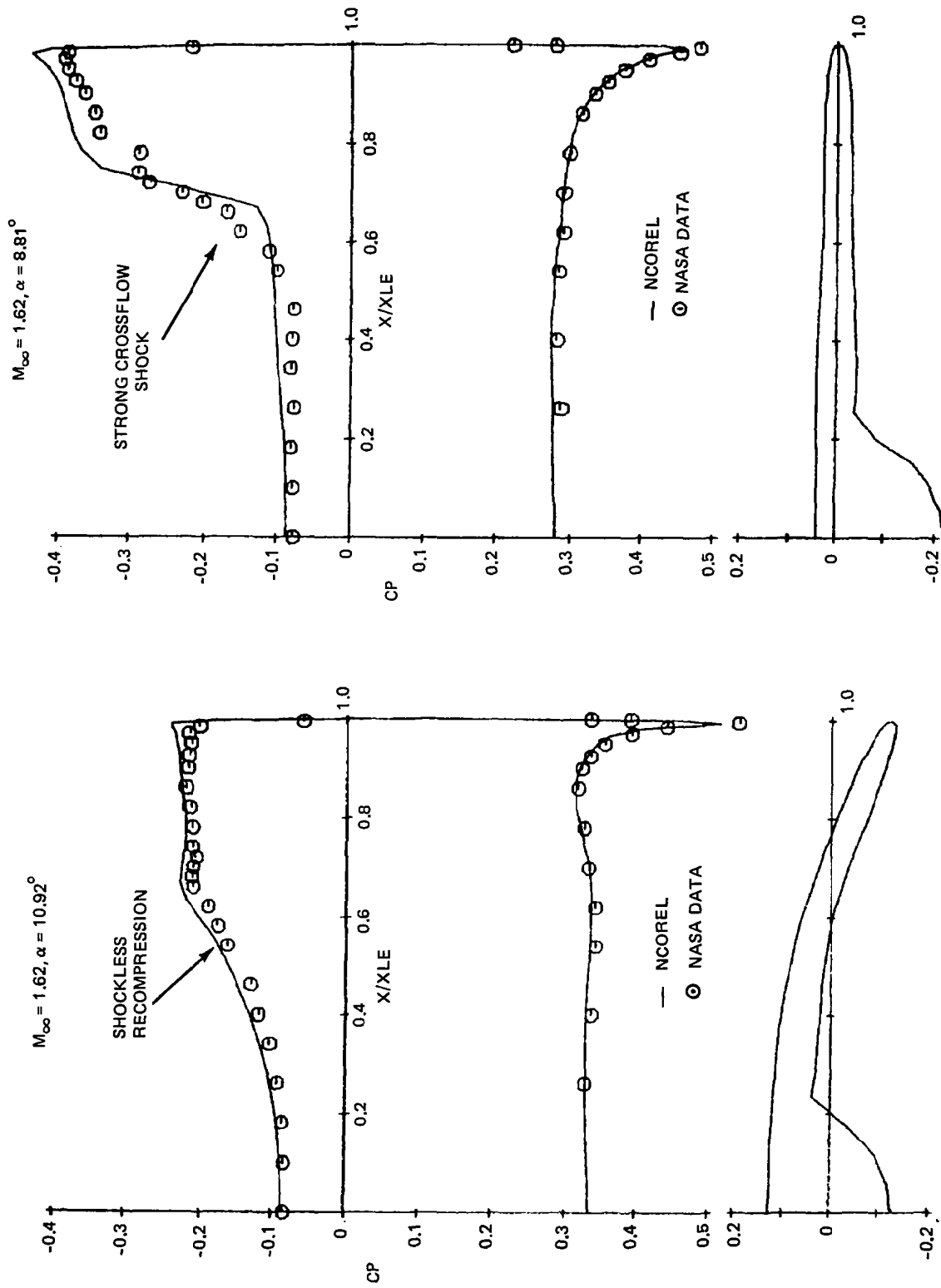


Figure 21 Spanwise Pressure Distributions on a Conical Cambered and a Flat Wing Section,  $M_\infty = 1.62$

2246-023W

computations were carried out on a (38 x 30 x 50) mesh where 38 points were distributed around the body and 50 radial marching steps or  $Z/L = 0.02$  were used. The conformal mapping was not implemented for these body shapes. The total run times ranged from 4 to 7 min on an IBM 370/168 with the spherical geometry generation requiring approximately 2 - 3 min of the total run time.

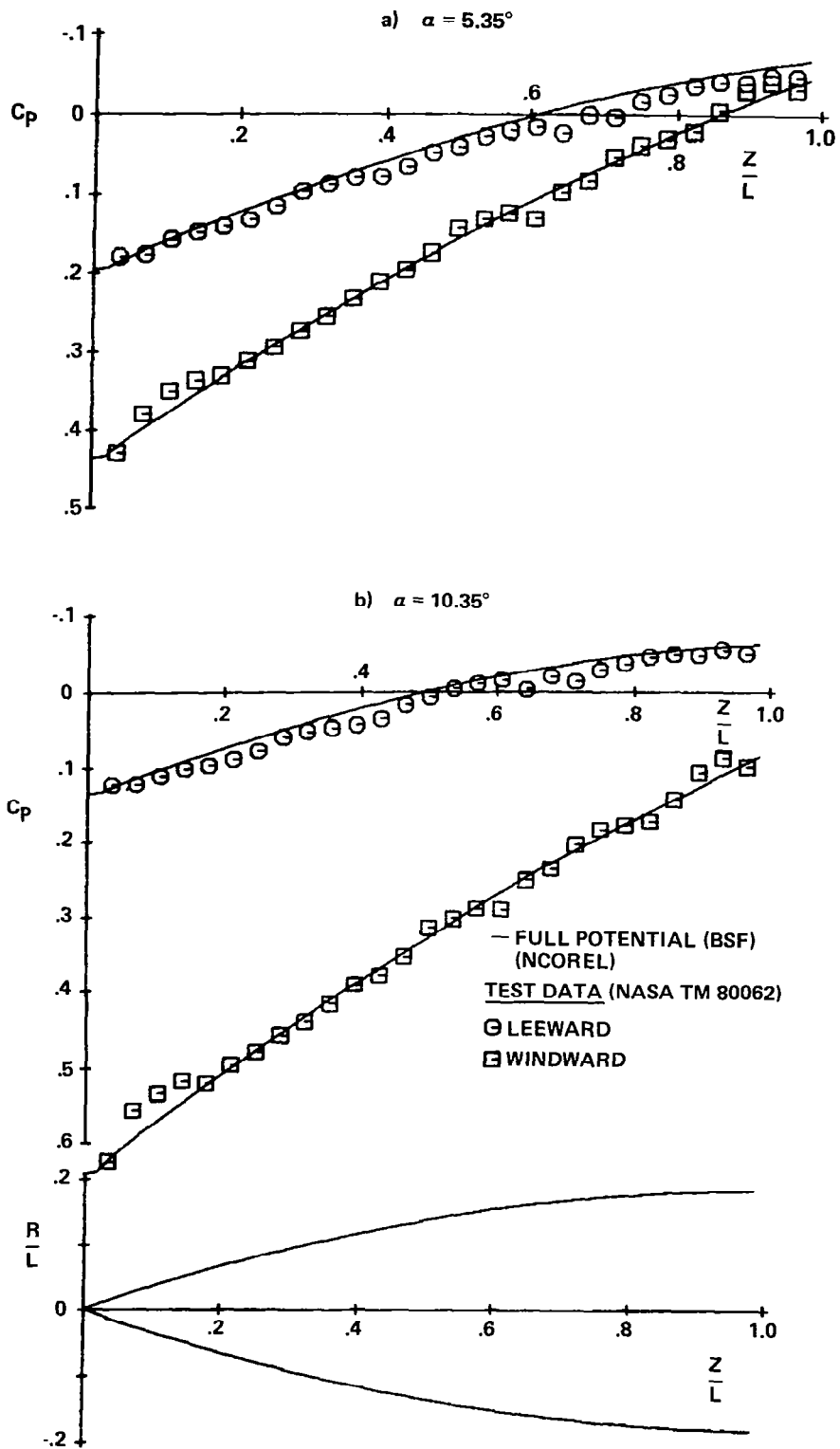
Figure 22a and 22b show the computed windward and leeward symmetry plane pressures compared to the test data at  $M_\infty = 1.70$  for a parabolic arc body with a lobed cross section at  $\alpha = 5.35^\circ$  and  $10.35^\circ$ , respectively. The test data do not exhibit a smooth behavior due to either probe or geometric inaccuracies. Excellent overall comparison is achieved at these angles of attack. Figure 23 shows a comparison of computed azimuthal pressure distributions with data for the same body at  $M_\infty = 1.70$ ,  $\alpha = 10.35^\circ$  for several axial locations. Excellent agreement in the azimuthal shape of the pressure distribution is achieved with a slight difference in the magnitude of the pressure levels.

Figure 24 shows another set of comparisons for a fuselage forebody shape at  $M_\infty = 1.70$ ,  $\alpha = 1.00^\circ$  and  $\alpha = 5.01^\circ$ . According to Ref. 11, the first five pressure taps were incorrectly located and hence do not necessarily lie on the symmetry planes and should be disregarded. Figure 25 shows the azimuthal pressure distributions for the same body at  $M_\infty = 1.70$ ,  $\alpha = 1.00^\circ$  and several axial locations.

Overall excellent agreement with the test data was achieved.

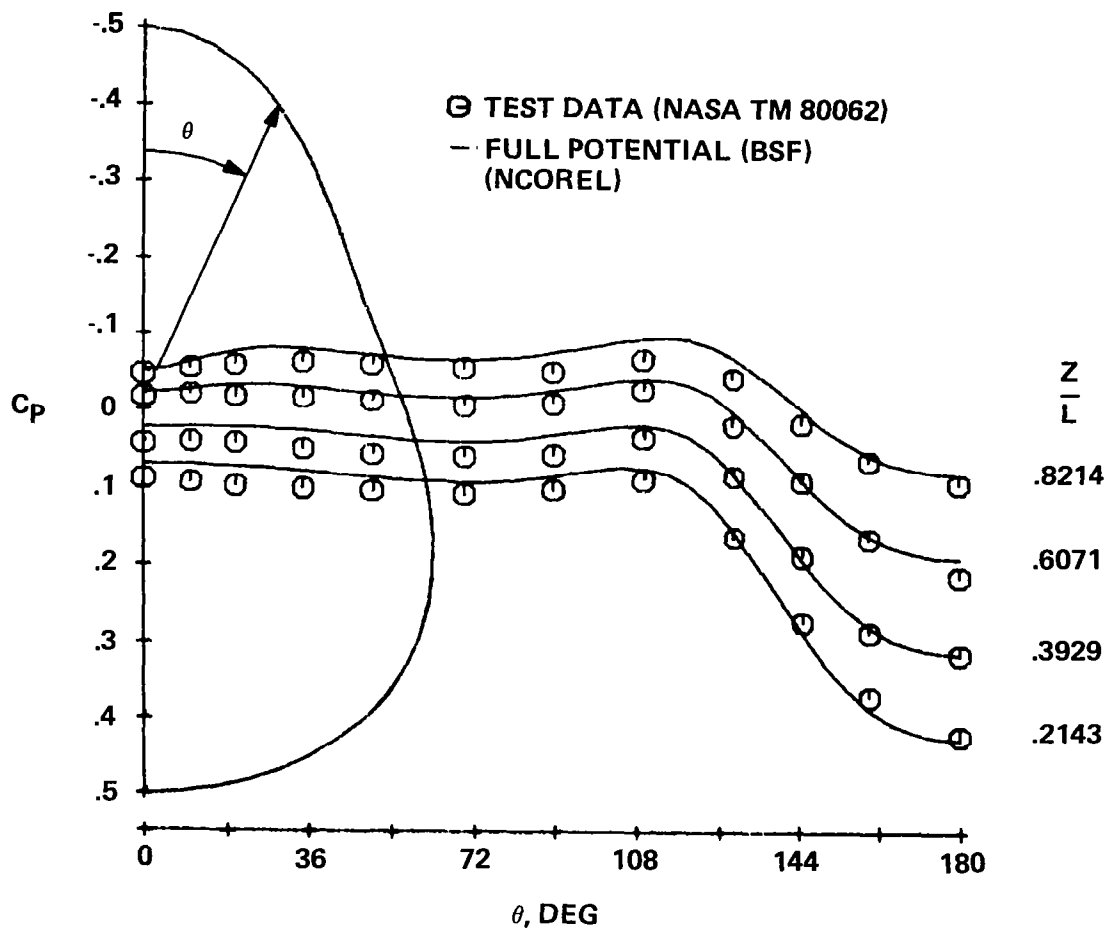
### 8.2.2 Missile Bodies

Experimental force and moment coefficients for two missile bodies are reported in Ref. 12. Circular and 3 to 1 elliptical cross section body shapes were developed from a minimum drag Haack-Adams area distribution. NCOREL was used to compute the body alone characteristics of these two shapes in Ref. 13. Figure 26a shows the moment and normal force coefficients as a function of angle of attack for the circular cross section body. A linear Woodward panel method calculation and experimental data points are also shown. NCOREL slightly overpredicts the moment and underpredicts the normal force. It is interesting to note the nonlinearity of the normal force with increasing angle



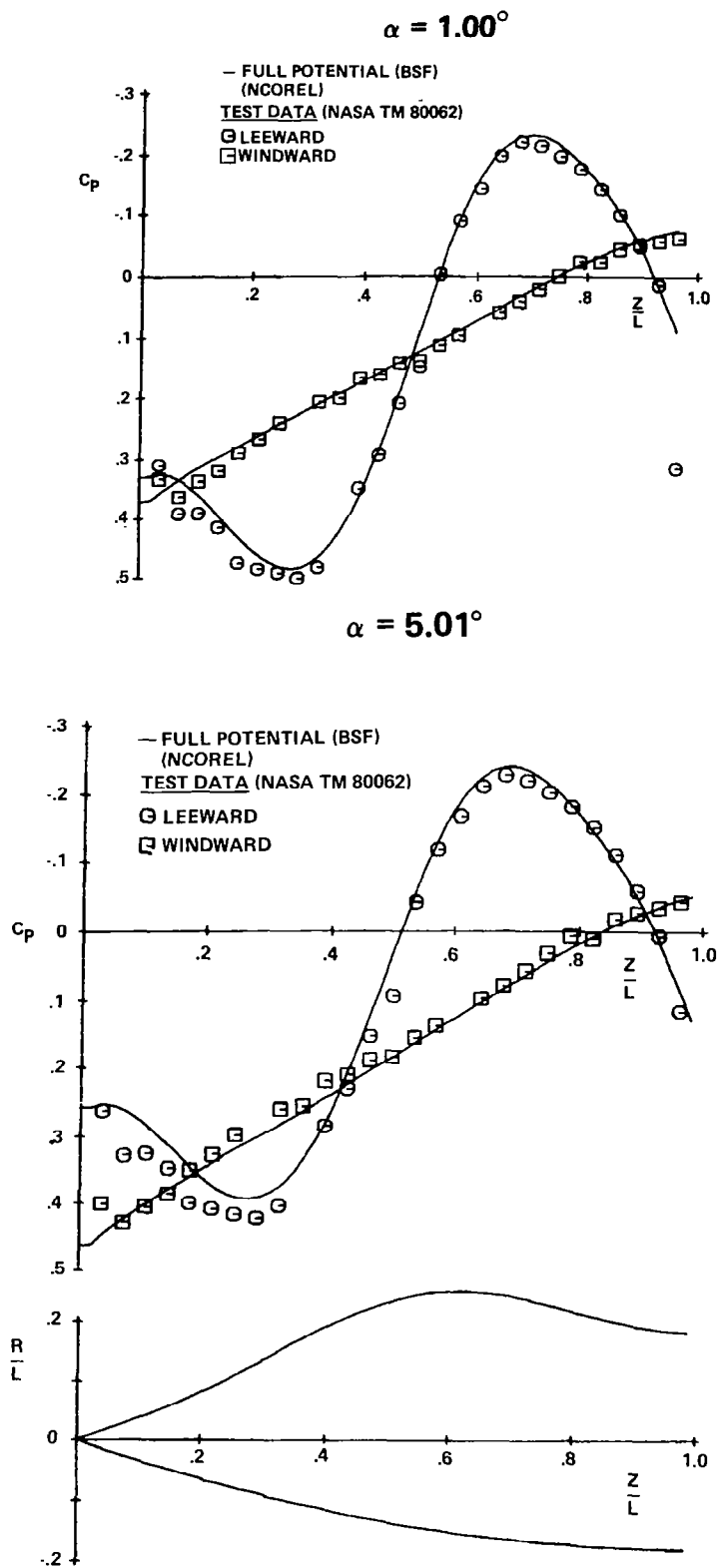
2246-029W

Figure 22 Axial Pressure Distribution on a Parabolic Arc Body with Lobed Cross Sections at  $M_\infty = 1.70$



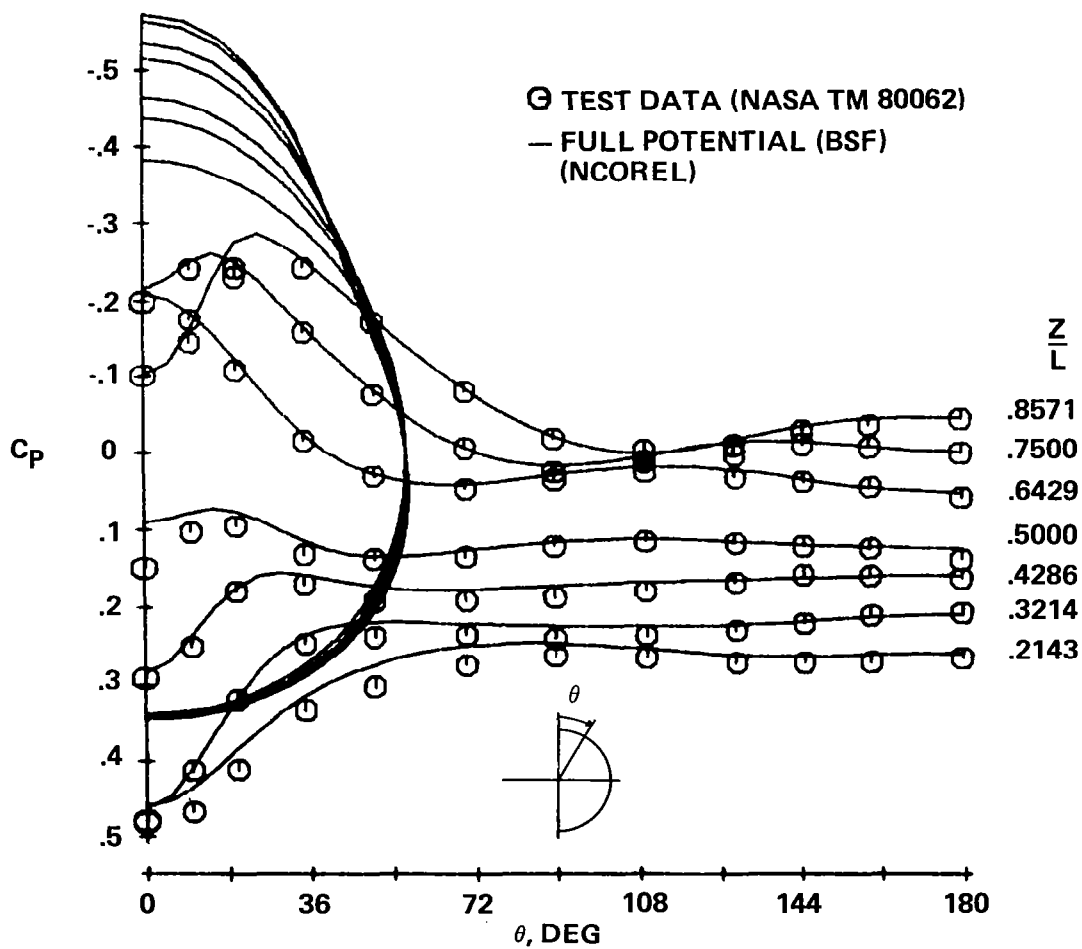
2246-032W

Figure 23 Azimuthal Pressure Distribution on a Parabolic Arc  
 Body with Lobed Cross Section,  $M_\infty = 1.70$ ,  $\alpha = 10.35^\circ$



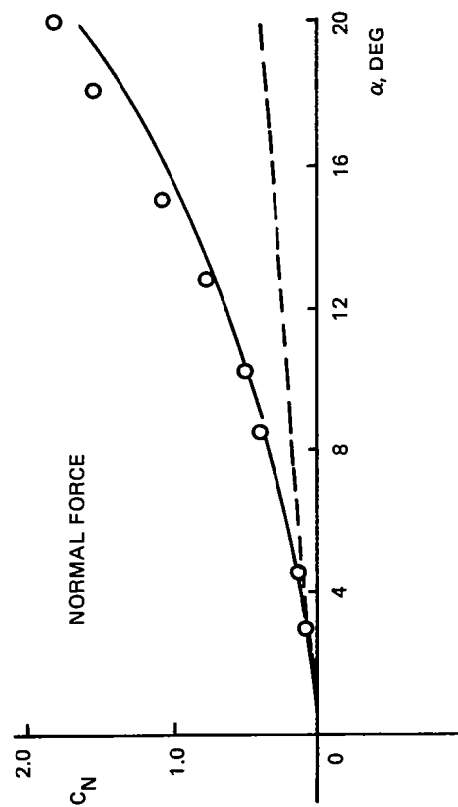
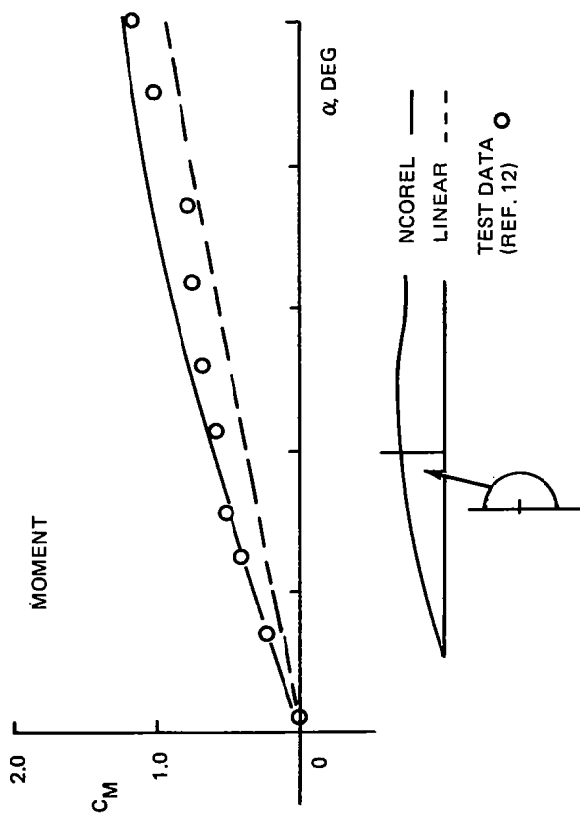
2246-031W

Figure 24 Axial Pressure Distribution on a Fuselage Forebody Shape,  $M_\infty = 1.70$

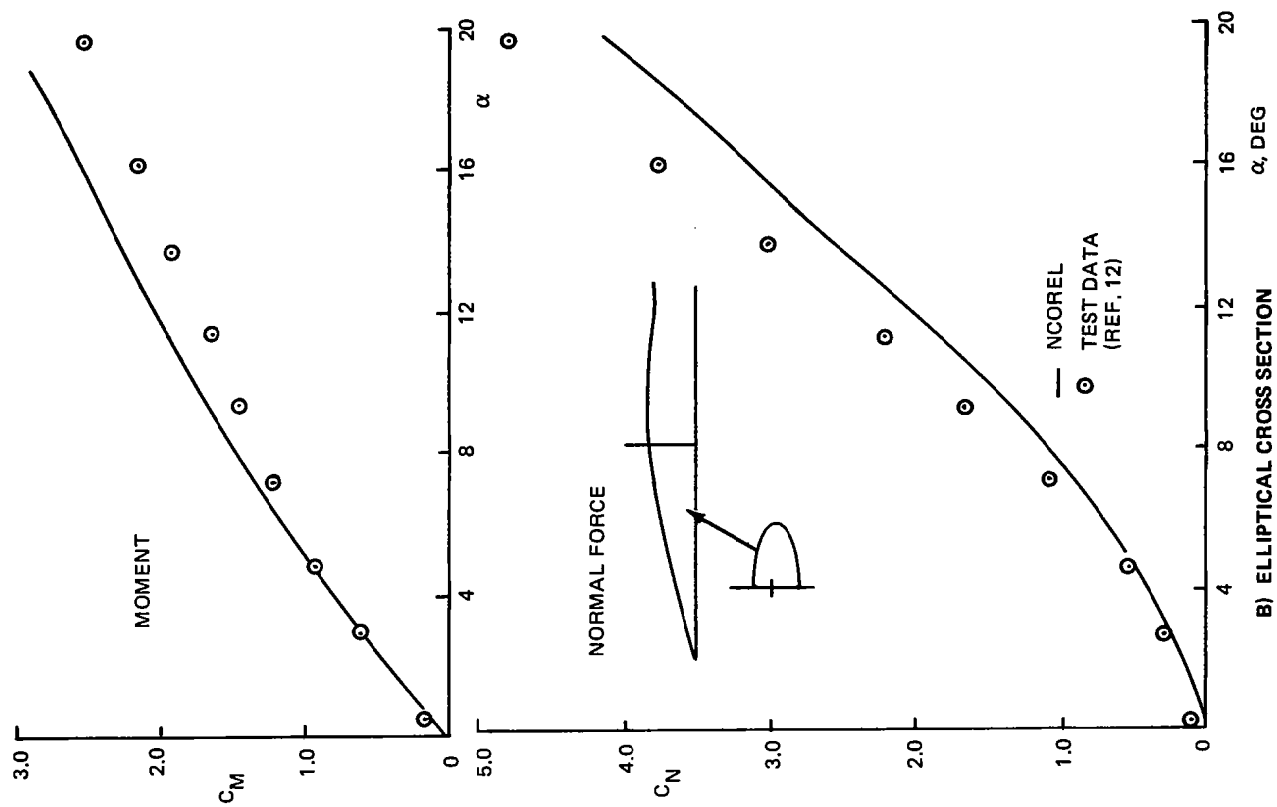


2246-033W

Figure 25 Azimuthal Pressure Distribution on a Fuselage Forebody  
 $M_\infty = 1.70, \alpha = 1^\circ$



A) CIRCULAR CROSS SECTION



B) ELLIPTICAL CROSS SECTION

Figure 26 Missile Body Moment and Normal Force Characteristics at  $M_{\infty} = 2.0$



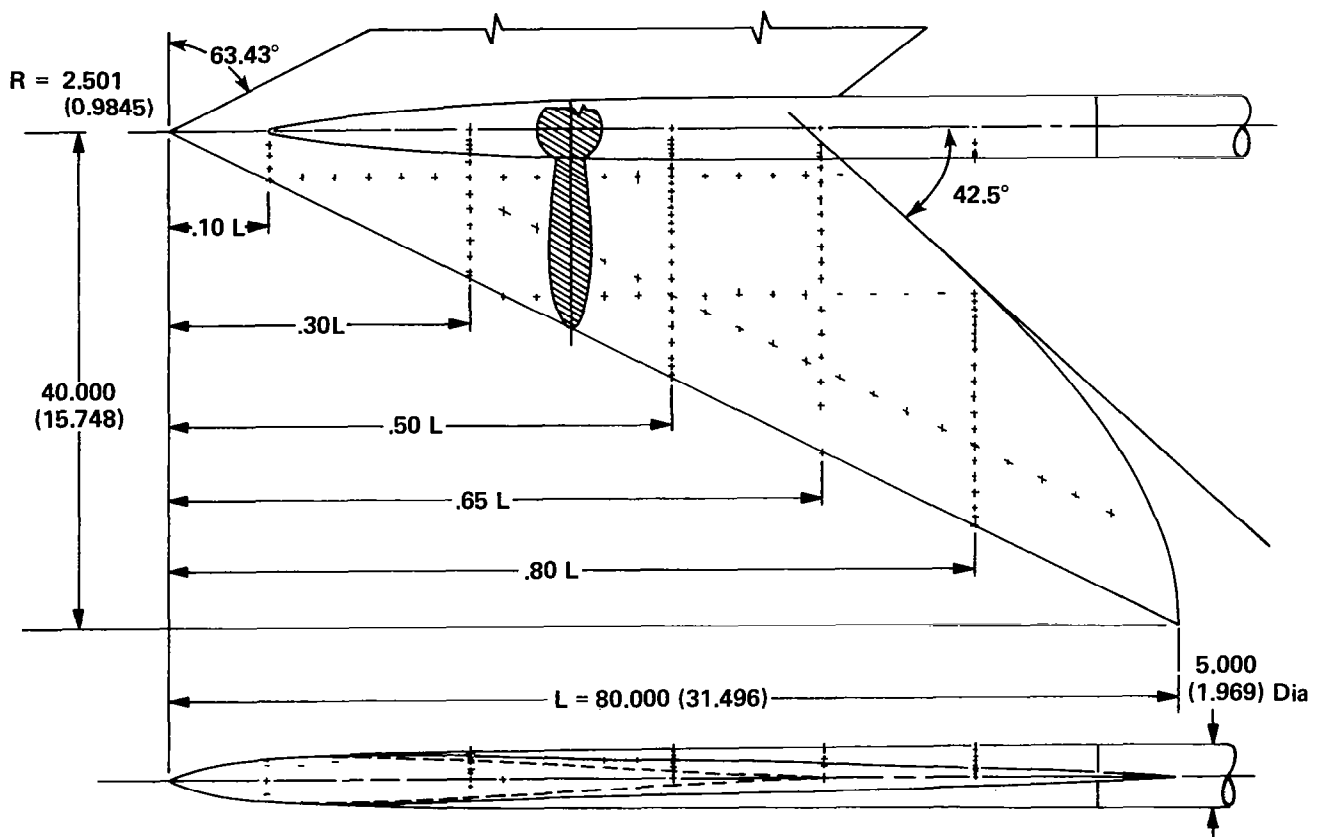
These curves dramatically demonstrate the need for a nonlinear method, especially at high angles of attack. The discrepancy between the experimental data and NCOREL is probably due to viscous effects that are entirely neglected in NCOREL.

### 8.2.3 Analytic Arrow Wing

Reference 14 reports on a series of wind tunnel tests for four analytically defined arrow wings. This experiment was selected because of the availability of detailed spanwise data at several stations for a three-dimensional configuration. The basic symmetrical wing configuration referred to as Model 1 with a sweep angle  $\Lambda = 63.43^\circ$  was used for the present study (see Fig. 27). The analytical geometry was kindly supplied by G. Moretti of PINY in the form of a computer subroutine.

The geometry consists of a wing with a straight leading edge and a circular centerbody emerging from the wing downstream of the apex. The variable sweep trailing edge of the wing remains a supersonic trailing edge for all Mach numbers tested. The geometry was run in NCOREL at the lowest test Mach number of 2.36. A (57 x 41) cross flow plane grid and 40 radial steps were used for the computation.

Figure 28 shows the correlation achieved for  $\alpha = 6^\circ$  and span stations  $Z/L = 0.30, 0.50, 0.65$ , and  $0.80$ . The computed results at a spanwise station were obtained by interpolation of the results from the spherical surfaces. The body has already emerged from the wing at the first span station (Fig. 28a), where  $Z/L = 0.30$ . The grid definition of the body is adequate at this station. The computed pressures do not indicate any localized spanwise effect due to the wing-body juncture, although the test data show a slight variation in the vicinity of the juncture. A cross flow shock is not indicated in either the experimental data or the computed results at this station. Figures 28b and 28c show two further downstream stations. The formation of a weak cross flow shock is now evident. At these stations the grid definition of the body is rather poor although the correlation in pressures remains excellent.

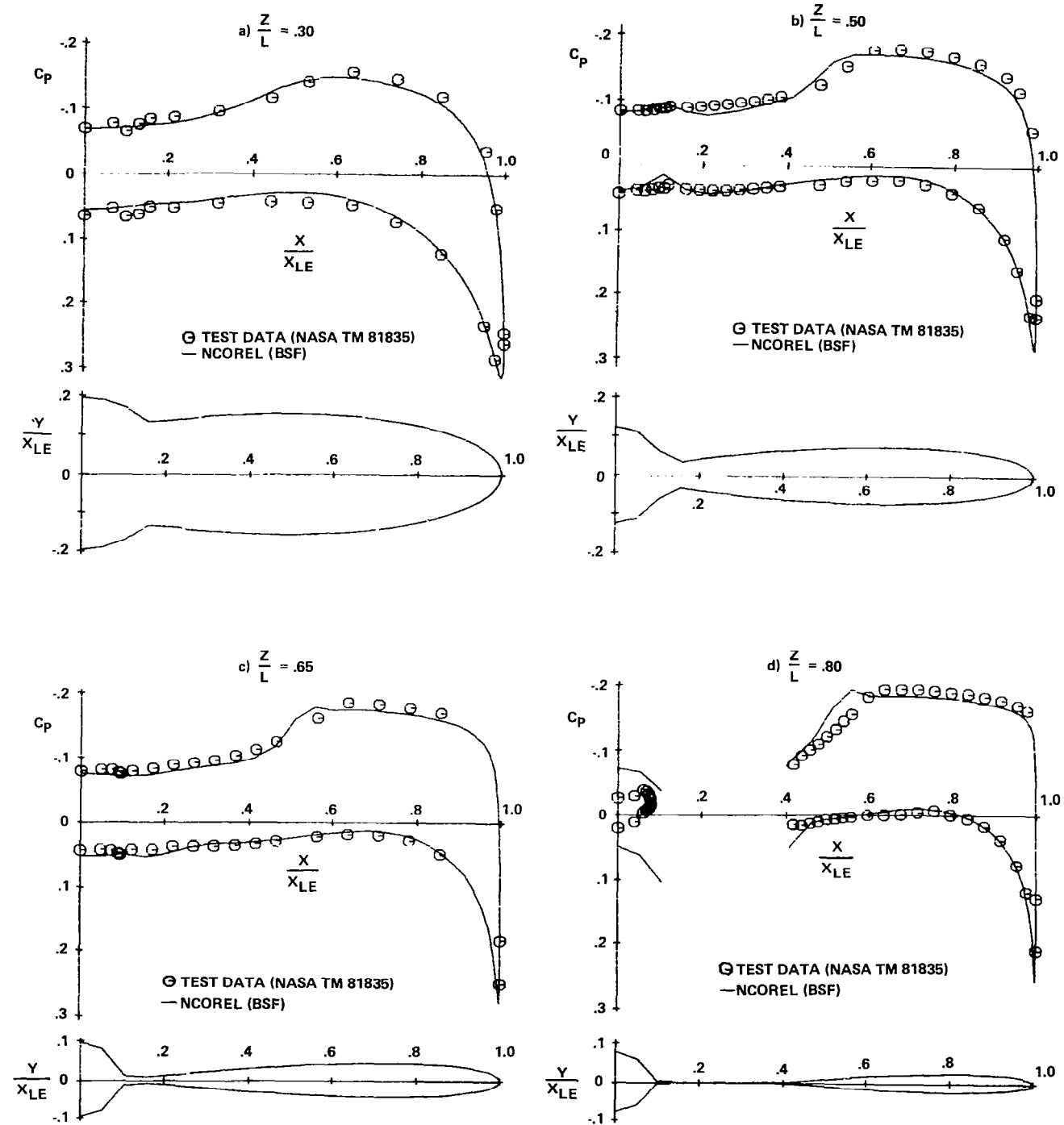


NOTE: DIMENSIONS ARE IN CM (IN.)

2246-030W

Figure 27 Arrow-wing Wind-tunnel Model Showing Pressure Orifice Locations (Ref. 14)

# NASA ARROW WING (MODEL 1)



2246-034W

Figure 28 Spanwise Pressure Distribution on an Analytically Defined Arrow Wing,  $M_\infty = 2.36$ ,  $\alpha = 6^\circ$

by the wake approximation. Remarkably good comparison is achieved on the wing surface using this approximation. The computed results indicate trailing edge shocks that occur due to the supersonic nature of the trailing edge. The local solution for the shocks in the vicinity of the trailing edge is not good because of the erroneous flat plate approximation as well as boundary layer effects and artificial smearing of the oblique trailing edge shocks. Smearing of the trailing edge shocks occur because grid points are not necessarily located on the exact trailing edge of the wing and also due to the use of numerical central difference formulae for the computation of body spanwise slopes. The computed body pressures do not correlate with the test data. This was expected because the wake of the wing has a definite influence on the body, unlike on the wing. Some difficulty in the geometry of the flat plate wake occurred as indicated in Fig. 28d by the wake crossover.

The computed results have a tendency to slightly underpredict the supercritical pressures and indicate a slightly downstream position of the cross flow shock in comparison with the test data. This discrepancy may in part be due to the rotational effects associated with the high Mach number of 2.36 which are neglected in the present potential theory.

Higher angles of attack were not computed because the experimental pressure distributions indicated a flat leeward pressure distribution with the absence of a cross flow shock. This is generally indicative of leeward surface boundary layer separation, and correlation with inviscid solutions would not be expected.

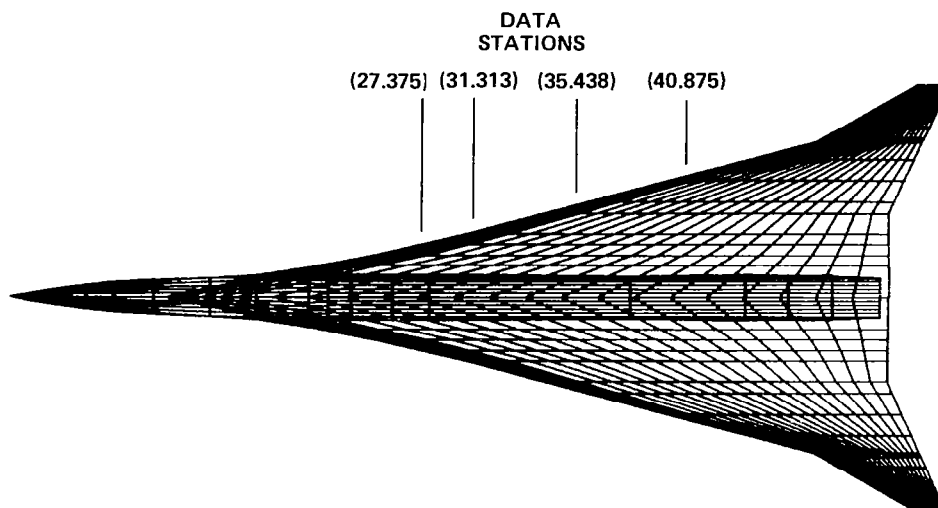
#### 8.2.4 Supersonic Cruise Aircraft

A more stringent test of the code in computing wing-body geometries is the type of configuration where the body origin lies upstream of the wing origin, which is typical of any realistic aircraft. This type of geometry leads to the formation of an embedded oblique wing shock. Reference 15 contains spanwise surface pressure data for a supersonic cruise aircraft configuration at Mach numbers 2.30, 2.96, and 3.30. Reference 15 was chosen because it also contains detailed measured geometric data of the complete aircraft in the form of an input data set consistent with the patch geometry requirement of Ref. 10.

Figure 29 shows the panel definition of the aircraft and the location of some of the pressure stations used for comparison defined in aircraft model coordinates (in.). The geometry data set of Ref. 15 was modified for use in NCOREL. The engine nacelles and vertical tails were removed. The wing model contains a total of 650 panels and the fuselage model, which was made simpler than that of Ref. 15, contains a total of 328 panels. The Joukowski mapping singularity was then tied to the evolution of the wing. Hence, the mapping singularity remains on the axis of the aircraft until the wing origin. Then the singularity moves continuously outward with the wing as the wing emerges from the fuselage. This procedure was found to be necessary because abrupt changes in singularity location cause abrupt changes in the mesh, leading to erroneous results. The camber of the wing centerline section was also modified to make the apex of the wing coincide with the origin of the fuselage so that the mapping singularity smoothly departs from the axis of the fuselage.

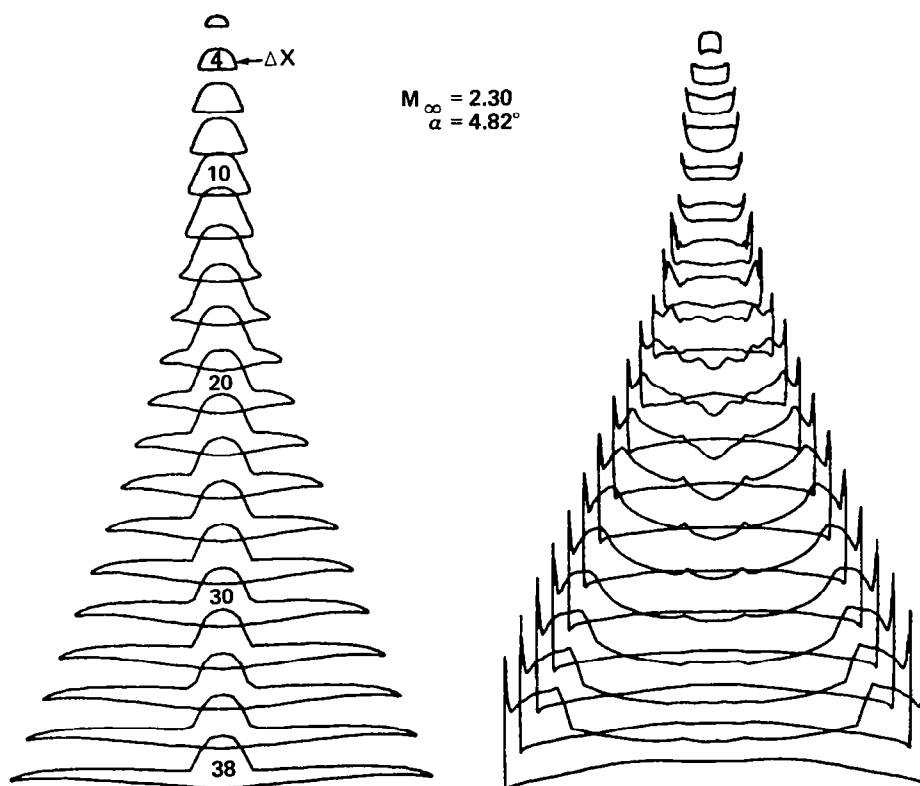
Some preliminary computations were carried out at  $M_\infty = 2.30$ . A  $(58 \times 58)$  cross sectional mesh was used with a marching step size of  $\Delta Z = 2$  which yielded approximately 23 steps to the centerline trailing edge of the wing. Figure 30 shows an isometric plot of the spanwise cross sections and pressure distributions at  $M_\infty = 2.30$ ,  $\alpha = 4.82^\circ$ . As noted earlier, the numerical program marches on spherical surfaces using the spherical cross sectional geometry. Figure 30 was obtained from the spherical data by linear interpolation. A large, low pressure spike occurs as the wing emerges from the fuselage ( $x \sim 14$ ). The spike remains throughout and a cross flow shock quickly develops. Interesting to note is the pressure depression that occurs due to the fuselage. Just after the wing emerges, the pressure distribution exhibits large oscillations on the leeward surface, causing convergence problems. This may be related to oscillations in the geometry or to the simultaneous development of the oblique embedded wing shock due to the wing emergence from the fuselage and the appearance of the supercritical cross flow shock.

If a thin wing (i.e., in comparison to the fuselage) emerges from the fuselage, a new scale to the problem is created. In the wing-body calculation, only a few points will be distributed between the newly emerged wing surface and oblique wing shock embedded in the fuselage flow field. As



2246-027W

**Figure 29** Input Panel Model of Supersonic Cruise Aircraft Showing Pressure Data Stations used for Comparison



2246-028W

**Figure 30** Isometric View of Spanwise Cross Sections and Pressure Distributions ( $\Delta X = 2$ )

the oblique wing shock moves away from the wing surface towards the bow shock, the resolution becomes better. It is suspected that this is the primary difficulty being encountered in the vicinity of the wing emergence from the fuselage. The lack of resolution can create oscillations and convergence problems especially if a supercritical region has developed. A stretching of the coordinates creating a cluster near the newly emerged wing surface may be necessary to alleviate this problem.

The computed results show a large suction spike at the leading edge with a steep adverse pressure gradient. The computed solution indicates that the suction spike induces a cross flow shock. The flow then expands slightly to further recompress through a second cross flow shock. This unusual behavior is most probably caused by the small nose radius and rather large camber. The suction spike would most probably cause the leading edge to separate. Figure 31 shows a series of comparisons at  $M_\infty = 2.30$  and  $\alpha = 4.82^\circ$  between a wing-body and wing alone calculation with the corresponding test data. The presence of the body has a minor effect on the windward pressures and a significant but local effect on the leeward surface, yielding a compression from the wing-body juncture to the centerline. Both wing and wing-body calculations exhibit leading edge suction spikes, with the wing-body exhibiting a more inward location and a slightly stronger cross flow shock. Overall the two calculations compare favorably with only minor and expected differences. The leeward surface experimental pressure data do not indicate a suction spike or a cross flow shock. The absence of a cross flow shock in the experimental data as the wing becomes thinner must be due to leading edge boundary layer separation.

The lack of correlation in the leeward surface pressures led to a closer inspection of the test data. Two intermediate stations where only leeward pressure data points were taken are plotted for comparison in Fig. 32a and 32b for  $\alpha = 2.81^\circ$  and  $\alpha = 4.82^\circ$  without the wing alone solutions. Except for the leading edge pressure spikes remarkably good correlation was achieved with the leeward experimental and theoretical pressures at these two intermediate stations. Interesting to note is that at the two intermediate stations the experimental pressures exhibit cross flow shocks at the higher angle of attack ( $\alpha = 4.82^\circ$ ). Also, if one compares the stations of Fig. 32 with the stations shown in Fig. 31, the experimental leeward data of the two intermediate

## SUPERSONIC CRUISE AIRCRAFT

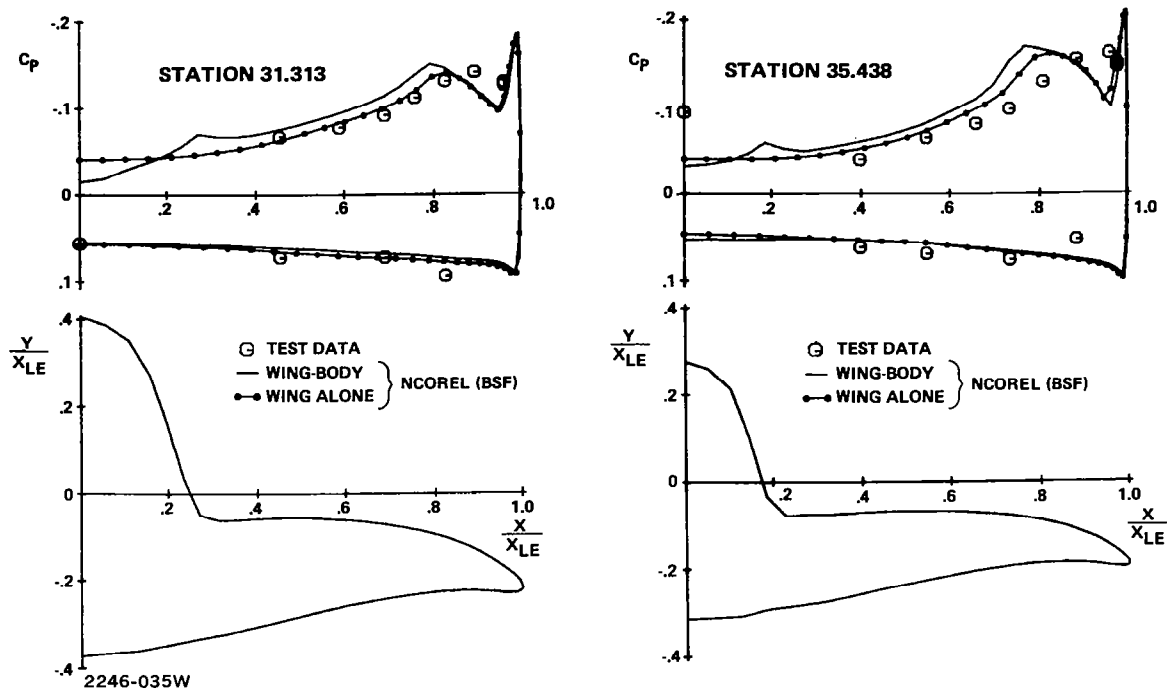


**Figure 31** Comparison of Computed Wing Alone and Wing-Body Configurations with Pressure Data for  $M_\infty = 2.30$   $\alpha = 4.82^\circ$

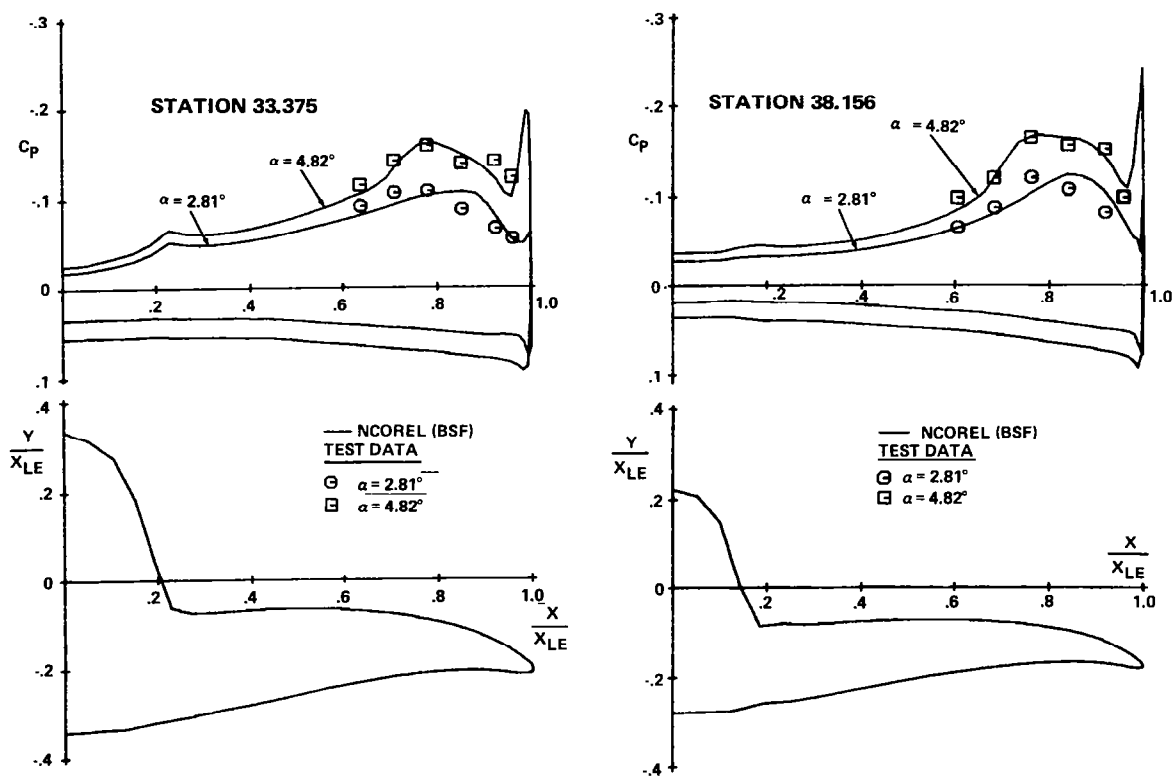


**Figure 32** Comparison with Surface Pressure Data for a Supersonic Cruise Aircraft at  $M_\infty = 2.30$ ,  $\alpha = 2.81^\circ$  and  $4.82^\circ$



stations are distinctly different from their neighboring stations which raises some concern about inconsistencies in the experimental data.

#### 8.2.5 Zero Lift Wave Drag of a Delta Wing

Figure 33 shows a series of numerical computations at several Mach numbers for a three dimensional delta wing ( $\Lambda = 71.57^\circ$ ) at zero angle of attack. The Weber version (see Ref. 16) of the Squire delta wing has a circular arc centerline thickness distribution with elliptic spanwise cross sections. To compute the entire wing in a spherical coordinate system, a flat plate was inserted for the wake geometry. This is a valid approximation since the wing is symmetric and at zero angle of attack. The computed pressures on the wing were integrated to obtain the zero lift wave drag values at several different Mach numbers and compared to experimental values and the Squire linearized analysis. This computation was suggested by Mason because it had been noted earlier in Ref 17 that linearized theory has a tendency to overpredict the drag. Hence, the opportunity exists of achieving lower levels of drag using a more accurate nonlinear analysis tool. The nonlinear code shows a marked improvement above Mach 1.8 for the difficult prediction of zero lift wave drag. The discrepancies at the lower Mach numbers are being investigated. At the Mach numbers 1.5 and 1.6, the linearized results show slightly better agreement. The accuracy of the nonlinear analysis depends upon the accuracy of capturing the oblique trailing edge shocks. To better resolve these shocks, a windward differencing was used to determine the numerical surface slopes in the radial marching direction. Less smearing of these shocks occurred when this was done and slightly better correlation was achieved. No attempts were made in the analysis to actually delineate the trailing edge of the wing. Aft of the trailing edge, the spherical cross sections take on a lobed appearance outboard of the wake region. A grid point on the body surface did not necessarily fall exactly on the trailing edge of the wing. Also, centered differences were used to determine the circumferential body slopes. All of this tends to artificially smear the oblique trailing edge shock. The surface pressures on the wing should not be influenced by the trailing edge shocks, but, unfortunately, the above numerical approximations that tend to smear the trailing edge affects the wing pressures slightly.

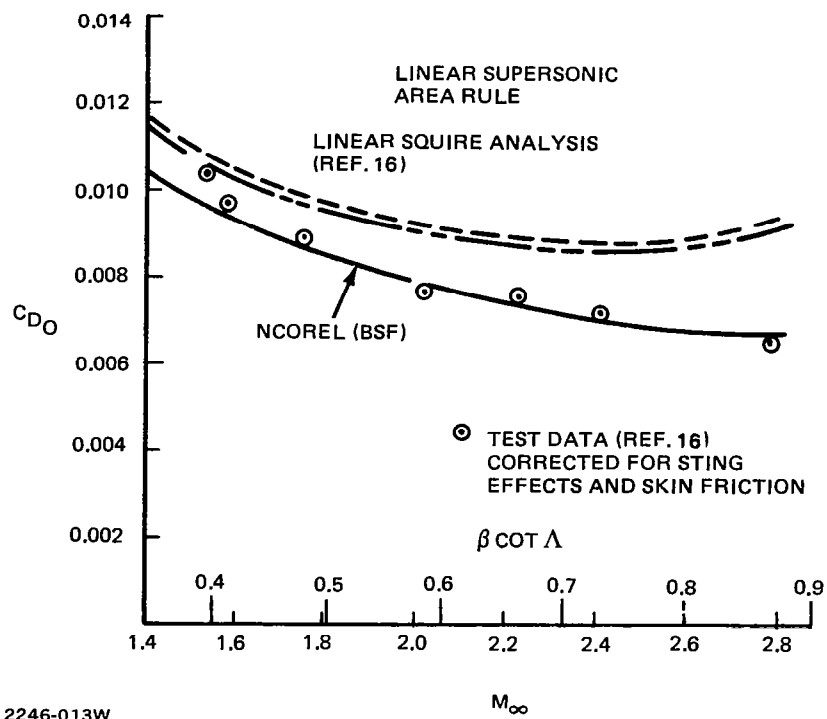
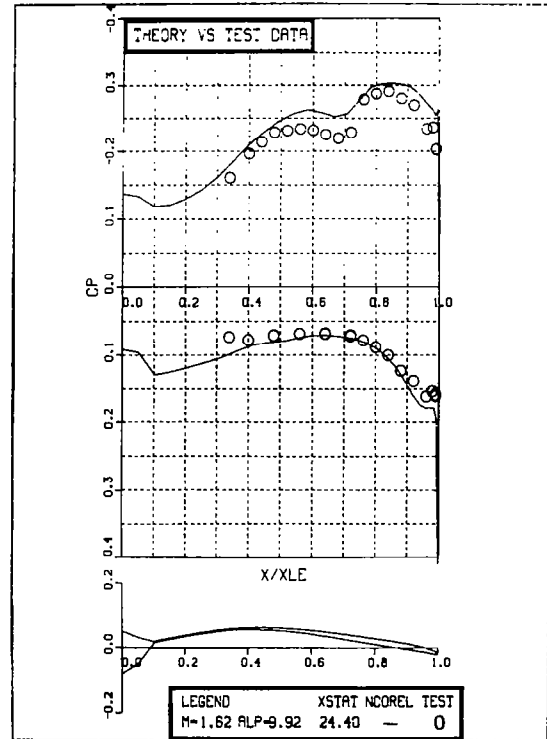
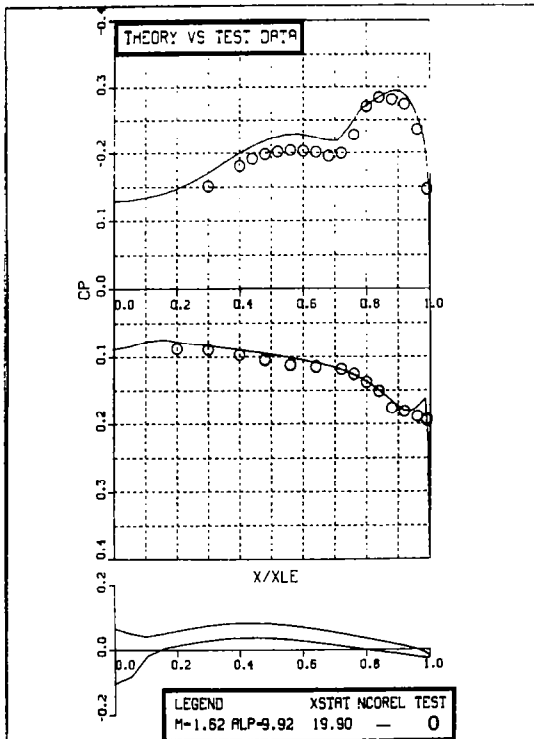
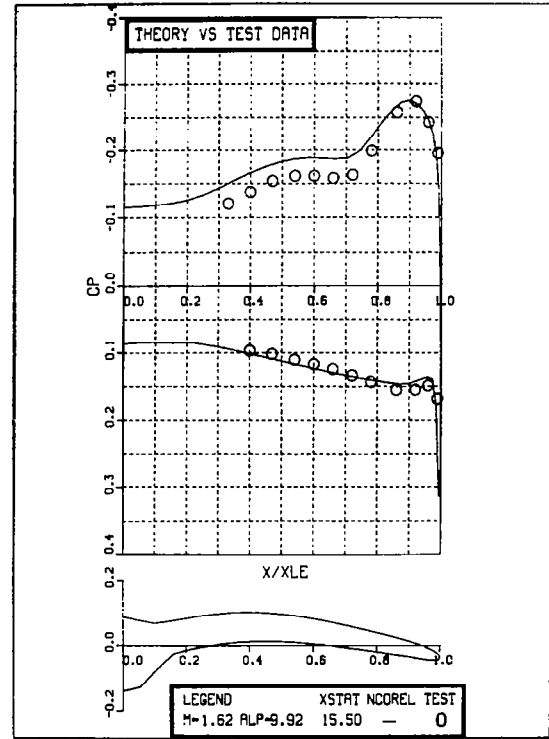
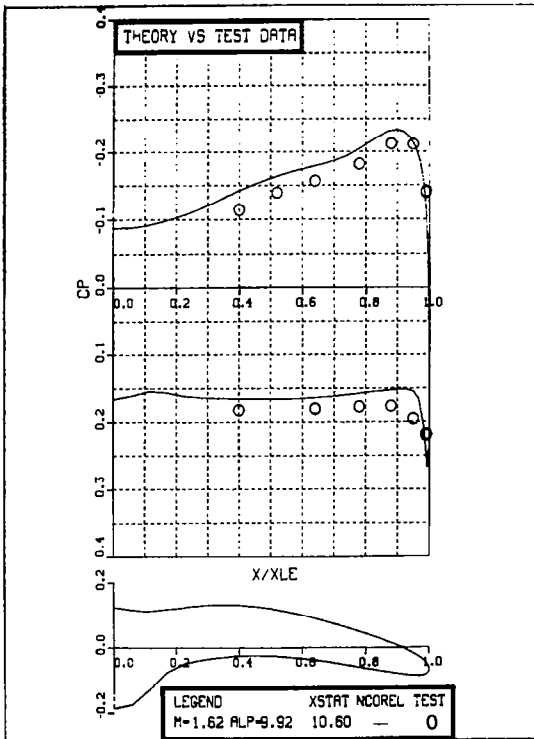


**Figure 33 Computed and Measured Zero Lift Wave Drag on the Squire Delta Wing**

#### 8.2.6 NASA/Grumman Demonstration Wing

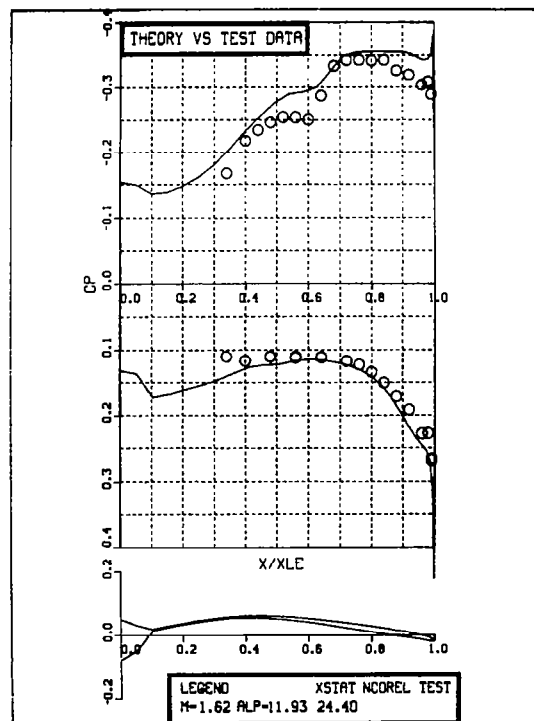
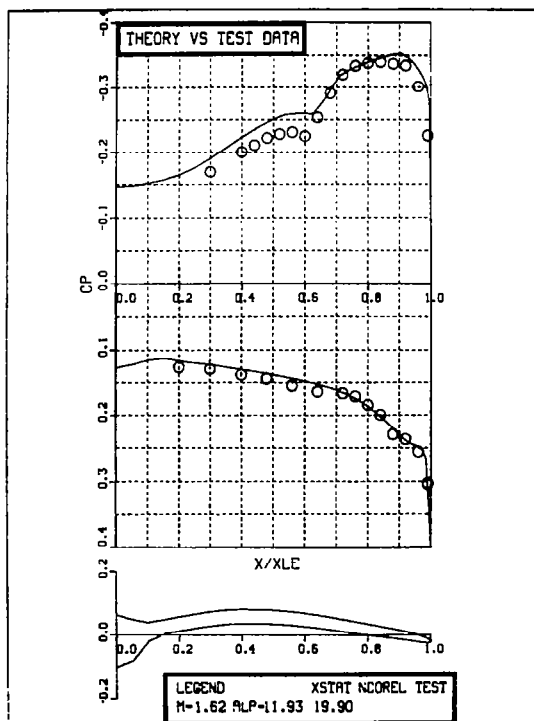
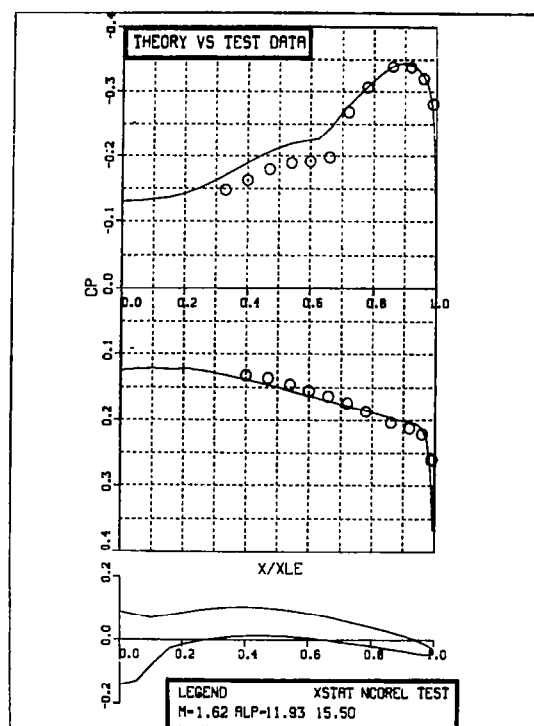
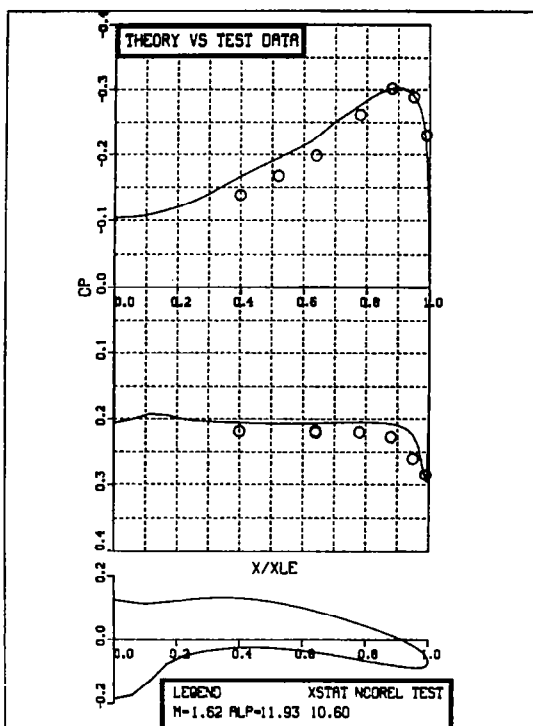
A three dimensional supersonic wing was designed by Grumman Engineering for NASA Langley and tested in the Langley Unitary Plan Wind Tunnel. This wing was designed with the aid of NCOREL at a design condition of  $M_\infty = 1.62$  and  $\alpha = 12^\circ$  with a lift coefficient  $C_L \sim 0.40$ . One of the objectives of this program was to use a nonlinear theory to design a realistic wing and achieve attached flow at the design condition by minimizing the strength of the cross flow shock. A post test evaluation of the wind tunnel results against the pretest predictions of NCOREL also was used as a validation of the accuracy of the code (see Ref. 6 and 7).

Four spanwise stations,  $x = 10.6, 15.50, 19.90$  and  $24.40$ , were instrumented for pressures. The last station occurs roughly at the centerline trailing edge of the wing. The results obtained with NCOREL (BSF) are for a  $(57 \times 57)$  crossflow mesh and a marching step size of one inch. This yields approximately 30 steps to the tip section of the wing. The NCOREL solutions are obtained on spherical surfaces. The code computes, by linear interpolation, both spanwise and chordwise pressure distributions. Figure 34 shows a comparison between the predictions of NCOREL and wind tunnel data at  $M_\infty = 1.62$ ,  $\alpha = 9.92^\circ$ . At the first station,  $x = 10.60$ , a slight shift in pressure levels is apparent between theory and experiment. The tunnel data indicates a higher pressure level on both windward and leeward surfaces. At  $x = 15.50$ , the windward and the leeward supercritical pressures are in excellent agreement. The experiment indicates a stronger compression and higher subcritical pressures on the leeward surface. This trend persists at the next two stations. At this condition, a distinct cross flow shock has not yet developed except possibly at the last station,  $x = 24.40$ . It is interesting to note that NCOREL has no difficulties computing down to the last station where the wing is very thin and almost a flat plate in the vicinity of the centerbody. With this grid the body definition is not very good at the last two stations. The centerbody causes an expansion to occur. Unfortunately, the wind tunnel model was not instrumented in the vicinity of the centerbody. Figure 35 shows the design condition of  $M_\infty = 1.62$ ,  $\alpha = 11.93^\circ$ . The same trends between NCOREL and experiment persist, but a cross flow shock develops at  $x = 19.90$ . The experiment seems to indicate a slightly stronger cross flow shock but excellent agreement in shock position is achieved. At



2246-041W

Figure 34 NCOREL Comparisons With DEMO Wing Surface Pressure Data,  $M_{\infty} = 1.62$ ,  $\alpha = 9.92^{\circ}$



2246-037W

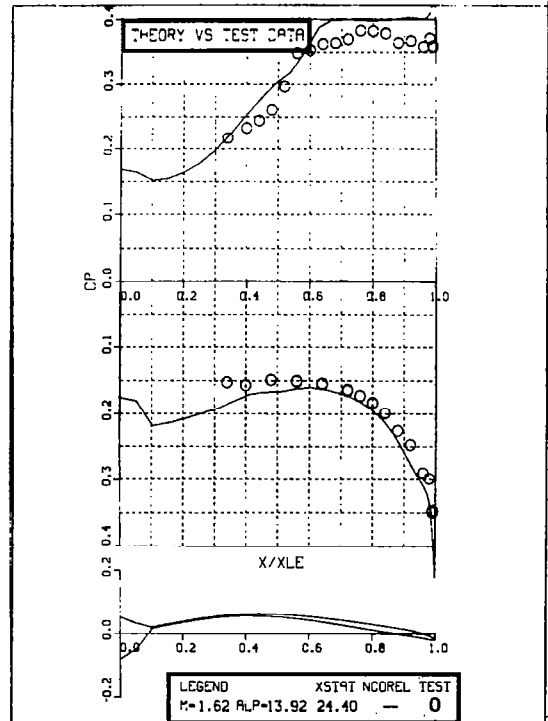
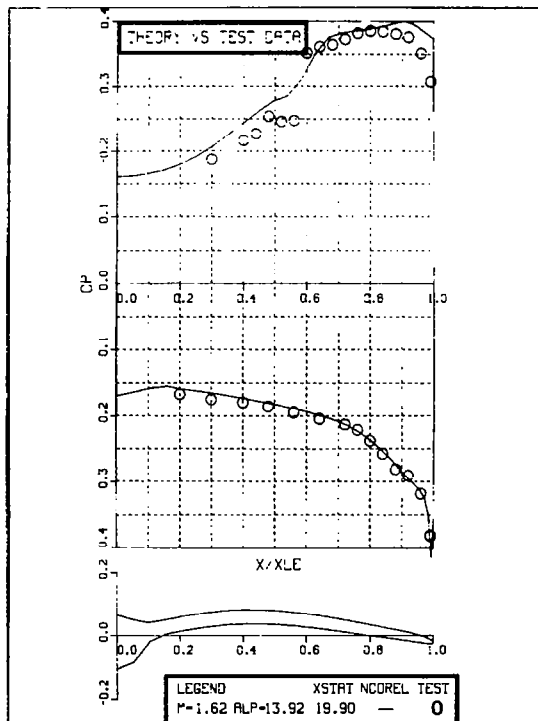
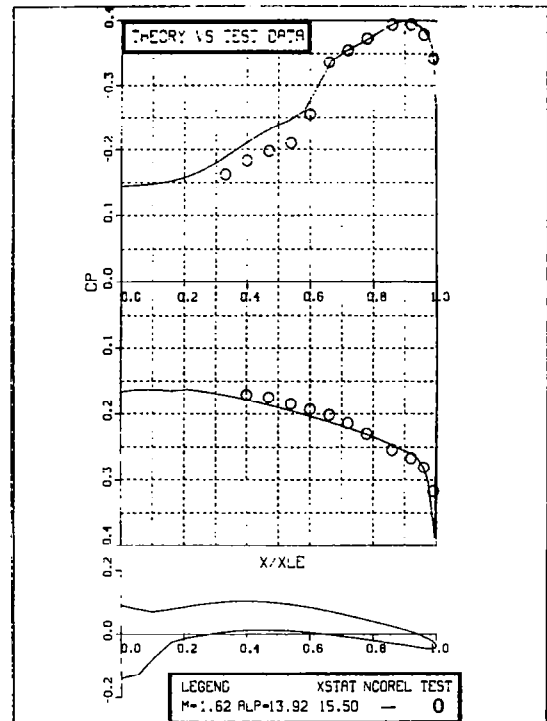
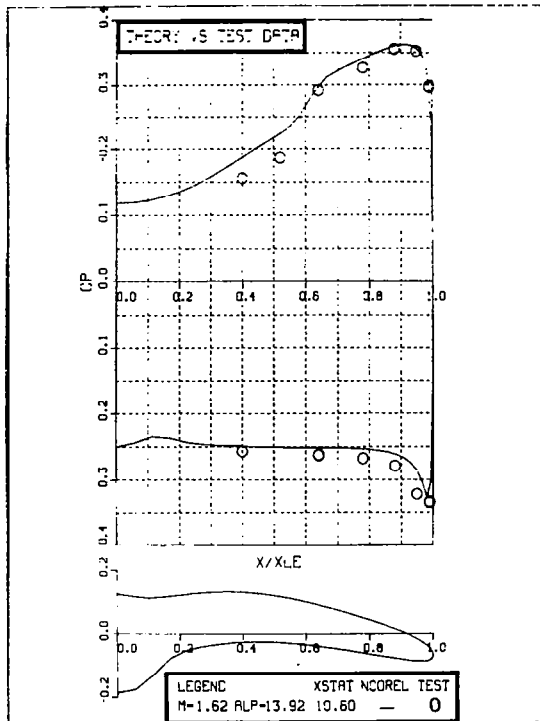
Figure 35. NCOREL Comparisons with DEMO Wing Surface Pressure Data,  $M_{\infty} = 1.62$ ,  $\alpha = 11.93^{\circ}$ .

the last station,  $x = 24.40$ , the experiment does not indicate the plateau in supercritical pressure that NCOREL predicts. The last plot, Fig. 36 shows the comparison at  $M_\infty = 1.62$ , and  $\alpha = 13.92$  which corresponds to a  $C_L \sim 0.47$ . In this figure, a crossflow shock develops at  $x = 10.60$ . A distinct shock is apparent in the test data at  $x = 19.90$ . NCOREL overpredicts the supercritical plateau at  $x = 24.40$ .

A comparison between NCOREL and test data at  $M_\infty = 2.00$ ,  $\alpha = 11.80^\circ$  is shown in Fig. 37. The test data represent the model with the alternate leading edge, and the NCOREL predictions are for the basic leading edge. The difference between the two leading edges are minor, with the alternate leading edge having slightly less camber very close to the leading edge. The agreement is excellent at all four stations. Overall, the agreement between the tunnel data and NCOREL is quite good.

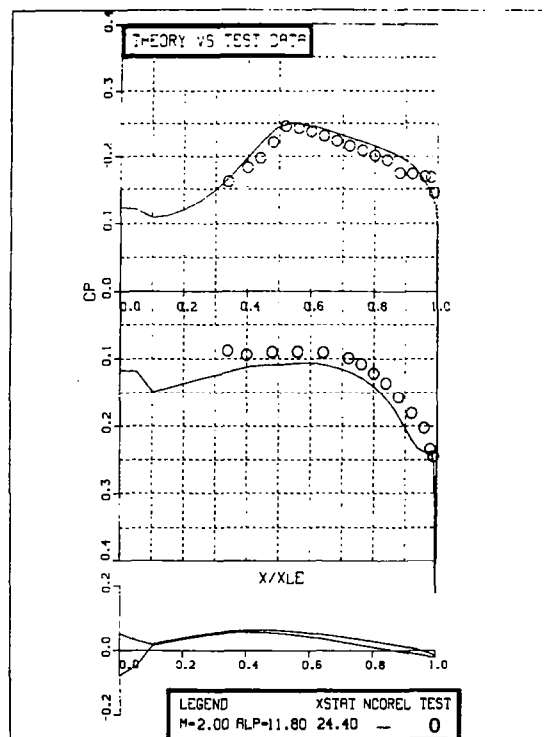
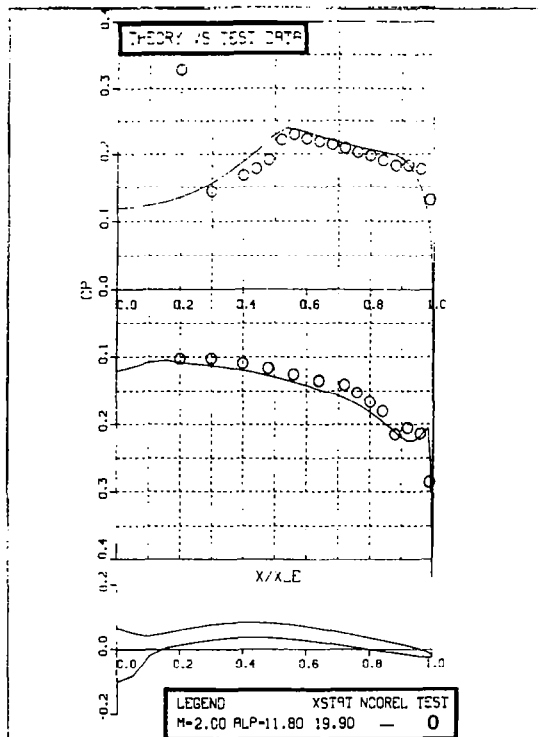
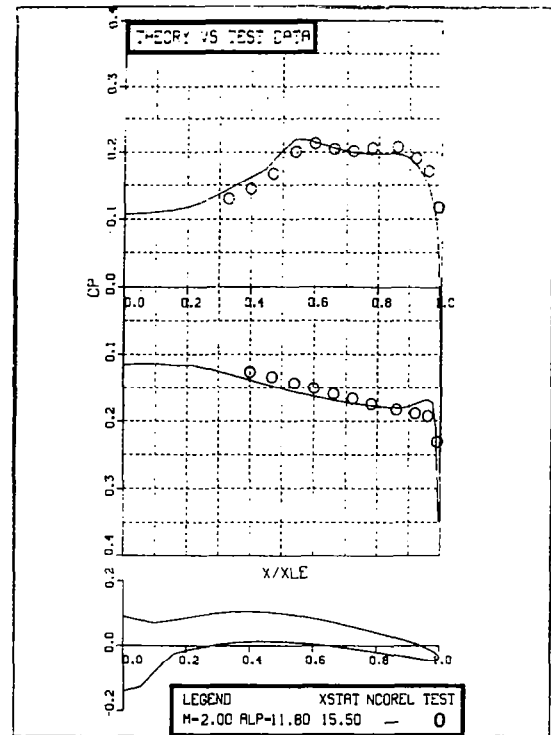
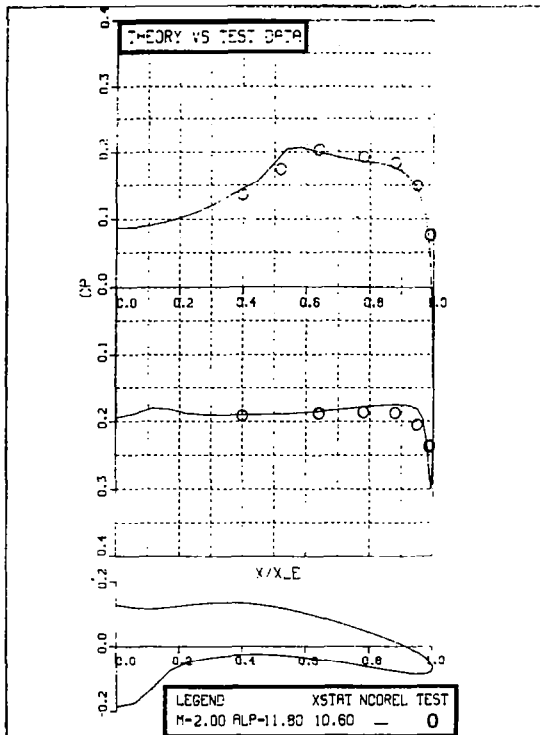
Figure 38 shows a series of isobar plots for the demonstration wing. The planform plotted is that computed by NCOREL where a small portion of the tip could not be computed. All the plots were generated by interpolating for 100 pressure coefficient levels between the limit of  $-0.5$  and  $+0.5$ . The dark regions indicate large pressure gradients. This occurs typically near the apex, leading edges and in the vicinity of crossflow shocks. On the leeward surface at  $\alpha = 7.92^\circ$ , a small compression occurs as the wing gets thinner toward the tip section. The crossflow compression develops with angle of attack and moves inboard. Finally, at  $\alpha = 13.92^\circ$ , a distinct cross flow shock is indicated in the isobar pattern. The leeward isobars become more parallel to the freestream with angle of attack. The windward surface isobar pattern does not change that dramatically with angle of attack. The compression due to the centerbody is quite apparent. An interesting feature is that the windward isobars tend to become parallel to the leading edge with angle of attack. The compression that occurs in the vicinity of the trailing edge is due to the trailing edge shock smearing.

As an interesting comparison, the equivalent flat wing was computed at approximately the same lift, i.e.,  $M_\infty = 1.62$ ,  $\alpha = 9.40^\circ$ . The flat wing has the same planform and thickness distribution of the DEMO wing. Figure 39 shows a comparison of the two isobar patterns. A very strong crossflow shock appears on the flat wing in comparison to the DEMO wing.



2246-039W

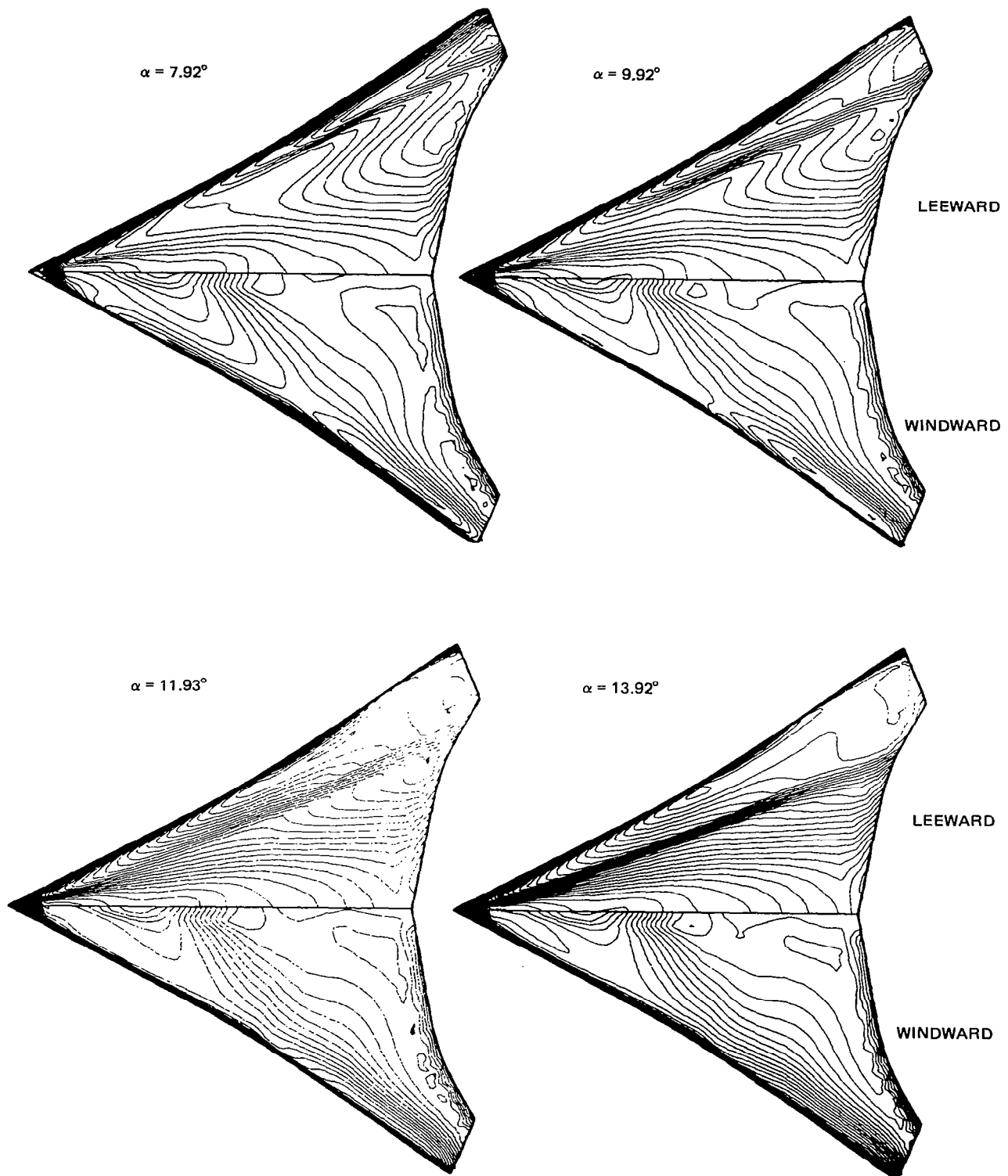
Figure 36 NCOREL Comparisons With DEMO Wing Surface Pressure Data,  $M_{\infty} = 1.62$ ,  $\alpha = 13.92^{\circ}$



2246-040W

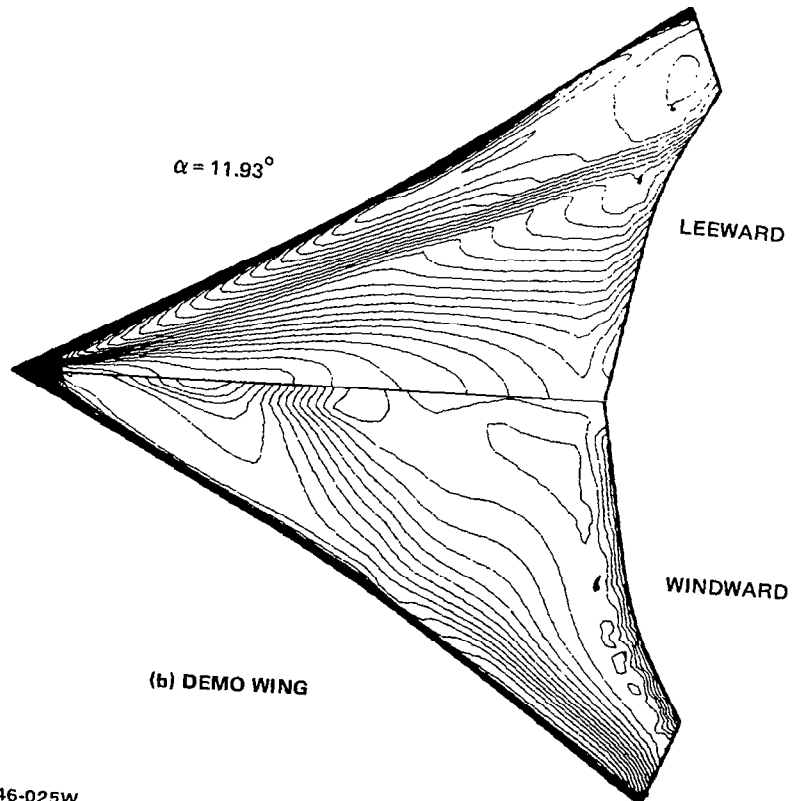
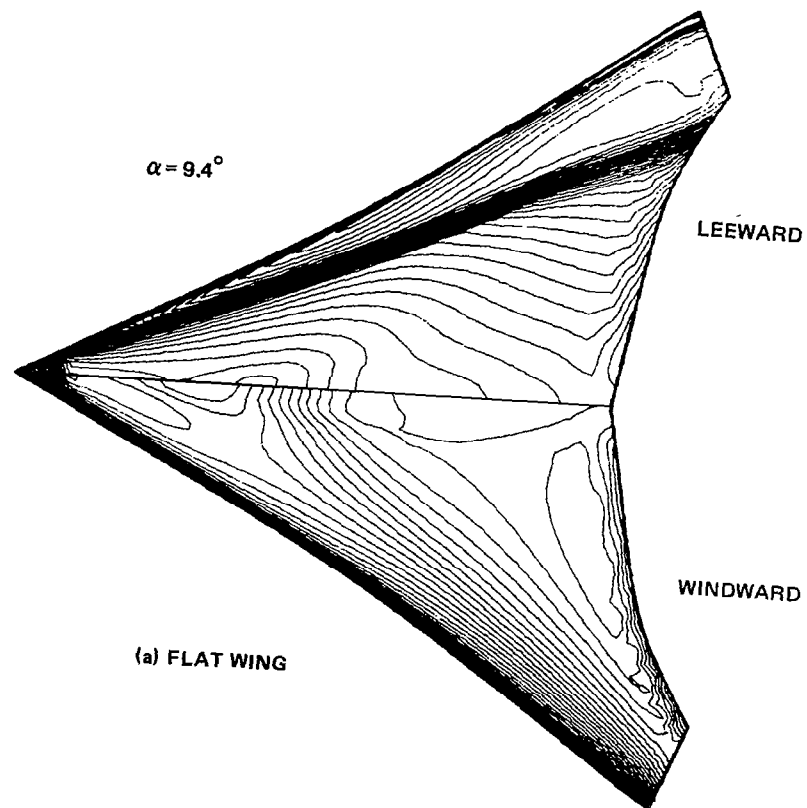
Figure 37 NCOREL Comparisons With DEMO Wing Surface Pressure Data,  $M_{\infty} = 2.00$ ,  $\alpha = 11.80^{\circ}$





2246-026W

Figure 38 Computed Isobar Patterns for the DEMO Wing,  $M_\infty = 1.62$



2246-025W

Figure 39 Computed Isobar Patterns at  $C_L = 0.40$ ,  $M_\infty = 1.62$

## 9 COMPUTER PROGRAM DESCRIPTION

### 9.1 ORGANIZATIONAL STRUCTURE

The NCOREL computer program in its segmented form requires about 215 K<sub>g</sub>, on a CDC computer. Segmentation was chosen over Overlay to reduce core requirements so that a more portable computer code would be created that could be run on either CDC or IBM machines. Segmentation, unlike Overlay, does not require changes in the source code to reduce core storage. Instead, a segmentation directives file is created that controls the sequential loading of subroutines in order to reduce core. A segmentation tree based on these directives is created that controls the sequential loading of subroutines in order to reduce core. The basic core requirements of the code is governed by the main level common blocks and subroutines and the branch segment or sublevel of the tree that requires the most core. Any number of other branches can be included in the logic without increasing core as long as the core of these branches are less than the core of the largest branch.

Figure 40 illustrates the basic subroutine dependence used in NCOREL and its branches or sublevels. Each level may have other subroutines included or secondary branches using other subroutines. The name of a branch or sublevel coincides with a subroutine name. The INCLUDE statement identifies other subroutines that are to be loaded simultaneously with the routine that the branch name identifies. Figure 41 further illustrates the breakdown and calling sequence of the somewhat complicated INITN branch. Figure 42 shows the segmentation directives for NCOREL. The GLOBAL statements include the labeled COMMON BLOCKS within a particular level. For example, the labeled common block named BLK1 is GLOBAL to the main level NCOREL. Hence, BLK1 is always stored in the main level and this information is available to any of the sublevels. In addition, the loading of any sublevel or branch does not destroy this information. This is true of all the labeled common blocks GLOBAL to the main level NCOREL. Any other common block information that is only specific to a sublevel is made GLOBAL to that sublevel. When that sublevel or branch is returned to main and another sublevel loaded, the information is lost or written over by the new sublevel being loaded. The CONUSE sublevel is a user supplied geometry package that needs a CONUSE subroutine. Any other subroutines that are required in CONUSE must be named

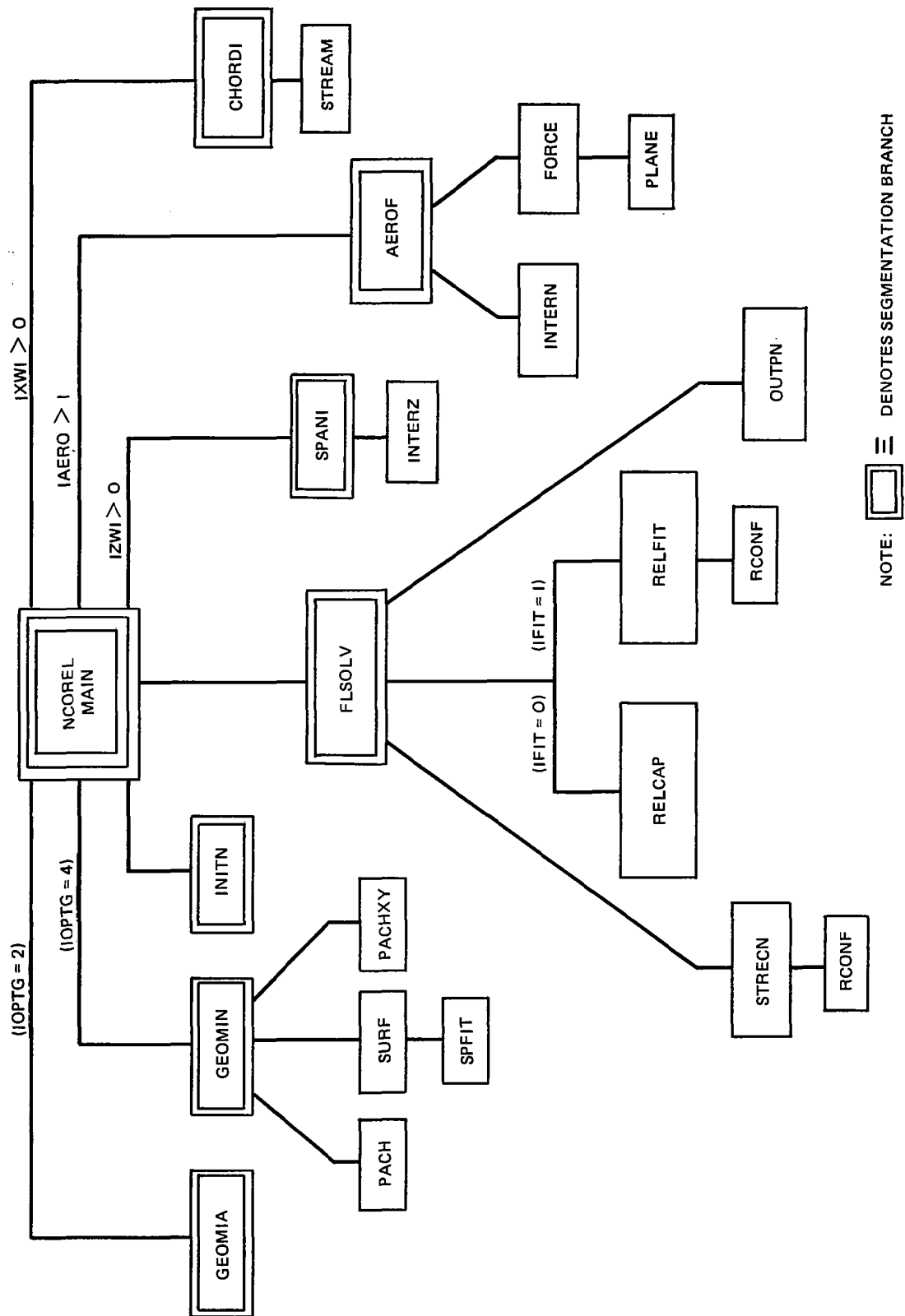


Figure 40 NCOREL Subroutine and Branch Organizational Chart

2246-002W

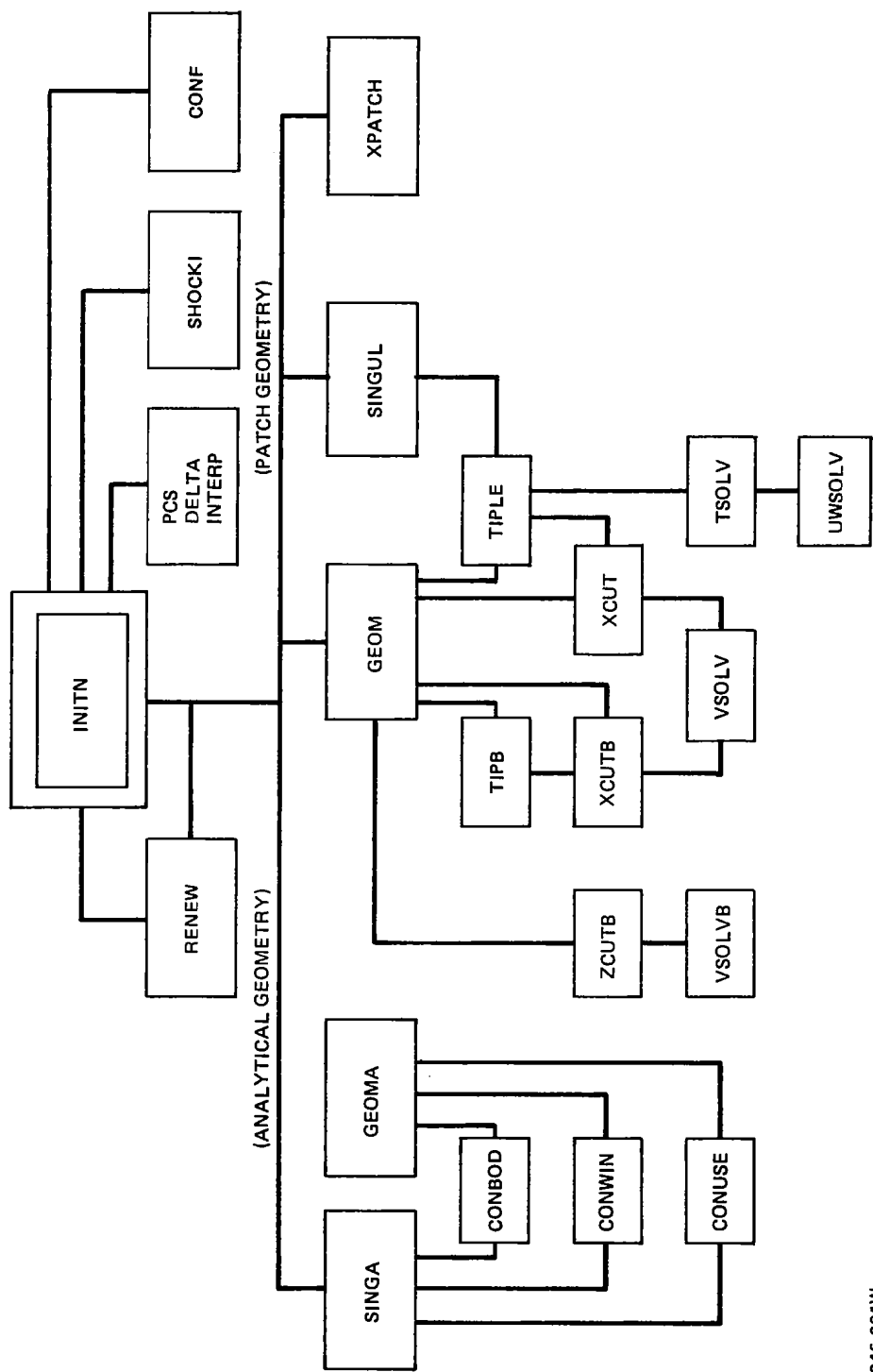


Figure 41 Subroutine Dependence in INITN Branch

2246-001W

# SEGLOAD DIRECTIVES.

```

      TREE      NCOREL-(INITN-(GEOM-(XCUT,XCUTB),
,GEOMA-(CONBOD,CONWIN,CONUSE)),
,FLSOLV-(STRECN,RELFIT,RELCAP,OUTPN),
,GEOMIN-(START,PACHXY,SURF-PACH-SPFIT),
,GEOMIA,SPANI,CHORDI,AEROF-(INTERN,FORCE))
*
      INCLUDE   PCS,INTERP,SHOCKI,GRAF,CONF,RCONF,DELTA,XTES
      GLOBAL    BLK1,GEO,TITL,RAD,BLK2,MAP,BLK2P
      GLOBAL    PATPLT,BOWSHK,PLO,DELZW1,DELZW2,DELZW3
      GLOBAL    DELZW4,DELZW5,DELZW6,INT,TE,SURVEY,AEROC
*
FLSOLV      GLOBAL    BLK3,BLK4
*
INITN       GLOBAL    TIP
INITN       INCLUDE   RENEW
*
GEOM        INCLUDE   XPATCH,SINGUL,VSOLV,VSOLVB
GEOM        GLOBAL    XPAT,XPATB,ERROR,FINDYM
*
XCUT        INCLUDE   TIFLE,TSOLV,UWSOLV
*
XCUTB       INCLUDE   ZCUTB,TIPB,YMBOD
*
FORCE       INCLUDE   PLANE
*
GEOMA       INCLUDE   SINGA
*
SPANI       INCLUDE   INTERZ
*
CHORDI      INCLUDE   STREAM
*
CONUSE      INCLUDE   AIRFOL
*
      END

```

**Figure 42 Segmentation Directives for NCOREL**

by the user in the INCLUDE statement. Figure 43 shows the segmentation tree diagram that is generated for a typical run. The only variation to the segmentation will occur in the INCLUDE statement for the user supplied CONUSE geometry. Segmentation reduces the core requirement by a factor of two to three. If large core is available, NCOREL can be run without segmentation as, for example, on a IBM 3033. Any small subroutines that are called throughout NCOREL have been included in the main level.

Figure 43 is also annotated to show the core required for each branch of the segmentation. The main program requires about 111 Kg. The relaxation routines that generate the cross flow solutions require about 164 Kg. The next largest branch, 174 Kg, involves the aerodynamic subroutines that interpolate and compute forces and moments. The largest branch of 212 Kg comes from the patch geometry subroutines. Hence, the patch geometry branch GEOM sets the core requirements for NCOREL.

## 9.2 SUBROUTINE DESCRIPTIONS

Table I groups the subroutines as to their function in NCOREL.

### MAIN PROGRAM NCOREL

This is the main program that reads and writes an echo of the input control data from TAPE 1. In addition, it controls the calling sequence of the sublevels. Any geometry initialization and reading of geometric data from TAPE 5 and storing of input parameters occurs within the main program.

```

TREE DIAGRAM.

*NCOREL (111K)
?
? _INITN (120K)
? ?
? ? _GEOB (210K)
? ? ?
? ? ? _XCUT
? ? ?
? ? ? _XCUTB
? ?
? ? _GEOBA (127K)
? ?
? ? _CONBOD
? ?
? ? _CONWIN
? ?
? ? _CONUSE
?
? _FLSOLV (164K)
? ?
? ? _STRECN
? ?
? ? _RELFIT
? ?
? ? _RELCAP
? ?
? ? _OUTPN
?
? _GEOBMIN (112K)
? ?
? ? _START (136K)
? ?
? ? _PACHXY
? ?
? ? _SURF
? ?
? ? _PACH
? ?
? ? _SPFIT
?
? _GEOBIA (112K)
?
? _SPANI (173K)
?
? _CHORDI (174K)
?
? _AEROF (111K)
?
? _INTERN
?
? _FORCE
FWA OF THE LOAD 1064
LWA+1 OF THE LOAD 213255

WRITTEN TO FILE ABS

TRANSFER ADDRESS -- NCOREL 76753

```

**Figure 43 Segmentation Tree Diagram for NCOREL**



**Table 1. Subroutine Groups**

**GROUP I**

(MAPPING, RELAXATION SOLUTION, AND SPHERICAL OUTPUT)

**GROUP IA**

**NCOREL (MAIN)**  
**INITN** – GEOMETRY MAPPING  
**FLSOLV**  
**STRECN** – METRICS  
**REL CAP** } RELAXATION  
**RELFIT** } SOLUTION  
**OUTPN** – SPHERICAL OUTPUT  
**RENEW** – REFINES  
MARCHING STEP

**GROUP IB**

(AUXILIARY PROGRAMS OF  
GROUP IA)  
**PCS** } PERIODIC CUBIC  
**DELTA** } SPLINE  
**INTERP** }  
**CONF** } WING MAPPING  
**RCONF** }  
**SHOCKI** – SHOCK GUESS

**GROUP II**

(ANALYTICAL OR USER  
SUPPLIED GEOMETRY)

**GEOMIA** – READ INPUT  
**GEOMA** – SPHERICAL CROSS  
CROSS SECTION  
**SINGA** – SINGULARITY  
LOCATION  
**CONBOD** – AXISYMMETRIC  
BODY  
**CONWIN** – ANALYTIC WINGS  
**CONUSE** – USER SUPPLIED

**GROUP III**

(HARRIS INPUT AND PATCH GEOMETRY)

**GROUP IIIA**

**GEOMIN**  
**START** – READS INPUT  
**GEOM** – SPHERICAL CROSS  
SECTION  
**SINGUL** – SINGULARITY  
**SURF** } PATCH GENERATION  
**PACH** }  
**SPFIT** – SPLINE FITTING  
**PACHXY** – PATCH CORNER  
POINTS  
**XPATCH** – SPHERICAL CUT  
PATCHES

**GROUP IIIB**

**XCUT** } TRANSVERSE  
**XCUTB** } SURFACE  
**ZCUTB** } COORDINATES  
**TIPLE** } SPHERICAL  
**TIPB** } LEADING EDGE  
**YMBOD**

**GROUP IIIC**

**VSOLV** } BI-CUBIC  
**VSOLVB** } PATCH EQUATION  
**TSOLV** } SOLVER  
**UWSOLV** }

<u>Subroutine Name</u>	<u>Purpose</u>
<u>GEOMIA</u>	Reads geometric parameters from TAPE5 and initializes and stores data used in the supplied analytical geometry package (IOPTG = 2).
<u>GEOMIN</u>	Reads Harris Wave Drag Input from TAPE5 and initializes data for Craidon Bi-Cubic Patch Geometry Option (IOPTG = 4).
( <u>START</u> )	Reads in Harris Wave Drag Input from TAPE5 and writes surface coordinate data on TAPE10.
( <u>SURF</u> )	Reads surface coordinate data from TAPE10 and controls writing of patches on TAPE 14.
( <u>PACH</u> )	Computes and writes Patch coefficient matrix on TAPE14.
( <u>SPFIT</u> )	Spline fits geometric surface data for patch definition.
( <u>PACHXY</u> )	Reads PATCH matrices from TAPE14 and computes and stores maximum and minimum coordinates of <u>BODY</u> and <u>WING</u> patches
<u>INITN</u>	Computes spherical geometry and mapped space body and shock information for relaxation solution
( <u>GEOM</u> )	Computes spherical geometry and singularity location at $r = r_0 + \Delta r$ where $r_0$ is the current solution station (IOPTG = 4).
( <u>XPATCH</u> )	Reads and sorts entire set of patches and stores patches required for spherical cut (IOPTG = 4).
( <u>SINGUL</u> )	Computes leading edge and singularity location at $r = r_0 + 2\Delta r$ (IOPTG = 4).
( <u>GEOMA</u> )	Computes spherical geometry and singularity at $r = r_0 + \Delta r$ . (IOPTG = 1, 2 or 3)
( <u>SINGA</u> )	Computes leading edge coordinates and singularity location at $r = r_0 + 2\Delta r$ . (IOPTG = 1, 2 or 3)
( <u>SHOCKI</u> )	Computes spherical coordinates of initial shock shape guess (BSF) or outer boundary (BSC)
( <u>CONF</u> )	Maps input body or shock physical spherical coordinates to mapped space.
( <u>PCS</u> )	Computes derivatives used in finding spline coefficients
( <u>DELTA</u> )	Determines spline fit parameters
( <u>INTERP</u> )	Interpolates from periodic cubic splines to find body or shock mapped space radii at mesh points.

<u>(RENEW)</u>	Recomputes body geometry when marching step size is refined.
<u>FLSOLV</u>	Controls the calling of subroutines STRECN, RELCAP, RELFIT, and OUTPN
<u>(STRECN)</u>	Computes mapping metrics, nonconical mesh derivatives, and freestream velocity components. Inverts mapping to obtain physical spherical mesh coordinates.
<u>(RELCAP)</u>	Computes spherical cross flow plane bow shock captured (BSC) relaxation solution for the reduced potential $F(I,J)$ when $IFIT = 0$ .
<u>(RELFIT)</u>	Computes spherical cross flow plane bow shock fit (BSF) relaxation solution for the reduced potential $F(I,J)$ when $IFIT = 1$ . Also recomputes mapped space bow shock coordinates $C(I)$ , its derivatives, and mesh metrics.
<u>(OUTPN)</u>	Outputs spherical cross flow plane solutions on TAPE6 and interpolates for cross flow sonic line and bow shock if $IFIT = 0$ . Also writes spherical solutions on TAPE7.
<u>(RCONF)</u>	Inverts mapping to obtain physical spherical coordinates given mapped space coordinates

NOTE: Two Cartesian coordinate systems are referenced and treated interchangeably in the geometry routines.  $Z_C = Y_A$ ,  $Y_C = Z_A$ ,  $Z_C = X_A$  where the subscript C refers to the cartesian coordinates associated with the spherical coordinate system and the subscript A refers to the standard aircraft coordinate system.

<u>SPANI</u>	Controls interpolation for transverse cross sectional data ( $Z_C = X_A = \text{constant}$ ) by reading arbitrary transverse locations specified as input on TAPE1.
<u>(INTERZ)</u>	Interpolates for a given $Z_C = X_A = \text{constant}$ station from spherical solutions read from TAPE7. Interpolated transverse coordinates and pressure data written on TAPE10.
<u>CHORDI</u>	Controls interpolation for chordwise data ( $X_C = Y_A = \text{constant}$ ) by reading for arbitrary chordwise locations specified as input on TAPE1.
<u>(STREAM)</u>	Interpolates for $X_C = Y_A = \text{constant}$ station from spherical data read from TAPE7. Writes interpolated coordinates and pressure data on TAPE14.
<u>AEROF</u>	Controls the computation of forces, moments, and areas.
<u>(INTERN)</u>	Interpolates and writes on TAPE2 transverse plane data used in force calculations from spherical data read from TAPE7.
<u>(FORCE)</u>	Computes forces, moments, and areas from set of quadrilateral panels determined by INTERN

(PLANE) Computes area, normal and axial force for a given triangular plane

XTES A subroutine used by CONUSE, INTERZ, STREAM, and INTERN to yield the  $(Z_{TE})_C$  or  $(X_{TE})_A$  given  $X_C$  or  $Y_A$ .

ANALYTICAL GEOMETRY SUBROUTINES  
(IOPTG = 1, 2, or 3)

GEOMA Iterates to find spherical geometry at  $r = r_0 + \Delta r$  where  $r_0$  is current solution station (IOPTG = 1, 2, or 3)

SINGA Computes leading edge coordinates and singularity location at  $r = r_0 + 2\Delta r$ . (IOPTG = 1, 2, or 3)

IOPTG = 1 (CONBOD) Given axial station  $Z_C$  or  $X_A$  computes radius of axisymmetric body of revolution. (NOTE: equation of body radius  $R = R(z_C)$  is supplied by user)

IOPTG = 2 (CONWIN) Analytical geometry package for conical and nonconical wings, bodies or wing-bodies. Given axial station  $Z_C$  or  $X_A$ , and spanwise coordinate  $X_C$  or  $Y_A$ , computes surface coordinate  $Y_C$  or  $Z_A$ .

IOPTG = 3 (CONUSE) User supplied geometry package simulates use of CONWIN

CRAIDON BI-CUBIC PATCH SUBROUTINES  
(IOPTG = 4)

GEOM Computes spherical surface geometry and singularity location from Harris Wave Drag Input and Bi-Cubic Surface Patches at  $r = r_0 + \Delta r$ .

(TIPB) Used in iteration procedure to find spherical maximum half-width of BODY cross section at given axial location. Given  $(Z, X)_C$  or  $(X, Y)_A$  it computes  $Y_C$  or  $Z_A$  of the body. Uses XCUTB, ZCUTB and MBOD.

(TIPLE) Used in iteration procedure to find spherical wing leading edge coordinates. Given  $(Z, X)_C$  or  $(X, Y)_A$  it computes the surface coordinate  $Y_C$  or  $Z_A$  of the leading edge. Uses TSOLV and XCUT.

(XCUTB) Used in iteration procedure to determine spherical BODY surface coordinates. Given  $(Z, X)_C$  or  $(X, Y)_A$  it computes  $Y_C$  or  $Z_A$ .

(XCUT) Used in iteration procedure to determine spherical WING surface coordinates. Given  $(Z, X)_C$  or  $(X, Y)_A$  it computes  $Y_C$  or  $Z_A$ .

(TSOLV) Used by TIPLE to compute WING leading edge coordinate from leading edge patches. Given  $U_{LE}$  and  $(Z, X)_C$  or  $(X, Y)_A$  it determines  $W$  by iteration to find  $Y_C$  or  $Z_A$ .

<u>(VSOLV)</u>	Used by XCUT and XCUTB, a Newton iteration method for finding U and W on a patch corresponding to given values of $(Z,X)_C$ or $(X,Y)_A$ yielding the surface coordinate $Y_C$ or $Z_A$ .
<u>(ZCUTB)</u>	Used by TIPB to find $X_C$ or $Y_A$ surface coordinate of a BODY patch given the coordinates $(Z,Y)_C$ or $(X,Z)_A$ .
<u>(VSOLVB)</u>	Newton iteration method for finding U and W on a BODY patch given $(Z,Y)_C$ or $(X,Z)_A$ yielding the surface coordinate $Y_C$ or $Z_A$ .
<u>(YMBOD)</u>	Determines maximum and minimum coordinates of a set of BODY patches. Used by TIPB

### 9.3 COMMON BLOCKS

The following is a partial description of the labeled common blocks used in the basic NCOREL subroutines. Labeled common blocks associated with the various geometry options are excluded.

<u>Label</u>	<u>Contents</u>
/BLK1/	LIN, LOUT, IC, JC, KT, DX, DY, WW, GA, EMINF, A02, GAMMA, RELW, DELMIN, PI, PIO2, ALP, IPLOT, EST, NOUT, JOUT, IRUN, IPUN, REWD, ISYM

<u>Variable</u>	<u>Definition</u>
LIN = 1	Input device for namelist data
LOUT = 6	Output print device
IC	Initial number of mesh points in X or $\theta$ direction
JC	Initial number of mesh points in Y or $\rho$ direction
KT	Maximum number of iterations in the relaxation routines
DX	Mesh size in computational X or $\theta$ direction
DY	Mesh size in computational Y or $\rho$ direction
WW	Over-relaxation parameter
GA	Specific heat ratio parameter
EMINF	Freestream Mach number
A02	Stagnation speed of sound squared,
GAMMA	Ratio of specific heats
RELW	Bow shock fit relaxation parameter
DELMIN	Convergence tolerance on potential solution
PI	$\pi$
PIO2	$\pi/2$
ALP	Angle of attack (radians)
IPLOT	Plotting parameter
EST	Coefficient of temporal artificial viscosity
NOUT	Print control parameter
IRUN	Restart control parameter
IPUN	Punch control parameter for restarting
REWD	Spherical termination station
ISYM	Symmetry control parameter

<u>Label</u>	<u>Contents</u>
/GEO/	NG, NS, AZ, BZ, NBOD
<u>Variable</u>	<u>Definition</u>
NG	Number of spherical cross sectional geometry points
NS	Mesh control parameter for bow shock capture
AZ	Tangent of leading edge planform half angle used in patch geometry
BZ	Not used
NBOD	Number of spherical body cross sectional geometry points

<u>Label</u>	<u>Contents</u>
/SURVEY/	KIT, IDIV
<u>Variable</u>	<u>Definition</u>
KIT	Number of iterations for convergence at an r-station
IDIV	IDIV = 0, spherical station has converged IDIV = 1, spherical station has diverged

<u>Label</u>	<u>Contents</u>
/TE/	IZW, ITE, ZTE, XTEBK, ZTIP
<u>Variable</u>	<u>Definition</u>
IZW	Print control for interpolated Z - stations
ITE	Triggers call of trailing edge subroutine XTES
ZTE	Default z-station for terminating force calculation
XTEBK	Spanwise location of break in trailing edge
ZTIP	Axial termination of wing tip

<u>Label</u>	<u>Contents</u>
/AERO/	CBAR, YCG, ZCG
<u>Variable</u>	<u>Definition</u>
CBAR	Aerodynamic chord used in moment coefficient definition
YCG	Vertical location of moment center
ZCG	Axial location of moment center

<u>Label</u>	<u>Contents</u>
/RAD/	R, DZ, KR, KRAD, IOPTG, IOPTS, EP, IFIT

<u>Variable</u>	<u>Definition</u>
-----------------	-------------------

R	Spherical r - station
DZ	Step size in marching direction
KR	Radial station integer KR = 1, conical station (R = 0) KR > 1, nonconical stations (R > 0)
KRAD	Marching step size refinement parameter
IOPTG	Geometry option parameter
IOPTS	Bow shock capture option parameter
EP	Bow shock guess parameter
IFIT	BSC or BSF option parameter

<u>Label</u>	<u>Contents</u>
--------------	-----------------

/MAP/	S0, S1, S2, PII, CSCAL, SOPR, S1PR, SON, S1N, S2N, SOPRN S1PRN, S2PRN
-------	--

Note: Complex numbers except for PII and CSCAL

<u>Variable</u>	<u>Definition</u>
-----------------	-------------------

S0	Singularity location in mapped space, $S_0$ , at r
S1	Complex conjugate of singularity location, $\bar{S}_0$ , at r
S2	Singularity shift in mapped space, at r
PII	$\pi$ , constant
CSCAL = 1.0	Not used
SOPR	Radial derivative of mapped singularity, $S_{0r}$ at r
S1PR	Radial derivative of conjugate, $\bar{S}_{0r}$ at r
S2PR	Radial derivative of singularity shift, $S_{2r}$ at r
SON	Singularity location in mapped space, $S_0$ , at $r + \Delta r$
S1N	Complex conjugate of singularity location, $\bar{S}_0$ , at $r = r + \Delta r$
S2N	Singularity shift in mapped space, at $r + \Delta r$
SOPRN	Radial derivative of mapped singularity, $S_{0r}$ at $r + \Delta r$
S1PRN	Radial derivative of conjugate, $\bar{S}_{0r}$ at $r + \Delta r$
S2PRN	Radial derivative of singularity shift, $S_{2r}$ at $r + \Delta r$

<u>Label</u>	<u>Contents</u>
--------------	-----------------

/BOWSHK/	THEB(201), RHOB(201), THES(201), RHOS(201)
----------	--

<u>Variable</u>	<u>Definition</u>
-----------------	-------------------

THEB	Body theta locations in mapped space from input geometry cross sectional points
RHOB	Body radii in mapped space from input geometry cross sectional points
THES	Bow shock theta locations in mapped space
RHOS	Bow shock radii in mapped space

<u>Label</u>	<u>Contents</u>
/PLO/	XXB(60), YYB(60)
<u>Variable</u>	<u>Definition</u>
XXB	Physical body spherical coordinates (X/Z) at mesh points
YYB	Physical body spherical coordinates (Y/Z) at mesh points

<u>Label</u>	<u>Contents</u>
/INT/	L(201), D(201)
<u>Variable</u>	<u>Definition</u>
L,D	Used in periodic spline fit routines

<u>Label</u>	<u>Contents</u>
/TIP/	XTIP, YTIP, XSIN, YSIN
<u>Variable</u>	<u>Definition</u>
XTIP	Leading edge physical coordinate x
YTIP	Leading edge physical coordinate y
XSIN	Singularity physical coordinate x
YSIN	Singularity physical coordinate y

Note: Labeled blocks /BLK2/, /BLK2P/, /BLK3/, and /BLK4/ are large core common blocks.

<u>Label</u>	<u>Contents</u>
/BLK2/	F(60,60), H(60,60), X(60), B(60), BPR(60) BSEC(60) C(60), CPR(60), CSEC(60), H1(60,60), H2(60,60)
<u>Variable</u>	<u>Definition</u>
F(I,J)	Reduced potential at R
H(I,J)	Mapping metrics for mesh at R
X(I)	Sheared computational coordinate
Y(I)	Sheared computational coordinate
B(I)	Body mapped radius
BPR(I)	Mapped body derivative, $B_{\theta}$
BSEC(I)	Mapped body derivative, $B_{\theta\theta}$
C(I)	Bow shock (BSF) or Outer Boundary (BSC) mapped radii
CPR(I)	Mapped bow shock/boundary derivative, $C_{\theta}$
CSEC(I)	Mapped bow shock/boundary derivative, $C_{\theta\theta}$
H1(I,J)	Nonconical mapped mesh derivative, $\rho_r$
H2(I,J)	Nonconical mapped mesh derivative, $\rho_{\theta r}$



<u>Label</u>	<u>Contents</u>
/BLK2P/	FP(60,60), FPP(60,60), BR(60), BRR(60), BRTH(60), CR(60), CRR(60), CRTH(60), BN(60), CN(60), CP(60), CPP(60)

<u>Variable</u>	<u>Definition</u>
FP(I,J)	Reduced potential at $R - \Delta R$
FPP(I,J)	Reduced potential at $R - 2\Delta R$
BR(I)	Nonconical mapped body derivative $B_R$
BRR(I)	Nonconical mapped body derivative $B_{RR}$
BRTH(I)	Nonconical mapped body derivative $B_{R\theta}$
CR(I)	Nonconical mapped bow shock/boundary derivative $C_R$
CRR(I)	Nonconical mapped bow shock/boundary derivative $C_{RR}$
CRTH(I)	Nonconical mapped bow shock/boundary derivative $C_{R\theta}$
BN(I)	Body mapped radius at $R + \Delta R$
CN(I)	Bow shock/boundary radius at $R + \Delta R$
CP(I)	Bow shock/boundary radius at $R - \Delta R$
CPP(I)	Bow shock/boundary radius at $R - 2\Delta R$

<u>Label</u>	<u>Contents</u>
/BLK3/	VI(60,60), UI(60,60), WI(60,60)

<u>Variable</u>	<u>Definition</u>
VI(I,J)	Freestream velocity component in mapped $p$ direction
UI(I,J)	Freestream velocity component in mapped $\theta$ direction
WI(I,J)	Freestream velocity component in spherical $r$ direction

<u>Label</u>	<u>Contents</u>
/BLK4/	HP(60,60,), H1P(60,60), H2P(60,60)

<u>Variable</u>	<u>Definition</u>
HP(I,J)	Mapping metrics at $R - \Delta R$
H1P(I,J)	Nonconical mapped mesh derivative at $R - \Delta R$
H2P(I,J)	Nonconical mapped mesh derivative at $R - \Delta R$

#### 9.4 I/O UNIT DEVICES


The following is a description of the I/O units utilized in NCOREL and their purpose.

<u>Unit</u>	<u>Usage</u>
TAPE1	Namelist input device Input for arbitrary spanwise and chordwise interpolation
TAPE2	Used in force computations (contains $z$ station data)

TAPE5	Input device for geometry data
TAPE6	Print device for output
TAPE7	Spherical data output device (surface coordinates, pressure and bow shock data)
TAPE8	Flow field data output device for restarting NCOREL at R > 0. Also, flow field data input device for restart.
TAPE10	Used in patch geometry definition; Chordwise interpolated data output device
TAPE14	Used in patch geometry definition; Spanwise interpolated data output device

Table 2 shows the I/O unit devices and the subroutines which utilize them.

**Table 2. External Device Usage**

	TAPE1	TAPE2	TAPE5	TAPE7	TAPE8	TAPE10	TAPE14
							
MAIN	X						
INITN					X		
OUTPN				X	X		
GEOMIA			X				
START			X			X	
SURF						X	X
PACH						X	X
PACHXY						X	X
XPATCH						X	X
AEROF		X		X			
INTERN		X		X			
FORCE		X					
SPANI	X			X			
INTERZ				X		X	
CHORDI	X			X			
STREAM 2240-004W				X			X



10.1 INPUT PARAMETERS

Card No. 1                      Description Title of Geometry

Card No. 2                      Title Describing Freestream Conditions

Note: Cards No. 1 and 2 are alphanumeric title cards and must be less than 80 characters.

Note: The remainder of the input is in namelist format. Recommended default values of certain parameters are suggested.

<u>Namelist Variable</u>	<u>Description</u>
EMINF	Mach Number ( $M > 1$ )
ALP	Angle of Attack (degrees)
ISYM	If ISYM = 0, half plane symmetry will be assumed.  If ISYM = 1, quarter plane symmetry is assumed.
GAMMA = 1.4	Ratio of Specific Heat
EST = -0.1	Coefficient of Temporal Artificial Viscosity ( $-5.0 < EST < 0.0$ )
IC	Circumferential Mesh Points (IC-1) (Maximum IC = 58), must be even number
JC	Radial Crossflow Mesh Points (JC-1) (Maximum JC = 58), must be even number

Note: IC and JC apply only for crude conical grid subject to conical mesh refinement. IC and JC must be even numbers.

KMAX (1)	Maximum number of iterations for each conical mesh
KMAX (2)	
KMAX (3)	
KREF	Conical grid refinements. Maximum two refinements. Refinement given by $2(IC-1)$ and $2(JC-1)$ . Final mesh not to exceed $IC = JC = 58$ . ( $1 < KREF < 3$ )
KMAXNC	Maximum nonconical iterations.

DMIN (1)	Convergence tolerances for each conical
DMIN (2)	grid. Nonconical tolerance given by
DMIN (3)	DMIN (1).

Note: Currently,  $10^{-5}$  to  $10^{-7}$  is used for the bow shock capturing (IFIT = 0) tolerance on the correction to potential.  $10^{-2}$  to  $10^{-4}$  is used for bow shock fitting (IFIT = 1) tolerance on maximum residual.

<u>Namelist Variable</u>	<u>Description</u>
W(1) = 1.5 W(2) = " W(3) = "	Relaxation parameter for SLOR scheme.
RELSHK(1) RELSHK(2) RELSHK(3)	Conical Bow Shock relaxation parameters. Bow shock fitting only. $0 < \text{RELSHK} < 1.0$
RELNC = 1.5	Nonconical bow shock fit relaxation parameter
IFIT	IFIT = 0, Bow Shock is captured IFIT = 1, Bow Shock is fit.
IOPTS	<u>Bow Shock capture options</u> IOPTS = 0, Outer boundary not conformed to shock shape.  IOPTS = 1, after first conical mesh bow shock is conformed to captured shock shape for further conical mesh refinements.  IOPTS = 2, Nonconical meshes are conformed to previous captured bow shock shape.
NS = 4 (IOPTS = 0) = 4-8 (IOPTS = 1,2)	Used in bow shock capturing scheme to position mesh beyond initial shock shape guess.
EP > 1.0 (IFIT = 0) > 1.0 (IFIT = 1)	If EP = 1.0, initial conical guess for bow shock shape is the rotated mach cone.

Note: For Bow Shock Fit, IFIT = 1, the following parameters must be set:  
IOPTS = 0, NS = 0.

NOUT	<u>Controls output print</u> , if NOUT = 0, no mapped plane variables and derivatives are output. Minimum output. If NOUT = 1, maximum mapped plane output.
JOUT	If JOUT = -1, minimum output for solution (only on body surface).

If JOUT = 0, body surface and shock surface (IFIT = 1) output and three coordinate lines are output from body to bow shock.

Namelist Variable

Description

	If JOUT = 1, maximum output of entire crossflow mesh. If JOUT > 1, every JOUT coordinate line from body surface to bow shock will be output.
IPUN	If IPUN = 0, the solution will not be punched out to restart. If IPUN = 1, the solution will be punched out on TAPE8.
IRUN	If IRUN = 0, new run If IRUN = 1, restart run, reads data from TAPE8
DZ	Marching Step size
KRR (1)	If KRR = 0, marching step size will not be refined.  If KRR > 0, marching step size will be decreased. New step size will be $DZ = DZ/KRR$  If KRR < 0, marching step size will be increased. New step size will be $DZ = DZ *  KRR $ . KRR constrained to -2.
KRR (2)	
KRR (3)	
KRR (4)	
KRR (5)	
RZNEW (1)	R stations at which marching step size is changed.
RZNEW (2)	
RZNEW (3)	
RZNEW (4)	
RZNEW (5)	
IOPTG	<u>Geometry Options</u>  If IOPTG = 1, axisymmetric body subroutine <u>CONBOD</u> is used to generate geometry (user supplied or altered).  If IOPTG = 2, subroutine <u>CONWIN</u> is used for geometry. This subroutine can generate conical and 3D wings or wing body with circular arc camber and elliptical cross section. Requires input on Tape 5.  If IOPTG = 3, subroutine <u>CONUSE</u> will be used to generate geometry. User supplied. Any input data should be read from TAPE5.

If IOPTG = 4, Craidon patch geometry routines are used with Harris wave drag input required on Tape 5.

NG                      Number of geometry points generated in cross flow plane. Generally, NG > IC after mesh refinement. (NG must be odd)

AZ                      Maximum half angle in degrees of configuration (for IOPTG = 4 only).

BZ = 1.0                Not used.

REND                    Solution terminates at R = REND.

NT                      Alternate termination of program after NT steps.

IPLLOT = 2              Inoperable.

IAERO                    If IAERO = 0, aerodynamic coefficients are not computed.

                          If IAERO = 1, aerodynamic coefficients are computed at end of output.

ZCG                     Axial moment center.

YCG                     Vertical moment center.

CBAR                    Aerodynamic chord used for nondimensional moment coefficient.

ITE                     If ITE = 0, trailing edge subroutine XTES will not be called. Force calculation will terminate at z = ZTE

                          If ITE = 1, trailing edge subroutine XTES will be called and used by force subroutines.

ZTE                     Default location of trailing edge. If ITE = 0, a straight trailing edge with zero sweep or a body will be assumed where forces are computed to z = ZTE.

IZW                     If IZW = 0, interpolated z - station data used in force calculation will not be printed.

                          If IZW = 1, interpolated z - station data will be printed.



IXWI                      If IXWI = 0, no chordwise stations are read for interpolation output.

                            If IXWI > 0, IXWI chordwise interpolation stations will be read from TAPE1 and x-station interpolated output will be printed.

IZWI                      If IZWI = 0, no spanwise stations are read for interpolation output.

                            If IZWI > 0, IZWI spanwise interpolation stations will be read from TAPE1 and z-station interpolated output will be printed.

#### Auxillary Input on TAPE1

This input uses a format of 10F7.4 and only occurs if either IXWI or IZWI are not zero.

#### IZWI Input Set:

Up to 25 arbitrary spanwise z stations can be input for interpolation.

#### IXWI Input Set:

Up to 25 arbitrary chordwise x-stations can be input for interpolation.

#### Geometric Input (TAPE 5)

#### IOPTG = 2

A total of six input cards corresponding to five geometric axial sections are required for this geometry option with Format 7F10.5.

Each card has the following format:

$$z, \delta_F, \delta_E, \delta_T, \delta_{TC}, \delta_P, \delta_B$$

where z refers to z-station and the remaining six numbers are angles in degrees.

<u>Card No.</u>	<u>Variables</u>
1	ZW1, DELFW1, DELEW1, DELTW1, DELCW1, DELPW1
2	ZW2, DELFW2, DELEW2, DELTW2, DELCW2, DELPW2
3	ZW3, DELFW3, DELEW3, DELTW3, DELCW3, DELPW3
4	ZW4, DELFW4, DELEW4, DELTW4, DELCW4, DELPW4

5	ZW5, DELFW5, DELEW5, DELTW5, DELCW5, DELPW5, DELPB5
6	ZW6, DELFW6, DELEW6, DELTW6, DELCW6, DELPW6, DELPB6
<u>Variable</u>	<u>Definition</u>
z	z- station
DELFW	Spanwise angular location for camber If DELFW = 0, entire spanwise section will have circular arc camber.
DELEW	Spanwise angular location for elliptical thickness distribution  If DELEW = 0, cross section will be elliptical.  If $0 < \text{DELEW} < \text{DELTW}$ , section inboard of DELEW has constant thickness, outboard of DELEW has elliptical thickness.
DELTW	Leading edge half angle ( $90^\circ - \Delta$ )
DELCW	Maximum circular arc leading edge camber angle
DELPW	Centerline half thickness angle of wing
DELPB	Centerline half thickness angle of wing-body cross section.

General Rules for Analytical Geometry Package (IOPTG = 2)

- 1) The geometry must be initiated with a circular cone at  $z = Z1$  with  $\text{DELFW1} = \text{DELTW1} = \text{DELPW1}$  and  $\text{DELEW1} = \text{DELCW1} = 0$ .
- 2) Card No. 2 for  $z = ZW2$  is identical to card No. 1 except  $\text{DELPW2} = 0$ .
- 3) The geometry will deform from a circular cone at  $z = ZW1$  to a conical geometry section between  $z = ZW3$  and  $z = ZW4$ .
- 4) The angular definitions of cards No. 3 and 4 must be identical, since a conical section is assumed between  $z = ZW3$  and  $z = ZW4$ .
- 5) Wing-body cross section can only be generated for  $z > ZW5$ . Body angular definition only required for card no. 5 and 6.

- 6) Conical wing-body or wing section will be generated between  $z = ZW5$  and  $z = ZW6$ . Angular definitions on cards 5 and 6 must be identical. If  $DELP = DELPB$  on cards 5 and 6, wing-body cross section will not be generated. If  $DELPB > DELP$ , a wing body cross section is generated.
- 7)  $DELE$  must be less than  $DELT$ .
- 8)  $DELF$  must be less than or equal to  $DELT$ .

#### Harris Wave Drag/Craidon Patch Geometry (IOPTG = 4)

This input is also read from TAPE5. A detailed description of this geometry input is located in several references and will not be repeated. (see Ref. 10)

Restrictions: Only wing, fuselage, or wing-body options apply to NCOREL. Fuselage must be treated as individual component and should be smooth (i.e., no corners). Wing definition must extend to centerline and origin of geometry must be at (0,0,0). For wing-body configurations, apex of wing should be on axis of coordinate system ( $Y_A = Z_A = 0$ ).

Note: Centerline wing or body twist should be removed from geometry and included in angle of attack. Severe centerline camber on bodies or wings that cause origin of coordinate or apex to lie outside of cross section will not run in NCOREL.

## 10.2 PRINTED OUTPUT

Note: The first set of printed output echoes the input parameters.

<u>Output Block</u>	<u>Description</u>
Spherical Geometry	NG Input Geometry points are printed at new radial station ( $R = R + DR$ ).
<u>Variable</u>	<u>Description</u>
IG	IG = 1, lower symmetry plane IG = NG, upper symmetry plane
R	Spherical Radius
x	Spanwise Coordinate
y	Vertical Coordinate
z	Axial Coordinate
OMEG	Spherical angle (degrees)
PSI	Spherical angle (degrees)
<u>Output Block</u>	<u>Description</u>
Map Singularity	The location of the mapping singularity and derivatives at the current R and new $R + \Delta R$ station are printed for both the physical and mapped space.
<u>Output Block</u>	<u>Description</u>
Body Mesh Data (Not printed if NOUT = 0)	Blocks of variables are printed for the body surface ( $J = 2$ ) used in solution at current R station.

### Block #1

<u>Variable</u>	<u>Description</u>
X	Mapped space circumferential coordinate ( $X = \theta$ )
B	Mapped space body radius ( $B = \rho$ )
BPR	Mapped Space body derivatives $B_\theta$
BSEC	$B_{\theta\theta}$
BR	$B_R$
BRR	$B_{RR}$
BRTH	$B_R$

### Block #2

<u>Variable</u>	<u>Description</u>
X	Mapped space circumferential coordinate ( $X = 0$ )
C	Mapped space shock (IFIT = 1) or outer boundary (IFIT = 0) radius  Mapped space shock or outer boundary derivatives
CPR	$C_\theta$
CSEC	$C_{\theta\theta}$
CR	$C_R$
CRR	$C_{RR}$
CRTH	$C_R$

### Block #3

X/Z Y/Z	Physical Space Body Mesh Coordinates
H UI VI WI	Mapping metric Mapped space freestream velocities
H1 H2	Radial mesh derivatives $\rho r$ Radial mesh derivatives $\rho \theta r$

### Block #4

	Metric derivatives in computational space
HX	$h_x$
HY	$h_y$
HR	$h_r$
H1X	$h_{1x}$
H1Y	$h_{1y}$
H1R	$h_{1r}$
H2X	$h_{2x}$

H2Y	$h_{2y}$
H2R	$H_{2R}$

#### Output Block

Solution Convergence History  
(Not printed if NOUT = 0)

<u>Variable</u>	<u>Description</u>
Iter	Iteration
DELMX	Maximum correction to potential
I J	Mesh point where maximum Correction occurs
DELAvg	Average correction
RESMX	Maximum residual
I J	Mesh point where maximum residual occurs
RESAvg	Average residual
KSUP	If IFIT = 0, number of supersonic points outside captured bow shock IFIT = 1, number of supersonic crossflow points
DELS	(Only printed if IFIT = 1) Maximum residual in shock jump equation
IS	Shock Mesh point where maximum residual occurs.

#### Output Block

##### Bow Shock Mesh Location

Only printed if IFIT = 0. The JS = J mesh location of the last supersonic point that occurs starting with J = JC-2 and decreasing J. The JS-1 mesh point corresponds to the subsonic side of the captured bow shock.

Note: The J mesh location must not exceed JC-3 or erroneous results may be obtained.

#### Output Block

Mesh and Solution

### Block #1

Body coordinates and surface data ( $J = 2, I = 2$  to  $IC$ )

<u>Variable</u>	<u>Description</u>
RHO	Cross flow mapped radius
F	Reduced potential
X/Z Y/Z Z	Physical space spherical coordinates
M	Total Mach number
$M_R$	Radial Mach number
MC	Cross flow Mach number
CP	Pressure coefficient

### Block #2

Bow shock coordinates and surface data ( $J = JC, I = 2$  to  $IC$ )  
Printed only if  $IFIT = 1$

Above output is printed for the bow shock surface.

### Block #3

#### RADIAL OUTPUT DATA IN CROSSFLOW PLANE

This output is printed only if  $JOUT > 0$ . Above printout occurs for  $I =$  constant and  $J = 2$  to  $JC$ . If  $JOUT = 0$ , Printout occurs at  $I = 2, I = 1 + \frac{IC}{2}$  and  $I = IC$ .

### Block #4

#### INTERPOLATED CROSSFLOW SONIC LINE

If  $JOUT > 0$ , the interpolated physical coordinates ( $X/Z, Y/Z$ ) of the embedded cross flow sonic line are printed.

#### INTERPOLATED BOW SHOCK

Occurs only if  $IFIT = 0$  and  $JOUT > 0$ , interpolated physical coordinates of the outer sonic line.

Note: The above printout occurs for each  $R$  station computed.

Note: The code will terminate at  $R = \text{REND}$  or after NT steps. If the message:

SOLUTION HAS DIVERGED AT  $R =$

the solution diverges and run will terminate and proceed to next set of output.

Output Block

END OF RUN ITERATION SURVEY

This set of output summarizes the number of iterations required for convergence at each R Station.

TOTAL NUMBER OF ITERATIONS =

This number reflects the total number of iterations required for the computation.

Output Block

If  $IZW = 1$  and  $IAERO = 1$ , spanwise data is interpolated and printed.

Output Block

AERODYNAMIC OUTPUT DATA

IF  $IAERO = 1$ , aerodynamic coefficients are computed.

Block #1

HALF CROSS SECTIONAL AREA

This output prints the cross sectional area for each of the interpolated z stations

Block #2

SECTIONAL OR INCREMENTAL AREAS, FORCES, AND COEFFICIENTS

This output prints the forces and moments on each spanwise increment for half of the symmetric configuration.

<u>Variable</u>	<u>Description</u>
Z	Axial Station
	<u>Incremental:</u>
SREF(DZ)	planform area



SAREA (DZ)	surface area
FN(DZ)	normal force
FA(DZ)	axial force
CN(DZ)	normal force coefficient
CA(DZ)	axial force coefficient
CL(DZ)	lift coefficient
CD(DZ)	drag coefficient
CM(DZ)	moment coefficient

Note: The above coefficients are nondimensionalized by the incremental span areas.

#### Block #2

#### AXIAL INTEGRATION OF AREAS AND COEFFICIENTS

<u>Variable</u>	<u>Description</u>
Z	axial station
XMIN	location of centerline or trailing edge of wing
XMAX	Maximum spanwise coordinate or leading edge of wing
SREF(Z)	planform area
STOT(Z)	surface area
CN(Z)	normal force coefficient
CA(Z)	axial force coefficient
CL(Z)	lift coefficient
CD(Z)	drag coefficient
CM(Z)	moment coefficient

Note: The last set of numbers represent the total areas, forces, and moments of the configuration. Coefficients are nondimensionalized by the computed planform area.

## Block #2

The freestream conditions, total lift, drag and moment coefficients, and the aerodynamic constants used in this computation are printed.

### 10.3 SAMPLE CASES

Figure 44 illustrates a sample user supplied CONUSE subroutine for generating the cross sectional coordinates of an arrow wing with 33 degrees leading edge sweep and 27.214 degrees trailing edge sweep with a symmetrical 4% thick NACA four digit airfoil specified for the chordwise thickness. The wake extension is specified by extending the trailing edge thickness.

Figure 45 illustrates two sample input data sets for  $M_\infty = 1.70$  and  $\alpha = 5^\circ$  with a marching step size  $DZ = 1.0$ . Figure 45a illustrates the input data for the bow shock capture method (BSC), and Fig. 45b illustrates the equivalent data set for the bow shock fit method (BSF).

Figure 46 illustrates the printed output when  $NOUT = 1$  and  $JOUT = 0$  for the BSF method. The first station printed is at  $R = 0$  or the conical station. The NG spherical geometry points are printed at  $R = R + \Delta R$ . The geometry is then assumed to be conical between  $R = 0$  and  $R = 1$ . The singularity location in both the physical and mapped space are printed. At the conical station ( $R = 0$ ), all the  $R$  derivatives of the body (B), bow shock or outer boundary (C), metric (H), mesh derivatives ( $H_1, H_2$ ), and mapped space singularity location ( $S_0$ ) and its conjugate ( $S_1 = \overline{S_0}$ ) as well as ( $S_2$ ) are identically zero.

Following the mapped space metric data, the iterative solution commences. For the BSF method, the solution is converged when both the maximum residual (RESMX) of the full potential equation and the maximum residual of the isentropic shock jump condition (DELS) are reduced to the specified tolerances. The tolerance specified in the input was  $10^{-3}$  for the maximum residual. An internal tolerance of  $10^{-5}$  has been set on the correction for the shock position C represented by DELCMX. DELS and DELSHK represent the maximum residual of the shock jump condition which is used at nonconical stations. The location (I,J) of the maximum correction and residual for the potential are given and the location of the maximum residual in the shock jump condition is also specified. For the conical station, the internal flow usually converges first followed by the shock jump condition. The body and shock solutions are then printed for the  $J = 2$  and  $J = JC$  rings. With  $JOUT = 0$ , the solution on three rays from  $J = 2$  (body) to  $J = JC$  (shock) are then printed for  $I = 2, 9, 16$  corresponding to the two symmetry planes ( $I = 2, 16$ ) and the leading edge ( $I = 9$ ).

This output repeats itself for each radial station. Spherical geometry data is always computed one station ahead of the solution. Hence, the spherical geometry is printed at  $R = 2$  and the solution is computed for  $R = 1$ . Figure 47 shows the differing output corresponding to the BSC method. In the BSC method, there is no shock jump condition and the parameter DELS is missing from the iteration listing. The tolerance is specified in the input as  $10^{-6}$  and applies to the maximum correction to the potential (DELMX). When DELMX converges to less than  $10^{-6}$ , the solution has been obtained. The first printout yields the circumferential bow shock location relative to the mesh. The body data ( $J = 2$ ) is then printed. The bow shock location is not printed since the shock has been captured. Rays from the body to the shock are also printed followed by the interpolated bow shock coordinates. The bow shock coordinates are interpolated as the outer cross flow sonic line. Pressure data is not interpolated for the bow shock because it is considered to be too inexact due to the capture method.

The next set of printed output occurs at the end of the run and gives a summary of the number of iterations required at each step and the total number of iterations. Figure 48 shows this set of output for the BSF input data. A total of 35 stations was computed. This output is designed to give the user a quick way to determine if the run was successful. Since the maximum number of iterations specified in the input was 200, all the stations have converged to the specified tolerance.

The user has the option of specifying arbitrary spanwise and chordwise stations where the pressure coefficient data will be interpolated. Figure 49 shows an example of this output.

The last set of printed output is shown in Fig 50 and corresponds to the aerodynamic output data for the BSF run.

100=	SUBROUTINE CONUSE(Z,XX,IFLAG,Y,NX,NY,NZ)	CON00010
110=	COMMON /TIP/XTIP,YTIP,XSING,YSING	CON00020
120=C		CON00030
130=C	ARROW WING WITH SPECIFIED AIRFOIL SECTION	CON00040
140=C		CON00050
150=	PI=3.14159265	CON00060
160=	X=XX	CON00070
170=	THLE=33.	CON00080
180=	THTE=62.786	CON00090
190=	TANTHL=TAN(THLE*PI/180.)	CON00100
200=	TANTHT=TAN(THTE*PI/180.)	CON00110
210=	XT=Z*TANTHL	CON00120
220=	CR=20.	CON00130
230=	ZA=CR*TANTHT/(TANTHT-TANTHL)	CON00140
240=	XA=ZA*TANTHL	CON00150
250=	IF (X.GT.XT) X=XT	CON00160
260=	IF (IFLAG.EQ.0) GO TO 500	CON00170
270=	ZLE=X/TANTHL	CON00180
280=	ZTE=CR+X/TANTHT	CON00190
290=	C=ZTE-ZLE	CON00200
300=	ZC=(Z-ZLE)/C	CON00210
310=	CALL AIRFOL(ZC,YTHC)	CON00220
320=	YTH=C*YTHC	CON00230
330=	IF (IFLAG.EQ.1) Y=YTH	CON00240
340=	IF (IFLAG.EQ.2) Y=-YTH	CON00250
350=	RETURN	CON00260
360=	500 YTIP=0.	CON00270
370=	XTIP=Z*TANTHL	CON00280
380=	ZC=Z/CR	CON00290
390=	CALL AIRFOL (ZC,YTHC)	CON00300
400=	YTH=CR*YTHC	CON00310
410=	XSING=SQRT(XTIP**2-YTH**2)	CON00320
420=	YSING=0.	CON00330
430=	RETURN	CON00340
440=	END	CON00350

2246-049W

Figure 44 Sample of CONUSE Subroutines

450=	SUBROUTINE <u>XTES</u> (X,ZTE,DUMMY)	CON00360
460=	COMMON/TE/IZW,ITE,XTEC,YTEBK,XTIP	CON00370
470=	IF (ITE,NE,0) YTEBK=0,	CON00380
480=	PI=3.14159265	CON00390
490=	CR=20,	CON00400
500=	THTE=62.786	CON00410
510=	THLE=33.00	CON00420
520=	TANTHL=TAN(THLE*PI/180.)	CON00430
530=	TANTHT=TAN(THTE*PI/180.0)	CON00440
540=	IF (ITE,NE,0) XTIP=CR*TANTHT/(TANTHT-TANTHL)	CON00450
550=	ZTE=CR+X/TANTHT	CON00460
560=	RETURN	CON00470
570=	END	CON00480
580=	SUBROUTINE <u>AIRFOL</u> (XC,YTH)	CON00490
590=	T=.04	CON00500
600=	IF (XC,GT,1.) X=1.0	CON00510
610=	IF (XC,LE,1.) X=XC	CON00520
620=	YTH=(T/.20)*(.2969*SQRT(X)-.126*X-.3516*X*X	CON00530
630=	1+.2843*X*X*X-.1015*X*X*X*X)	CON00540
640=	RETURN	CON00550
650=	END	CON00560

2246-049W

**Figure 44 Sample of CONUSE Subroutines**

```

100= 4-DIGIT AIROIL...ARROW WING
110= M=1.70,ALP=5.00,THC=30.00,DELC=1.000
120= $INPUT IC=16,JC=16,KMAX(1)=200,KMAX(2)=200,KREF=1,IPL0T=2,KRR(1)=0,KRR(2)=0,
130= KRR(3)=0,KRR(4)=0,KRR(5)=0,DZ=1.,RZNEW(1)=100.,RZNEW(2)=100.,RZNEW(3)=900.,
140= RZNEW(4)=1000.,RZNEW(5)=1000.,EMINF=1.70,ALP=5.00,AZ=33.00,BZ=1.000,
150= GAMMA=1.4,EP=1.40,IOPTG=3,IOPTS=0,IFIT=0,IAERO=1,IZW=0,ITE=1,ISYM=0,
160= IXWI=10,IZWI=5,ZTE=20.00,CBAR=14.747,YCG=0.,ZCG=16.701,
170= RELSHK(1)=.50,RELSHK(2)=.25,RELSHK(3)=.10,RELNC=1.5,KMAXNC=200,
180= W(1)=1.5,W(2)=1.5,DMIN(1)=1.E-6,DMIN(2)=1.E-6,EST=-1.E-1,NS=4,NT=50,W(3)=1.5,
190= NOUT=1,JOUT=0,NG=39,IRUN=0,IPUN=0,REND=34.,DMIN(3)=1.E-6,KMAX(3)=200 $END)
200=5.0 10.0 15.0 20.0 25.0
210=0.0 2.0 4.0 6.0 8.0 10.0 12.0 14.0 16.0 18.0 CHORDI
..

```

..

```

100= 4-DIGIT AIROIL...ARROW WING
110= M=1.70,ALP=5.00,THC=30.00,DELC=1.000
120= $INPUT IC=16,JC=16,KMAX(1)=200,KMAX(2)=200,KREF=1,IPL0T=2,KRR(1)=0,KRR(2)=0,
130= KRR(3)=0,KRR(4)=0,KRR(5)=0,DZ=1.,RZNEW(1)=100.,RZNEW(2)=100.,RZNEW(3)=900.,
140= RZNEW(4)=1000.,RZNEW(5)=1000.,EMINF=1.70,ALP=5.00,AZ=33.00,BZ=1.000,
150= GAMMA=1.4,EP=1.0,IOPTG=3,IOPTS=0,IFIT=1,IAERO=1,IZW=0,ITE=1,ISYM=0,
160= IXWI=10,IZWI=5,ZTE=20.00,CBAR=14.747,YCG=0.,ZCG=16.701,
170= RELSHK(1)=.50,RELSHK(2)=.25,RELSHK(3)=.10,RELNC=1.5,KMAXNC=200,
180= W(1)=1.5,W(2)=1.5,DMIN(1)=1.E-3,DMIN(2)=1.E-3,EST=-1.E-1,NS=0,NT=50,W(3)=1.5,
190= NOUT=1,JOUT=0,NG=39,IRUN=0,IPUN=0,REND=34.,DMIN(3)=1.E-3,KMAX(3)=200 $END
200=5.0 10.0 15.0 20.0 25.0
210=0.0 2.0 4.0 6.0 8.0 10.0 12.0 14.0 16.0 18.0 CHORDI
..

```

COMMAND-

2246-048W

Figure 45 Sample Input Data Sets

```

NCOREL

NON-CONICAL RELAXATION SOLUTION

      MINF=1.700      ALF= 5.000

IC= 16      JC= 16      KMAX1= 200      KMAX2= 200      KMAX3= 200      KMAXNC= 200      KREF=1

      IFLOT= 2      NT= 50      NOUT= 1      JOUT= 0      IRUN= 0
      GAMMA=1.40      WW1=1.500      WW2=1.500      WW3=1.500      EST= -.10      DMIN1= .10E-02      DMIN2= .10E-02      DMIN3= .10E-02

4-DIGIT AIRFOIL...ARROW WING

      AZ=33.000      EZ= 1.000      NG= 39      NS= 0      IFIT= 1
      IXWI=10      IZWI= 5      IZW= 0      ITE= 1      ZTE= 20.0000
      AERODYNAMIC CONSTANTS      CRAR= 14.7470      YCG= 0.0000      ZCG= 16.7010

      ISYM= 0

```

#### RADIAL STEP SIZE PARAMETERS AND OPTIONS

```

DR= 1.000      NR= 50      IFUN= 0      REND= 34.00000      IOFTG= 3      IOFTS= 0      IAERO= 1      EP= 1.00

```

#### BOW SHOCK RELAXATION PARAMETERS

```

RELSHK(1)= .50      RELSHK(2)= .25      RELSHK(3)= .10      RELNC= 1.50

```

#### RADIAL STEP SIZE REFINEMENT PARAMETERS

```

KRR(1)= 0      KRR(2)= 0      KRR(3)= 0      KRR(4)= 0      KRR(5)= 0
RZNEW(1)= 100.00000      RZNEW(2)= 100.00000      RZNEW(3)= 900.00000      RZNEW(4)=1000.00000      RZNEW(5)=1000.00000

```



\*\*\* SPHERICAL CUT GEOMETRY INPUT COORDINATES \*\*\*

LEADING EDGE OR MAXIMUM HALF WIDTH COORDINATES

IG	R	X	Y	Z	OMEG	PSI	XTIP=	.54464E+00	YTIP=	0.	ZTIP=	.83867E+00	OMTIP=	0.	PSID=	.33000E+02	RTIP=	.10000E+01
1	.10000E+01	0.	-.23414E+00	.97220E+00	-.90000E+02	.13541E+02												
2	.10000E+01	.44976E-01	-.22661E+00	.97295E+00	-.78774E+02	.13357E+02												
3	.10000E+01	.89645E-01	-.21853E+00	.97171E+00	-.67695E+02	.13662E+02												
4	.10000E+01	.13370E+00	-.20990E+00	.96854E+00	-.57504E+02	.14410E+02												
5	.10000E+01	.17684E+00	-.20071E+00	.96356E+00	-.48618E+02	.15316E+02												
6	.10000E+01	.21878E+00	-.19997E+00	.95690E+00	-.41117E+02	.16882E+02												
7	.10000E+01	.25922E+00	-.18066E+00	.94877E+00	-.34873E+02	.18419E+02												
8	.10000E+01	.29789E+00	-.16978E+00	.93938E+00	-.29680E+02	.20052E+02												
9	.10000E+01	.33452E+00	-.15834E+00	.92899E+00	-.25329E+02	.21722E+02												
10	.10000E+01	.36887E+00	-.14633E+00	.91789E+00	-.21638E+02	.23381E+02												
11	.10000E+01	.40070E+00	-.13378E+00	.90639E+00	-.18463E+02	.24989E+02												
12	.10000E+01	.42980E+00	-.12070E+00	.89482E+00	-.15686E+02	.26514E+02												
13	.10000E+01	.45595E+00	-.10709E+00	.88354E+00	-.13218E+02	.27928E+02												
14	.10000E+01	.47900E+00	-.92994E-01	.87288E+00	-.10987E+02	.29205E+02												
15	.10000E+01	.49877E+00	-.78429E-01	.86318E+00	-.89364E+01	.30324E+02												
16	.10000E+01	.51513E+00	-.63433E-01	.85476E+00	-.70201E+01	.31267E+02												
17	.10000E+01	.52797E+00	-.48045E-01	.84790E+00	-.51996E+01	.32016E+02												
18	.10000E+01	.53721E+00	-.32310E-01	.84283E+00	-.34419E+01	.32560E+02												
19	.10000E+01	.54278E+00	-.16278E-01	.83972E+00	-.17178E+01	.32890E+02												
20	.10000E+01	.54464E+00	-.22070E-07	.83867E+00	-.23217E-05	.33000E+02												
21	.10000E+01	.54278E+00	.16278E-01	.83972E+00	.17178E+01	.32890E+02												
22	.10000E+01	.53721E+00	.32310E-01	.84283E+00	.34419E+01	.32560E+02												
23	.10000E+01	.52797E+00	.48045E-01	.84790E+00	.51996E+01	.32016E+02												
24	.10000E+01	.51513E+00	.63433E-01	.85476E+00	.70201E+01	.31267E+02												
25	.10000E+01	.49877E+00	.78429E-01	.86318E+00	.89364E+01	.30324E+02												
26	.10000E+01	.47900E+00	.92994E-01	.87288E+00	.10987E+02	.29205E+02												
27	.10000E+01	.45595E+00	.10709E+00	.88354E+00	.13218E+02	.27928E+02												
28	.10000E+01	.42980E+00	.12070E+00	.89482E+00	.15686E+02	.26514E+02												
29	.10000E+01	.40070E+00	.13378E+00	.90639E+00	.18463E+02	.24989E+02												
30	.10000E+01	.36887E+00	.14633E+00	.91789E+00	.21638E+02	.23381E+02												
31	.10000E+01	.33452E+00	.15834E+00	.92899E+00	.25329E+02	.21722E+02												
32	.10000E+01	.29789E+00	.16978E+00	.93938E+00	.29680E+02	.20052E+02												
33	.10000E+01	.25922E+00	.18066E+00	.94877E+00	.34873E+02	.18419E+02												
34	.10000E+01	.21878E+00	.19097E+00	.95690E+00	.41117E+02	.16882E+02												
35	.10000E+01	.17684E+00	.20071E+00	.96356E+00	.48618E+02	.15316E+02												
36	.10000E+01	.13370E+00	.20990E+00	.96854E+00	.57504E+02	.14410E+02												
37	.10000E+01	.89645E-01	.21853E+00	.97171E+00	.67695E+02	.13662E+02												
38	.10000E+01	.44976E-01	.22661E+00	.97295E+00	.78774E+02	.13357E+02												
39	.10000E+01	0.	.23414E+00	.97220E+00	.90000E+02	.13541E+02												

SINGULARITY LOCATION IN PHYSICAL SPACE AT R= 1.000

Figure 46 Sample Printed Output for BSF Method (Sheet 2 of 14)

XSIN/Z= .59424 YSIN/Z= 0.00000 -YSIN/Z= 0.00000

SINGULARITY LOCATION IN MAPPED SPACE AT CURRENT STATION  
 S0= .2747E+00 0. S1= .2747E+00 0. S2= 0. 0. 0.

SINGULARITY LOCATION IN MAPPED SPACE AT NEW STATION  
 S0N= .2747E+00 0. SIN= .2747E+00 0. S2N= 0. 0. 0.

XTIP= 1.08928 YTIIP= 0.00000 ZTIIP= 1.67734 QMTIP= 0.00000 PSID= 33.00000 RTIP= 2.00000

SINGULARITY LOCATION IN PHYSICAL SPACE AT R= 2.000  
 XSIN/Z= .62537 YSIN/Z= 0.00000 -YSIN/Z= 0.00000

SINGULARITY DERIVATIVES AT CURRENT STATION S0PR= 0. 0. 0. S1PR= 0. 0. 0.  
 SINGULARITY DERIVATIVE AT CURRENT STATION S2PR= 0. 0. 0.  
 SINGULARITY DERIVATIVES AT NEW STATION S0PRN= .6159E-02 0. 0. S1PRN= .6159E-02 0. 0.  
 SINGULARITY DERIVATIVE AT NEW STATION S2PRN= 0. 0. 0.

FSIMU= 36.031879  
 SHOCK1

R= 0.000

I	X	B	BFR	BSEC	BR	BRK	BRTH
2	-.15708E+01	.20899E+00	0.	-.24553E+00	0.	0.	0.
3	-.13464E+01	.20281E+00	-.22043E-01	.49070E-01	0.	0.	0.
4	-.11220E+01	.19910E+00	-.12548E-01	.35555E-01	0.	0.	0.
5	-.89760E+00	.19718E+00	-.52650E-02	.29357E-01	0.	0.	0.
6	-.67320E+00	.19673E+00	.15416E-02	.31309E-01	0.	0.	0.
7	-.44880E+00	.19787E+00	.93857E-02	.38603E-01	0.	0.	0.
8	-.22440E+00	.20095E+00	-.12588E-01	-.10065E-01	0.	0.	0.
9	-.71054E-14	.20352E+00	-.17316E-11	-.10213E+00	0.	0.	0.
10	.22440E+00	.20095E+00	-.12588E-01	-.10065E-01	0.	0.	0.
11	.44880E+00	.19787E+00	-.93857E-02	.38603E-01	0.	0.	0.
12	.67320E+00	.19673E+00	-.15416E-02	.31309E-01	0.	0.	0.
13	.89760E+00	.19718E+00	.52650E-02	.29357E-01	0.	0.	0.
14	.11220E+01	.19910E+00	.12548E-01	.35555E-01	0.	0.	0.
15	.13464E+01	.20281E+00	.22043E-01	.49070E-01	0.	0.	0.
16	.15708E+01	.20899E+00	0.	-.24553E+00	0.	0.	0.

R= 0.000

I	X	C	CFR	CSEC	CR	CRR	CRTH
2	-.15708E+01	.33409E+00	0.	-.16121E+00	0.	0.	0.
3	-.13464E+01	.33003E+00	-.35046E-01	-.15114E+00	0.	0.	0.

Figure 46 Sample Printed Output for BSF Method (Sheet 3 of 14)

4	-.11220E+01	.31836E+00	-.65495E-01	-.12025E+00	0.	0.	0.
5	-.89760E+00	.30044E+00	-.86408E-01	-.66146E-01	0.	0.	0.
6	-.67320E+00	.27958E+00	-.92040E-01	.15954E-01	0.	0.	0.
7	-.44880E+00	.25933E+00	-.75499E-01	.13147E+00	0.	0.	0.
8	-.22440E+00	.24570E+00	-.30908E-01	.26595E+00	0.	0.	0.
9	-.71054E-14	.24546E+00	.37044E-01	.33969E+00	0.	0.	0.
10	.22440E+00	.26232E+00	.10570E+00	.27222E+00	0.	0.	0.
11	.44880E+00	.29290E+00	.14982E+00	.12102E+00	0.	0.	0.
12	.67320E+00	.32956E+00	.14081E+00	-.23060E-01	0.	0.	0.
13	.89760E+00	.36507E+00	.14357E+00	-.13060E+00	0.	0.	0.
14	.11220E+01	.39400E+00	.10620E+00	-.20247E+00	0.	0.	0.
15	.13464E+01	.41273E+00	.56158E-01	-.24357E+00	0.	0.	0.
16	.15708E+01	.41920E+00	0.	-.25695E+00	0.	0.	0.

R= 0.000

I	J	X/Z	Y/Z	H	z	UI	VI	WI	H1	H2
2	2	-.21243E-14	-.24084E+00	.28240E+01	.84953E-15	-.31799E+00	-.31799E+00	.94810E+000.		0.
3	2	.13377E+00	-.21751E+00	.28100E+01	-.10254E+00	-.30488E+00	-.30488E+00	.94686E+000.		0.
4	2	.26156E+00	-.19286E+00	.26321E+01	-.19701E+00	-.30596E+00	-.30596E+00	.93144E+000.		0.
5	2	.38025E+00	-.16526E+00	.23176E+01	-.27148E+00	-.32215E+00	-.32215E+00	.90693E+000.		0.
6	2	.48486E+00	-.13325E+00	.19129E+01	-.31259E+00	-.35851E+00	-.35851E+00	.87963E+000.		0.
7	2	.56920E+00	-.95849E-01	.14827E+01	-.29623E+00	-.42460E+00	-.42460E+00	.85555E+000.		0.
8	2	.62703E+00	-.51972E-01	.11328E+01	-.16994E+00	-.51635E+00	-.51635E+00	.83935E+000.		0.
9	2	.64941E+00	-.17264E-14	.10012E+01	.87156E-01	-.54257E+00	-.54257E+00	.83548E+000.		0.
10	2	.62703E+00	.51972E-01	.11328E+01	.31854E+00	-.42555E+00	-.42555E+00	.84702E+000.		0.
11	2	.56920E+00	.95849E-01	.14827E+01	.40136E+00	-.28632E+00	-.28632E+00	.87002E+000.		0.
12	2	.48486E+00	.13325E+00	.19129E+01	.38558E+00	-.20158E+00	-.20158E+00	.90039E+000.		0.
13	2	.38025E+00	.16526E+00	.23176E+01	.32204E+00	-.15747E+00	-.15747E+00	.93354E+000.		0.
14	2	.26156E+00	.19286E+00	.26321E+01	.22991E+00	-.13779E+00	-.13779E+00	.96341E+000.		0.
15	2	.13377E+00	.21751E+00	.28100E+01	.11933E+00	-.13531E+00	-.13531E+00	.98359E+000.		0.
16	2	.11566E-13	.24084E+00	.28240E+01	.10086E-13	-.14852E+00	-.14852E+00	.98891E+000.		0.

I	J	HX	HY	HR	H1X	H1Y	H1R	H2X	H2Y	H2R
2	2	0.	-.16314E+00	0.	0.	0.	0.	0.	0.	0.
3	2	-.19198E+00	-.17093E+00	0.	0.	0.	0.	0.	0.	0.
4	2	-.49237E+00	-.14353E+00	0.	0.	0.	0.	0.	0.	0.
5	2	-.71920E+00	-.92505E-01	0.	0.	0.	0.	0.	0.	0.
6	2	-.83490E+00	-.35720E-01	0.	0.	0.	0.	0.	0.	0.
7	2	-.78004E+00	.10475E-01	0.	0.	0.	0.	0.	0.	0.
8	2	-.48149E+00	.36705E-01	0.	0.	0.	0.	0.	0.	0.
9	2	-.43627E-11	.47551E-01	0.	0.	0.	0.	0.	0.	0.
10	2	.48149E+00	.50339E-01	0.	0.	0.	0.	0.	0.	0.
11	2	.78004E+00	.16066E-01	0.	0.	0.	0.	0.	0.	0.
12	2	.83490E+00	-.57715E-01	0.	0.	0.	0.	0.	0.	0.
13	2	.71920E+00	-.15107E+00	0.	0.	0.	0.	0.	0.	0.
14	2	.49237E+00	-.23608E+00	0.	0.	0.	0.	0.	0.	0.
15	2	.19198E+00	-.28386E+00	0.	0.	0.	0.	0.	0.	0.

Figure 46 Sample Printed Output for BSF Method (Sheet 4 of 14)

16	2	0.	- .2757E+00	0.	0.	0.	0.	0.	0.	0.	0.
ITER	DELMX	I	J	DELAUG	RESMX	I	J	RESAVG	KSUP	DELS	IS
1	-.4046E-01	4	2	.9137E-02	-.1473E+03	9	2	.5284E+01	0	.14E-02	11
2	-.2285E-01	2	2	.7841E-02	-.1252E+02	8	3	.2359E+01	0	.24E+00	9
3	-.2157E-01	9	2	.6810E-02	-.3866E+02	8	2	.1859E+01	0	.51E-01	3
4	-.1271E-01	2	2	.4081E-02	-.9429E+01	2	2	.9032E+00	0	.66E-01	2
5	-.8075E-02	2	2	.2574E-02	-.9602E+01	2	2	.6260E+00	0	.47E-01	7
6	-.7358E-02	2	2	.2252E-02	-.5712E+01	3	2	.5211E+00	0	.43E-01	2
7	-.4817E-02	5	2	.1514E-02	-.4993E+01	2	2	.3749E+00	0	.31E-01	7
8	-.6246E-02	2	8	.1489E-02	-.3440E+01	3	2	.3271E+00	0	.31E-01	2
9	.3524E-02	2	11	.1015E-02	-.3208E+01	2	2	.2432E+00	0	.21E-01	5
10	-.6047E-02	2	8	.1098E-02	-.2084E+01	3	2	.2308E+00	0	.26E-01	2
11	.4424E-02	2	10	.8073E-03	-.2081E+01	2	2	.1772E+00	0	.16E-01	5
12	-.5572E-02	2	9	.8597E-03	-.1403E+01	5	2	.1726E+00	0	.20E-01	2
13	.4601E-02	2	10	.6752E-03	-.1329E+01	2	2	.1413E+00	0	.12E-01	2
14	-.5026E-02	2	9	.6882E-03	-.1009E+01	5	2	.1375E+00	0	.16E-01	2
15	.4235E-02	2	10	.5509E-03	-.9241E+00	2	2	.1135E+00	0	.12E-01	2
16	-.4314E-02	2	9	.5465E-03	-.7413E+00	5	2	.1097E+00	0	.13E-01	2
17	.3710E-02	2	10	.4464E-03	-.6927E+00	2	2	.9164E-01	0	.11E-01	2
18	-.3630E-02	2	9	.4358E-03	-.6007E+00	2	8	.8782E-01	0	.11E-01	2
19	.3173E-02	2	10	.3633E-03	-.5466E+00	2	2	.7469E-01	0	.93E-02	2
20	-.3029E-02	2	9	.3503E-03	-.5025E+00	2	9	.7090E-01	0	.88E-02	2
21	.2683E-02	2	10	.2980E-03	-.4453E+00	2	2	.6137E-01	0	.80E-02	2
22	-.2525E-02	2	9	.2845E-03	-.4195E+00	2	9	.5777E-01	0	.74E-02	2
23	.2259E-02	2	10	.2461E-03	.3728E+00	2	9	.5075E-01	0	.68E-02	2
24	-.2107E-02	2	9	.2330E-03	-.3504E+00	2	9	.4746E-01	0	.62E-02	2
25	.1900E-02	2	10	.2045E-03	.3136E+00	2	9	.4219E-01	0	.58E-02	2
26	-.1762E-02	2	10	.1924E-03	-.2932E+00	2	9	.3925E-01	0	.52E-02	2
27	.1597E-02	2	10	.1707E-03	.2638E+00	2	9	.3520E-01	0	.49E-02	2
28	-.1476E-02	2	10	.1597E-03	-.2456E+00	2	9	.3264E-01	0	.44E-02	2
29	.1343E-02	2	10	.1429E-03	.2220E+00	2	9	.2946E-01	0	.41E-02	2
30	-.1239E-02	2	10	.1332E-03	-.2061E+00	2	9	.2725E-01	0	.37E-02	2
31	.1130E-02	2	10	.1199E-03	.1869E+00	2	9	.2471E-01	0	.35E-02	2
32	-.1042E-02	2	10	.1114E-03	.1746E+00	2	2	.2281E-01	0	.31E-02	2
33	.9518E-03	2	10	.1008E-03	.1574E+00	2	9	.2076E-01	0	.29E-02	2
34	-.8762E-03	2	10	.9338E-04	.1476E+00	2	2	.1914E-01	0	.26E-02	2
35	.8017E-03	2	10	.8485E-04	.1327E+00	2	9	.1746E-01	0	.25E-02	2
36	-.7377E-03	2	10	.7843E-04	.1246E+00	2	2	.1609E-01	0	.22E-02	2
37	.6756E-03	2	10	.7147E-04	.1118E+00	2	9	.1470E-01	0	.21E-02	2
38	-.6213E-03	2	10	.6595E-04	.1051E+00	2	2	.1354E-01	0	.19E-02	2
39	.5695E-03	2	10	.6023E-04	.9430E-01	2	9	.1239E-01	0	.17E-02	2
40	-.5236E-03	2	10	.5551E-04	.8860E-01	2	2	.1140E-01	0	.16E-02	2
41	.4801E-03	2	10	.5078E-04	-.7963E-01	2	2	.1044E-01	0	.15E-02	2
42	-.4413E-03	2	10	.4675E-04	.7468E-01	2	2	.9600E-02	0	.13E-02	2
43	.4049E-03	2	10	.4282E-04	-.6727E-01	2	2	.8799E-02	0	.12E-02	2

Figure 46 Sample Printed Output for BSF Method (Sheet 5 of 14)

44	-,3721E-03	2	10	,3939E-04	,6296E-01	2	2	,8090E-02	0	,11E-02	2
45	-,3414E-03	2	10	,3611E-04	-,5682E-01	2	2	,7420E-02	0	,10E-02	2
46	-,3137E-03	2	10	,3320E-04	,5304E-01	2	2	,6820E-02	0	,95E-03	2
47	-,2880E-03	2	10	,3046E-04	-,4801E-01	2	2	,6257E-02	0	,88E-03	2
48	-,2646E-03	2	10	,2799E-04	-,4474E-01	2	2	,5750E-02	0	,80E-03	2
49	-,2429E-03	2	10	,2569E-04	-,4053E-01	2	2	,5277E-02	0	,74E-03	2
50	-,2231E-03	2	10	,2360E-04	,3769E-01	2	2	,4849E-02	0	,68E-03	2
51	-,2049E-03	2	10	,2167E-04	-,3423E-01	2	2	,4451E-02	0	,63E-03	2
52	-,1882E-03	2	10	,1990E-04	,3177E-01	2	2	,4089E-02	0	,57E-03	2
53	-,1728E-03	2	10	,1828E-04	-,2889E-01	2	2	,3754E-02	0	,53E-03	2
54	-,1587E-03	2	10	,1679E-04	,2678E-01	2	2	,3449E-02	0	,48E-03	2
55	-,1458E-03	2	10	,1542E-04	-,2440E-01	2	2	,3167E-02	0	,45E-03	2
56	-,1339E-03	2	10	,1416E-04	,2259E-01	2	2	,2909E-02	0	,41E-03	2
57	-,1230E-03	2	10	,1301E-04	-,2060E-01	2	2	,2671E-02	0	,38E-03	2
58	-,1129E-03	2	10	,1194E-04	,1904E-01	2	2	,2454E-02	0	,34E-03	2
59	-,1037E-03	2	10	,1097E-04	-,1740E-01	2	2	,2253E-02	0	,32E-03	2
60	-,9527E-04	2	10	,1007E-04	,1605E-01	2	2	,2070E-02	0	,29E-03	2
61	-,8749E-04	2	10	,9234E-05	,1467E-01	2	2	,1901E-02	0	,27E-03	2
62	-,8036E-04	2	10	,8498E-05	,1354E-01	2	2	,1746E-02	0	,24E-03	2
63	-,7380E-04	2	10	,7806E-05	-,1238E-01	2	2	,1603E-02	0	,23E-03	2
64	-,6779E-04	2	10	,7169E-05	,1141E-01	2	2	,1473E-02	0	,21E-03	2
65	-,6226E-04	2	10	,6585E-05	-,1044E-01	2	2	,1352E-02	0	,19E-03	2
66	-,5718E-04	2	10	,6047E-05	,9624E-02	2	2	,1242E-02	0	,17E-03	2
67	-,5252E-04	2	10	,5555E-05	-,8815E-02	2	2	,1141E-02	0	,16E-03	2
68	-,4824E-04	2	10	,5101E-05	,8117E-02	2	2	,1048E-02	0	,15E-03	2
69	-,4430E-04	2	10	,4686E-05	-,7435E-02	2	2	,9624E-03	0	,14E-03	2
70	-,4069E-04	2	10	,4303E-05	,6846E-02	2	2	,8839E-03	0	,12E-03	2
71	-,3737E-04	2	10	,3953E-05	-,6273E-02	2	2	,8119E-03	0	,11E-03	2
72	-,3432E-04	2	10	,3630E-05	,5774E-02	2	2	,7457E-03	0	,10E-03	2
73	-,3152E-04	2	10	,3334E-05	-,5295E-02	2	2	,6849E-03	0	,96E-04	2
74	-,2895E-04	2	10	,3062E-05	,4870E-02	2	2	,6290E-03	0	,88E-04	2
75	-,2659E-04	2	10	,2813E-05	-,4466E-02	2	2	,5777E-03	0	,81E-04	2
76	-,2442E-04	2	10	,2583E-05	,4108E-02	2	2	,5304E-03	0	,75E-04	2
77	-,2243E-04	2	10	,2373E-05	-,3767E-02	2	2	,4873E-03	0	,68E-04	2
78	-,2060E-04	2	10	,2179E-05	,3466E-02	2	2	,4474E-03	0	,63E-04	2
79	-,1892E-04	2	10	,2001E-05	-,3179E-02	2	2	,4111E-03	0	,58E-04	2
80	-,1738E-04	2	10	,1838E-05	,2923E-02	2	2	,3776E-03	0	,53E-04	2
81	-,1594E-04	2	10	,1688E-05	-,2682E-02	2	2	,3468E-03	0	,49E-04	2
82	-,1466E-04	2	10	,1551E-05	,2465E-02	2	2	,3185E-03	0	,45E-04	2
83	-,1347E-04	2	10	,1424E-05	-,2262E-02	2	2	,2925E-03	0	,41E-04	2
84	-,1237E-04	2	10	,1308E-05	,2079E-02	2	2	,2687E-03	0	,38E-04	2
85	-,1136E-04	2	10	,1201E-05	-,1908E-02	2	2	,2468E-03	0	,35E-04	2
86	-,1043E-04	2	10	,1103E-05	,1734E-02	2	2	,2266E-03	0	,32E-04	2
87	-,9582E-05	2	10	,1013E-05	-,1610E-02	2	2	,2082E-03	0	,29E-04	2
88	-,8801E-05	2	10	,9308E-06	,1480E-02	2	2	,1912E-03	0	,27E-04	2
89	-,8083E-05	2	10	,8549E-06	-,1358E-02	2	2	,1756E-03	0	,25E-04	2
90	-,7424E-05	2	10	,7852E-06	,1248E-02	2	2	,1613E-03	0	,23E-04	2
91	-,6819E-05	2	10	,7212E-06	-,1146E-02	2	2	,1481E-03	0	,21E-04	2
92	-,6263E-05	2	10	,6623E-06	,1053E-02	2	2	,1361E-03	0	,19E-04	2
93	-,5752E-05	2	10	,6083E-06	-,9665E-03	2	2	,1250E-03	0	,18E-04	2
94	-,5283E-05	2	10	,5587E-06	,8885E-03	2	2	,1148E-03	0	,16E-04	2

Figure 46 Sample Printed Output for BSF Method (Sheet 6 of 14)

DELCHK= .16122E-04 DELCHK= .93354E-05

R= 0.000

JRINS= 2

BODY COORDINATES AND SURFACE DATA

I	RHO	F	X/Z	Y/Z	Z	M	MR	MC	CF
2	.20899E+00	-.11761E+00	-.21243E-14	-.24084E+00	0.	.13000E+01	.13000E+01	.67920E-04	.38624E+00
3	.20281E+00	-.11985E+00	.13377E+00	-.21751E+00	0.	.12976E+01	.12940E+01	.96358E-01	.38922E+00
4	.19910E+00	-.11570E+00	.26156E+00	-.19286E+00	0.	.12891E+01	.12742E+01	.19517E+00	.39941E+00
5	.19718E+00	-.10749E+00	.38025E+00	-.16526E+00	0.	.12743E+01	.12452E+01	.27048E+00	.41751E+00
6	.19673E+00	-.97417E-01	.48486E+00	-.13325E+00	0.	.12505E+01	.12129E+01	.30436E+00	.44705E+00
7	.19787E+00	-.87375E-01	.56920E+00	.95849E-01	0.	.12129E+01	.11827E+01	.26929E+00	.49498E+00
8	.20095E+00	-.78816E-01	.62703E+00	-.51972E-01	0.	.11643E+01	.11604E+01	.95325E-01	.55940E+00
9	.20352E+00	-.73104E-01	.64941E+00	-.17264E-14	0.	.12017E+01	.11713E+01	.26863E+00	.50965E+00
10	.20095E+00	-.70798E-01	.62703E+00	.51972E-01	0.	.13725E+01	.12326E+01	.60372E+00	.30259E+00
11	.19787E+00	-.69452E-01	.56920E+00	.95849E-01	0.	.14681E+01	.12960E+01	.68958E+00	.20166E+00
12	.19673E+00	-.69286E-01	.48486E+00	.13325E+00	0.	.14875E+01	.13509E+01	.62270E+00	.18248E+00
13	.19718E+00	-.70134E-01	.38025E+00	.16526E+00	0.	.14911E+01	.14044E+01	.50101E+00	.17894E+00
14	.19910E+00	-.71278E-01	.26156E+00	.19286E+00	0.	.14931E+01	.14517E+01	.34906E+00	.17698E+00
15	.20281E+00	-.71614E-01	.13377E+00	.21751E+00	0.	.14954E+01	.14847E+01	.17795E+00	.17482E+00
16	.20899E+00	-.69916E-01	.11566E-13	.24084E+00	0.	.14965E+01	.14965E+01	.27258E-07	.17370E+00

JRINS= 16

BOW SHOCK COORDINATES AND SURFACE DATA

I	RHO	F	X/Z	Y/Z	Z	M	MR	MC	CF
2	.40719E+00	0.	-.14232E-14	-.82977E+00	0.	.14032E+01	.11359E+01	.82371E+00	.26901E+00
3	.40530E+00	0.	.23179E+00	-.80632E+00	0.	.13996E+01	.11325E+01	.82241E+00	.27285E+00
4	.40002E+00	0.	.45054E+00	-.73822E+00	0.	.13895E+01	.11230E+01	.81825E+00	.28383E+00
5	.39234E+00	0.	.64449E+00	-.63170E+00	0.	.13751E+01	.11100E+01	.81157E+00	.29971E+00
6	.38382E+00	0.	.80420E+00	-.49572E+00	0.	.13597E+01	.10972E+01	.80299E+00	.31693E+00
7	.37643E+00	0.	.92351E+00	-.34023E+00	0.	.13483E+01	.10886E+01	.79544E+00	.32987E+00
8	.37245E+00	0.	.10003E+01	-.17365E+00	0.	.13466E+01	.10876E+01	.79407E+00	.33175E+00
9	.37393E+00	0.	.10352E+01	-.56067E-14	0.	.13596E+01	.10962E+01	.80424E+00	.33170E+00
10	.38161E+00	0.	.10276E+01	.18074E+00	0.	.13879E+01	.11153E+01	.82603E+00	.28558E+00
11	.39438E+00	0.	.97336E+00	.36734E+00	0.	.14267E+01	.11438E+01	.85276E+00	.24398E+00
12	.41002E+00	0.	.86816E+00	.55264E+00	0.	.14689E+01	.11784E+01	.87685E+00	.20087E+00
13	.42608E+00	0.	.71104E+00	.72375E+00	0.	.15079E+01	.12137E+01	.89480E+00	.16274E+00
14	.44014E+00	0.	.50622E+00	.86461E+00	0.	.15392E+01	.12437E+01	.90692E+00	.13345E+00
15	.44987E+00	0.	.26375E+00	.95849E+00	0.	.15595E+01	.12634E+01	.91425E+00	.11507E+00
16	.45336E+00	0.	.19437E-13	.99162E+00	0.	.15665E+01	.12702E+01	.91678E+00	.10881E+00

Figure 46 Sample Printed Output for BSF Method (Sheet 7 of 14)

RADIAL OUTPUT DATA IN CROSSFLOW PLANE

IRING= 2

J	RHO	F	X/Z	Y/Z	Z	M	MR	MC	CF
2	.20899E+00	-.11761E+00	-.21243E-14	-.24084E+00	0.	.13000E+01	.13000E+01	.67920E-04	.38624E+00
3	.22313E+00	-.10544E+00	-.24931E-14	-.28264E+00	0.	.13009E+01	.12987E+01	.75897E-01	.38518E+00
4	.23730E+00	-.94142E-01	-.55314E-15	-.32367E+00	0.	.13033E+01	.12951E+01	.14585E+00	.38236E+00
5	.25146E+00	-.83567E-01	-.62468E-15	-.36422E+00	0.	.13067E+01	.12894E+01	.21161E+00	.37830E+00
6	.26562E+00	-.73620E-01	-.69378E-15	-.40451E+00	0.	.13110E+01	.12820E+01	.27421E+00	.37322E+00
7	.27978E+00	-.64235E-01	-.76280E-15	-.44475E+00	0.	.13160E+01	.12728E+01	.33429E+00	.36726E+00
8	.29393E+00	-.55359E-01	-.83202E-15	-.48511E+00	0.	.13218E+01	.12622E+01	.39234E+00	.36048E+00
9	.30809E+00	-.46957E-01	-.90173E-15	-.52575E+00	0.	.13283E+01	.12502E+01	.44871E+00	.35290E+00
10	.32225E+00	-.39001E-01	-.97218E-15	-.56683E+00	0.	.13355E+01	.12369E+01	.50370E+00	.34449E+00
11	.33640E+00	-.31471E-01	-.10436E-14	-.60846E+00	0.	.13436E+01	.12224E+01	.55760E+00	.33520E+00
12	.35056E+00	-.24355E-01	-.11162E-14	-.65080E+00	0.	.13526E+01	.12069E+01	.61071E+00	.32492E+00
13	.36472E+00	-.17645E-01	-.11902E-14	-.69397E+00	0.	.13627E+01	.11903E+01	.66339E+00	.31348E+00
14	.37887E+00	-.11342E-01	-.12659E-14	-.73810E+00	0.	.13743E+01	.11729E+01	.71610E+00	.30059E+00
15	.39303E+00	-.54533E-02	-.13435E-14	-.78332E+00	0.	.13877E+01	.11548E+01	.76957E+00	.28573E+00
16	.40719E+00	0.	-.14232E-14	-.82977E+00	0.	.14032E+01	.11359E+01	.82371E+00	.26901E+00

IRING= 9

J	RHO	F	X/Z	Y/Z	Z	M	MR	MC	CF
2	.20352E+00	-.73104E-01	.64941E+00	-.17264E-14	0.	.12017E+01	.11713E+01	.26863E+00	.50965E+00
3	.21589E+00	-.66622E-01	.66767E+00	-.20066E-14	0.	.11968E+01	.11695E+01	.25457E+00	.51601E+00
4	.22786E+00	-.60355E-01	.68767E+00	-.23818E-14	0.	.12021E+01	.11684E+01	.28224E+00	.50917E+00
5	.24004E+00	-.54287E-01	.70922E+00	-.25535E-14	0.	.12115E+01	.11671E+01	.32487E+00	.49687E+00
6	.25221E+00	-.48409E-01	.73233E+00	-.28230E-14	0.	.12228E+01	.11650E+01	.37138E+00	.48225E+00
7	.26438E+00	-.42717E-01	.75678E+00	-.30915E-14	0.	.12349E+01	.11620E+01	.41804E+00	.46669E+00
8	.27655E+00	-.37209E-01	.78255E+00	-.33600E-14	0.	.12475E+01	.11581E+01	.46375E+00	.45079E+00
9	.28872E+00	-.31884E-01	.80962E+00	-.36295E-14	0.	.12603E+01	.11532E+01	.50831E+00	.43479E+00
10	.30090E+00	-.26745E-01	.83797E+00	-.39007E-14	0.	.12732E+01	.11474E+01	.55180E+00	.41878E+00
11	.31307E+00	-.21793E-01	.86757E+00	-.41745E-14	0.	.12864E+01	.11408E+01	.59443E+00	.40273E+00
12	.32524E+00	-.17030E-01	.89845E+00	-.44515E-14	0.	.12998E+01	.11333E+01	.63645E+00	.38654E+00
13	.33741E+00	-.12462E-01	.93062E+00	-.47325E-14	0.	.13136E+01	.11251E+01	.67813E+00	.37008E+00
14	.34959E+00	-.80944E-02	.96411E+00	-.50183E-14	0.	.13281E+01	.11161E+01	.71982E+00	.35312E+00
15	.36176E+00	-.39362E-02	.99896E+00	-.53094E-14	0.	.13435E+01	.11065E+01	.76196E+00	.33534E+00
16	.37393E+00	0.	.10352E+01	-.56067E-14	0.	.13596E+01	.10962E+01	.80424E+00	.31700E+00

IRING= 16

J	RHO	F	X/Z	Y/Z	Z	M	MR	MC	CF
2	.20899E+00	-.69916E-01	.11566E-13	.24084E+00	0.	.14965E+01	.14965E+01	.27258E-07	.17370E+00

3	.22645E+00	-.62853E-01	.11959E-13	.29226E+00	0.	.14968E+01	.14946E+01	.80358E-01	.17343E+00
4	.24390E+00	-.56209E-01	.11584E-13	.34261E+00	0.	.14976E+01	.14895E+01	.15616E+00	.17262E+00
5	.26136E+00	-.49920E-01	.13268E-13	.39239E+00	0.	.14989E+01	.14814E+01	.22849E+00	.17135E+00
6	.27881E+00	-.43950E-01	.14945E-13	.44200E+00	0.	.15007E+01	.14708E+01	.29801E+00	.16964E+00
7	.29627E+00	-.38277E-01	.13134E-13	.49179E+00	0.	.15030E+01	.14580E+01	.36513E+00	.16746E+00
8	.31372E+00	-.32885E-01	.14476E-13	.54203E+00	0.	.15058E+01	.14430E+01	.43019E+00	.16477E+00
9	.33118E+00	-.27768E-01	.15837E-13	.59302E+00	0.	.15092E+01	.14262E+01	.49346E+00	.16153E+00
10	.34863E+00	-.22921E-01	.17225E-13	.64499E+00	0.	.15133E+01	.14077E+01	.55519E+00	.15767E+00
11	.36609E+00	-.18345E-01	.18646E-13	.69819E+00	0.	.15181E+01	.13877E+01	.61566E+00	.15308E+00
12	.38354E+00	-.14046E-01	.20107E-13	.75288E+00	0.	.15240E+01	.13662E+01	.67517E+00	.14760E+00
13	.40100E+00	-.10034E-01	.15863E-13	.80930E+00	0.	.15311E+01	.13436E+01	.73420E+00	.14097E+00
14	.41845E+00	-.63292E-02	.17008E-13	.86770E+00	0.	.15400E+01	.13199E+01	.79347E+00	.13274E+00
15	.43591E+00	-.29629E-02	.18197E-13	.92838E+00	0.	.15519E+01	.12955E+01	.85453E+00	.12191E+00
16	.45336E+00	0.	.19437E-13	.99162E+00	0.	.15665E+01	.12702E+01	.91678E+00	.10881E+00

\*\*\* SPHERICAL CUT GEOMETRY INPUT COORDINATES \*\*\*

LEADING EDGE OR MAXIMUM HALF WIDTH COORDINATES

XTIP= .10893E+01 YTIP= 0. ZTIP= .16773E+01 QMTIP= 0. PSID= .33000E+02 RTIP= .20000E+01

IG	R	X	Y	Z	OMEG	FSI
1	.20000E+01	0.	-.31081E+00	.19757E+01	-.90000E+02	.89404E+01
2	.20000E+01	.89952E-01	-.30171E+00	.19751E+01	-.73399E+02	.90572E+01
3	.20000E+01	.17929E+00	-.29187E+00	.19704E+01	-.58439E+02	.98617E+01
4	.20000E+01	.26740E+00	-.28126E+00	.19620E+01	-.46447E+02	.11189E+02
5	.20000E+01	.35369E+00	-.26985E+00	.19499E+01	-.37343E+02	.12852E+02
6	.20000E+01	.43766E+00	-.25761E+00	.19345E+01	-.30487E+02	.14707E+02
7	.20000E+01	.51844E+00	-.24452E+00	.19161E+01	-.25251E+02	.16655E+02
8	.20000E+01	.59578E+00	-.23058E+00	.18952E+01	-.21158E+02	.18638E+02
9	.20000E+01	.66905E+00	-.21576E+00	.18724E+01	-.17874E+02	.20578E+02
10	.20000E+01	.73775E+00	-.20007E+00	.18482E+01	-.15173E+02	.22470E+02
11	.20000E+01	.80141E+00	-.18351E+00	.18232E+01	-.12897E+02	.24272E+02
12	.20000E+01	.85959E+00	-.16609E+00	.17982E+01	-.10936E+02	.25960E+02
13	.20000E+01	.91191E+00	-.14782E+00	.17739E+01	-.92077E+01	.27510E+02
14	.20000E+01	.95799E+00	-.12875E+00	.17509E+01	-.76544E+01	.28901E+02
15	.20000E+01	.99753E+00	-.10890E+00	.17300E+01	-.62304E+01	.30114E+02
16	.20000E+01	.10303E+01	-.88333E-01	.17119E+01	-.45005E+01	.31132E+02
17	.20000E+01	.10559E+01	-.67092E-01	.16972E+01	-.36355E+01	.31940E+02
18	.20000E+01	.10744E+01	-.45244E-01	.16863E+01	-.24113E+01	.32526E+02
19	.20000E+01	.10856E+01	-.22856E-01	.16796E+01	-.12062E+01	.32881E+02
20	.20000E+01	.10893E+01	-.46832E-05	.16773E+01	-.24633E-03	.33000E+02
21	.20000E+01	.10856E+01	.22856E-01	.16796E+01	.12062E+01	.32881E+02
22	.20000E+01	.10744E+01	.45244E-01	.16863E+01	.24113E+01	.32526E+02
23	.20000E+01	.10559E+01	.67092E-01	.16972E+01	.36355E+01	.31940E+02
24	.20000E+01	.10303E+01	.88333E-01	.17119E+01	.45005E+01	.31132E+02
25	.20000E+01	.99753E+00	.10890E+00	.17300E+01	.62304E+01	.30114E+02



26	.20000E+01	.53799E+00	.12875E+00	.17509E+01	.76544E+01	.28901E+02
27	.20000E+01	.91191E+00	.14782E+00	.17739E+01	.92077E+01	.27510E+02
28	.20000E+01	.85959E+00	.16609E+00	.17982E+01	.10936E+02	.25960E+02
29	.20000E+01	.80141E+00	.18351E+00	.18232E+01	.12897E+02	.24272E+02
30	.20000E+01	.73775E+00	.20007E+00	.18482E+01	.15173E+02	.22470E+02
31	.20000E+01	.66905E+00	.21576E+00	.18724E+01	.17874E+02	.20578E+02
32	.20000E+01	.59578E+00	.23058E+00	.18952E+01	.21158E+02	.18628E+02
33	.20000E+01	.51844E+00	.24452E+00	.19161E+01	.25351E+02	.16655E+02
34	.20000E+01	.43756E+00	.25761E+00	.19345E+01	.30487E+02	.14707E+02
35	.20000E+01	.35369E+00	.26985E+00	.19499E+01	.37342E+02	.12852E+02
36	.20000E+01	.26740E+00	.28124E+00	.19620E+01	.46447E+02	.11189E+02
37	.20000E+01	.17929E+00	.29187E+00	.19704E+01	.58439E+02	.98617E+01
38	.20000E+01	.89952E-01	.30171E+00	.19751E+01	.73399E+02	.90572E+01
39	.20000E+01	0.	.31081E+00	.19757E+01	.90000E+02	.89404E+01

SINGULARITY LOCATION IN PHYSICAL SPACE AT R= 2.000

XSIN/Z= .62557 YSIN/Z= 0.00000 -YSIN/Z= 0.00000

SINGULARITY LOCATION IN MAPPED SPACE AT CURRENT STATION

SO= .2747E+00 0. S1= .2747E+00 0. S2= 0. 0.

SINGULARITY LOCATION IN MAPPED SPACE AT NEW STATION

SON= .2870E+00 0. S1N= .2870E+00 0. S2N= 0. 0.

XTIP= 1.63392 YTIP= 0.00000 ZTIP= 2.51601 OMTIP= 0.00000 PSID= 33.00000 RTIP= 3.00000

SINGULARITY LOCATION IN PHYSICAL SPACE AT R= 3.000

XSIN/Z= .63538 YSIN/Z= 0.00000 -YSIN/Z= 0.00000

SINGULARITY DERIVATIVES AT CURRENT STATION SOFR=

SINGULARITY DERIVATIVE AT CURRENT STATION S2PR= 0. S1PR= .6159E-02 0. S1PR= .6159E-02 0.

SINGULARITY DERIVATIVES AT NEW STATION SOFRN=

SINGULARITY DERIVATIVE AT NEW STATION S2PRN= 0. S1PRN= .8061E-02 0. S1PRN= .8061E-02 0.

R= 1.000

I	X	B	BFR	RSEC	BR	RRR	BRTH
2	-.15708E+01	.20899E+00	0.	-.24553E+00	-.10582E-01	-.21164E-01	0.
3	-.13464E+01	.20281E+00	-.22043E-01	.49070E-01	-.91127E-02	-.18225E-01	.53257E-02
4	-.11220E+01	.19910E+00	-.12548E-01	.35555E-01	-.81919E-02	-.16384E-01	.31722E-02
5	-.89760E+00	.19718E+00	-.52650E-02	.29357E-01	-.76890E-02	-.15378E-01	.13850E-02
6	-.67320E+00	.19673E+00	.15416E-02	.31309E-01	-.75703E-02	-.15141E-01	-.50923E-03
7	-.4880E+00	.19787E+00	.93857E-02	.38603E-01	-.79175E-02	-.15835E-01	-.27701E-02
8	-.122440E+00	.20095E+00	.12588E-01	-.10065E-01	-.88135E-02	-.17627E-01	-.32978E-02
9	-.71054E-14	.20352E+00	-.17316E-11	-.10213E+00	-.93976E-02	-.18795E-01	-.26566E-09

10	.22440E+00	.20995E+00	-.12588E-01	-.10065E-01	-.88135E-02	-.17627E-01	.32978E-02
11	.44880E+00	.19787E+00	-.93857E-02	.38603E-01	-.79175E-02	-.15835E-01	.27701E-02
12	.67320E+00	.19673E+00	-.15416E-02	.31309E-01	-.75703E-02	-.15141E-01	.50923E-03
13	.89760E+00	.19728E+00	.52650E-02	.29357E-01	-.76890E-02	-.15378E-01	-.13850E-02
14	.11220E+01	.19910E+00	.12548E-01	.35555E-01	-.81919E-02	-.16384E-01	-.31722E-02
15	.13464E+01	.20281E+00	.22043E-01	.49070E-01	-.91127E-02	-.18225E-01	-.53257E-02
16	.15708E+01	.20899E+00	0.	-.24553E+00	-.10582E-01	-.21164E-01	0.

R= 1.000

I	J	X	C	Y/Z	H	UI	VI	WI	H1	H2	CRTH
2	2	-.15708E+01	.40719E+00	0.	-.74904E-01	0.	0.	0.	0.	0.	0.
3	3	-.13464E+01	.40530E+00	-.15981E-01	-.67533E-01	0.	0.	0.	0.	0.	0.
4	4	-.11220E+01	.40002E+00	-.28881E-01	-.47435E-01	0.	0.	0.	0.	0.	0.
5	5	-.89760E+00	.39234E+00	-.36080E-01	-.16728E-01	0.	0.	0.	0.	0.	0.
6	6	-.67320E+00	.38382E+00	-.35454E-01	.22304E-01	0.	0.	0.	0.	0.	0.
7	7	-.44880E+00	.37643E+00	-.25345E-01	.67793E-01	0.	0.	0.	0.	0.	0.
8	8	-.22440E+00	.37245E+00	-.55662E-02	.10849E+00	0.	0.	0.	0.	0.	0.
9	9	-.71054E-14	.37393E+00	.20421E-01	.12312E+00	0.	0.	0.	0.	0.	0.
10	10	.22440E+00	.38161E+00	.45565E-01	.10098E+00	0.	0.	0.	0.	0.	0.
11	11	.44880E+00	.39438E+00	.63301E-01	.57098E-01	0.	0.	0.	0.	0.	0.
12	12	.67320E+00	.41002E+00	.70636E-01	.82747E-02	0.	0.	0.	0.	0.	0.
13	13	.89760E+00	.42608E+00	.67104E-01	-.39750E-01	0.	0.	0.	0.	0.	0.
14	14	.11220E+01	.44014E+00	.52993E-01	-.86016E-01	0.	0.	0.	0.	0.	0.
15	15	.13464E+01	.44987E+00	.29466E-01	-.12368E+00	0.	0.	0.	0.	0.	0.
16	16	.15708E+01	.45336E+00	0.	-.13894E+00	0.	0.	0.	0.	0.	0.

R= 1.000

I	J	HX	HY	HR	H1X	H1Y	H1R	H2X	H2Y	H2R
2	2	-.21243E-14	-.24084E+00	.28240E+01	.84953E-15	-.31799E+00	-.31799E+00	.94810E+00	.28266E-02	.67712E-17
3	3	.13377E+00	-.21751E+00	.28100E+01	-.10254E+00	-.30488E+00	-.30488E+00	.94686E+00	.27841E-02	.88846E-03
4	4	.26156E+00	-.19286E+00	.26321E+01	-.19701E+00	-.30596E+00	-.30596E+00	.93144E+00	.25665E-02	.18251E-02
5	5	.38025E+00	-.16526E+00	.23176E+01	-.27148E+00	-.32215E+00	-.32215E+00	.90693E+00	.20919E-02	.28816E-02
6	6	.48486E+00	-.13325E+00	.19129E+01	-.31259E+00	-.35851E+00	-.35851E+00	.87963E+00	.11159E-02	.41070E-02
7	7	.56920E+00	-.95849E-01	.14827E+01	-.29623E+00	-.42460E+00	-.42460E+00	.85555E+00	.95915E-03	.52941E-02
8	8	.62703E+00	-.51972E-01	.11328E+01	-.16994E+00	-.51435E+00	-.51435E+00	.83935E+00	.48509E-02	.48521E-02
9	9	.64941E+00	-.17264E-14	.10012E+01	.87156E-01	-.54257E+00	-.54257E+00	.83548E+00	.76327E-02	.19919E-15
10	10	.62703E+00	.51972E-01	.11328E+01	.31854E+00	-.42555E+00	-.42555E+00	.84702E+00	.48509E-02	.48521E-02
11	11	.56920E+00	.95849E-01	.14827E+01	.40136E+00	-.28632E+00	-.28632E+00	.87002E+00	.95915E-03	.52941E-02
12	12	.48486E+00	.13325E+00	.19129E+01	.38558E+00	-.20158E+00	-.20158E+00	.90039E+00	.11159E-02	.41070E-02
13	13	.38025E+00	.16526E+00	.23176E+01	.32204E+00	-.15747E+00	-.15747E+00	.93354E+00	.20919E-02	.28816E-02
14	14	.26156E+00	.19286E+00	.26321E+01	.22999E+00	-.13779E+00	-.13779E+00	.96341E+00	.25665E-02	.18251E-02
15	15	.13377E+00	.21751E+00	.28100E+01	.11933E+00	-.13531E+00	-.13531E+00	.98359E+00	.27841E-02	.88846E-03
16	16	.11566E-13	.24084E+00	.28240E+01	.10086E-13	-.14852E+00	-.14852E+00	.98891E+00	.28266E-02	.77384E-16

Figure 46 Sample Printed Output for BSF Method (Sheet 11 of 14)

2	2	0,	-	.25973E+00	-	.97070E-01	0,	-	.15108E-03	.27701E-02	0,	.19344E-18	.68435E-17					
3	2	-	.19198E+00	-	.27362E+00	-	.86194E-01	-	.26009E-03	-	.17765E-03	.27281E-02	-	.18251E-02	-	.29105E-04	-	.89763E-03
4	2	-	.49237E+00	-	.24352E+00	-	.69502E-01	-	.69217E-03	-	.26363E-03	.24912E-02	-	.19932E-02	-	.41168E-04	-	.18369E-02
5	2	-	.71920E+00	-	.17624E+00	-	.48604E-01	-	.14504E-02	-	.42055E-03	.19759E-02	-	.22818E-02	-	.17968E-04	-	.28767E-02
6	2	-	.83490E+00	-	.82308E-01	-	.23313E-01	-	.30511E-02	-	.63510E-03	.93600E-03	-	.24125E-02	-	.26744E-03	-	.40312E-02
7	2	-	.78004E+00	.29110E-01	.90353E-02	-	.59668E-02	-	.68304E-03	-	.11712E-02	.74515E-03	.96767E-03	-	.49937E-02			
8	2	-	.48149E+00	.14055E+00	.50561E-01	-	.66735E-02	.56045E-02	.56045E-02	.56045E-02	.56045E-02	.52941E-02	.52941E-02	-	.19096E-02	-	.41652E-02	
9	2	-	.43627E-11	.19460E+00	.75120E-01	-	.18957E-13	.25228E-02	.66588E-02	.97042E-02	.10966E-15	-	.15686E-15					
10	2	.48149E+00	.14805E+00	.50555E-01	.66735E-02	.58666E-03	-	.46506E-02	.52941E-02	.52941E-02	.20168E-02	.41634E-02						
11	2	.78004E+00	.31681E-01	.89352E-02	.59668E-02	-	.175408E-03	-	.11724E-02	-	.74515E-03	-	.10625E-02	.49944E-02				
12	2	.83490E+00	-.94541E-01	.23489E-01	.30511E-02	-.72479E-03	.93581E-03	.93581E-03	.24125E-02	-	.30209E-03	.40319E-02						
13	2	.71920E+00	-.20779E+00	-.48858E-01	.14504E-02	-.49285E-03	.19760E-02	.22818E-02	-	.19381E-04	.28771E-02							
14	2	.49237E+00	-.29356E+00	-.69838E-01	.69217E-03	-.31562E-03	.24914E-02	.19932E-02	.50287E-04	.18371E-02								
15	2	.19198E+00	-.33538E+00	-.86594E-01	.26009E-03	-.21610E-03	.27283E-02	-	.18251E-02	.35888E-04	.89773E-03							
16	2	0,	-	.32160E+00	-	.97484E-01	0,	-	.18573E-03	.27703E-02	.27547E-17	.78219E-16						

ITER	DELMX	I	J	DELAUG	RESMX	I	J	RESAVG	KSUP	DELS	IS
------	-------	---	---	--------	-------	---	---	--------	------	------	----

1	.5340E-02	16	2	.6268E-03	.4786E+01	3	2	.2163E+00	0	.33E-02	2
2	.2064E-02	2	2	.2888E-03	.1132E+01	2	2	.6268E-01	0	.77E-03	16
3	.9331E-03	2	2	.1317E-03	.3613E+00	2	2	.2516E-01	0	.47E-03	3
4	.2890E-03	15	2	.4864E-04	.8738E-01	2	2	.9022E-02	0	.47E-03	2
5	.1602E-03	16	2	.2344E-04	.4670E-01	16	2	.4304E-02	0	.23E-03	2
6	.8098E-04	15	3	.1316E-04	.2063E-01	15	3	.2462E-02	0	.71E-04	10
7	.4911E-04	16	2	.9126E-05	.1369E-01	16	2	.1709E-02	0	.54E-04	10
8	.2594E-04	15	3	.5279E-05	.6604E-02	15	3	.9844E-03	0	.41E-04	9
9	.1647E-04	16	2	.3863E-05	.4478E-02	16	2	.7297E-03	0	.28E-04	8
10	.8898E-05	15	3	.2619E-05	.2267E-02	15	3	.4973E-03	0	.18E-04	9
11	.5817E-05	16	2	.1759E-05	.1558E-02	16	2	.3316E-03	0	.12E-04	8
12	.3187E-05	15	3	.1056E-05	.8495E-03	2	2	.1997E-03	0	.73E-05	7

R= 1.000

JRING= 2

BODY COORDINATES AND SURFACE DATA

I	RHO	F	X/Z	Y/Z	Z	M	MR	MC	CP			
2	.20899E+00	-	.11113E+00	-	.21243E-14	-	.24084E+00	.97220E+00	.13520E+01	.13510E+01	.51103E-01	.32563E+00
3	.20281E+00	-	.11361E+00	.13377E+00	-	.21751E+00	.96891E+00	.13457E+01	.13408E+01	.11421E+00	.33281E+00	
4	.19910E+00	-	.11052E+00	.26156E+00	-	.19286E+00	.95104E+00	.13312E+01	.13136E+01	.21593E+00	.34944E+00	
5	.19718E+00	-	.10365E+00	.38025E+00	-	.16526E+00	.92375E+00	.13092E+01	.12758E+01	.29363E+00	.37536E+00	
6	.19673E+00	-	.94840E-01	.48486E+00	-	.13325E+00	.89341E+00	.12775E+01	.12348E+01	.32730E+00	.41359E+00	

Figure 46 Sample Printed Output for BSF Method (Sheet 12 of 14)

7	.19787E+00	-.85778E-01	.56920E+00	-.95849E-01	.86608E+00	.12314E+01	.11969E+01	.28940E+00	.47124E+00
8	.20095E+00	-.77853E-01	.62703E+00	-.51972E-01	.84640E+00	.11730E+01	.11679E+01	.10959E+00	.54772E+00
9	.20352E+00	-.72443E-01	.64941E+00	-.17264E-14	.83867E+00	.12047E+01	.11754E+01	.26392E+00	.50570E+00
10	.20095E+00	-.70122E-01	.62703E+00	.51972E-01	.84640E+00	.13844E+01	.12410E+01	.61340E+00	.28944E+00
11	.19787E+00	-.68263E-01	.56920E+00	.95849E-01	.86608E+00	.14924E+01	.13112E+01	.71275E+00	.17769E+00
12	.19767E+00	-.67023E-01	.48486E+00	.13325E+00	.89341E+00	.15194E+01	.13724E+01	.65199E+00	.15188E+00
13	.19718E+00	-.66389E-01	.38025E+00	.16526E+00	.92375E+00	.15280E+01	.14329E+01	.53045E+00	.14367E+00
14	.19910E+00	-.65934E-01	.26156E+00	.19286E+00	.95104E+00	.15339E+01	.14875E+01	.37444E+00	.13835E+00
15	.20281E+00	-.64983E-01	.13377E+00	.21751E+00	.96891E+00	.15391E+01	.15265E+01	.19652E+00	.13356E+00
16	.20899E+00	-.62942E-01	.11566E-13	.24084E+00	.97220E+00	.15417E+01	.15406E+01	.58359E-01	.13119E+00

JRING= 16

# ROW SHOCK COORDINATES AND SURFACE DATA

I	RHO	F	X/Z	Y/Z	Z	M	MR	MC	CP
2	.40719E+00	0.	-.14232E-14	-.82977E+00	.76957E+00	.14020E+01	.11355E+01	.82234E+00	.27029E+00
3	.40530E+00	0.	.23179E+00	-.80632E+00	.76609E+00	.13992E+01	.11323E+01	.82194E+00	.27327E+00
4	.40002E+00	0.	.45054E+00	-.73822E+00	.75637E+00	.13900E+01	.11232E+01	.81887E+00	.28325E+00
5	.39234E+00	0.	.64449E+00	-.63170E+00	.74239E+00	.13763E+01	.11105E+01	.81297E+00	.29834E+00
6	.38382E+00	0.	.80420E+00	-.49572E+00	.72692E+00	.13616E+01	.10980E+01	.80522E+00	.31473E+00
7	.37643E+00	0.	.92351E+00	-.34023E+00	.71272E+00	.13506E+01	.10896E+01	.79811E+00	.32717E+00
8	.37245E+00	0.	.10003E+01	-.17365E+00	.70173E+00	.13488E+01	.10885E+01	.79656E+00	.32924E+00
9	.37393E+00	0.	.10352E+01	-.36067E-14	.69477E+00	.13609E+01	.10967E+01	.80568E+00	.31558E+00
10	.38161E+00	0.	.10276E+01	.18074E+00	.69195E+00	.13879E+01	.11153E+01	.82606E+00	.28555E+00
11	.39438E+00	0.	.97336E+00	.36734E+00	.69298E+00	.14256E+01	.11434E+01	.85144E+00	.24517E+00
12	.41002E+00	0.	.86816E+00	.55264E+00	.69688E+00	.14669E+01	.11777E+01	.87457E+00	.20280E+00
13	.42608E+00	0.	.71104E+00	.72375E+00	.70197E+00	.15056E+01	.12129E+01	.89206E+00	.16494E+00
14	.44014E+00	0.	.50622E+00	.86461E+00	.70643E+00	.15368E+01	.12428E+01	.90394E+00	.13569E+00
15	.44987E+00	0.	.26375E+00	.95849E+00	.70919E+00	.15568E+01	.12625E+01	.91095E+00	.11747E+00
16	.45336E+00	0.	.19437E-13	.99162E+00	.71007E+00	.15635E+01	.12692E+01	.91300E+00	.11153E+00

# RADIAL OUTPUT DATA IN CROSSFLOW PLANE

IRING= 2

J	RHO	F	X/Z	Y/Z	Z	M	MR	MC	CP
2	.20899E+00	-.11112E+00	-.21243E-14	-.24084E+00	.97220E+00	.13520E+01	.13510E+01	.51103E-01	.32563E+00
3	.22315E+00	-.10012E+00	-.24931E-14	-.28264E+00	.96230E+00	.13477E+01	.13423E+01	.12096E+00	.33046E+00
4	.23730E+00	-.89798E-01	-.55514E-15	-.32367E+00	.95140E+00	.13452E+01	.13323E+01	.18599E+00	.33334E+00
5	.25146E+00	-.80059E-01	-.62468E-15	-.36422E+00	.93962E+00	.13440E+01	.13210E+01	.24749E+00	.33470E+00
6	.26562E+00	-.70826E-01	-.69378E-15	-.40451E+00	.92703E+00	.13440E+01	.13086E+01	.30622E+00	.33478E+00
7	.27978E+00	-.62050E-01	-.76280E-15	-.44475E+00	.91371E+00	.13449E+01	.12951E+01	.36269E+00	.33371E+00
8	.29393E+00	-.53693E-01	-.83202E-15	-.48511E+00	.89972E+00	.13468E+01	.12805E+01	.41728E+00	.33157E+00
9	.30809E+00	-.45727E-01	-.90173E-15	-.52573E+00	.88512E+00	.13496E+01	.12650E+01	.47029E+00	.32838E+00
10	.32225E+00	-.38132E-01	-.97218E-15	-.56683E+00	.86996E+00	.13533E+01	.12485E+01	.52201E+00	.32416E+00

Figure 46 Sample Printed Output for BSF Method (Sheet 13 of 14)

11	.33640E+00	-.30895E-01	-.10436E-14	-.60846E+00	.85429E+00	.13580E+01	.12313E+01	.57268E+00	.31885E+00
12	.35056E+00	-.24008E-01	-.11162E-14	-.65080E+00	.83814E+00	.13637E+01	.12133E+01	.62259E+00	.31238E+00
13	.36472E+00	-.17467E-01	-.11902E-14	-.69397E+00	.82155E+00	.13707E+01	.11946E+01	.67206E+00	.30457E+00
14	.37887E+00	-.11277E-01	-.12659E-14	-.73810E+00	.80457E+00	.13792E+01	.11754E+01	.72153E+00	.29516E+00
15	.39303E+00	-.54473E-02	-.13435E-14	-.78332E+00	.78723E+00	.13896E+01	.11537E+01	.77169E+00	.28368E+00
16	.40719E+00	0.	-.14233E-14	-.82977E+00	.76957E+00	.14020E+01	.11355E+01	.82234E+00	.27029E+00

IRING= 9

J	RHO	F	X/Z	Y/Z	Z	M	MR	MC	CF
2	.20352E+00	-.72443E-01	.64941E+00	-.17264E-14	.83867E+00	.12047E+01	.11754E+01	.26392E+00	.50570E+00
3	.21569E+00	-.65988E-01	.66767E+00	-.20066E-14	.83166E+00	.12011E+01	.11742E+01	.25290E+00	.51033E+00
4	.22786E+00	-.59764E-01	.68767E+00	-.22818E-14	.82397E+00	.12073E+01	.11735E+01	.28374E+00	.50233E+00
5	.24004E+00	-.53749E-01	.70926E+00	-.25335E-14	.81567E+00	.12173E+01	.11721E+01	.32847E+00	.48933E+00
6	.25221E+00	-.47930E-01	.73233E+00	-.28230E-14	.80679E+00	.12289E+01	.11699E+01	.37620E+00	.47440E+00
7	.26438E+00	-.42300E-01	.75678E+00	-.30915E-14	.79740E+00	.12411E+01	.11666E+01	.42350E+00	.45684E+00
8	.27655E+00	-.36856E-01	.78255E+00	-.33600E-14	.78753E+00	.12536E+01	.11623E+01	.46946E+00	.44318E+00
9	.28872E+00	-.31594E-01	.80962E+00	-.36295E-14	.77721E+00	.12661E+01	.11570E+01	.51399E+00	.42762E+00
10	.30090E+00	-.26514E-01	.83797E+00	-.39007E-14	.76647E+00	.12786E+01	.11508E+01	.55724E+00	.41219E+00
11	.31307E+00	-.21617E-01	.86757E+00	-.41745E-14	.75535E+00	.12912E+01	.11436E+01	.59948E+00	.39683E+00
12	.32524E+00	-.16905E-01	.89845E+00	-.44515E-14	.74387E+00	.13041E+01	.11357E+01	.64097E+00	.38142E+00
13	.33741E+00	-.12380E-01	.93062E+00	-.47325E-14	.73204E+00	.13172E+01	.11269E+01	.68202E+00	.36581E+00
14	.34959E+00	-.80484E-02	.96411E+00	-.50183E-14	.71991E+00	.13310E+01	.11175E+01	.72298E+00	.34974E+00
15	.36176E+00	-.39177E-02	.99894E+00	-.53094E-14	.70748E+00	.13456E+01	.11074E+01	.76429E+00	.33294E+00
16	.37393E+00	0.	.10352E+01	-.56067E-14	.69477E+00	.13609E+01	.10967E+01	.80568E+00	.31558E+00

IRING= 16

J	RHO	F	X/Z	Y/Z	Z	M	MR	MC	CF
2	.20899E+00	-.62942E-01	.11566E-13	.24084E+00	.97220E+00	.15417E+01	.15406E+01	.58359E-01	.13119E+00
3	.22645E+00	-.57401E-01	.11959E-13	.29226E+00	.95985E+00	.15368E+01	.15314E+01	.12893E+00	.13565E+00
4	.24390E+00	-.51965E-01	.11584E-13	.34261E+00	.94402E+00	.15328E+01	.15200E+01	.19743E+00	.13937E+00
5	.26136E+00	-.46655E-01	.13268E-13	.39239E+00	.93090E+00	.15296E+01	.15067E+01	.26381E+00	.14236E+00
6	.27881E+00	-.41482E-01	.14945E-13	.44200E+00	.91464E+00	.15271E+01	.14914E+01	.32820E+00	.14463E+00
7	.29627E+00	-.36459E-01	.13134E-13	.49179E+00	.89736E+00	.15255E+01	.14746E+01	.39076E+00	.14619E+00
8	.31372E+00	-.31593E-01	.14476E-13	.54203E+00	.87916E+00	.15246E+01	.14562E+01	.45166E+00	.14700E+00
9	.33118E+00	-.26894E-01	.15837E-13	.59302E+00	.86013E+00	.15246E+01	.14363E+01	.51108E+00	.14703E+00
10	.34863E+00	-.22373E-01	.17225E-13	.64499E+00	.84036E+00	.15254E+01	.14152E+01	.56922E+00	.14622E+00
11	.36609E+00	-.18043E-01	.18644E-13	.69819E+00	.81993E+00	.15273E+01	.13930E+01	.62631E+00	.14447E+00
12	.38354E+00	-.13918E-01	.20107E-13	.75288E+00	.79889E+00	.15304E+01	.13697E+01	.68265E+00	.14163E+00
13	.40100E+00	-.10017E-01	.15863E-13	.80930E+00	.77733E+00	.15349E+01	.13455E+01	.73868E+00	.13744E+00
14	.41845E+00	-.63657E-02	.17008E-13	.86770E+00	.75530E+00	.15414E+01	.13205E+01	.79512E+00	.13145E+00
15	.43591E+00	-.30036E-02	.18197E-13	.92838E+00	.73286E+00	.15511E+01	.12951E+01	.85346E+00	.12267E+00
16	.45336E+00	0.	.19437E-13	.99162E+00	.71007E+00	.15635E+01	.12692E+01	.91300E+00	.11153E+00

NCOREL

NON-CONICAL RELAXATION SOLUTION

MINF=1.700 ALP= 5.000

IC= 16 JC= 16 KMAX1= 200 KMAX2= 200 KMAX3= 200 KMAXNC= 200 KREF=1

IFLOT= 2 NT= 50 NDUT= 1 JOUT= 0 IRUN= 0

GAMMA=1.40 WW1=1.500 WW2=1.500 WW3=1.500 EST= -.10 DMIN1= .10E-05 DMIN2= .10E-05 DMIN3= .10E-05

4-DIGIT AIRFOIL...ARROW WING

AZ=33.000 BZ= 1.000 NG= 39 NS= 4 IFIT= 0

IXWI=10 IZWI= 5 IZW= 0 ITE= 1 ZTE= 20.0000

AERODYNAMIC CONSTANTS CBAR= 14.7470 YCG= 0.0000 ZCG= 16.7010

ISYM= 0

# RADIAL STEP SIZE PARAMETERS AND OPTIONS

DR= 1.000 NR= 50 IPUN= 0 REID= 34.00000 IDPTS= 3 IDPTS= 0 IAERO= 1 EF= 1.40

# BOW SHOCK RELAXATION PARAMETERS

RELSHK(1)= .50 RELSHK(2)= .25 RELSHK(3)= .10 RELNC= 1.50

# RADIAL STEP SIZE REFINEMENT PARAMETERS

KRR(1)= 0 KRR(2)= 0 KRR(3)= 0 KRR(4)= 0 KRR(5)= 0

RZNEW(1)= 100.00000 RZNEW(2)= 100.00000 RZNEW(3)= 900.00000 RZNEW(4)=1000.00000 RZNEW(5)=1000.00000

2246-045W

Figure 47 Sample Printed Output for BSC Method (Sheet 1 of 14)

\*\*\* SPHERICAL CUT GEOMETRY INPUT COORDINATES \*\*\*

LEADING EDGE OR MAXIMUM HALF WIDTH COORDINATES

		XTIP=	.54464E+00	YTIP=	0.	ZTIP=	.83867E+00	DMTIF=	0.	PSID=	.33000E+02	RTIP=	.10000E+01
IG	R	X	Y	Z	OMEG	PSI							
1	.10000E+01	0.	-.23414E+00	.97220E+00	-.90000E+02	.13541E+02							
2	.10000E+01	.44976E-01	-.22661E+00	.97295E+00	-.78774E+02	.13357E+02							
3	.10000E+01	.89645E-01	-.21853E+00	.97171E+00	-.67695E+02	.13662E+02							
4	.10000E+01	.13370E+00	-.20990E+00	.96854E+00	-.57504E+02	.14410E+02							
5	.10000E+01	.17684E+00	-.20071E+00	.96356E+00	-.48618E+02	.15516E+02							
6	.10000E+01	.21878E+00	-.19097E+00	.95690E+00	-.41117E+02	.16882E+02							
7	.10000E+01	.25922E+00	-.18066E+00	.94877E+00	-.34873E+02	.18419E+02							
8	.10000E+01	.29789E+00	-.16978E+00	.93938E+00	-.29680E+02	.20052E+02							
9	.10000E+01	.33452E+00	-.15834E+00	.92899E+00	-.25329E+02	.21722E+02							
10	.10000E+01	.36887E+00	-.14633E+00	.91789E+00	-.21638E+02	.23381E+02							
11	.10000E+01	.40070E+00	-.13378E+00	.90639E+00	-.18463E+02	.24989E+02							
12	.10000E+01	.42980E+00	-.12070E+00	.89482E+00	-.15686E+02	.26514E+02							
13	.10000E+01	.45395E+00	-.11070E+00	.88354E+00	-.13218E+02	.27928E+02							
14	.10000E+01	.47900E+00	-.92994E-01	.87288E+00	-.10987E+02	.29205E+02							
15	.10000E+01	.49877E+00	-.78429E-01	.86318E+00	-.89364E+01	.30324E+02							
16	.10000E+01	.51513E+00	-.63433E-01	.85476E+00	-.70201E+01	.31267E+02							
17	.10000E+01	.52797E+00	-.48045E-01	.84790E+00	-.51996E+01	.32016E+02							
18	.10000E+01	.53721E+00	-.32310E-01	.84283E+00	-.34419E+01	.32560E+02							
19	.10000E+01	.54278E+00	-.16278E-01	.83972E+00	-.17178E+01	.32890E+02							
20	.10000E+01	.54464E+00	-.22070E-07	.83867E+00	-.23217E-05	.33000E+02							
21	.10000E+01	.54278E+00	.16278E-01	.83972E+00	.17178E+01	.32890E+02							
22	.10000E+01	.53721E+00	.32310E-01	.84283E+00	.34419E+01	.32560E+02							
23	.10000E+01	.52797E+00	.48045E-01	.84790E+00	.51996E+01	.32016E+02							
24	.10000E+01	.51513E+00	.63433E-01	.85476E+00	.70201E+01	.31267E+02							
25	.10000E+01	.49877E+00	.78429E-01	.86318E+00	.89364E+01	.30324E+02							
26	.10000E+01	.47900E+00	.92994E-01	.87288E+00	.10987E+02	.29205E+02							
27	.10000E+01	.45395E+00	.10709E+00	.88354E+00	.13218E+02	.27928E+02							
28	.10000E+01	.42980E+00	.12070E+00	.89482E+00	.15686E+02	.26514E+02							
29	.10000E+01	.40070E+00	.13378E+00	.90639E+00	.18463E+02	.24989E+02							
30	.10000E+01	.36887E+00	.14633E+00	.91789E+00	.21638E+02	.23381E+02							
31	.10000E+01	.33452E+00	.15834E+00	.92899E+00	.25329E+02	.21722E+02							
32	.10000E+01	.29789E+00	.16978E+00	.93938E+00	.29680E+02	.20052E+02							
33	.10000E+01	.25922E+00	.18066E+00	.94877E+00	.34873E+02	.18419E+02							
34	.10000E+01	.21878E+00	.19097E+00	.95690E+00	.41117E+02	.16882E+02							
35	.10000E+01	.17684E+00	.20071E+00	.96356E+00	.48618E+02	.15516E+02							
36	.10000E+01	.13370E+00	.20990E+00	.96854E+00	.57504E+02	.14410E+02							
37	.10000E+01	.89645E-01	.21853E+00	.97171E+00	.67695E+02	.13662E+02							
38	.10000E+01	.44976E-01	.22661E+00	.97295E+00	.78774E+02	.13357E+02							
39	.10000E+01	0.	.23414E+00	.97220E+00	.90000E+02	.13541E+02							

2246-045W

Figure 47 Sample Printed Output for BSC Method (Sheet 2 of 14)

SINGULARITY LOCATION IN PHYSICAL SPACE AT R= 1.000  
 XSIN/Z= .59424 YSIN/Z= 0.00000 -YSIN/Z= 0.00000

SINGULARITY LOCATION IN MAPPED SPACE AT CURRENT STATION  
 S0= .2747E+00 0. S1= .2747E+00 0. S2= 0. 0.

SINGULARITY LOCATION IN MAPPED SPACE AT NEW STATION  
 S0N= .2747E+00 0. S1N= .2747E+00 0. S2N= 0. 0.

XTIP= 1.08928 YTIP= 0.00000 ZTIP= 1.67734 DMTIP= 0.00000 PSID= 33.00000 RTIP= 2.00000

SINGULARITY LOCATION IN PHYSICAL SPACE AT R= 2.000  
 XSIN/Z= .62557 YSIN/Z= 0.00000 -YSIN/Z= 0.00000

SINGULARITY DERIVATIVES AT CURRENT STATION S0PR= 0. 0. S1PR= 0. 0.  
 SINGULARITY DERIVATIVE AT CURRENT STATION S2PR= 0. 0.  
 SINGULARITY DERIVATIVES AT NEW STATION S0PRN= .6159E-02 0. S1PRN= .6159E-02 0.  
 SINGULARITY DERIVATIVE AT NEW STATION S2PRN= 0. 0.  
 PSIMU= 36.031879  
 SHOCKI

R= 0.000

I	X	B	BPR	BSEC	BR	BRR	BRTH
2	-.15708E+01	.20899E+00	0.	-.24553E+00	0.	0.	0.
3	-.13464E+01	.20281E+00	-.22043E-01	.49070E-01	0.	0.	0.
4	-.11220E+01	.19910E+00	-.12548E-01	.35555E-01	0.	0.	0.
5	-.89760E+00	.19718E+00	-.52650E-02	.29357E-01	0.	0.	0.
6	-.67320E+00	.19673E+00	.15416E-02	.31309E-01	0.	0.	0.
7	-.44880E+00	.19787E+00	.93857E-02	.38603E-01	0.	0.	0.
8	-.22440E+00	.20095E+00	.12588E-01	-.10065E-01	0.	0.	0.
9	-.71054E-14	.20352E+00	-.17316E-11	-.10213E+00	0.	0.	0.
10	.22440E+00	.20095E+00	-.12588E-01	-.10065E-01	0.	0.	0.
11	.44880E+00	.19787E+00	-.93857E-02	.38603E-01	0.	0.	0.
12	.67320E+00	.19673E+00	-.15416E-02	.31309E-01	0.	0.	0.
13	.89760E+00	.19718E+00	.52650E-02	.29357E-01	0.	0.	0.
14	.11220E+01	.19910E+00	.12548E-01	.35555E-01	0.	0.	0.
15	.13464E+01	.20281E+00	.22043E-01	.49070E-01	0.	0.	0.
16	.15708E+01	.20899E+00	0.	-.24553E+00	0.	0.	0.

R= 0.000

I	X	C	CPR	CSEC	CR	CRR	CRTH
2	-.15708E+01	.49170E+00	0.	-.64481E-01	0.	0.	0.

2246-045W

Figure 47 Sample Printed Output for BSC Method (Sheet 3 of 14)



3	-.13464E+01	.49008E+00	-.26059E-01	-.16777E+00	0.	0.	0.
4	-.11220E+01	.48001E+00	-.58190E-01	-.11860E+00	0.	0.	0.
5	-.89760E+00	.46397E+00	-.76381E-01	-.43527E-01	0.	0.	0.
6	-.67320E+00	.44573E+00	-.75266E-01	.53456E-01	0.	0.	0.
7	-.44880E+00	.43019E+00	-.51272E-01	.16040E+00	0.	0.	0.
8	-.22440E+00	.42272E+00	-.27591E-02	.27197E+00	0.	0.	0.
9	-.71054E-14	.42895E+00	.66030E-01	.34112E+00	0.	0.	0.
10	.22440E+00	.45235E+00	.13259E+00	.25214E+00	0.	0.	0.
11	.44880E+00	.48846E+00	.17371E+00	.11434E+00	0.	0.	0.
12	.67320E+00	.53031E+00	.18394E+00	-.23211E-01	0.	0.	0.
13	.89760E+00	.57101E+00	.16464E+00	-.14880E+00	0.	0.	0.
14	.11220E+01	.60420E+00	.12036E+00	-.24586E+00	0.	0.	0.
15	.13464E+01	.62502E+00	.58153E-01	-.30853E+00	0.	0.	0.
16	.15708E+01	.63030E+00	0.	-.20976E+00	0.	0.	0.

R= 0.000

I	J	X/Z	Y/Z	H	UI	VI	WI	H1	H2
2	2	-.21243E-14	-.24084E+00	.28240E+01	.84953E-15	-.31799E+00	.94810E+000.		0.
3	2	.13377E+00	-.21751E+00	.28100E+01	-.10254E+00	-.30488E+00	.94686E+000.		0.
4	2	.26156E+00	-.19286E+00	.26321E+01	-.19701E+00	-.30596E+00	.93144E+000.		0.
5	2	.38025E+00	-.16526E+00	.23176E+01	-.27148E+00	-.32215E+00	.90693E+000.		0.
6	2	.48486E+00	-.13325E+00	.19129E+01	-.31259E+00	-.35851E+00	.87963E+000.		0.
7	2	.56920E+00	-.95849E-01	.14827E+01	-.29623E+00	-.42460E+00	.85555E+000.		0.
8	2	.62703E+00	-.51972E-01	.11328E+01	-.16994E+00	-.51635E+00	.83935E+000.		0.
9	2	.64941E+00	-.17264E-14	.10012E+01	.87156E-01	-.54257E+00	.83548E+000.		0.
10	2	.62703E+00	.51972E-01	.11328E+01	.31854E+00	-.42555E+00	.84702E+000.		0.
11	2	.56920E+00	.95849E-01	.14827E+01	.40136E+00	-.28632E+00	.87002E+000.		0.
12	2	.48486E+00	.13325E+00	.19129E+01	.38558E+00	-.20158E+00	.90039E+000.		0.
13	2	.38025E+00	.16526E+00	.23176E+01	.32204E+00	-.15747E+00	.93354E+000.		0.
14	2	.26156E+00	.19286E+00	.26321E+01	.22991E+00	-.13779E+00	.96341E+000.		0.
15	2	.13377E+00	.21751E+00	.28100E+01	.11933E+00	-.13531E+00	.98359E+000.		0.
16	2	.11566E-13	.24084E+00	.28240E+01	.10086E-13	-.14852E+00	.98891E+000.		0.

I	J	HX	HY	HR	H1X	H1Y	H1R	H2X	H2Y	H2R
2	2	0.	-.37363E+00	0.	0.	0.	0.	0.	0.	0.
3	2	-.19198E+00	-.39192E+00	0.	0.	0.	0.	0.	0.	0.
4	2	-.49237E+00	-.34407E+00	0.	0.	0.	0.	0.	0.	0.
5	2	-.71920E+00	-.24384E+00	0.	0.	0.	0.	0.	0.	0.
6	2	-.83490E+00	-.11168E+00	0.	0.	0.	0.	0.	0.	0.
7	2	-.78004E+00	.36485E-01	0.	0.	0.	0.	0.	0.	0.
8	2	-.48149E+00	.18161E+00	0.	0.	0.	0.	0.	0.	0.
9	2	-.43627E-11	.25891E+00	0.	0.	0.	0.	0.	0.	0.
10	2	.48149E+00	.20573E+00	0.	0.	0.	0.	0.	0.	0.
11	2	.78004E+00	.43174E-01	0.	0.	0.	0.	0.	0.	0.
12	2	.83490E+00	-.15495E+00	0.	0.	0.	0.	0.	0.	0.
13	2	.71920E+00	-.35036E+00	0.	0.	0.	0.	0.	0.	0.
14	2	.49237E+00	-.50791E+00	0.	0.	0.	0.	0.	0.	0.

2246-045W

Figure 47 Sample Printed Output for BSC Method (Sheet 4 of 14)

15 2 .19198E+00 -.58903E+00 0. 0. 0. 0. 0. 0. 0.  
 16 2 0. -.56834E+00 0. 0. 0. 0. 0. 0. 0. 0.

ITER	DELX	I	J	DELAG	RESMX	I	J	RESAVG	KSUF
1	-.3615E-01	3	2	.3897E-02	-.3520E+02	4	2	.1993E+01	111
2	-.2085E-01	2	2	.3646E-02	-.9898E+01	8	3	.1009E+01	103
3	-.1394E-01	2	2	.3108E-02	-.4796E+01	8	5	.7847E+00	98
4	-.9415E-02	2	2	.2609E-02	-.5359E+01	8	6	.6301E+00	91
5	-.6907E-02	2	2	.2328E-02	-.4809E+01	8	7	.5310E+00	84
6	-.5446E-02	2	2	.2127E-02	-.3148E+01	8	8	.4625E+00	78
7	-.4578E-02	2	2	.1875E-02	-.2325E+01	7	9	.3971E+00	73
8	-.3786E-02	2	2	.1665E-02	-.2555E+01	8	9	.3430E+00	69
9	-.3431E-02	5	2	.1589E-02	-.1807E+01	7	10	.3144E+00	65
10	-.3101E-02	4	2	.1394E-02	-.2063E+01	8	10	.2824E+00	63
11	-.2789E-02	2	2	.1133E-02	-.8750E+00	9	10	.2213E+00	56
12	-.2334E-02	2	2	.1061E-02	-.1409E+01	8	11	.1999E+00	54
13	-.2018E-02	6	9	.9994E-03	-.1299E+01	9	11	.1879E+00	52
14	-.1914E-02	5	2	.8612E-03	-.9029E+00	5	11	.1631E+00	51
15	-.1947E-02	4	2	.7878E-03	-.7725E+00	4	11	.1441E+00	49
16	-.2044E-02	3	2	.7498E-03	-.8783E+00	2	11	.1346E+00	46
17	-.2071E-02	2	2	.7093E-03	-.9925E+00	8	12	.1272E+00	46
18	-.1645E-02	2	2	.6199E-03	-.9284E+00	9	12	.1124E+00	46
19	-.1575E-02	6	12	.5094E-03	-.7709E+00	6	12	.9238E-01	44
20	-.1324E-02	6	12	.4223E-03	-.8219E+00	6	12	.7578E-01	44
21	-.9642E-03	10	12	.3668E-03	-.5344E+00	6	12	.6473E-01	43
22	-.1256E-02	5	12	.3321E-03	-.4653E+00	5	12	.5833E-01	43
23	-.1481E-02	5	12	.3021E-03	-.6719E+00	5	12	.5362E-01	43
24	-.1129E-02	5	12	.2593E-03	-.6229E+00	5	12	.4708E-01	43
25	-.6585E-03	5	12	.2116E-03	-.4051E+00	5	12	.3882E-01	43
26	-.5637E-03	4	12	.1748E-03	-.2207E+00	5	12	.3163E-01	42
27	-.9478E-03	4	12	.1541E-03	-.3215E+00	4	12	.2723E-01	42
28	-.1130E-02	4	12	.1432E-03	-.4389E+00	4	12	.2518E-01	42
29	-.1002E-02	4	12	.1327E-03	-.4484E+00	4	12	.2368E-01	42
30	-.6980E-03	4	12	.1168E-03	-.3528E+00	4	12	.2123E-01	42
31	-.4153E-03	4	12	.9645E-04	-.2313E+00	4	12	.1769E-01	42
32	-.3296E-03	3	12	.7933E-04	-.1442E+00	4	12	.1429E-01	41
33	-.6212E-03	3	12	.7663E-04	-.1905E+00	3	12	.1309E-01	39
34	-.8884E-03	3	12	.8740E-04	-.2980E+00	3	12	.1436E-01	39
35	-.1011E-02	3	12	.1020E-03	-.3796E+00	3	12	.1672E-01	39
36	-.9349E-03	3	12	.1129E-03	-.3933E+00	3	12	.1862E-01	38
37	-.1299E-02	2	12	.1352E-03	-.4075E+00	2	12	.2177E-01	38
38	-.1753E-02	2	12	.1495E-03	-.6652E+00	2	12	.2450E-01	38
39	-.1474E-02	2	12	.1391E-03	-.6859E+00	2	12	.2391E-01	38
40	-.9026E-03	2	12	.1103E-03	-.4773E+00	2	12	.1976E-01	38
41	-.4328E-03	2	12	.7802E-04	-.2495E+00	2	12	.1435E-01	38
42	-.2376E-03	2	2	.5184E-04	-.1057E+00	2	12	.9664E-02	38

2246-045W Figure 47 Sample Printed Output for BSC Method (Sheet 5 of 14)

43	-.1321E-03	2	2	.3490E-04	-.4541E-01	11	12	.6445E-02	38
44	-.9438E-04	11	12	.2488E-04	-.3780E-01	11	12	.4453E-02	38
45	-.7604E-04	13	11	.1916E-04	-.3055E-01	11	12	.3267E-02	38
46	-.6787E-04	13	11	.1572E-04	-.2419E-01	11	12	.2550E-02	38
47	-.5967E-04	13	11	.1344E-04	-.1893E-01	11	12	.2106E-02	38
48	-.5183E-04	13	11	.1169E-04	-.1472E-01	11	12	.1802E-02	38
49	-.4462E-04	13	11	.1008E-04	-.1143E-01	11	12	.1548E-02	38
50	-.3814E-04	13	11	.8643E-05	-.9825E-02	13	11	.1327E-02	38
51	-.3243E-04	13	11	.7406E-05	-.8429E-02	13	11	.1141E-02	38
52	-.2748E-04	13	11	.6363E-05	-.7197E-02	13	11	.9833E-03	38
53	-.2322E-04	13	11	.5469E-05	-.6122E-02	13	11	.8466E-03	38
54	-.1958E-04	13	11	.4691E-05	-.5195E-02	13	11	.7268E-03	38
55	-.1649E-04	13	11	.4012E-05	-.4398E-02	13	11	.6217E-03	38
56	-.1388E-04	13	11	.3421E-05	-.3718E-02	13	11	.5302E-03	38
57	-.1167E-04	13	11	.2911E-05	-.3139E-02	13	11	.4510E-03	38
58	-.9809E-05	13	11	.2471E-05	-.2647E-02	13	11	.3829E-03	38
59	-.8242E-05	13	11	.2093E-05	-.2231E-02	13	11	.3244E-03	38
60	-.6923E-05	13	11	.1771E-05	-.1879E-02	13	11	.2746E-03	38
61	-.5818E-05	13	11	.1497E-05	-.1582E-02	13	11	.2321E-03	38
62	-.4887E-05	13	11	.1264E-05	-.1331E-02	13	11	.1960E-03	38
63	-.4105E-05	13	11	.1066E-05	-.1120E-02	13	11	.1654E-03	38
64	-.3448E-05	13	11	.8992E-06	-.9422E-03	13	11	.1394E-03	38
65	-.2897E-05	13	11	.7577E-06	-.7924E-03	13	11	.1175E-03	38
66	-.2433E-05	13	11	.6383E-06	-.6663E-03	13	11	.9901E-04	38
67	-.2044E-05	13	11	.5374E-06	-.5601E-03	13	11	.8338E-04	38
68	-.1717E-05	13	11	.4524E-06	-.4709E-03	13	11	.7019E-04	38
69	-.1442E-05	13	11	.3807E-06	-.3958E-03	13	11	.5907E-04	38
70	-.1212E-05	13	11	.3203E-06	-.3327E-03	13	11	.4970E-04	38
71	-.1018E-05	13	11	.2694E-06	-.2796E-03	13	11	.4181E-04	38
72	-.8551E-06	13	11	.2266E-06	-.2350E-03	13	11	.3516E-04	38

ROW SHOCK MESH LOCATION

(IS) 2 3 4 5 6 7 8 9 10 11 12 13 14 15 16  
(JS) 13 13 13 13 13 13 13 13 13 12 12 11 11 11

R= 0.000

JRING= 2

BODY COORDINATES AND SURFACE DATA

I	RHO	F	X/Z	Y/Z	Z	M	HR	MC	CP
2	.20899E+00	-.12342E+00	-.21243E-14	-.24084E+00	0.	.12879E+01	.12879E+01	.11544E-05	.40085E+00
3	.20821E+00	-.12546E+00	.13377E+00	-.21751E+00	0.	.12855E+01	.12822E+01	.91569E-01	.40383E+00
4	.19910E+00	-.12076E+00	.26156E+00	-.19286E+00	0.	.12771E+01	.12634E+01	.18426E+00	.41408E+00

2246-045W

Figure 47 Sample Printed Output for BSC Method (Sheet 6 of 14)

J	RHD	F	X/Z	Y/Z	Z	M	MR	MC	CP
5	.19718E+00	-.11182E+00	.38025E+00	-.16526E+00	0.	.12625E+01	.12357E+01	.25876E+00	.43205E+00
6	.19673E+00	-.10101E+00	.48486E+00	-.13325E+00	0.	.12397E+01	.12048E+01	.29200E+00	.46063E+00
7	.19787E+00	-.90424E-01	.56920E+00	-.95849E-01	0.	.12045E+01	.11761E+01	.26004E+00	.50593E+00
8	.20095E+00	-.81653E-01	.62703E+00	-.51972E-01	0.	.11588E+01	.11549E+01	.94564E-01	.56691E+00
9	.20352E+00	-.76108E-01	.64941E+00	-.17264E-14	0.	.11927E+01	.11647E+01	.25683E+00	.52148E+00
10	.20095E+00	-.74309E-01	.62703E+00	.51972E-01	0.	.13554E+01	.12228E+01	.58461E+00	.32177E+00
11	.19787E+00	-.73559E-01	.56920E+00	.95849E-01	0.	.14511E+01	.12849E+01	.67433E+00	.21876E+00
12	.19673E+00	-.73848E-01	.48486E+00	.13325E+00	0.	.14735E+01	.13396E+01	.61386E+00	.19620E+00
13	.19718E+00	-.74977E-01	.38025E+00	.16526E+00	0.	.14788E+01	.13930E+01	.49641E+00	.19099E+00
14	.19910E+00	-.76262E-01	.26156E+00	.19286E+00	0.	.14813E+01	.14401E+01	.34693E+00	.18851E+00
15	.20281E+00	-.76643E-01	.13377E+00	.21751E+00	0.	.14836E+01	.14730E+01	.17736E+00	.18627E+00
16	.20899E+00	-.74926E-01	.11566E-13	.24084E+00	0.	.14847E+01	.14847E+01	.76187E-05	.18516E+00

# RADIAL OUTPUT DATA IN CROSSFLOW PLANE

IRING= 2

J	RHD	F	X/Z	Y/Z	Z	M	MR	MC	CP
2	.20899E+00	-.12342E+00	-.21243E-14	-.24084E+00	0.	.12879E+01	.12879E+01	.11544E-05	.40085E+00
3	.22918E+00	-.10642E+00	-.26481E-14	-.30022E+00	0.	.12879E+01	.12852E+01	.10749E+00	.39872E+00
4	.24938E+00	-.91063E-01	-.61448E-15	-.35827E+00	0.	.12943E+01	.12781E+01	.20413E+00	.39317E+00
5	.26957E+00	-.77036E-01	-.71305E-15	-.41574E+00	0.	.13008E+01	.12672E+01	.29386E+00	.38532E+00
6	.28977E+00	-.64134E-01	-.81161E-15	-.47321E+00	0.	.13090E+01	.12530E+01	.37870E+00	.37556E+00
7	.30996E+00	-.52232E-01	-.91099E-15	-.53115E+00	0.	.13188E+01	.12360E+01	.45993E+00	.36401E+00
8	.33015E+00	-.41247E-01	-.10119E-14	-.59000E+00	0.	.13302E+01	.12164E+01	.53850E+00	.35062E+00
9	.35035E+00	-.31129E-01	-.11151E-14	-.65016E+00	0.	.13437E+01	.11945E+01	.61532E+00	.33513E+00
10	.37054E+00	-.21858E-01	-.12212E-14	-.71200E+00	0.	.13596E+01	.11706E+01	.69148E+00	.31701E+00
11	.39074E+00	-.13440E-01	-.13308E-14	-.77590E+00	0.	.13792E+01	.11451E+01	.76870E+00	.29511E+00
12	.41093E+00	-.59292E-02	-.14446E-14	-.84227E+00	0.	.14057E+01	.11187E+01	.85110E+00	.26631E+00
13	.43112E+00	.50505E-03	-.15633E-14	-.91150E+00	0.	.15602E+01	.11189E+01	.10873E+01	.11447E+00
14	.45132E+00	-.52904E-05	-.16878E-14	-.98407E+00	0.	.17137E+01	.11064E+01	.13087E+01	-.10131E-01
15	.47151E+00	0.	-.18188E-14	-.10605E+01	0.	.16998E+01	.10540E+01	.13336E+01	.11237E-03
16	.49170E+00	0.	-.19573E-14	-.11412E+01	0.	.17000E+01	.10047E+01	.13714E+01	.14049E-13

IRING= 9

J	RHD	F	X/Z	Y/Z	Z	M	MR	MC	CP
2	.20352E+00	-.76108E-01	.64941E+00	-.17264E-14	0.	.11927E+01	.11647E+01	.25683E+00	.52148E+00
3	.21962E+00	-.67572E-01	.67395E+00	-.20959E-14	0.	.11894E+01	.11627E+01	.25051E+00	.52586E+00
4	.23572E+00	-.59377E-01	.70144E+00	-.24575E-14	0.	.11992E+01	.11612E+01	.29942E+00	.51290E+00
5	.25182E+00	-.51493E-01	.73158E+00	-.28145E-14	0.	.12132E+01	.11586E+01	.35988E+00	.49459E+00
6	.26793E+00	-.43912E-01	.76415E+00	-.31697E-14	0.	.12286E+01	.11544E+01	.42040E+00	.47477E+00
7	.28403E+00	-.36629E-01	.79903E+00	-.35254E-14	0.	.12444E+01	.11486E+01	.47871E+00	.45473E+00
8	.30013E+00	-.29643E-01	.83615E+00	-.38836E-14	0.	.12602E+01	.11411E+01	.53470E+00	.43489E+00
9	.31623E+00	-.22955E-01	.87548E+00	-.42461E-14	0.	.12760E+01	.11321E+01	.58869E+00	.41534E+00

2246-045W

Figure 47 Sample Printed Output for BSC Method (Sheet 7 of 14)

10	.33234E+00	-.16567E-01	.91704E+00	-.46148E-14	0.	.12919E+01	.11216E+01	.64108E+00	.39601E+00
11	.34844E+00	-.10483E-01	.96089E+00	-.49911E-14	0.	.13080E+01	.11098E+01	.69226E+00	.37677E+00
12	.36454E+00	-.47069E-02	.10071E+01	-.53768E-14	0.	.13244E+01	.10966E+01	.74254E+00	.35747E+00
13	.38044E+00	.75358E-03	.10558E+01	-.57735E-14	0.	.15223E+01	.11227E+01	.10280E+01	.14918E+00
14	.39674E+00	-.88834E-05	.11071E+01	-.61828E-14	0.	.17326E+01	.11432E+01	.13019E+01	-.23760E-01
15	.41285E+00	0.	.11613E+01	-.66066E-14	0.	.16996E+01	.11050E+01	.12914E+01	.28826E-03
16	.42895E+00	0.	.12184E+01	-.70468E-14	0.	.17000E+01	.10744E+01	.13174E+01	.21074E-13

IRING= 16

J	RHO	F	X/Z	Y/Z	Z	M	MR	MC	CF
2	.20899E+00	-.74926E-01	.11566E-13	.24084E+00	0.	.14847E+01	.14847E+01	.76187E-05	.18516E+00
3	.23908E+00	-.63032E-01	.11117E-13	.32879E+00	0.	.14855E+01	.14794E+01	.13430E+00	.18446E+00
4	.26918E+00	-.52183E-01	.14019E-13	.41462E+00	0.	.14876E+01	.14652E+01	.25733E+00	.18231E+00
5	.29927E+00	-.42204E-01	.13364E-13	.50040E+00	0.	.14912E+01	.14439E+01	.37245E+00	.17886E+00
6	.32937E+00	-.33013E-01	.15695E-13	.58768E+00	0.	.14962E+01	.14166E+01	.48143E+00	.17398E+00
7	.35946E+00	-.24582E-01	.18103E-13	.67783E+00	0.	.15030E+01	.13843E+01	.58555E+00	.16742E+00
8	.38955E+00	-.16914E-01	.20620E-13	.77210E+00	0.	.15122E+01	.13476E+01	.68615E+00	.15864E+00
9	.41965E+00	-.10054E-01	.17088E-13	.87178E+00	0.	.15252E+01	.13074E+01	.78535E+00	.14645E+00
10	.44974E+00	-.41162E-02	.19175E-13	.97827E+00	0.	.15467E+01	.12533E+01	.88951E+00	.12665E+00
11	.47983E+00	.52600E-03	.21427E-13	.10932E+01	0.	.16353E+01	.12360E+01	.10707E+01	.50389E-01
12	.50993E+00	-.15723E-04	.23881E-13	.12184E+01	0.	.17096E+01	.11914E+01	.12261E+01	-.70886E-02
13	.54002E+00	.29370E-06	.26582E-13	.13561E+01	0.	.16997E+01	.11243E+01	.12748E+01	.23055E-03
14	.57011E+00	-.46014E-08	.29585E-13	.15093E+01	0.	.17000E+01	.10589E+01	.13300E+01	-.46429E-05
15	.60021E+00	0.	.32960E-13	.16816E+01	0.	.17000E+01	.99297E+00	.13799E+01	.78043E-07
16	.63030E+00	0.	.36801E-13	.18775E+01	0.	.17000E+01	.92691E+00	.14251E+01	.14049E-13

# INTERPOLATED CAPTURED ROW SHOCK COORDINATES

X/Z	Y/Z
-.15194E-14	-.88591E+00
.24273E+00	-.85896E+00
-.46897E+00	-.78047E+00
.66421E+00	-.65923E+00
.81886E+00	-.50887E+00
.93090E+00	-.34427E+00
.10058E+01	-.17508E+00
.10510E+01	-.57346E-14
.10639E+01	.19003E+00
.10217E+01	.39302E+00
.90970E+00	.58865E+00
.74479E+00	.76926E+00
.52719E+00	.91097E+00
.27529E+00	.10119E+01
.20549E-13	.10483E+01

Figure 47 Sample Printed Output for BSC Method (Sheet 8 of 14)

2246-045W

\*\*\* SPHERICAL CUT GEOMETRY INPUT COORDINATES \*\*\*

LEADING EDGE OR MAXIMUM HALF WIDTH COORDINATES

XTIP=	.10893E+01	YTIP=	0.	ZTIP=	.16773E+01	DMTIP=	0.	PSID=	.33000E+02	RTIP=	.20000E+01
IG	R	X	Y	Z	DMEG	PSI					
1	.20000E+01	0.	-.31081E+00	.19757E+01	-.90000E+02	.89404E+01					
2	.20000E+01	.89952E-01	-.30171E+00	.19751E+01	-.73399E+02	.90572E+01					
3	.20000E+01	.17929E+00	-.29187E+00	.19704E+01	-.58439E+02	.98617E+01					
4	.20000E+01	.26740E+00	-.28126E+00	.19620E+01	-.46447E+02	.11189E+02					
5	.20000E+01	.35369E+00	-.26985E+00	.19499E+01	-.37342E+02	.12852E+02					
6	.20000E+01	.43756E+00	-.25761E+00	.19345E+01	-.30487E+02	.14707E+02					
7	.20000E+01	.51844E+00	-.24452E+00	.19161E+01	-.25251E+02	.16655E+02					
8	.20000E+01	.59578E+00	-.23058E+00	.18952E+01	-.21158E+02	.18628E+02					
9	.20000E+01	.66905E+00	-.21576E+00	.18724E+01	-.17874E+02	.20578E+02					
10	.20000E+01	.73775E+00	-.20007E+00	.18482E+01	-.15173E+02	.22470E+02					
11	.20000E+01	.80141E+00	-.18351E+00	.18232E+01	-.12897E+02	.24272E+02					
12	.20000E+01	.85959E+00	-.16609E+00	.17982E+01	-.10936E+02	.25960E+02					
13	.20000E+01	.91191E+00	-.14782E+00	.17739E+01	-.92077E+01	.27510E+02					
14	.20000E+01	.95799E+00	-.12875E+00	.17509E+01	-.76544E+01	.28901E+02					
15	.20000E+01	.99753E+00	-.10890E+00	.17300E+01	-.62304E+01	.30114E+02					
16	.20000E+01	.10303E+01	-.88333E-01	.17119E+01	-.49005E+01	.31132E+02					
17	.20000E+01	.10559E+01	-.67092E-01	.16972E+01	-.36355E+01	.31940E+02					
18	.20000E+01	.10744E+01	-.45244E-01	.16863E+01	-.24113E+01	.32526E+02					
19	.20000E+01	.10856E+01	-.22856E-01	.16796E+01	-.12062E+01	.32881E+02					
20	.20000E+01	.10893E+01	-.46832E-05	.16773E+01	-.24633E-03	.33000E+02					
21	.20000E+01	.10856E+01	.22856E-01	.16796E+01	.12062E+01	.32881E+02					
22	.20000E+01	.10744E+01	.45244E-01	.16863E+01	.24113E+01	.32526E+02					
23	.20000E+01	.10559E+01	.67092E-01	.16972E+01	.36355E+01	.31940E+02					
24	.20000E+01	.10303E+01	.88333E-01	.17119E+01	.49005E+01	.31132E+02					
25	.20000E+01	.99753E+00	.10890E+00	.17300E+01	.62304E+01	.30114E+02					
26	.20000E+01	.95799E+00	.12875E+00	.17509E+01	.76544E+01	.28901E+02					
27	.20000E+01	.91191E+00	.14782E+00	.17739E+01	.92077E+01	.27510E+02					
28	.20000E+01	.85959E+00	.16609E+00	.17982E+01	.10936E+02	.25960E+02					
29	.20000E+01	.80141E+00	.18351E+00	.18232E+01	.12897E+02	.24272E+02					
30	.20000E+01	.73775E+00	.20007E+00	.18482E+01	.15173E+02	.22470E+02					
31	.20000E+01	.66905E+00	.21576E+00	.18724E+01	.17874E+02	.20578E+02					
32	.20000E+01	.59578E+00	.23058E+00	.18952E+01	.21158E+02	.18628E+02					
33	.20000E+01	.51844E+00	.24452E+00	.19161E+01	.25251E+02	.16655E+02					
34	.20000E+01	.43756E+00	.25761E+00	.19345E+01	.30487E+02	.14707E+02					
35	.20000E+01	.35369E+00	.26985E+00	.19499E+01	.37342E+02	.12852E+02					
36	.20000E+01	.26740E+00	.28126E+00	.19620E+01	.46447E+02	.11189E+02					
37	.20000E+01	.17929E+00	.29187E+00	.19704E+01	.58439E+02	.98617E+01					
38	.20000E+01	.89952E-01	.30171E+00	.19751E+01	.73399E+02	.90572E+01					
39	.20000E+01	0.	.31081E+00	.19757E+01	.90000E+02	.89404E+01					

Figure 47 Sample Printed Output for BSC Method (Sheet 9 of 14)

SINGULARITY LOCATION IN PHYSICAL SPACE AT R= 2.000  
 X SIN/Z= .62557 Y SIN/Z= 0.00000 -Y SIN/Z= 0.00000

SINGULARITY LOCATION IN MAPPED SPACE AT CURRENT STATION  
 S0= .2747E+00 0. S1= .2747E+00 0. S2= 0. 0.

SINGULARITY LOCATION IN MAPPED SPACE AT NEW STATION  
 SON= .2870E+00 0. SIN= .2870E+00 0. S2N= 0. 0.

XTIP= 1.63392 YTIP= 0.00000 ZTIP= 2.51601 DM TIP= 0.00000 PSID= 33.00000 RTIP= 3.00000

SINGULARITY LOCATION IN PHYSICAL SPACE AT R= 3.000  
 X SIN/Z= .63538 Y SIN/Z= 0.00000 -Y SIN/Z= 0.00000

SINGULARITY DERIVATIVES AT CURRENT STATION S0PR= .6159E-02 0. S1PR= .6159E-02 0.  
 SINGULARITY DERIVATIVE AT CURRENT STATION S2PR= 0. 0.  
 SINGULARITY DERIVATIVES AT NEW STATION S0PRN= .8061E-02 0. S1PRN= .8061E-02 0.  
 SINGULARITY DERIVATIVE AT NEW STATION S2PRN= 0. 0.

R= 1.000

I	X	B	BPR	BSEC	BR	BRR	BRTH
2	-.15708E+01	.20899E+00	0.	-.24553E+00	-.10582E-01	-.21164E-01	0.
3	-.13464E+01	.20281E+00	-.22043E-01	.49070E-01	-.91127E-02	-.18225E-01	.53257E-02
4	-.11220E+01	.19910E+00	-.12548E-01	.35355E-01	-.81919E-02	-.16384E-01	.31722E-02
5	-.89760E+00	.19718E+00	-.52650E-02	.29357E-01	-.76890E-02	-.15378E-01	.13850E-02
6	-.67320E+00	.19673E+00	.15416E-02	.31309E-01	-.75703E-02	-.15141E-01	-.50923E-03
7	-.44880E+00	.19787E+00	.93857E-02	.38603E-01	-.79175E-02	-.15835E-01	-.27701E-02
8	-.22440E+00	.20095E+00	.12588E-01	-.10065E-01	-.88135E-02	-.17627E-01	-.32978E-02
9	-.71054E-14	.20352E+00	-.17316E-11	-.10213E+00	-.93976E-02	-.18795E-01	-.26566E-09
10	.22440E+00	.20095E+00	-.12588E-01	-.10065E-01	-.88135E-02	-.17627E-01	.32978E-02
11	.44880E+00	.19787E+00	-.93857E-02	.38603E-01	-.79175E-02	-.15835E-01	.27701E-02
12	.67320E+00	.19673E+00	-.15416E-02	.31309E-01	-.75703E-02	-.15141E-01	.50923E-03
13	.89760E+00	.19718E+00	.52650E-02	.29357E-01	-.76890E-02	-.15378E-01	-.13850E-02
14	.11220E+01	.19910E+00	.12548E-01	.35355E-01	-.81919E-02	-.16384E-01	-.31722E-02
15	.13464E+01	.20281E+00	.22043E-01	.49070E-01	-.91127E-02	-.18225E-01	-.53257E-02
16	.15708E+01	.20899E+00	0.	-.24553E+00	-.10582E-01	-.21164E-01	0.

R= 1.000

I	X	C	CFR	CSEC	CR	CRR	CRTH
2	-.15708E+01	.49170E+00	0.	-.64481E-01	0.	0.	0.
3	-.13464E+01	.49008E+00	-.26059E-01	-.16777E+00	0.	0.	0.

2246-045W

Figure 47 Sample Printed Output for BSC Method (Sheet 10 of 14)

I	J	X/Z	Y/Z	H	UI	VI	WI	H1	H2
4	2	-11220E+01	.48001E+00	-.58190E-01	-.11860E+00	0.	0.	0.	0.
5	2	-.89760E+00	.46397E+00	-.76381E-01	-.43527E-01	0.	0.	0.	0.
6	2	-.67320E+00	.44573E+00	-.75266E-01	.53456E-01	0.	0.	0.	0.
7	2	-.44880E+00	.43019E+00	-.51272E-01	.16040E+00	0.	0.	0.	0.
8	2	-.22440E+00	.42272E+00	-.27591E-02	.27197E+00	0.	0.	0.	0.
9	2	-.71054E-14	.42895E+00	.66030E-01	.34112E+00	0.	0.	0.	0.
10	2	.22440E+00	.45235E+00	.13259E+00	.25214E+00	0.	0.	0.	0.
11	2	.44880E+00	.48846E+00	.17371E+00	.11434E+00	0.	0.	0.	0.
12	2	.67320E+00	.53031E+00	.18394E+00	-.23211E-01	0.	0.	0.	0.
13	2	.89760E+00	.57101E+00	.16464E+00	-.14880E+00	0.	0.	0.	0.
14	2	.11220E+01	.60420E+00	.12036E+00	-.24586E+00	0.	0.	0.	0.
15	2	.13464E+01	.62502E+00	.58153E-01	-.30853E+00	0.	0.	0.	0.
16	2	.15708E+01	.63030E+00	0.	-.20976E+00	0.	0.	0.	0.

R= 1.000

I	J	HX	HY	HR	H1X	H1Y	H1R	H2X	H2Y	H2R
2	2	0.	-.37363E+00	-.97896E-01	0.	-.21424E-03	.27704E-02	0.	.28174E-18	.68450E-17
3	2	-.19198E+00	-.39192E+00	-.87026E-01	-.26009E-03	-.25047E-03	.27285E-02	-.18251E-02	-.42201E-04	-.89783E-03
4	2	-.49237E+00	-.34407E+00	-.70235E-01	-.69217E-03	-.36694E-03	.24916E-02	-.19932E-02	-.59830E-04	-.18373E-02
5	2	-.71920E+00	-.24384E+00	-.49194E-01	-.14506E-02	-.57377E-03	.19762E-02	-.22818E-02	.20002E-04	-.28776E-02
6	2	-.83490E+00	-.11168E+00	-.23768E-01	-.30511E-02	-.84747E-03	.93552E-03	-.24125E-02	.34748E-03	-.40330E-02
7	2	-.78004E+00	.36485E-01	.87042E-02	-.59668E-02	-.90556E-03	-.11752E-02	-.74515E-03	.12494E-02	-.49960E-02
8	2	-.48149E+00	.18161E+00	.50521E-01	-.66735E-02	.69586E-03	-.46573E-02	.52941E-02	.25078E-02	-.41545E-02
9	2	-.43627E-11	.25891E+00	.75553E-01	-.18957E-13	.34243E-02	-.66334E-02	.97042E-02	.15167E-15	-.15493E-15
10	2	.48149E+00	.20573E+00	.50486E-01	.66735E-02	.76434E-03	-.46633E-02	.52941E-02	-.28739E-02	.41469E-02
11	2	.78004E+00	.43174E-01	.82345E-02	.59668E-02	-.11615E-02	-.11807E-02	-.74515E-03	-.15454E-02	.49993E-02
12	2	.83490E+00	-.15495E+00	-.24615E-01	.30511E-02	-.11402E-02	.93475E-03	-.24125E-02	-.44470E-03	.40363E-02
13	2	.71920E+00	-.35036E+00	-.50444E-01	.14506E-02	-.80043E-03	.19767E-02	-.22818E-02	-.14832E-04	.28795E-02
14	2	.49237E+00	-.50791E+00	-.71895E-01	.69217E-03	.52373E-03	.24924E-02	-.19932E-02	.93470E-04	.18384E-02
15	2	.19198E+00	-.58903E+00	-.88992E-01	.26009E-03	-.36278E-03	.27293E-02	-.18251E-02	.65087E-04	.89829E-03

Figure 47 Sample Printed Output for BSC Method (Sheet 11 of 14)

2246-045W



16 2 0, -56834E+00 -,99924E-01 0, -,31471E-03 ,27712E-02 0, ,50351E-17 ,78270E-16

ITER	DELHX	I	J	DELAHG	RESMX	I	J	RESAVG	KSUP
1	.4727E-02	16	2	.4450E-03	.3479E+01	3	2	.1654E+00	38
2	.1993E-02	2	2	.2354E-03	.1071E+01	2	2	.6078E-01	38
3	.9347E-03	2	2	.1266E-03	.3571E+00	2	2	.2868E-01	38
4	.3766E-03	2	2	.6321E-04	.1138E+00	2	2	.1385E-01	38
5	.1572E-03	16	2	.3401E-04	.4617E-01	16	2	.7513E-02	38
6	.7512E-04	15	2	.1774E-04	.2132E-01	15	2	.4111E-02	38
7	.4181E-04	16	2	.1005E-04	.1226E-01	16	2	.2443E-02	38
8	.1982E-04	2	2	.5364E-05	-.9397E-02	14	11	.1372E-02	38
9	-.1511E-04	14	11	.3112E-05	-.7932E-02	14	11	.8192E-03	38
10	-.1272E-04	14	11	.2003E-05	.6691E-02	14	11	.5021E-03	38
11	-.1071E-04	14	11	.1510E-05	-.5641E-02	14	11	.3314E-03	38
12	-.9012E-05	14	11	.1380E-05	-.4754E-02	14	11	.2653E-03	38
13	-.7587E-05	14	11	.1310E-05	-.4006E-02	14	11	.2273E-03	38
14	-.6388E-05	14	11	.1264E-05	-.3376E-02	14	11	.2185E-03	38
15	-.5380E-05	14	11	.1147E-05	-.2845E-02	14	11	.1993E-03	38
16	-.4532E-05	14	11	.1025E-05	-.2397E-02	14	11	.1790E-03	38
17	-.3818E-05	14	11	.8916E-06	-.2020E-02	14	11	.1561E-03	38
18	-.3218E-05	14	11	.7683E-06	-.1703E-02	14	11	.1346E-03	38
19	-.2712E-05	14	11	.6529E-06	-.1436E-02	14	11	.1144E-03	38
20	-.2286E-05	14	11	.5521E-06	-.1211E-02	14	11	.9675E-04	38
21	-.1928E-05	14	11	.4637E-06	-.1021E-02	14	11	.8119E-04	38
22	-.1625E-05	14	11	.3886E-06	-.8609E-03	14	11	.6802E-04	38
23	-.1371E-05	14	11	.3246E-06	-.7260E-03	14	11	.5678E-04	38
24	-.1156E-05	14	11	.2709E-06	-.6124E-03	14	11	.4736E-04	38
25	-.9748E-06	14	11	.2259E-06	-.5165E-03	14	11	.3945E-04	38

ROW SHOCK MESH LOCATION

(IS) 2 3 4 5 6 7 8 9 10 11 12 13 14 15 16  
 (JS) 13 13 13 13 13 13 13 13 13 13 12 12 11 11 11

R= 1.000

JRING= 2

BODY COORDINATES AND SURFACE DATA

I RHO F X/Z Y/Z Z H MR MC CP

2246-045W

Figure 47 Sample Printed Output for BSC Method (Sheet 12 of 14)

2	.20899E+00	-.11687E+00	-.21243E-14	-.24084E+00	.97220E+00	.13397E+01	.13388E+01	.50696E-01	.33965E+00
3	.20281E+00	-.11915E+00	.13377E+00	-.21751E+00	.94891E+00	.13335E+01	.13289E+01	.10962E+00	.34688E+00
4	.19910E+00	-.11553E+00	.26156E+00	-.19286E+00	.95104E+00	.13190E+01	.13026E+01	.20721E+00	.36373E+00
5	.19718E+00	-.10795E+00	.38025E+00	-.16524E+00	.92375E+00	.12971E+01	.12661E+01	.28214E+00	.38973E+00
6	.19673E+00	-.98424E-01	.48486E+00	-.13325E+00	.89341E+00	.12664E+01	.12266E+01	.42717E+00	.31527E+00
7	.19787E+00	-.88842E-01	.56920E+00	-.95849E-01	.86608E+00	.12227E+01	.11901E+01	.28056E+00	.48230E+00
8	.20095E+00	-.80720E-01	.62703E+00	-.51972E-01	.84640E+00	.11673E+01	.11622E+01	.10917E+00	.55333E+00
9	.20352E+00	-.75486E-01	.64941E+00	-.17264E-14	.83867E+00	.11956E+01	.11687E+01	.25196E+00	.51770E+00
10	.20095E+00	-.73676E-01	.62703E+00	.51972E-01	.84640E+00	.13667E+01	.12309E+01	.59387E+00	.30907E+00
11	.19787E+00	-.72426E-01	.56920E+00	.95849E-01	.86608E+00	.14744E+01	.12994E+01	.69665E+00	.19540E+00
12	.19673E+00	-.71672E-01	.48486E+00	.13325E+00	.89341E+00	.15042E+01	.13603E+01	.64211E+00	.16626E+00
13	.19718E+00	-.71363E-01	.38025E+00	.16524E+00	.92375E+00	.15144E+01	.14205E+01	.52488E+00	.15660E+00
14	.19910E+00	-.71094E-01	.26156E+00	.19286E+00	.95104E+00	.15208E+01	.14747E+01	.37145E+00	.15060E+00
15	.20281E+00	-.70238E-01	.13377E+00	.21751E+00	.94891E+00	.15258E+01	.15133E+01	.19508E+00	.14584E+00
16	.20899E+00	-.68240E-01	.11566E-13	.24084E+00	.97220E+00	.15282E+01	.15271E+01	.57834E-01	.14363E+00

# RADIAL OUTPUT DATA IN CROSSFLOW PLANE

IRING= 2

J	RHO	F	X/Z	Y/Z	Z	M	MR	MC	CP
2	.20899E+00	-.11687E+00	-.21243E-14	-.24084E+00	.97220E+00	.13397E+01	.13388E+01	.50696E-01	.33965E+00
3	.22918E+00	-.10145E+00	-.26481E-14	-.30022E+00	.95777E+00	.13352E+01	.13268E+01	.15018E+00	.34481E+00
4	.24938E+00	-.87358E-01	-.61448E-15	-.35827E+00	.94140E+00	.13340E+01	.13120E+01	.24078E+00	.34630E+00
5	.26957E+00	-.74345E-01	-.71305E-15	-.41574E+00	.92338E+00	.13350E+01	.12948E+01	.32540E+00	.34506E+00
6	.28977E+00	-.62264E-01	-.81161E-15	-.47321E+00	.90390E+00	.13381E+01	.12751E+01	.40563E+00	.34150E+00
7	.30996E+00	-.51020E-01	-.91099E-15	-.53115E+00	.88315E+00	.13431E+01	.12534E+01	.48251E+00	.33576E+00
8	.33015E+00	-.40551E-01	-.10119E-14	-.59000E+00	.86127E+00	.13500E+01	.12298E+01	.55688E+00	.32784E+00
9	.35035E+00	-.30825E-01	-.11151E-14	-.65016E+00	.83838E+00	.13591E+01	.12045E+01	.62954E+00	.31754E+00
10	.37054E+00	-.21830E-01	-.12212E-14	-.71200E+00	.81461E+00	.13708E+01	.11778E+01	.70149E+00	.30439E+00
11	.39074E+00	-.13580E-01	-.13308E-14	-.77590E+00	.79007E+00	.13862E+01	.11498E+01	.77427E+00	.28741E+00
12	.41093E+00	-.61303E-02	-.14446E-14	-.84227E+00	.76485E+00	.14079E+01	.11213E+01	.85136E+00	.26396E+00
13	.43112E+00	.37019E-03	-.15633E-14	-.91150E+00	.73905E+00	.15563E+01	.11185E+01	.10821E+01	.11795E+00
14	.45132E+00	-.29253E-05	-.16878E-14	-.98407E+00	.71276E+00	.17100E+01	.11055E+01	.13046E+01	-.73982E-02
15	.47151E+00	0.	-.18188E-14	-.10605E+01	.68607E+00	.16999E+01	.10541E+01	.13337E+01	.61919E-04
16	.49170E+00	0.	-.19573E-14	-.11413E+01	.65904E+00	.17000E+01	.10047E+01	.13714E+01	.14049E-13

IRING= 9

J	RHO	F	X/Z	Y/Z	Z	M	MR	MC	CP
2	.20352E+00	-.75486E-01	.64941E+00	-.17264E-14	.83867E+00	.11956E+01	.11687E+01	.25196E+00	.51770E+00
3	.21962E+00	-.66991E-01	.67395E+00	-.20959E-14	.82925E+00	.11938E+01	.11673E+01	.24993E+00	.52003E+00
4	.23572E+00	-.58860E-01	.70144E+00	-.24575E-14	.81868E+00	.12046E+01	.11660E+01	.30244E+00	.50589E+00
5	.25182E+00	-.51055E-01	.73158E+00	-.28145E-14	.80708E+00	.12190E+01	.11631E+01	.36468E+00	.48718E+00
6	.26793E+00	-.43557E-01	.76415E+00	-.31697E-14	.79457E+00	.12343E+01	.11585E+01	.42589E+00	.46750E+00

2246-045W

Figure 47 Sample Printed Output for BSC Method (Sheet 13 of 14)

J	RHO	F	X/Z	Y/Z	Z	H	MR	MC	CP
7	.28403E+00	-.36357E-01	.79903E+00	-.35254E-14	.78124E+00	.12497E+01	.11521E+01	.48423E+00	.44801E+00
8	.30013E+00	-.29449E-01	.83615E+00	-.38836E-14	.76716E+00	.12649E+01	.11440E+01	.53981E+00	.42902E+00
9	.31623E+00	-.22828E-01	.87548E+00	-.42461E-14	.75240E+00	.12799E+01	.11343E+01	.59308E+00	.41054E+00
10	.33234E+00	-.16495E-01	.91704E+00	-.46148E-14	.73702E+00	.12949E+01	.11231E+01	.64450E+00	.39246E+00
11	.34844E+00	-.10450E-01	.96089E+00	-.49911E-14	.72107E+00	.13098E+01	.11105E+01	.69447E+00	.37460E+00
12	.36454E+00	-.46959E-02	.10071E+01	-.57768E-14	.70460E+00	.13249E+01	.10968E+01	.74335E+00	.35679E+00
13	.38064E+00	.76345E-03	.10558E+01	-.57735E-14	.68766E+00	.15223E+01	.11227E+01	.10284E+01	.14895E+00
14	.39674E+00	-.77578E-05	.11071E+01	-.61828E-14	.67029E+00	.17331E+01	.11433E+01	.13024E+01	-.24105E-01
15	.41285E+00	0.	.11612E+01	-.66066E-14	.65254E+00	.16997E+01	.11050E+01	.12914E+01	.25224E-03
16	.42895E+00	0.	.12184E+01	-.70468E-14	.63444E+00	.17000E+01	.10744E+01	.13174E+01	.21074E-13

IRING= 16

# INTERPOLATED CAPTURED ROW SHOCK COORDINATES

X/Z	Y/Z
-.15211E-14	-.88686E+00
.24288E+00	-.85970E+00
.46918E+00	-.78095E+00
.66445E+00	-.65956E+00
.81909E+00	-.50908E+00
.93099E+00	-.34432E+00
.10057E+01	-.17506E+00
.10510E+01	-.57339E-14
.10642E+01	.19010E+00
.10231E+01	.39376E+00
.91140E+00	.59012E+00
.74785E+00	.77334E+00
.52903E+00	.91505E+00
.27602E+00	.10153E+01
.20618E-13	.10519E+01

2246-045W

Figure 47 Sample Printed Output for BSC Method (Sheet 14 of 14)

# END OF RUN ITERATION SURVEY

(R)	0.0	1.0	2.0	3.0	4.0	5.0	6.0	7.0	8.0	9.0	10.0	11.0	12.0	13.0	14.0
(ITER)	94	12	16	15	15	13	12	14	15	17	17	19	19	19	18
(R)	15.0	16.0	17.0	18.0	19.0	20.0	21.0	22.0	23.0	24.0	25.0	26.0	27.0	28.0	29.0
(ITER)	19	18	18	19	19	19	18	18	18	18	18	19	19	19	19
(R)	30.0	31.0	32.0	33.0	34.0										
(ITER)	19	20	20	20	20										

TOTAL NUMBER OF ITERATIONS= 692

2246-047W

Figure 48 Summary of Convergence History

\*\*\* INTERPOLATED Z STATIONS SPECIFIED AS INPUT \*\*\*

ZI= 5.0000

I	XI	YI	CPI
1	-.00000	-.39603	.07728
2	.66285	-.37143	.07778
3	1.30799	-.33800	.08309
4	1.91370	-.29407	.09831
5	2.44957	-.23809	.12895
6	2.87706	-.16922	.18559
7	3.15500	-.08784	.30383
8	3.24704	-.00000	.25285
9	3.15500	.08784	-.10914
10	2.87706	.16922	-.13759
11	2.44957	.23809	-.12083
12	1.91370	.29407	-.10324
13	1.30799	.33800	-.09038
14	.66285	.37143	-.08015
15	.00000	.39603	-.07548

ZI= 10.0000

I	XI	YI	CPI
1	-.00000	-.35294	.05442
2	1.32423	-.35352	.05389
3	2.61471	-.34361	.05582
4	3.82715	-.31877	.06462
5	4.90017	-.27327	.08654
6	5.75615	-.20285	.13149
7	6.31274	-.10753	.23908
8	6.49408	-.00000	-.12945
9	6.31274	.10753	-.21065
10	5.75615	.20285	-.19996
11	4.90017	.27327	-.16707
12	3.82715	.31877	-.13311
13	2.61471	.34361	-.11060
14	1.32423	.35352	-.09730
15	.00000	.35294	-.09219

2246-043W

Figure 49 Spanwise and Chordwise Interpolation Output (Sheet 1 of 6)

ZI= 15.0000

I	XI	YI	CFI
1	-.00000	-.21070	.04085
2	1.98525	-.23922	.04068
3	3.91938	-.25920	.04149
4	5.73572	-.26562	.04637
5	7.34247	-.24928	.06147
6	8.62395	-.20021	.09557
7	9.45795	-.11299	.16495
8	9.74111	-.00000	-.32318
9	9.45795	.11299	-.29193
10	8.62395	.20021	-.23577
11	7.34247	.24928	-.19094
12	5.73572	.26562	-.14698
13	3.91938	.25920	-.11968
14	1.98525	.23922	-.10640
15	.00000	.21070	-.10221

ZI= 20.0000

I	XI	YI	CFI
1	-.00000	-.00840	.04819
2	2.64587	-.06772	.03052
3	5.22308	-.11878	.03064
4	7.64268	-.15732	.03403
5	9.78240	-.17672	.04287
6	11.48870	-.16412	.06683
7	12.59977	-.10371	.09909
8	12.98815	-.00000	-.34928
9	12.59977	.10371	-.34131
10	11.48870	.16412	-.26006
11	9.78240	.17672	-.20577
12	7.64268	.15732	-.15503
13	5.22308	.11878	-.12645
14	2.64587	.06772	-.11334
15	.00000	.00840	-.09520

2246-043W

Figure 49 Spanwise and Chordwise Interpolation Output (Sheet 2 of 6)

TRAILING EDGE LOCATION, XTE= 9.72310 ZTE= 25.00000

ZI= 25.0000

I	XI	YI	CPI
1	-.00000	-.00840	.08614
2	3.30727	-.00697	.10399
3	6.52838	-.00554	.10487
4	9.55182	-.00722	.06062
5	12.22453	-.05786	.03136
6	14.35473	-.08715	.04167
7	15.74159	-.07489	.04227
8	16.23519	-.00000	-.34990
9	15.74159	.07489	-.37036
10	14.35473	.08715	-.27660
11	12.22453	.05786	-.21016
12	9.55182	.00722	-.13860
13	6.52838	.00554	-.07414
14	3.30727	.00697	-.05247
15	.00000	.00840	-.06078

2246-043W

Figure 49 Spanwise and Chordwise Interpolation Output (Sheet 3 of 6)

# CHORDWISE INTERPOLATION PROGRAM

XSPAN= 0.00000

UPPER SURFACE

LOWER SURFACE

ZUP	YUP	CPU	ZLO	YLO	CPL
0.00000	0.00000	.17370	0.00000	0.00000	.38624
1.97570	.31081	-.04595	1.97570	-.31081	.09929
2.97885	.35563	-.06174	2.97885	-.35563	.09352
3.98170	.38216	-.06950	3.98170	-.38216	.08517
4.98430	.39596	-.07541	4.98430	-.39596	.07730
5.98664	.40013	-.07993	5.98664	-.40013	.07116
6.98875	.39667	-.08361	6.98875	-.39667	.06607
7.99063	.38700	-.08678	7.99063	-.38700	.06173
8.99230	.37220	-.08962	8.99230	-.37220	.05789
9.99376	.35308	-.09218	9.99376	-.35308	.05444
10.99504	.33030	-.09451	10.99504	-.33030	.05131
11.99614	.30435	-.09665	11.99614	-.30435	.04845
12.99708	.27560	-.09872	12.99708	-.27560	.04585
13.99787	.24434	-.10048	13.99787	-.24434	.04330
14.99852	.21075	-.10220	14.99852	-.21075	.04085
15.99904	.17492	-.10400	15.99904	-.17492	.03847
16.99945	.13687	-.10584	16.99945	-.13687	.03602
17.99974	.09653	-.10779	17.99974	-.09653	.03343
18.99992	.05378	-.10991	18.99992	-.05378	.03061
20.00000	.00840	-.09520	20.00000	-.00840	.04819

2246-043W

Figure 49 Spanwise and Chordwise Interpolation Output (Sheet 4 of 6)



XSPAN= 2.00000  
 ITEU= 26 ITL= 26  
 ZTE= 21.02848

UPPER SURFACE			LOWER SURFACE		
ZUP	YUP	CPU	ZLO	YLO	CPL
3.07973	-.00000	.33169	3.07973	-.00000	.33169
3.17301	.07431	-.03599	3.17301	-.07431	.34399
3.46086	.14408	-.09853	3.46086	-.14408	.22219
3.47890	.14825	-.10180	3.47890	-.14825	.21518
4.08379	.22248	-.10538	4.08379	-.22248	.14268
4.56970	.25828	-.10689	4.56970	-.25828	.11944
5.22535	.29749	-.10540	5.22535	-.29749	.09610
5.64143	.31330	-.10583	5.64143	-.31330	.08898
6.68999	.34133	-.10489	6.68999	-.34133	.07542
7.64750	.35593	-.10331	7.64750	-.35593	.06621
7.73635	.35654	-.10338	7.73635	-.35654	.06566
8.75433	.35710	-.10383	8.75433	-.35710	.06027
9.77240	.35048	-.10426	9.77240	-.35048	.05581
10.79047	.33787	-.10469	10.79047	-.33787	.05203
11.80849	.32021	-.10510	11.80849	-.32021	.04878
12.82645	.29824	-.10560	12.82645	-.29824	.04598
13.84431	.27256	-.10597	13.84431	-.27256	.04338
14.86206	.24363	-.10643	14.86206	-.24363	.04099
15.11175	.23589	-.10657	15.11175	-.23589	.04044
15.86684	.21173	-.10754	15.86684	-.21173	.03881
16.86733	.17727	-.10889	16.86733	-.17727	.03661
17.86771	.14037	-.11039	17.86771	-.14037	.03428
18.86799	.10099	-.11208	18.86799	-.10099	.03172
19.86817	.05900	-.10969	19.86817	-.05900	.03385
20.86826	.02727	-.10037	20.86826	-.02727	.05001
21.02848	.02407	-.09760	21.02848	-.02407	.05389

XSPAN= 4.00000  
 ITEU= 22 ITL= 22  
 ZTE= 22.05696

UPPER SURFACE			LOWER SURFACE		
ZUP	YUP	CPU	ZLO	YLO	CPL
6.15946	-.00000	.19495	6.15946	-.00000	.19495
6.33707	.09505	-.14306	6.33707	-.09505	.28337
6.92546	.18444	-.16764	6.92546	-.18444	.16423
6.94887	.18780	-.16839	6.94887	-.18780	.15984

2246-043W

Figure 49 Spanwise and Chordwise Interpolation Output (Sheet 5 of 6)

8.05636	.26235	-.15583	8.05636	-.26235	.10335
8.16225	.26849	-.15452	8.16225	-.26849	.09875
9.14929	.29552	-.14607	9.14929	-.29552	.08085
10.23871	.31443	-.13663	10.23871	-.31443	.06517
10.45198	.31673	-.13476	10.45198	-.31673	.06253
11.29578	.31493	-.13202	11.29578	-.31493	.05720
12.34501	.30629	-.12871	12.34501	-.30629	.05177
13.39427	.29170	-.12547	13.39427	-.29170	.04723
14.44349	.27193	-.12244	14.44349	-.27193	.04345
15.30941	.25205	-.12011	15.30941	-.25205	.04081
15.48715	.24736	-.12005	15.48715	-.24736	.04041
16.50477	.21780	-.11983	16.50477	-.21780	.03819
17.52230	.18526	-.11982	17.52230	-.18526	.03597
18.53974	.14988	-.12010	18.53974	-.14988	.03361
19.55709	.11169	-.12055	19.55709	-.11169	.03104
20.57435	.07052	-.11790	20.57435	-.07052	.03293
21.59151	.03523	-.10704	21.59151	-.03523	.04904
22.05696	.02743	-.09984	22.05696	-.02743	.06060

XSFAN= 6.00000  
 ITEU= 19 ITL= 19  
 ZTE= 23.08543

UPPER SURFACE

LOWER SURFACE

ZUP	YUP	CPU	ZLO	YLO	CPL
9.23919	-.00000	-.04739	9.23919	-.00000	-.04739
9.50436	.10638	-.20300	9.50436	-.10638	.24458
10.38997	.20062	-.20370	10.38997	-.20062	.13207
10.42393	.20398	-.20357	10.42393	-.20398	.12810
11.52230	.24688	-.18870	11.52230	-.24688	.09363
12.24808	.26873	-.17902	12.24808	-.26873	.07433
12.63881	.27099	-.17541	12.63881	-.27099	.06992
13.72848	.27128	-.16553	13.72848	-.27128	.05917
14.81817	.26416	-.15590	14.81817	-.26416	.05036
15.69327	.25346	-.14837	15.69327	-.25346	.04446
15.89987	.24919	-.14767	15.89987	-.24919	.04373
16.94894	.22423	-.14415	16.94894	-.22423	.04039
17.99795	.19537	-.14092	17.99795	-.19537	.03737
19.04687	.16294	-.13805	19.04687	-.16294	.03448
20.09573	.12713	-.13570	20.09573	-.12713	.03144
21.14450	.08800	-.13377	21.14450	-.08800	.02872
22.19319	.04469	-.12918	22.19319	-.04469	.03073
22.97659	.01309	-.11341	22.97659	-.01309	.04981
23.08543	.00947	-.11103	23.08543	-.00947	.05301

\*\*\*\*\*

# AERODYNAMIC OUTPUT DATA

\*\*\*\*\*

## HALF CROSS SECTIONAL AREA DISTRIBUTION

Z	SCROSS
0.00000	0.00000
1.00000	.20819
2.00000	.55948
3.00000	.97662
4.00000	1.42677
5.00000	1.88807
6.00000	2.34389
7.00000	2.78081
8.00000	3.18756
9.00000	3.55460
10.00000	3.87332
11.00000	4.13655
12.00000	4.33762
13.00000	4.47041
14.00000	4.52880
15.00000	4.50700
16.00000	4.39962
17.00000	4.20076
18.00000	3.90370
19.00000	3.50109
20.00000	2.98429
21.45990	2.19138
23.10232	1.40859
24.89038	.77216
26.71825	.31971
28.37856	.07883

2246-044W

Figure 50 Aerodynamic Output (Sheet 1 of 3)

# SECTIONAL OR INCREMENTAL AREAS, FORCES, AND COEFFICIENTS

Z	SAREA(DZ)	FN(DZ)	FA(DZ)	CN(DZ)	CA(DZ)	CL(DZ)	CR(DZ)	CM(DZ)
1.00000	.32471	.07324	.05949	.22557	.18321	.20875	.20217	.24570
2.00000	.97412	.20680	.07443	.21230	.07641	.20483	.09462	.21844
3.00000	1.62352	.33387	.04802	.20565	.02958	.20229	.04739	.19786
4.00000	2.27293	.47781	.03846	.21022	.01692	.20794	.03518	.18811
5.00000	2.92234	.61823	.03081	.21155	.01054	.20983	.02894	.17499
6.00000	3.57175	.75740	.02374	.21205	.00665	.21067	.02510	.16104
7.00000	4.22115	.89582	.01664	.21222	.00394	.21107	.02242	.14678
8.00000	4.87056	1.03360	.00912	.21221	.00187	.21124	.02036	.13238
9.00000	5.51997	1.17034	.00111	.21202	.00020	.21119	.01868	.11787
10.00000	6.16938	1.30603	-.00737	.21170	-.00119	.21099	.01726	.10332
11.00000	6.81878	1.44085	-.01602	.21131	-.00235	.21071	.01608	.08879
12.00000	7.46819	1.57487	-.02222	.21088	-.00297	.21033	.01542	.07431
13.00000	8.11760	1.70801	-.02474	.21041	-.00305	.20987	.01530	.05986
14.00000	8.76701	1.83954	-.02536	.20983	-.00289	.20928	.01541	.04546
15.00000	9.41641	1.96919	-.02476	.20912	-.00263	.20856	.01561	.03113
16.00000	10.06582	2.09752	-.02289	.20838	-.00227	.20779	.01590	.01688
17.00000	10.71523	2.22432	-.01971	.20759	-.00184	.20696	.01626	.00274
18.00000	11.36464	2.34930	-.01513	.20672	-.00133	.20605	.01669	-.01129
19.00000	12.01404	2.47219	-.00910	.20578	-.00076	.20506	.01718	-.02519
20.00000	12.66345	2.59538	-.00275	.20495	-.00022	.20419	.01765	-.03898
21.45990	17.58115	3.72662	-.00093	.21197	-.00005	.21116	.01842	-.05778
23.10232	16.47943	3.79054	.00482	.23002	.00029	.22912	.02034	-.08680
24.89038	13.96837	3.55280	.00916	.25435	.00066	.25332	.02282	-.12534
26.71825	9.99903	2.82527	.01055	.28255	.00106	.28139	.02568	-.17343
28.37856	5.33184	1.63494	.00961	.30664	.00180	.30531	.02852	-.22370

2246-044W

Figure 50 Aerodynamic Output (Sheet 2 of 3)

# AXIAL INTEGRATION OF AREAS AND COEFFICIENTS

Z	XMIN	XMAX	SREF(Z)	STOT(Z)	CN(Z)	CA(Z)	CL(Z)	CD(Z)	CM(Z)
1.00000	0.00000	.64941	.32471	.74559	.22557	.18321	.20875	.20217	.24570
2.00000	0.00000	1.29882	1.29882	2.86624	.21562	.10311	.20581	.12151	.22525
3.00000	0.00000	1.94822	2.92234	6.28671	.21008	.06226	.20385	.08033	.21004
4.00000	0.00000	2.59763	5.19527	11.00096	.21014	.04243	.20564	.06058	.20044
5.00000	0.00000	3.24704	8.11760	17.00674	.21065	.03095	.20715	.04919	.19128
6.00000	0.00000	3.89645	11.68935	24.30304	.21108	.02352	.20822	.04183	.18204
7.00000	0.00000	4.54585	15.91050	32.88942	.21138	.01833	.20898	.03668	.17268
8.00000	0.00000	5.19526	20.78105	42.76583	.21158	.01447	.20951	.03286	.16324
9.00000	0.00000	5.84467	26.30102	53.93248	.21167	.01148	.20986	.02988	.15372
10.00000	0.00000	6.49408	32.47039	66.38963	.21167	.00907	.21008	.02748	.14414
11.00000	0.00000	7.14348	39.28917	80.13765	.21161	.00709	.21019	.02550	.13454
12.00000	0.00000	7.79289	46.75736	95.17692	.21149	.00548	.21021	.02389	.12497
13.00000	0.00000	8.44230	54.87495	111.50786	.21133	.00422	.21016	.02262	.11529
14.00000	0.00000	9.09171	63.64195	129.13098	.21113	.00324	.21004	.02163	.10567
15.00000	0.00000	9.74111	73.05836	148.04676	.21087	.00248	.20985	.02085	.09606
16.00000	0.00000	10.39052	83.12418	168.25572	.21057	.00191	.20960	.02025	.08648
17.00000	0.00000	11.03993	93.83940	189.75842	.21023	.00148	.20930	.01980	.07691
18.00000	0.00000	11.68934	105.20404	212.55540	.20985	.00118	.20895	.01946	.06739
19.00000	0.00000	12.33874	117.21808	236.64731	.20943	.00098	.20855	.01923	.05790
20.00000	0.00000	12.98815	129.88153	262.03486	.20899	.00086	.20812	.01907	.04845
21.45990	2.83895	13.93622	147.46268	297.27303	.20935	.00075	.20849	.01899	.03579
23.10232	6.03283	15.00282	163.94211	330.30009	.21143	.00071	.21056	.01913	.02346
24.89038	9.50994	16.16400	177.91048	358.28966	.21479	.00070	.21392	.01942	.01178
26.71825	13.06446	17.35104	187.90952	378.32038	.21840	.00072	.21751	.01975	.00192
28.37856	16.29313	18.42926	193.24136	388.99795	.22084	.00075	.21993	.01999	-.00430

MINF= 1.7000

ALPHA= 5.0000

CL= .21993

CD= .01999

CM= -.00430

## AERODYNAMIC CONSTANTS

SREF= 193.24136

CBAR= 14.7470

ZCG= 16.7010

YCG= 0.0000

Figure 50 Aerodynamic Output (Sheet 3 of 3)



## 11 REFERENCES

1. Grossman, B., "Numerical Procedure for the Computation of Irrotational Conical Flows," AIAA J., Vol. 17, No. 8, Aug 1979, pp. 828-837.
2. Mason, W.H. and Rosen, B.S., "The COREL and W12SC3 Computer Programs for Supersonic Wing Design and Analysis, NASA CR-3676, 1983.
3. Grossman, B., and Siclari, M.J., "The Nonlinear Supersonic Potential Flow Over Delta Wings," AIAA Paper No. 80-0269, presented at AIAA 18th Aerospace Sciences Meeting, Pasadena, CA, Jan 1980.
4. Siclari, M.J., Marconi, F., and Grossman, B., "Analysis and Design of Supersonic Aircraft Based on Inviscid Nonlinear Eulerian Equations," AFWAL TRE-80-3110, Part I and II, Oct 1980.
5. Miller, D., Landrum, E.J., Townsend, J.C., and Mason, W.H., "Pressure and Force Data for a Flat Wing and a Warped Conical Wing Having a Shockless Recompression at Mach 1.62," NASA TP-1759, April 1981.
6. Mason, W.H., "Experimental Pressure Distributions and Aerodynamic Characteristics of a Demonstration Wing for a Wing Concept for Supersonic Maneuvering," Grumman Aerodynamics Report, 393-82-02, July 1982.
7. Mason, W.H., Miller, D.S., Pittman, J.L., and Siclari, M.J., "A Supersonic Maneuver Wing Designed for Nonlinear Attached Flow", AIAA Paper No. 83-0425, Jan 1983.
8. Jameson, A., "Iterative Solution of Transonic Flow Over Airfoils and Wings, Including Flows at Mach 1," Comm. Pure Appl. Math., Vol 27, pp. 283, 309, May 1974.
9. Siclari, M.J., "Supersonic Nonlinear Potential Flows with Subsonic Regions and Implicit Isentropic Shock Fitting," AIAA-81-1201, presented at AIAA 14th Fluid and Plasma Dynamics Conference, Palo Alto, CA, June 1981.
10. Craidon, C.B., "A Computer Program for Fitting Smooth Surfaces to an Aircraft Configuration and Other Three-Dimensional Geometries," NASA TM X-3206, June 1975.
11. Townsend, J.C., Howell, D.T., Collins, I.K. and Hayes, C., "Surface Pressure Data on a Series of Analytic Forebodies at Mach Numbers From 1.70 to 4.50 and Combined Angles of Attack and Sideslip," NASA TM-80062, June 1979.
12. Graves, E.B., "Aerodynamic Characteristics of a Monoplanar Missile Concept with Bodies of Circular and Elliptical Cross Sections," NASA TM-74079, Dec 1977.
13. Laiosa, J. and Boppe, C.W., "A New Hybrid Approach to Supersonic Aircraft Analysis", AIAA Paper No. 83-0340. Presented at AIAA 21st Aerospace Sciences Meeting, Reno, Nevada.

14. Townsend, J.C., "Pressure Data for Four Analytically Defined Arrow Wings in Supersonic Flow," NASA TM-81835, Sept 1980.
15. Shrout, B.L., Corlett, W.A. and Collins, I.K., "Surface Pressure Data for a Supersonic-Cruise Airplane Configuration at Mach Numbers of 2.30, 2.96, and 3.30," NASA TM-80061, May 1979.
16. Weber, J. and King, C., "Analysis of the Zero-Lift Drag Measured on Delta Wings," ARC R&M 3818, June 1976.
17. Mason, W.H., and Da Forno, G., "Opportunities for Supersonic Performance Gains Through Non-Linear Aerodynamics," AIAA Paper No. 79-1527, July 1979.



1. Report No. NASA CR-3694		2. Government Accession No.		3. Recipient's Catalog No.	
4. Title and Subtitle THE NCOREL COMPUTER PROGRAM FOR 3D NONLINEAR SUPERSONIC POTENTIAL FLOW COMPUTATIONS				5. Report Date August 1983	
				6. Performing Organization Code	
7. Author(s) Michael J. Siclari				8. Performing Organization Report No.	
9. Performing Organization Name and Address Grumman Aerospace Corporation Bethpage, New York 11714				10. Work Unit No.	
				11. Contract or Grant No. NAS1-16758	
12. Sponsoring Agency Name and Address National Aeronautics and Space Administration Washington, DC 20546				13. Type of Report and Period Covered Contractor Report	
				14. Sponsoring Agency Code	
15. Supplementary Notes Langley Technical Monitor: David Miller Final Report					
16. Abstract <p>An innovative computational technique (NCOREL) has been established for the treatment of three dimensional supersonic flows. The method is nonlinear in that it solves the nonconservative finite difference analog of the full potential equation and can predict the formation of supercritical cross flow regions, embedded and bow shocks.</p> <p>The method implicitly computes a conical flow at the apex (<math>R = 0</math>) of a spherical coordinate system and uses a fully implicit marching technique to obtain three dimensional cross flow solutions. This implies that the radial Mach number must remain supersonic. The cross flow solutions are obtained by using type dependent transonic relaxation techniques with the type dependency linked to the character of the cross flow velocity (i.e., subsonic/supersonic).</p> <p>The spherical coordinate system and marching on spherical surfaces is ideally suited to the computation of wing flows at low supersonic Mach numbers due to the elimination of the subsonic axial Mach number problems that exist in other marching codes that utilize Cartesian transverse marching planes.</p> <p>NCOREL has been applied successfully to a wide variety of body and wing configurations in the Mach number range from 1.5 to 3. The method represents a significant advancement in accuracy over linear methods. This report describes the practical application and use of the computer program NCOREL.</p>					
17. Key Words (Suggested by Author(s)) Supersonic Flow Nonlinear Potential Flow NCOREL			18. Distribution Statement Unclassified - Unlimited  Subject Category 02		
19. Security Classif. (of this report) Unclassified	20. Security Classif. (of this page) Unclassified	21. No. of Pages 170	22. Price A08		